TECHNISCHE UNIVERSITÄT DRESDEN

Internationales Hochschulinstitut Zittau

New Secretory Peroxidases and Peroxygenases from Saprotrophic Fungi of Kenyan Forests

DISSERTATION

zur Erlangung des akademischen Grades

Doctor rerum naturalium

(Dr. rer. nat.)

vorgelegt

dem Bereich Mathematik und Naturwissenschaften der Technischen Universität Dresden

von
M.Sc. Virginia Wambui Kimani

Geboren am 26. März 1985 in Kiambu (Kenya)

Verteidigt am 07. November 2019

Gutachter:
Herr Prof. Dr. Martin Hofrichter (TU Dresden – IHI Zittau)
Herr Prof. Richard P. Beckett (Universität KwaZulu-Natal, Südafrika)

Die Dissertation wurde in der Zeit von 01. Oktober 2015 bis zum 27. Mai 2019 im Internationalen Hochschulinstitut Zittau der TU Dresden angefertigt.

TECHNISCHE UNIVERSITÄT DRESDEN

Internationales Hochschulinstitut Zittau

New Secretory Peroxidases and Peroxygenases from Saprotrophic Fungi of Kenyan Forests

DISSERTATION

for obtaining the academic degree

Doctor rerum naturalium

(Dr. rer. nat.)

submitted to the

School of Science
of the Technical University Dresden

from
M.Sc. Virginia Wambui Kimani

born on 26. March 1985 in Kiambu (Kenya)

defended on 07th of November 2019

Reviewers:
Herr Prof. Dr. Martin Hofrichter (TU Dresden – IHI Zittau)
Herr Prof. Richard P. Beckett (University KwaZulu-Natal, Südafrika)

The Dissertation was prepared from 01. October 2015 till 27. May 2019 at the International Institute Zittau from the TU Dresden

TABLE OF CONTENTS

LIST OF ABBREVIATIONS V

ZUSAMMENFASSUNG VII

SUMMARY IX

MUHTASARI XI

1 INTRODUCTION 1

1.1 Degradation of lignocellulose by higher fungi 1

1.1.1 Plant cell wall composition 1

1.1.2 Lignocellulose degrading fungi 3

1.1.2.1 White-rot fungi (WRF) and litter-decomposing fungi (LDF) 5

1.1.2.2 Brown-rot fungi (BRF) 7

1.1.2.3 Soft-rot fungi (SRF) 8

1.1.2.4 Further groups of saprotrophic fungi inhabiting wood and soil 10

1.1.3 Enzymatic degradation of the lignocellulosic complex 12

1.1.3.1 Degradation of cellulose 12

1.1.3.2 Degradation of hemicelluloses 13

1.1.3.3 Degradation of lignin 14

1.2 Heme peroxidases 16

1.2.1 Fungal class II peroxidases 18

1.2.2 Dye-decolorizing peroxidase (DyP) 20

1.2.3 Unspecific peroxygenases (UPO) 23

1.3 Lignocellulose-degrading fungi from tropical regions 30

1.4 Relatives of fungal isolates 31

1.4.1 The genus *Psathyrella* 31

1.4.2 The genus *Xylaria* 33

1.5 Objectives of the study 34

2 MATERIAL AND METHODS 35

2.1 Collection sites of Kenyan fungi 35

2.2 Media and fungal cultivation conditions 36

2.2.1 Malt extract agar media (MA media) 37

2.2.2 Isolation of Kenyan fungi 37

2.2.3 Liquid cultivation 37

2.2.4 Agar plate screening for extracellular oxidoreductase activities 38

2.3 Enzyme assays 39
2.3.1 Rapid screening for oxidoreductases in microtiter plates 39
2.3.2 ABTS oxidation 40
2.3.3 Veratryl alcohol oxidation 40
2.3.4 Manganese oxidation 41
2.4 Production of peroxidases 41
2.4.1 Production of the UPO from *P. aberdarensis* (*Pab*UPO) 41
2.4.2 Production of the DyP from *X. grammica* (*Xgr*DyP) 42
2.5 Enzyme purification 43
2.5.1 Preparation of enzyme crude extract 43
2.5.2 Fast protein liquid chromatography (FPLC) 43
2.5.2.1 Purification of the UPO from *P. aberdarensis (PabUPO*) 43
2.5.2.2 Purification of the DyP-type peroxidase from *X. grammica* (*Xgr*DyP) 44
2.6 Enzyme characterization 44
2.6.1 Protein determination 44
2.6.2 Protein electrophoresis 44
2.6.2.1 Sodium dodecyl sulfate polyacrylamide gel electrophoresis (SDS-PAGE) 44
2.6.2.2 Native isoelectric focusing (IEF) 45
2.6.3 Determination of pH-optima and stability 45
2.6.3.1 pH-Optima and stability of the UPOs from *P. aberdarensis* (*Pab*UPO) 45
2.6.3.2 pH-Optima of the DyP from *X. grammica* (*Xgr*DyP) 46
2.6.4 Kinetic parameters 46
2.7 Peptide sequencing 46
2.8 Substrate conversion by *Pab*UPO 47
2.8.1 Halogenation of phenol 47
2.8.2 Hydroxylation of naphthalene 47
2.8.3 Hydroxylation of anisole (methoxybenzene) 47
2.8.4 Conversion of toluene (methylbenzene) 48
2.8.5 Conversion of oseltamivir 48
2.8.6 Oxidation of 5-formyl-2-furancarboxylic acid (FFCA) 48
2.9 High performance liquid chromatography (HPLC) 49
2.9.1 Reversed phase high performance liquid chromatography (RP-HPLC) 49
2.9.1.1 Halogenation of phenol and oxygenation of naphthalene 49

2.9.1.2 Oxygenation of anisole and toluene 49
2.9.1.3 Conversion of oseltamivir 50
2.9.1.4 Conversion of 5-formyl-2-furancarboxylic acid (FFCA) 50
2.9.2 Size exclusion chromatography - high performance liquid chromatography (SEC-HPLC) 50
2.10 Molecular work 51
2.10.1 Identification of isolated fungi 51
2.10.2 ITS sequencing 51
2.10.3 DNA isolation and genome sequencing 51
2.10.4 Assembly and genome annotation 52
2.11 Phylogenetic analysis 53
2.12 Homology modelling 53

3 RESULTS 54
3.1 Isolation and identification of fungal strains 54
3.2 *Psathyrella aberdarensis*: a new species of Psathyrellaceae 56
3.2.1 Diagnosis of *Psathyrella aberdarensis* 56
3.2.2 Description of *Psathyrella aberdarensis* 56
3.3 Enzyme screening and strain selection 59
3.4 Optimization of UPO production by *Psathyrella aberdarensis* 66
3.5 Purification of *Psathyrella aberdarensis* UPO (*Pab*UPO) 67
3.6 UV-visible spectra of the *P. aberdarensis* UPOs 69
3.7 Electrophoretic analyses of the *P. aberdarensis* UPOs 70
3.8 pH Optima and stabilities of the *P. aberdarensis* UPOs 70
3.9 Kinetic parameters of purified UPOs from *P. aberdarensis* 73
3.10 Peroxygenase-specific reactions catalyzed by *Pab*UPOs 74
3.10.1 Halogenation of phenol 74
3.10.3 Hydroxylation of naphthalene 77
3.10.4 Hydroxylation of anisole 78
3.10.5 Conversion of toluene 79
3.10.6 Conversion of oseltamivir 81
3.10.7 *O*-Demethylenation of nitrobenzodioxole 81
3.10.8 Conversion of FFCA into FDCA 82
3.11 The *Psathyrella aberdarensis* genome 83
3.11.1 Assembly and quality assessment of *P. aberdarensis* draft genome 83
3.11.2 *Pab*UPO encoding genes and their deduced protein sequences 84

3.11.3 Classification of the lignocellulytic enzymes in the *Psathyrella* genome ... 88
3.11.3.1 Glycoside Hydrolases ... 88
3.11.3.2 Oxidoreductases ... 90
3.12 Production and purification of a DyP from *Xylaria grammica* ... 92
3.13 Characterization of the *X. grammica* DyP ... 95
3.14 Kinetic parameters of the purified *X. grammica* DyP ... 97
3.15 The *Xylaria grammica* genome ... 97
3.15.1 Assembly and quality assessment of the *X. grammica* draft genome ... 97
3.15.2 *Xgr*DyP encoding genes and their deduced protein sequences ... 98
3.15.3 Classification of lignocellulytic enzymes in the *X. grammica* genome ... 100
3.15.3.1 Glycoside Hydrolases ... 101
3.15.3.2 Oxidoreductases ... 102

4 DISCUSSION ... 105
4.1 Setting up a culture collection of Kenyan fungi ... 105
4.2 First description of a new *Psathyrella* species ... 106
4.3 Agar-plate screening of fungal isolates for oxidoreductases ... 108
4.4 Production of oxidoreductases by Kenyan isolates in liquid culture ... 110
4.5 Comparison of *Pab*UPOs with other fungal peroxygenases ... 113
4.5.1 General aspects ... 113
4.5.1 Physicochemical optima and stabilities of *Pab*UPOs ... 114
4.5.2 Catalytic properties of *P. aberdarensis* UPOs ... 116
4.5.3 Structural aspects of the *Pab*UPOs ... 119
4.6 Comparison of *Xgr*DyP with other fungal DyP-type peroxidases ... 122
4.6.1 General aspects ... 122
4.6.2 Catalytic properties of *X. grammica* DyP ... 123
4.6.3 Structural aspects of the DyP of *X. grammica* (*Xgr*DyP) ... 127
4.6.4 Eco-physiological classification of *P. aberdarensis* and *X. grammica* ... 131

5 CONCLUSION AND OUTLOOK ... 133

6 REFERENCES ... 137

7 APPENDIX ... 156

LIST OF ABBREVIATIONS

AAOs	Aryl alcohol oxidases
A. dest	Distilled water
*Aae*UPO	*Agrocybe aegerita* unspecific peroxygenase
ABTS	2,2'-azino-*bis*(3-ethylbenzthiazoline-6-sulphonic acid)
ACN	Acetonitrile
AEX	Anion exchange chromatography
BA	Benzyl alcohol
*Bad*DyP	*Bjerkandera adusta* dyp-type peroxidase
BSA	Bovine serum albumin
*Cgl*UPO	*Chaetomium globusum* unspecific peroxygenase
CPO	Chloroperoxidase
*Cra*UPO	*Coprinellus radians* unspecific peroxygenase
CRO	Copper radical oxidase
*Cve*UPO	*Coprinopsis verticillata* unspecific peroxygenase
DMP	2,6-dimethoxyphenol
DyP	Dye-decolorizing peroxidase
EC	Enzyme commision
ESI-MS	Electrospray ionization mass spectrometer
$FADH_2$	Reduced flavin adenine dinucleotide (dihydro form)
FDCA	2,5-furandicarboxylic acid
FFCA	5-formyl-2-furancarboxylic acid
FPLC	Fast protein liquid chromatography
HA	Humic acid
HPLC	High performance liquid chromatography
IEF	Isoelectric focusing
k_{cat}	Catalytic constant
kDa	Kilodalton
K_m	Michaelis-Menten constant
LiP	Lignin peroxidase
LPMOs	Lytic polysaccharide monooxygenases
MnP	Manganese peroxidase
*Mro*UPO	*Marasmius rotula* unspecific peroxygenase

MS	Mass spectrometry
MW	Molecular weight
*Mwe*UPO	*Marasmius wettsteini* unspecific peroxygenase
NAD^+	Oxidized nicotinamide adenine dinucleotide
NBD	5-nitro-1,3-benzodioxole
NOS	Nitric oxide synthase
P450s	Cytochrome P450-dependent monooxygenases
*Pab*UPO	*Psathyrella aberdarensis* unspecific peroxygenase
PAH	Polycyclic aromatic hydrocarbon
PCA	Principal component analysis
pI	Isoelectric point
POD	Peroxidase
SDS-PAGE	Sodium dodecyl sulphate polyacrylamide gel electrophoresis
SEC	Size exclusion chromatography
UPO	Unspecific peroxygenase
VA	Veratryl alcohol
VP	Versatile peroxidase
*Xgr*DyP	*Xylaria grammica* dyp-type peroxidase

ZUSAMMENFASSUNG

Die vorliegende Dissertation befasst sich vor dem Hintergrund von pilzlicher Ökophysiologie und Umweltbiotechnologie mit der Isolierung, Reinigung und Charakterisierung von neuartigen Oxidoreduktasen aus kenianischen Pilzen (Eumycota). Unter Verwendung von selektiven, antibiotikahaltigen Agarmedien wurde 2016 eine Stammsammlung von 43 pilzlichen Isolaten angelegt, die Totholz, Laubstreu und Boden besiedelnde Arten umfasst und drei verschiedene kenianische Waldtypen und Biodiversitätsschwerpunkte berücksichtigt (ostafrikanische Regen-, Berg- und Küstenwälder). Die Isolate gehörten zu 21 Familien aus drei (Unter)stämmen: Basidiomycota, Ascomycota und Mucoromycotina. Unter ihnen befanden sich Weißfäulepilze und Streuzersetzer (aus den Familien Polyporaceae und Strophariceae), ein polyporaler Braunfäulepilz (*Fomitopsis meliae*) und zwei Vertreter der Familie Xylariaceae, die eine Moderfäule hervorrufen. Auf Grundlage morphologischer und molekularbiologischer Analysen konnte eine neue Art der Blätterpilz-Gattung *Psathyrella* identifiziert und als *P. aberdarensis* beschrieben werden. Extrazelluläre Aktivitäten von Unspezifischer Peroxygenase (UPO, EC 1.11.2.1) and DyP-Typ-Peroxidase (DyP, EC 1.11.1.19) wurden für einige der pilzlichen Isolate nachgewiesen, u.a. für *P. aberdarensis* (*Pab*UPO) und den ascomycetalen Moderfäulepilz *Xylaria grammica* (*Xgr*DyP). Die zugehörigen Enzymproteine wurden gereinigt und biochemisch characterisiert. Die *Pab*UPOs werden in Form von drei verschiedenen Isoenzymen/Isoformen exprimiert und realisieren ungewöhnlich breite pH-Profile bei entsprechend hoher Enzymstabilität. Sie gehören zur Proteinfamilie der “langen” UPOs und katalysieren typische Peroxygenierungen, u.a. die Oxidation von Alkoholen, die Spaltung von Ethern, die Demethylenierung, die Oxygenierung aromatischer Ringe und – darüber hinaus – die Oxidation von Formylfurancarbonsäure zu Furandicarbonsäure (eine spezifische Reaktion, die für die Herstellung von biobasierten Polyestern aus nachwachsenden Rohstoffen von Bedeutung ist). Bei der *Xgr*DyP handelt es sich um die erste Wildtyp-DyP eines Ascomyceten; sie ist in der Lage, Peroxidase-Substrate wie ABTS und 2,6-Dimethoxyphenol, aber auch den Anthrachinon-Farbstoff Reactive Blue 5, Veratrylalkohol, und – bemerkenswerterweise – Mangan (Mn^{2+}) zu oxidieren, was auf neue physiologische Funktionen dieses Enzymtyps hinweist. Die Genome der beiden Enzymbildner wurden sequenziert und annotiert, was die Identifizierung der zugehörigen Enzyme-kodierenden Gene erlaubte. Neben den beiden exprimierten *Pab*UPO-Genen

wurden 46 weitere putative UPO-Sequencen im *Psathyrella*-Genom gefunden. Aufgrund des Fehlens ligninolytischer Klasse-II-Peroxidasen in den Genomen beider Pilze wird angenommen, dass die charakterisierten Hämperoxidasen von ökophysiologischer Bedeutung für alternative Wege des Abbaus von Lignozellulosen oder Humus sind. Auf Basis des gefundenen Kernbestands an lignocellulolytischen CAZy-Enzymen (d.h. Cellulasen, lytische Polysaccharid-Monooxygenasen, Laccase, H_2O_2-bildende Oxidasen), können *P. aberdarensis* and *X. grammica* den ökophysiologischen Gruppen der streuzersetzenden Weißfäulepilze bzw. holzbesiedelnden Moderfäulepilze zugerechnet werden.

SUMMARY

The present dissertation deals, against the background of fungal eco-physiology and environmental biotechnology, with the isolation, purification and characterization of new fungal oxidoreducatses from Kenyan fungi (Eumycota). By using selective agar media supplemented with antibiotics, a culture collection comprising 43 fungal isolates dwelling in deadwood, leaf-litter and soil was established in 2016, considering three different Kenyan forest types and biodiversity hotspots (East African rainforest, mountain and coastal forests). The isolates turned out to belong to 21 families of the (sub)phyla Basidiomycota, Ascomycota and Mucoromycotina. Among them were white-rot and litter-decomposing fungi (from the families Polyporaceae and Strophariceae), a polyporous brown-rot species (*Fomitopsis meliae*) and two members of the family Xylariaceae causing soft-rot. By morphological and molecular analyses, a new species of the agaric genus *Psathyrella* was identified and described as *Psathyrella aberdarensis*. Extracellular activities of unspecific peroxygenase (UPO, EC 1.11.2.1) and DyP-type peroxidase (DyP, EC 1.11.1.19) were demonstrated for a few of the fungal isolates, among them *P. aberdarensis* (*Pab*UPO) and the soft-rot ascomycete *Xylaria grammica* (*Xgr*DyP), respectively. The corresponding enzyme proteins were purified and characterized. *Pab*UPOs occur in form of three different isoenzymes/isoforms realizing unusually broad pH-profiles and stabilities. They belong to the clade of 'long' UPOs and catalyze typical peroxygenations, i.e. alcohol oxidation, ether cleavage, demethylenation, aromatic ring oxygenation, and beyond that, the oxidation of formylfuran carboxylic acid into furandicarboxylic acid (a specific reaction in the preparation of bio-based polyesters from renewable building blocks). *Xgr*DyP is the first wild-type DyP reported for an ascomycetous fungus and was found to oxidize peroxidase substrates such as ABTS and 2,6-DMP but also Reactive Blue 5, veratryl alcohol and notably manganese (Mn^{2+}), suggesting novel physiological functions of this enzyme type. The genomes of both producer species were sequenced and annotated, which allowed the identification of the corresponding enzyme-encoding genes. Besides the two expressed *Pab*UPO genes, a further 46 putative UPO sequences were identified in the *Psathyrella* genome. Due to the absence of ligninolytic class II peroxidases in the genomes of both fungi, the characterized heme peroxidases may be of eco-physiological relevance for alternative pathways degrading lignocellulosic materials or humus. Based on the core set of lignocellulolytic CAZy enzymes (i.e. cellulases, lytic monosaccharide monooxygenases,

laccase, H_2O_2-generating oxidases), *P. aberdarensis* and *X. grammica* can be classified within the eco-physiological groups of litter-decomposing white-rot and wood-colonizing soft-rot fungi, respectively.

MUHTASARI

Tasnifu hii inaangazia utendakazi wa kuvu katika mazingira na bayo-teknolojia ya kimazingira, utengaji, usafishaji na ubainishaji wa vimeng'enya vipya aina ya oxidoreducatses kutoka kwa kuvu (Eumycota) kutoka Kenya. Kwa kutumia agar iliyoongezwa dawa za kuzuia bakteria, mkusanyiko wa kuvu 43 zinazopatikana kwenye miti ilioza, matawi na udongo ulibuniwa mwaka 2016, kuzingatia misitu mitatu ya Kenya, (Msitu wenye mvua nyingi Afrika Mashariki, mlima na misitu ya pwani). Kuvu hizo zilizotengwa zilibainika kuwa za familia 21 za familia ndogo ya kuvu aina ya phyla Basidiomycota, Ascomycota na Mucoromycotina. Miongoni mwao zilikuwa kuvu zinazosababisha muozo mweupe na zile zinazoozesha matawi (kutoka familia aina ya Polyporaceae na Strophariceae), aina ya kuvu yenye vipenyezo (*Fomitopsis meliae*) na kuvu mbili za familia ya Xylariaceae. Kupitia changanuzi za kimaumbile na kimasi, aina mpya ya familia ndogo ya uyoga ya *Psathyrella* ilitambuliwa na kuitwa *Psathyrella aberdarensis*. Michakato ya nje ya seli ya kimeng'enya chenye protini cha peroxygenase (UPO, EC 1.11.2.1) na kimeng'enya kinachochuja rangi cha peroxidase (DyP, EC 1.11.1.19) ilionekena kwenye kuvu chache zilizotengwa, ikiwemo *Psathyrella aberdarensis* (*Pab*UPO) na ile inayosababisha muozo hafifu ya ascomycete *Xylaria grammica* (*Xgr*DyP), mtawalia. Protini hizo za kimeng'enya zilisafishwa na kubainishwa. Vimeng'enya vya *Pab*UPO hupatikana katika aina tatu tofauti na hufikia viwango visivyo vya kawaida vya asidi na uthabiti. Vimeng'enya hivyo vinahusishwa na vimeng'enya virefu vya UPOs na huchochea michakato ya kawaida ya utengenezaji kemikali k.v utiaji oxijeni kwenye kemikali za asili ya pombe, umomonyoaji viyeyusho vya ether, mchakato wa kuondoa kemikali ya methyl kwenye furushi la kemikali (demethylenation), mchakato wa kutia oxijeni kwenye kemikali zenye mfumo wa duara (aromatic ring oxygenation), na zaidi ya hapo, ubadilishaji wa asidi aina ya formylfuran carboxylic hadi asidi aina ya furandicarboxylic kupitia utiaji oxijeni (mchakato mahususi katika utengenezaji wa bidhaa za polyester kwa njia ya kibaiolojia inayotumia chembe za kurejeshwa upya). Kimeng'enya kinachochuja rangi cha *Xgr*DyP ni kimeng'enya cha kwanza kugunduliwa kwa kuvu ya ascomycetous, na kilionekana kutekeleza mchakato wa kubadili nyenzo za utendakazi za kimeng'enya peroxidase kama vile ABTS na 2,6-DMP, pia Reactive Blue 5, kemikali ghafi ya veratryl na hasa madini ya manganese (Mn^{2+}), na hivyo kuashiria umuhimu wa kimeng'enya hiki katika utendakazi wa vimeng'enya vya aina hii. Mfumo wa asidi nasaba na jeni za aina zalishaji zilipangwa na kuelezewa, hatua iliyowezesha

utambulizi wa jeni zinazozalisha vimeng'enya. Mbali na jeni hizo mbili za kimeng'enya *Pab*UPO, vimeng'enya vingine 46 ambavyo matumizi yao hayajulikani, viligunduliwa kwenye jeni na asidi nasaba ya *Psathyrella*. Kutokana na ukosefu wa vimeng'enya dhahiri vya daraja ya pili vya peroxidases kwenye jeni na asidi nasaba ya kuvu hizo mbili, vimeng'enya vya peroxidases vilivyobainishwa, labda vina umuhimu kwenye physiologia mbadala za kumomonyoa ngome ya seli za mimea ama mboji. Kuambatana na mpangalio mkuu wa vimeng'enya vya kikabohaidreti vinavyoweza kumomonyoa ngome ya seli za mimea (k.v cellulases, lytic monosaccharide monooxygenases, laccase, vimeng'enya vinavyotoa kemikali ya H_2O_2 vya oxidases), *P. aberdarensis* na *X. grammica* vinaweza kuainishwa katika makundi ya physiologia-kimazingira ya kuvu zinazosababisha muozo mweupe wa matawi na majani, na kuvu za mitini zinazosababisha muozo hafifu, mtawalia.

1 INTRODUCTION

1.1 Degradation of lignocellulose by higher fungi

1.1.1 Plant cell wall composition

Lignocelluloses are becoming more and more economically important as raw materials for biotechnological and industrial applications, not at least against the background of intensified utilization of biomass in connection with the biorefinery concept and the idea of sustainable development (Mapemba et al. 2007, Jørgensen et al. 2007, Kamm and Kamm 2004). Such materials are found in all terrestrial ecosystems and represent the largest source of renewable organic compounds in the biosphere (Peters 2007). Concerning origin, condensation grade and composition, different types of lignocelluloses can be distinguished: compact softwood and hardwood of coniferous and deciduous (broad-leaved) trees and shrubs as well as straw-and hay-like materials from grasses, crops (in first place from cereals) and other annual herbal plants (Peters 2007). Lignocelluloses result from the synthesis of complex cell-wall polymers, which provide rigidity and mechanical stability and protect the plants from microbial attack (Monties and Fukushima 2001). The particular properties of lignocelluloses as natural 'composite material' are based on the structure of their major polymeric components: cellulose (forming the backbone fibers), hemicelluloses (xylan or glucomannan, covering the cellulose fibers) and lignin (acting as the molecular glue) (Monties and Fukushima 2001, Busch et al. 2006). From the biotechnological point of view, the enzymatic disintegration of the cell-wall complex is an attractive and challenging goal, as it would deliver sugars for fermentation (glucose, other hexoses, pentoses) and bioethanol production as well as aromatic compounds from lignin as raw material for the chemical industry (Mapemba et al. 2007, Jørgensen et al. 2007, Kamm and Kamm 2004, Busch et al. 2006).

Cellulose is the most abundant component of lignocelluloses (35-45%) comprising a non-branched polysaccharide made up entirely of cellobiose subunits, which consist of two β-1,4-linked D-glucose molecules, forming a linear polymeric chain varying in length between 8,000 and 15,000 residues (Fig. 1.1) (Brown 2004). Cellulose appears in sheets of glucopyranose rings lying in a plane with successive sheets stacked on top of another to form a three-dimensional structure. The β-1,4-linked cellobiose chains may appear more complex at the macroscopic level, since the cellulosic polymer is intricately associated with hemicelluloses and lignin (Shawn 2009). **Hemicelluloses** (e.g. xylan in

hardwood, glucomannan in softwood) are branched heteropolymers making up between 15% and 35% of lignocellulosic biomass; they can contain pentoses (e.g. β-D-xylose), hexoses (β-D-galactose) and/or uronic acids (e.g. galacturonic acid; Fig. 1.1) (Kirk and Cullen, 1998). The monomers are linked together via different glycosidic bonds (e.g. β-1,4-, β-1,3- or α-1,2-linkages). Typically, poylmeric xylan (e.g. glucuronoxylan or arabinoxylan) is bridged by ester bonds to carboxylic or phenolic groups of hydroxycinnamic acids (e.g. to ferulic or *p*-coumaric acid) of the lignin molecule (Liyama et al. 1994, Buranov and Mazza 2008). Such ester bonds are specific lignin-hemicellulose cross-links that reduce the biodegradability of cell walls (Hartley and Ford 1989, Koshijima and Watanabe 2003).

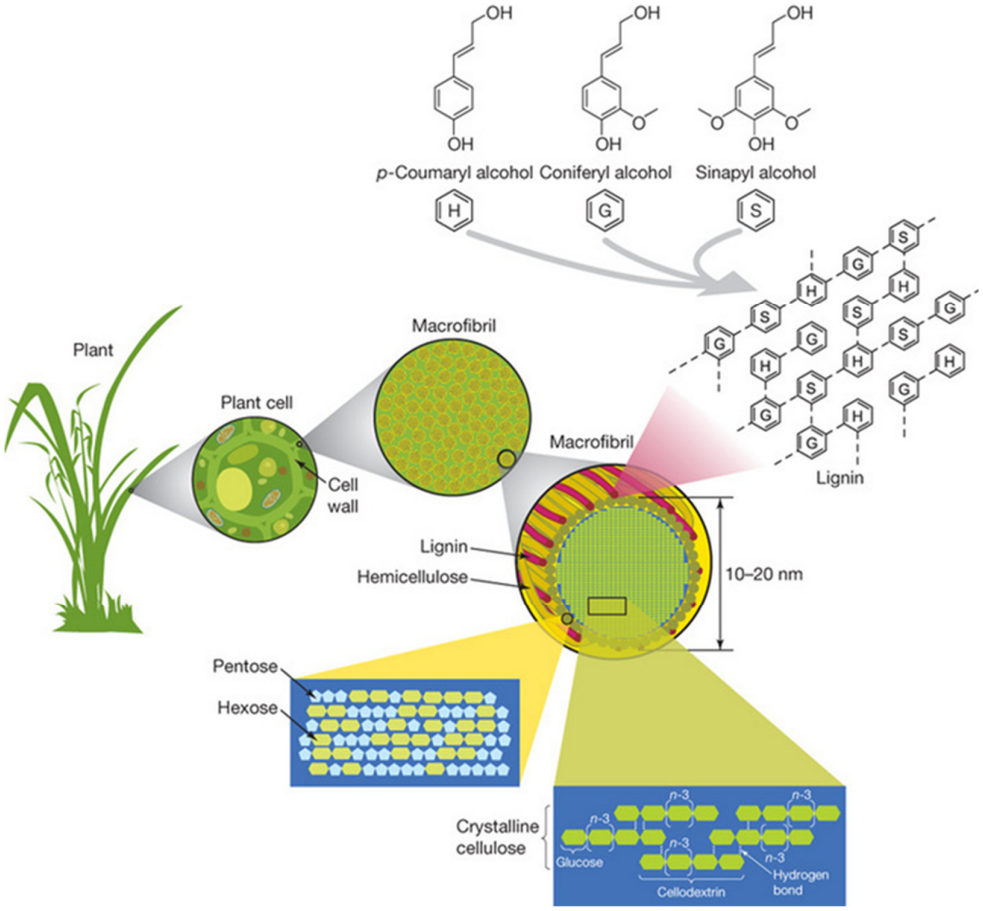

Fig. 1.1: Plant cell wall structure (Rubin 2008)

Lignin (10-30%) represents the third polymeric component of lignocelluloses and the most abundant form of aromatic carbon in the biosphere (Boerjan et al. 2003, Chen and Sarkanen 2010). It is an amorphous and heterogenous polymer present in all layers of woody cell walls and the most recalcitrant component of plant biomass. Lignin establishes

a three-dimensional network of phenylpropanoid subunits originating from coniferyl, sinapyl and *p*-coumaryl alcohols (Fig. 1.1; Rubin 2008), which are polymerized to guaiacyl-(G), syringyl-(S) and hydroxyphenyl-(H) type lignin subunits via the action of plant laccases and peroxidases (Higuchi 2006). The subunits are joined together by a variety of bond types including carbon-carbon and ether bonds, of which the β-aryl ether (β-*O*-4) bond is the most abundant one (Adler 1977, Mäkelä et al. 2014). Because of its complicated structure with diverse non-hydrolysable inter-monomeric bonds, the microbial degradation of lignin requires unspecific extracellular oxidoreductases (Kirk and Farrell 1987) and low-molecular weight oxidants (redox mediators), i.e. reactive metal cations and/or aromatic radicals (Evans et al. 1994).

1.1.2 Lignocellulose degrading fungi

To get access to the fermentable and assimilable polysaccharides and sugars, it is necessary to remove, at least in parts, the recalcitrant lignin polymer ('lignin barrier'). There are different microbial strategies to accomplish this, but the most efficient enzymatic systems have been developed by filamentous fungi. Among them, there is a polyphyletic group, the so-called 'higher fungi', which can be distinguished from other fungi ('microfungi', molds) by the temporary development of complex macroscopic fruiting bodies (sporocarps producing sexually formed meiospores), commonly known as mushrooms, toadstools, puffballs, morels etc. Their fungal mycelia growing preferably in the upper soil, leaf and needle litter, deadwood or living plants are of biotechnological relevance, since they secrete sets of powerful biocatalysts ('digestion enzymes'), which can degrade almost any natural organic material including the lignocellulosic complex (Fig. 1.1 & 1.2). About 20% of the higher fungi belong to the Basidiomycota (formerly basidiomycetes) and 80% to the Ascomycota (ascomycetes)[1]. Depending on their mode of living, they can be categorized as either saprotrophic (saprobic), phytopathogenic or symbiotic (mycorrhizal) fungi. The former group can be further divided into five ecological types: white-rot, brown-rot and soft-rot fungi colonizing wood (logs, branches, stumps) as well as litter-decomposing and dung-dwelling (coprophilic) fungi colonizing the top soil layer (leaf/needle/grass litter) or animal droppings (Hatakka 1994, Hatakka and Hammel 2010). All these fungi have two types of extracellular biocatalytic systems

[1] The ending 'mycetes' is indicative for a class of fungi while 'mycota' stands for a phylum (division). Nevertheless, the terms 'basidiomycetes' and 'ascomycetes' have been frequently used (and are also used herein) in a more general way actually pertaining the respective fungal phyla.

available, which can attack all components of the lignocellulosic complex (although to different extent). The hydrolytic system consists of diverse hydrolases (glycosidases, esterases) and is responsible for polysaccharide breakdown into sugars; the oxidative system attacks crystalline cellulose (by lytic polysaccharide monooxygenases or biological FENTON chemistry) and helps to overcome the lignin barrier by radical-mediated reactions initiated by peroxidases and/or laccases (Hatakka and Hammel 2010, Hatakka 1994).

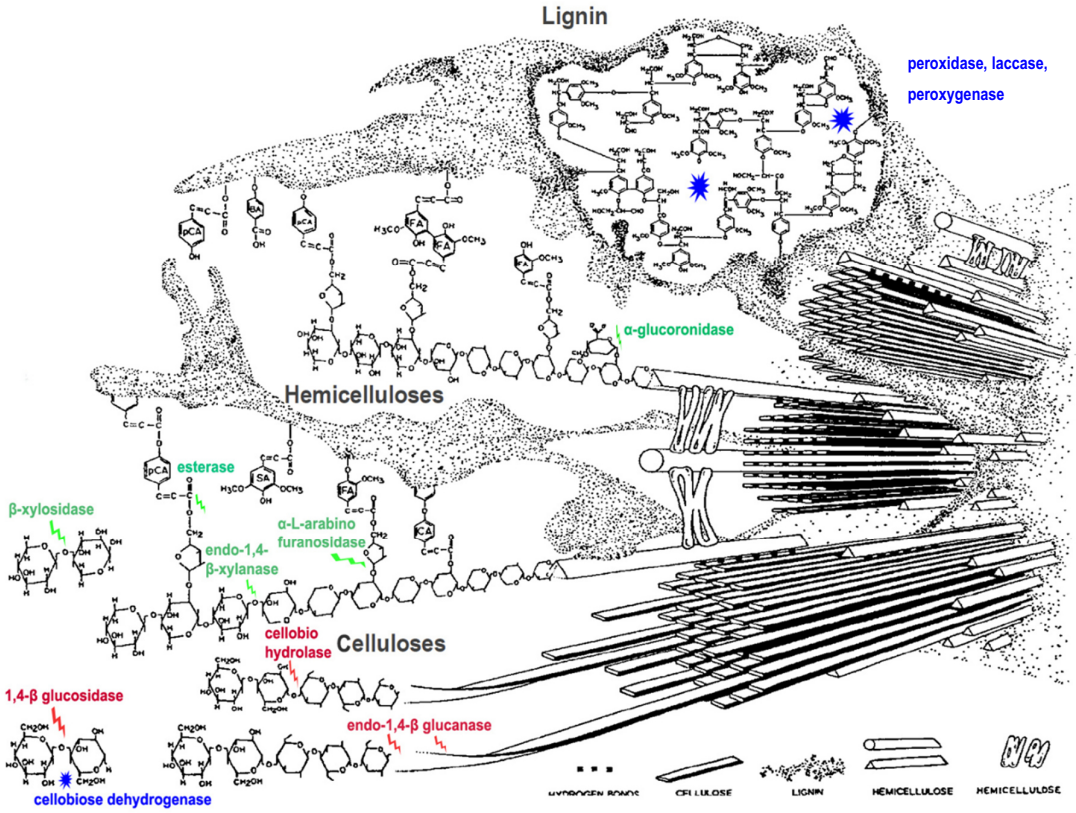

Fig. 1.2: Arrangement of polysaccharides and lignin in the plant cell-wall. Structural models of lignin, hemicelluloses and cellulose are given along with enzymes that attack them. Blue – oxidoreductases (including ligninolytic enzymes), green and red – hydrolases (hemicellulolytic and cellulolytic enzymes, respectively). The schematic model represents the secondary wall of a non-woody plant characterized by the presence of lignin units, and cinnamic [*p*-coumaric acid (*p*CA) and ferulic acid (FA)] acid bridges between lignin and polysaccharides (Bidlack et al. 1992).

1.1.2.1 White-rot fungi (WRF) and litter-decomposing fungi (LDF)

White-rot fungi (WRF) are Basidiomycota (mainly mushroom-forming Agaricomycetes) capable of efficiently degrading woody lignocelluloses (compact wood) including lignin, and most scientific work in this field has focused on representatives of these fungi over the last decades (Kirk and Farrell 1987, Hatakka 1994, Hofrichter et al. 2001, Martínez et al. 2006, Kersten and Cullen 2007, Hatakka and Hammel 2010, Krah et al. 2018). **Litter-decomposing fungi (LDF)** are actually WRF that colonize the uppermost soil layer (leaf litter) where they degrade small lignocellulosic materials such as leaves, needles, twigs and bark. Wood-dwelling WRF can be found within several orders, e.g. Polyporales, Hymenochaetales, Auriculariales and some among the Agaricales (Worrall et al. 1997), while LDF are exclusively represented by members of the Agaricales (Hintikka 1970, Osono 2007, Steffen et al. 2002). White-rot of wood is characterized by the degradation of lignin and hemicelluloses leaving behind whitish rotten fragments enriched in cellulose. LDF degrade lignin, polyphenols and humic substances along with remaining polysaccharides in forest or lawn litter causing the so-called white-rot of humus (Fig. 1.3 & 1.4; Hintikka 1970, Osono 2007, Voříšková and Baldrian, 2013, Barrasa et al. 2014).

Fig. 1.3: Characteristic visual appearance of wood decayed by a white-rot fungus (left) and fruiting bodies of *Fomes fomentarius* on a beech log as an example of a typical white-rot fungus (Photo: R. Ullrich 2008).

LDF physiologically resemble WRF (though they are somewhat 'weaker' in degrading woody lignocelluloses), produce similar sets of enzymes but have a higher competitive potential towards other microorganisms (e.g. soil bacteria). WRF are particularly known to degrade recalcitrant non-phenolic lignin structures (chap. 1.1.1). The degradation process proceeds either in an unselective manner, in the course of which cellulose, hemicellulose and lignin components are degraded simultaneously or it is a selective

process that results in the preferential decay of lignin (and hemicelluloses) and a relative accumulation of cellulose. Furthermore, both simultaneous and selective wood decay can take place at the same time on/in a log in dependence of the region and the properties of wood (Blanchette et al. 1990). For decades, *Phanerochaete chrysosporium* had been the model fungus of white-rot and lignin degradation (Kirk 1984), but meanwhile numerous other and ecologically more relevant fungi have been made available (e.g. *Ceriporiopsis subvermispora*, *Phlebia radiata*, *Phlebia* sp. *Nf*b19, *Pleurotus eryngii*; Lundell 1993, Martínez et al. 1994, Hatakka 2001, Hildén et al. 2008). Biodegradation of lignin ('ligninolysis') by WRF is a strict aerobic oxidative process based on the secretion of high-redox potential heme peroxidases belonging to the protein subfamily of 'class II peroxidases' (class II POD), i.e. lignin peroxidase (LiP), manganese peroxidase (MnP) and versatile peroxidase (VP), the latter being a functional hybrid of the first two enzymes (Hofrichter et al. 2010). Various WRF and LDF produce different combinations of these enzymes, but not all of these major enzymes are necessarily required to degrade lignin, leading to the assumption that there is more than one ecologically successful strategy for the degradation of lignin (Hatakka 1994, 2001).

Fig. 1.4: Fruiting bodies of agaric litter-decomposing fungi (*Mycena* sp.) growing in the uppermost soil layer in Kakamega forest, Kenya (Photo: Kimani 2016).

Copper-containing laccase (Lac) is another enzyme involved in the oxidation and modification of lignin; it attacks phenolic lignin moieties resulting in the formation of phenoxy radicals and in turn in coupling but also fission reactions (Kuhad et al. 1997, Leonowicz et al. 1999). Overall ligninolysis seems to be an unspecific process regarding the enzymatic reactions involved and finally leads to unstable lignin radicals including

free diffusible species that destabilize the polymer in a way that it partially disintegrates. As the result, water-soluble, aromatic lignin fragments emerge that can be further oxidized to CO_2 (lignin mineralization; Hatakka and Uusi-Rauva 1983, Dorado et al. 1999, Hatakka and Hammel 2010). Basically, lignin degradation is a co-metabolic process requiring an additional carbon source (usually sugars deriving from hemicelluloses or cellulose) and lignin as such (i.e. as 'sole' carbon source) cannot serve as growth substrate for fungi. Therefore, auxiliary enzymes like sugar-providing polysaccharide hydrolases are indirectly involved in lignin degradation by WRF along with oxidases supplying the ligninolytic peroxidases with hydrogen peroxide (Hatakka and Hammel 2010).

1.1.2.2 Brown-rot fungi (BRF)

Brown-rot fungi (BRF) represent only 7 to 10% of the wood-rot basidiomycetes. They are more frequently found on gymnosperm wood (conifers) and degrade the lignocellulosic complex into brown cubical wood fragments with characteristic cracks (cubical fracture) consisting mainly of lignin (Fig. 1.5; Ryvarden 1991, Hatakka and Hammel, 2010). Taxonomically, BRF and WRF species can be present in the same basidiomycetous order (Polyporales[2]) but – according to modern phylogeny – never in the same family or even in the same genus (Krah et al. 2018). Eco-physiologically, BRF substantially differ from WRF, since they extensively degrade cellulose and hemicelluloses in compact wood but modify lignin only to some extent (Eriksson et al. 1990, Hatakka 1994, Skrede et al. 2011). Intensively studied BRF are *Coniophora puteana*, *Gloeophyllum trabeum*, *Laetiporus sulphureus*, *Postia placenta* and *Serpula lacrymans*, the latter being a notorious, highly destructive agent of houses (Martínez et al. 2005, Hatakka 1994). To attack the recalcitrant crystalline cellulose, BRF use an alternative biochemical strategy comprising hydrolytic enzymes (e.g. endocellulases) and/or oxidative LPMO in combination with a unique non-enzymatic system based on hydroxyl radicals (•OH) formed via the FENTON reaction (Kirk and Farrell 1987, Jensen et al. 2001, Arantes et al. 2012).

[2] In addition to Polyporales, BRF are found in the orders Gloeophyllales and Boletales.

Fig. 1.5: Characteristic visual appearance of wood (*Malus* sp.) decayed by a brown-rot fungus (BRF, left; Photo: R. Ullrich 2009) and basidiocarp of *Fomitopsis pinicola* as an example of a typical BRF (right; Photo: R. Ullrich 2013).

The biological FENTON reaction of BRF depends on the presence of extracellular iron (Fe^{2+}/Fe^{3+}), oxalic acid, hydrogen peroxide (H_2O_2), benzoquinones and membrane-bound quinone reductases (Jensen et al. 2001, Wei et al. 2010, Gómez-Toribio et al. 2009). The *in-situ* formed hydroxyl radicals are highly reactive and cause the breakdown of crystalline cellulose and the partial oxidation (demethoxylation and re-polymerization) of lignin. Similar reactions were proposed to be involved in other fungal rot-types (white-rot, soft-rot) as well, although their actual contribution to the overall rotting process remains vague (Gómez-Toribio et al. 2009, Arantes et al. 2012).

1.1.2.3 Soft-rot fungi (SRF)

Soft-rot is generally caused by ascomycetous fungi (in particular by members of the order Xylariales) and their asexual states (anamorphs) formerly classified as 'deuteromycetes'. They are common on deadwood of broad-leaved trees and predominantly contribute to cellulose degradation but to a lesser extent than basidiomycetes do (Blanchette 1995, Boddy 2001). SRF tolerate wide ranges of temperature, humidity and pH and may grow in wood that has permanent contact to water (Daniel and Nilsson 1998). They attack various hardwood types (but scarcely softwood) and create unique cavities[3] in the wood cell walls (Shary et al. 2007). In addition to cavities, most SRF produce an erosion of the cell wall from the lumen inward toward the middle lamella. Soft-rot decay is divided into

[3] In contrast, WRF and BRF more or less evenly degrade the wood in vicinity of their hyphae without cavity formation.

two types designated as type 1 and type 2, which can be only reliably differentiated by microscopic inspection (Corbett 1965). Type 1 is characterized by the invasion of the lumen of wood cells and longitudinally oriented cavities formed within the secondary cell wall and type 2 involves massive erosion of the secondary cell wall also outward from the cell lumen (Daniel and Nilsson 1998, Daniel 2003, Kutz 2005). The latter rot-type is a diffuse form of cell wall degradation where cellulose and hemicelluloses are extensively degraded, while lignin is just modified to a limited extent.

Fig. 1.6: Ascocarps of *Xylaria longipes* as the example of a typical soft-rot fungus (SRF) on a deadwood log, probably of *Acer pseudoplatanus* (Photo: R. Ullrich 2013).

In advanced stages of soft-rot decay, the entire secondary wall can be completely degraded but the middle lamella will not be affected (Blanchette et al. 2004, Blanchette et al. 1990, Findlay 1984; Nilsson et al. 1989). Outwardly, an intensive soft-rot of type 2 may resemble white-rot. Fungi causing such intensive soft-rot belong to the family Xylariaceae (Fig. 1.6; e.g. to the genera *Daldinia, Hypoxylon, Kretzschmaria* and *Xylaria*; Anagnost 1998, Pointing et al. 2003, Liers et al. 2006, Schwarze 2007, Büttner et al. 2018). The lignin-degrading potential of these fungi was demonstrated with radiolabeled synthetic lignin (dehydrogenation polymer, ^{14}C-DHP). Not least, due to the absence of an efficient enzyme machinery based on class II PODs in SRF, synthetic lignin was just mineralized to moderate extent (up to ~10% $^{14}CO_2$; Liers et al. 2006). In contrast, LDF and WRF were shown to form between 20% and 75% $^{14}CO_2$ from synthetic lignin under comparable conditions, as demonstrated e.g. for *Nematoloma frowardii* (syn. *Phlebia* sp. *Nf*b19), *Pleurotus ostreatus, Agrocybe praecox, Collybia dryophila* and *Stropharia rugosoannulata* (Hofrichter et al. 1999, Steffen et al. 2000, Steffen 2003).

So far, it has been shown that members of the Xylariaceae merely secrete Lac and various polysaccharide hydrolases (e.g. xylanases, endoglucanase as well as an exceptional bifunctional GH78 enzyme combining feruloyl esterase and rhamnosidase activities; Liers et al. 2006; Nghi et al. 2012). As 'enzyme cocktail', these biocatalysts seem to be capable of synergistically attacking the lignocellulosic complex causing the typical soft-rot (type 2) appearance of wood. Furthermore, the *in-vitro* oxidation and fission of 'adlerol' (a non-phenolic lignin model dimer that contains a characteristic β-*O*-4 ether linkage) was demonstrated for purified *Xylaria polymorpha* laccase (*Xpo*Lac) in the presence of a synthetic redox mediator (Liers et al. 2007). Notably, the release of water-soluble aromatic fragments including ferulic acid was achieved by the treatment of rape straw with an 'enzyme cocktail' comprising *Xpo*Lac and bifunctional GH78 from the same fungus (Nghi 2012). Despite these findings, several aspects of wood degradation by SRF are still open, particularly the question, whether they can secrete any type of extracellular peroxidase.

1.1.2.4 Further groups of saprotrophic fungi inhabiting wood and soil

The classification of WRF and BRF in terms of their degradation mechanism has been used extensively (Liese, 1970, Erikkson et al. 1990, Hatakka and Hammel 2010). However, the advent of a large number of newly sequenced fungal genomes has demonstrated that this 'simple' classification is not applicable to all wood-degrading basidiomycetes (Riley et al. 2014, Floudas et al. 2015). A few examples of special types of wood-inhabiting and lignocellulose-degrading fungi have recently been classified besides the classic WRF-BRF scheme; they cause a so-called 'unresolved' type of wood-rot (**'uncertain' wood-rot fungi = URF**; Riley et al. 2014; Reina et al. 2019). Thus, fungi like *Botryobasidium botryosum*, *Jaapia argillacea* or *Schizophyllum commune* are lacking ligninolytic class II PODs (i.e. LiP, MnP, VP) but nonetheless show similarities to WRF regarding other carbohydrate- and lignin-active enzymes predicted in their genomes. Moreover, it has been shown that these URF are able to degrade all polymeric components of the plant cell wall, actually a characteristic of WRF (Riley et al., 2014). This suggests that – as in the case of SRF – certain aspects of wood and particular lignin degradation by URF are still unclear.

Coprophilous fungi, syn. **dung-dwelling fungi (DDF**) represent a large ecological group of saprotrophic Ascomycota, Basidiomycota and other fungal taxa colonizing and

decomposing the droppings (dung, manure, faeces) of diverse animals thereby fulfilling an important ecosystem function (Fig. 1.7; Mueller et al. 2004, Sarrocco, 2016). In particular, the dung of herbivores is a good fungal substrate, since it contains important nutrients and minerals (ammonium, phosphate, sulfate, etc.), metals and trace elements, vitamins as well as undigested lignocellulose that – along with bacterial biomass – can be utilized as carbon source. On the other hand, the pH in dung is rather alkaline (pH 8.0-9.0) and the competitive pressure by bacteria is exceptional high, which requires special adaptations on the part of DDF (in other fungal habitats such as leaf/needle litter or wood acidic pH conditions prevail, i.e. pH 3.0-6.0). Due to the high nitrogen-content, microbial competition and variable composition of dung, DDF often occur just during specific successional stages. Depending on their taxonomic affiliation, they can secrete a potpourri of extracellular enzymes including many polysaccharide-digesting hydrolases (Sarrocco, 2016, Couturier et al., 2016), laccases and MnPs. The latter enzymes were determined both *in situ* in compost cultures and *in silico* in the genome of the commercial white button mushroom (*Agaricus bisporus*) that prefers aged dung-compost mixtures as growth substrate (Lankinen 2004, Morin et al. 2012).

Fig. 1.7: An example of a coprophilous agaric mushroom (Basidiomycota) growing on elephant dung in the Aberdare forest, Kenya (Photo: Kimani 2016).

The fungal succession on dung typically starts with saprotrophic Mucoromycotina ('zygomycetes', e.g. *Pilobolus, Circinella* or *Cunnihamella*), which are responsible for the degradation of sugars and pectins. They quickly disappear when the nutrients are depleted and then colonization by ascomycetous fungi sets in. They are mainly involved

in the degradation of cellulose and hemicelluloses and are replaced by basidiomycetous agarics[4] like *Coprinus, Coprinopsis* and *Coprinellus* (e.g. *Coprinopsis verticillata*, Anh et al. 2007) or *Collybia*, *Marasmius* and *Mycena* (Hofrichter et al. 2009). These fungi typically degrade residual cellulose by removing the 'last lignin barrier'; as the result, a humified dung develops that is the perfect growth substrates for plants (Ludwig, 2001, Sarrocco, 2016, Couturier et al., 2016).

1.1.3 Enzymatic degradation of the lignocellulosic complex

A large and diverse set of hydrolases and oxidoreductases are required for the complete conversion of the three main components of the plant cell wall into monomeric, dimeric and oligomeric fragments, thus providing fungi with suitable carbon and energy sources (Hatakka and Hammel 2010, Lundell et al. 2010). These enzymes may be classified either according to the biochemical reaction that they catalyze according to the IUBMB Enzyme Nomenclature List (EC numbers; www.enzyme-database.org/), or they can be grouped on the basis of their phylogeny (i.e. amino acid sequences) within the database of carbohydrate-active enzymes, the CAZy database (www.cazy.org). The latter comprises glycoside hydrolases (GH), glycosyl transferases (GT), polysaccharide lyases (PL), carbohydrate esterases (CE) and auxiliary activities (AA). In addition, carbohydrate-binding modules (CBM) are classified as associated units within the CAZy database (Lombard et al., 2014). Most of the lignin-modifying enzymes (LME) are classified in the AA group, among them the high-redox potential class II POD (i.e. LiP, VP and MnP) as well as Lac and LPMO but also oxidases (e.g. sugar oxidases, aryl alcohol oxidase) responsible for the generation of H_2O_2, the co-substrate of peroxidases.

1.1.3.1 Degradation of cellulose

Cellulose consists of crystalline and amorphous parts and is therefore difficult to degrade by microorganism. Mainly wood-decay fungi[5] (WRF, BRF, SRF) and LDF are able to accomplish efficient cellulose break-down into sugars by using cellulases, which hydrolytically cleave the β-1,4-glycosidic bonds. These enzymes are organized within

[4] An agaric is a type of basidiomycetous fruiting body (mushroom) characterized by the presence of a cap (pileus) with gills on its underside and a clearly differentiated stalk (stipe). The prototype of this fruiting body is represented by *Agaricus bisporus*.

[5] It should be noted that there are also efficient bacterial degraders of cellulose such as *Cellulomonas* spp., anaerobic, cellulosome-possessing *Clostridium* spp. and celluloytic myxobacteria, but they do not substantially depolymerize lignin and hence preferentially dwell soil environments (Mathews et al. 2015.).

specific complexes that contain catalytic and non-catalytic domains, with the following three major components: β-1,4-endoglucanase (EG, EC 3.2.1.4), β-1,4-exoglucanase/ cellobiohydrolase (CBH, EC 3.2.1.91) and β-glucosidase (BGL, EC 3.2.1.21) (van den Brink and de Vries 2011). EG acts randomly at various sites within the cellulose fiber resulting in opened up sites that then can be further degraded by CBH (Lynd et al. 1991, Sánchez 2009). The latter enzyme is highly abundant and makes up between 40% and 70% of the fungal cellulase complex. These enzymes are also capable of degrading recalcitrant crystalline cellulose (though rather slowly) and they remove dimers or monomers at the cellulose chain ends. The synergistic action of EG and CBH may result in a continuous release of cellobiose molecules. Hydrolysis of terminal non-reducing sugar residues in respective glucosides is subsequently catalyzed by β-glucosidase releasing two β-D-glucose molecules (Rowell 1992, Sánchez 2009, Pérez et al. 2002).

Another possibility for fungi to degrade cellulose and its oligomers is accomplished by an oxidative mechanisms that involves the synergistic action of cellobiose dehydrogenase (CDH, EC 1.1.99.18) and LPMO (EC 1.14.99.54; formerly known as GH61). The former enzyme oxidizes cellobiose and related oligosaccharides to the corresponding lactones (Ludwig et al. 2010). CDH transfers the gained electrons in turn to LPMO, which catalyzes the copper-dependent hydroxylation of crystalline cellulose, leading to the oxidative cleavage of glycosidic β-1,4-bonds and formation of sugar derivatives either oxidized at C1 or C4 (Langston et al. 2011, Eijsink et al. 2019). Furthermore, CDH can participate in the production of reactive radicals through FENTON chemistry (chap. 1.1.2.2) suggesting its involvement in lignin modification as well (Henriksson et al. 2000).

1.1.3.2 Degradation of hemicelluloses

Hemicelluloses and pectin are structurally heterogenic polymers and thus their efficient degradation requires a variety of hydrolytic enzyme activities. To achieve complete break-down, all substitutions at the polymeric backbones have to be released. This requires different enzymes categorized into at least twelve GH families, which catalyze the hydrolysis of different types of glycosidic linkages within cell-wall polysaccharides (van den Brink and de Vries 2011). Due to the similar structure of the xyloglucan backbone and the cellulose chain (both are β-1-4-linked), hydrolysis of both occurs in a similar manner and by similar sets of enzymes acting at external and internal parts of the

chains as well as on respective sugar dimers. Endo-1,4-β-xylanase (EC 3.2.1.8) randomly cleaves the glycosidic bonds in the xylan backbone, which leads in a reduced degree of polymerization of the substrate. That way, initially oligomers and later mono-, di- and trisaccharides of β-D-xylopyranose appear. Subsequently, β-xylosidase liberates D-xylose from the non-reducing end of small xylo-oligosaccharides and xylobiose (Polizeli et al. 2005). Accessory enzymes such as α-L-arabinofuranosidases, α-L-rhamnosidases, α-galactosidase as well as acetyl xylan and feruloyl esterases are responsible for the further release of diverse monomers and short oligomers from the side chains of the xylan backbone (de Vries and Visser 2001).

1.1.3.3 Degradation of lignin

Lignin has a complex and recalcitrant overall structure, which does not contain hydrolysable linkages and thus requires a versatile set of secretory oxidative enzymes, in first place ligninolytic class II heme peroxidases (class II POD), and low-molecular effectors and redox-mediators (Kirk and Cullen, 1998, Hofrichter 2002, Hatakka and Hammel, 2010, Brink et al. 2019). The most efficient peroxidases are MnP, LiP and VP, which use H_2O_2 as cosubstrate within their reaction cycle (Martínez et al. 2009). MnP (EC 1.11.1.13) oxidizes Mn^{2+} into Mn^{3+}, which is – in its chelated form – highly diffusible and capable of oxidizing diverse target structures (up to 1.1 V) such as phenolics, carboxylic groups, thiols, *N*-heterocycles and the double bonds in unsaturated fatty acids and lipids (Glenn et al. 1986, Wariishi et al. 1992, Hofrichter 2002, Hofrichter et al. 2010). The primary products are radicals that tend to undergo subsequent oxidation and depolymerization reactions. Not least, due to its high abundance among (all) WRF and LDF, MnP seems to be the key enzyme of fungal ligninolysis (Hofrichter et al. 2010). LiP (EC 1.11.1.14) preferably catalyzes the one-electron oxidation of non-phenolic lignin structures with high redox potential (up to 1.5 V) including respective lignin model compounds such as veratryl alcohol and adlerol (non-phenolic β-*O*-4 dimer). The oxidation of the latter leads to C_α-C_β-cleavage within the dimeric molecule giving rise to veratraldehyde, guaiacol and ring fission products (Hammel et al. 1993, Lundell et al. 1993, Hofrichter et al. 2010). VP (EC 1.11.1.16) combines catalytic properties of both MnP and LiP, since it contains an exposed, catalytically active tryptophan (as LiP does) and also the three conserved acidic amino acids of MnP (two glutamates and one aspartate) near the active site where Mn^{2+} binds (Ruiz-Dueñas et al., 2008; Hofrichter et al. 2010).

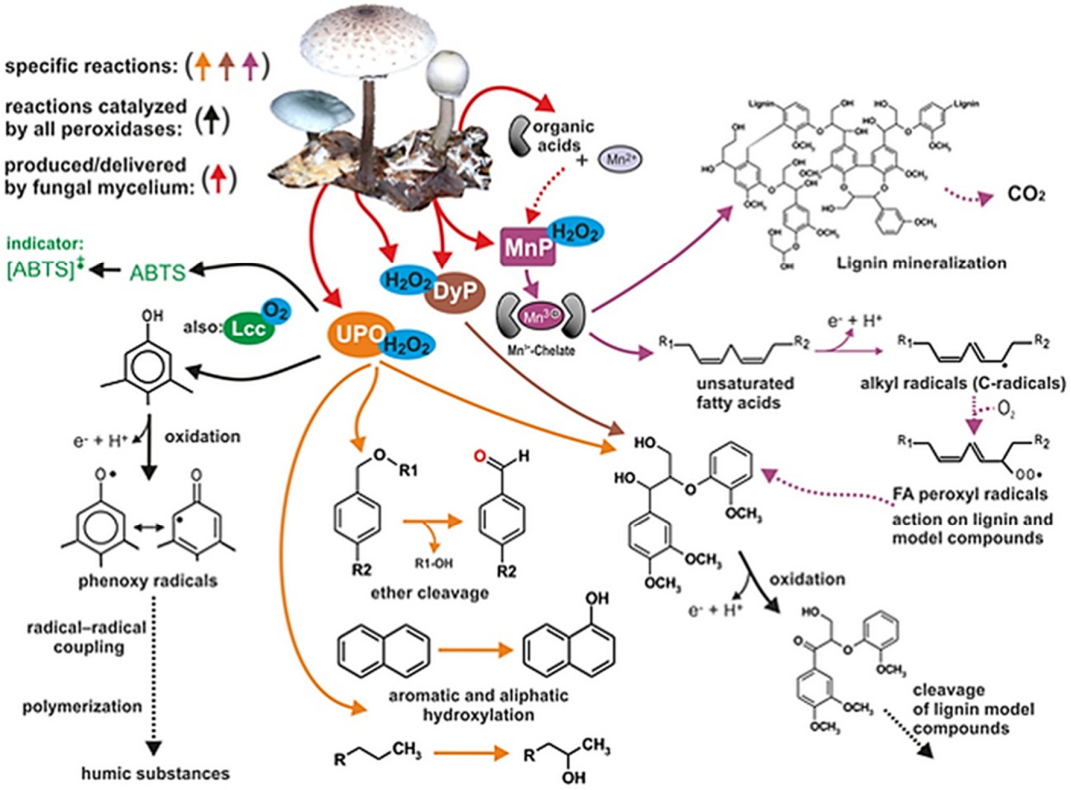

Fig. 1.8: Schematic summary of enzymatic lignin degradation and modification (Kellner et al. 2014).

Moreover, a certain role in lignin modification can be also assumed for unspecific peroxygenase (UPO, EC 1.11.2.1) and dye-decolorizing peroxidase (DyP, EC 1.11.1.19). Both heme peroxidases belonging to separate (super)families of heme proteins, have high-redox potentials (1.3 and 1.5 V, respectively) and thus can oxidize non-phenolic lignin model compounds (Kinne et al. 2009, Liers et al. 2013, Hofrichter et al. 2010). They have been frequently found in the genomes of wood-rot fungi (Basidiomycota, Ascomycota) and even beyond that in basal fungal groups (UPO) and bacteria (DyP). Moreover, they were shown to be widely expressed in leaf and needle litter across a range of forest ecosystems in Europe and the US dominated by *Fagus*, *Picea*, *Acer*, *Quercus* and *Populus* (Kellner et al. 2014). However, the actual role of these enzymes in lignin degradation (if any) as well as their 'ulterior' natural substrates remain nebulous and their identification will be a challenging task of future investigations (Fig. 1.8; Hofrichter et al. 2015, 2019).

Apart from heme peroxidases, laccases (Lac, EC 1.10.3.2), a group of multicopper oxidases, also participate in lignin modification[6] (Bourbonnais and Paice, 1990, Kellner et al., 2014) (Fig. 1.8). These enzymes can be divided in Lac with high (up to 0.8 V) and low (<0.6 V) redox potentials and only the former group, mainly secreted by WRF/LDF and a few SRF, is capable of attacking the phenolic subunits present in lignin (Bourbonnais and Paice 1990, Munk et al. 2015). Redox-mediators such as hydroxyanthranilic acid, hydroxybenzotriazole, methyl syringate or *p*-hydroxycinnamic acids can help to overcome the 'redox-potential limit' of Lac, which was demonstrated in several *in vitro* studies (Eggert et al. 1996, Liers et al. 2006, Camarero et al. 2008). However, it is questionable whether similar compounds play a comparable role in natural lignin breakdown (Li et al. 2001, Munk et al. 2015).

Since the above described peroxidases need H_2O_2 as cosubstrate to complete their reaction cycles, its generation plays an important role in lignocellulose modification and ligninolysis (Kersten and Cullen 2007). Abundant peroxide-supplying enzymes, meanwhile found in several secretomes ('exo-proteomes') of wood-rot basidiomycetes and ascomycetes, are aryl alcohol oxidase (AAO, EC 1.1.3.7), alcohol oxidase (EC 1.1.3.13), glyoxal oxidase (GLOX, EC 1.2.3.15), glucose oxidase (GOD, EC 1.1.3.4) and pyranose oxidase (EC 1.1.3.10). These oxidases convert their substrates into corresponding oxidized products (i.e. aldehydes, carboxylic acids and lactones) while reducing O_2 to H_2O_2 (Hernandez-Ortega et al. 2012). Among them, copper-radical oxidases like GLOX or galactose oxidases (GAO, EC 1.1.3.9) exhibit broad substrate spectra that include various aromatic and aliphatic aldehydes emerging during lignocellulose decomposition (Kersten and Kirk 1987, Guillén et al., 1990, Whittaker et al. 1996; Kersten and Cullen 2007, 2014).

1.2 Heme peroxidases

Peroxidases are grouped under EC 1.11.x and can be divided into heme peroxidases containing an iron protoporphyrin IX as prosthetic group in the active site and non-heme peroxidases bearing instead metals (e.g. vanadium haloperoxidase), redox-active cysteine (Cys-SH, e.g. peroxiredoxin) or selenocysteine (Cys-SeH, e.g. glutathione peroxidase) or other prosthetic groups (e.g. thioredoxin in prostaglandin synthase). They are found in all

[6] More precisely, laccases should be rather designated as 'lignin-modifying' than 'lignin-degrading' or 'ligninolytic' enzymes, since coupling and re-polymerizing reactions prevail over bond scissions during laccase action on lignin (Lundell et al. 2010).

domains of life and utilize H_2O_2 or organic hydroperoxides as electron acceptors in the oxidation of various substrates (Welinder et al. 1992, Dunford 1999, Hofrichter et al. 2010, Zámocký and Obinger 2010). For a long time, heme peroxidases had just been classified into two large protein superfamilies: the peroxidase-cycloxygenases (formerly mammalian or animal peroxidases, e.g. thyroid peroxidase, lactoperoxidase) and the peroxidase-catalases (formerly non-animal peroxidases or plant/fungal peroxidases) (Welinder et al. 1992). Later, the small protein family of bacterial di-heme cytochrome c peroxidases was added (Fulop et al. 1995).

The catalase-peroxidase superfamily comprises three main families designated as 'classes': class I – intracellular and/or bacterial catalases and peroxidases, class II – secreted fungal peroxidases including MnP, LiP and VP, and class III – secreted plant peroxidases such as horseradish peroxidase (Welinder et al. 1992, Zámocky et al. 2009, Lundell et al. 2010, Hofrichter et al. 2010). Because of protein sequences, molecular architecture and mechanistic properties noticeably diverging from the above mentioned heme peroxidases, two new (super)families[7] of microbial heme peroxidases were supplemented about ten years ago: the heme-thiolate peroxidases (also designated as 'haloperoxidases') comprising *Caldariomyces fumago* chloroperoxidase (*Cfu*CPO) and thousands of unspecific peroxygenases (UPO) from all fungal phyla as well as the DyP protein family[8] from fungi and bacteria (Conesa et al. 2002, Sugano et al. 2009, Pecyna et al. 2009, Hofrichter et al. 2010) (Fig. 1.9).

[7] It is still under discussion whether heme-thiolate peroxidases and peroxygenases represent a separate protein family or superfamily (Hofrichter et al. 2015).

[8] DyP proteins belong with chlorite dismutases and EfeB to the so-called CDE superfamily (Goblirsch et al. 2011).

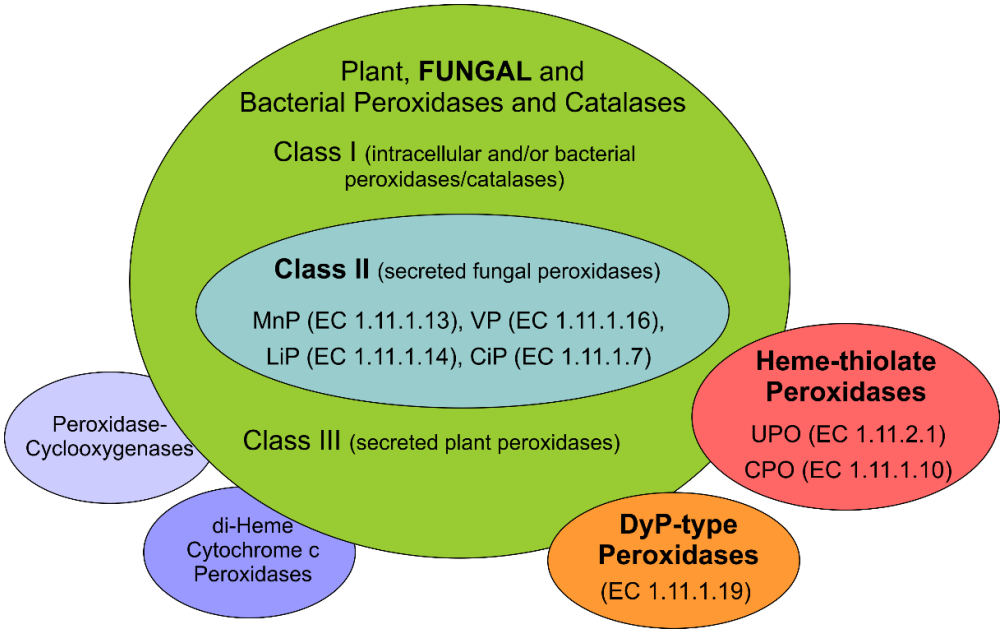

Fig. 1.9: Classification of the protein (super)families of heme peroxidases (modified according to Hofrichter et al. 2010, 2015, Reina 2016).

1.2.1 Fungal class II peroxidases

Class II peroxidases (class II POD) of the catalase-peroxidase superfamily contain fungal 'generic' peroxidases (GP) that oxidize phenolics (EC 1.11.1.7) and occur both in Basidiomycota and Ascomycota; the prototypical representative is a peroxidase of the ink-cap *Coprinopsis cinerea* that has a relatively low redox potential (around 0.9 V) compared to ligninolytic class II POD (Hofrichter et al. 2010, Liers et al. 2014). The latter comprises LiP, VP and different MnP types, which all exhibit exceptional broad substrate spectra (chap. 1.1.3.3). Their redox potentials vary between 1.1 and 1.5 V, which is 'high' enough to oxidize recalcitrant polymeric lignin structures (Dunford 1999, Hammel and Cullen 2008, Martinez et al. 2009, Hofrichter et al. 2010; chap. 1.1.1). The three enzymes have been intensively studied regarding ligninolysis over the last three decades (Hofrichter et al. 2010). Their heme environment (active site) is highly conserved and accomplishes the peroxidative reaction cycle. It is characterized by the presence of a proximal and a distal histidine (His) residue as well as of a distal arginine (Arg) (Dunford 1991). The proximal His serves as 5th heme ligand, the distal His as acid-base catalyst for H_2O_2-binding and Arg as charge stabilizer.

In the resting peroxidases, one water molecule is loosely bound to the ferric heme iron (Fe^{3+}) at the distal side [heme-Fe^{3+}---H_2O]. If the catalytic cycle starts, the distal side will

replace H_2O by H_2O_2 approaching through a narrow solvent access channel found in all three ligninolytic peroxidases (Piontek et al. 1993, Poulos 1993, Sundaramoorthy et al. 1994, Ruiz-Dueñaz et al. 1999). Oxidation of ferric iron (Fe^{3+}) and heme by the bound peroxide (compound 0) gives the key intermediate compound I (C-I) and water (Fig.1.10). C-I is a highly reactive oxo-ferryl heme-radical species [•heme-Fe^{4+}=O], which reacts – in the classic peroxidase cycle – with a first aromatic substrate molecule (AH, electron donor) via one-electron oxidation leading to compound II (C-II) and a substrate radical (A•). C-II [heme-Fe^{4+}=O] is still active enough to react with a second substrate molecule to form a second substrate radical and the resting enzyme. In the case of LiP (Fig. 1.10b), AH is typically a non-phenolic aromatic compound with high redox potential (whereas it is a phenol with lower redox-potential in the case of GP; cycle not shown). This cycle is just slightly modulated in the case of MnP, in which the electron donating substrate AH is replaced by Mn^{2+} that is oxidized to Mn^{3+}. VP can either use Mn^{2+}, phenols or non-phenolic aromatics, thus combining the catalytic properties of MnP, GP and LiP (Camarero et al. 1999, Hofrichter et al. 2010).

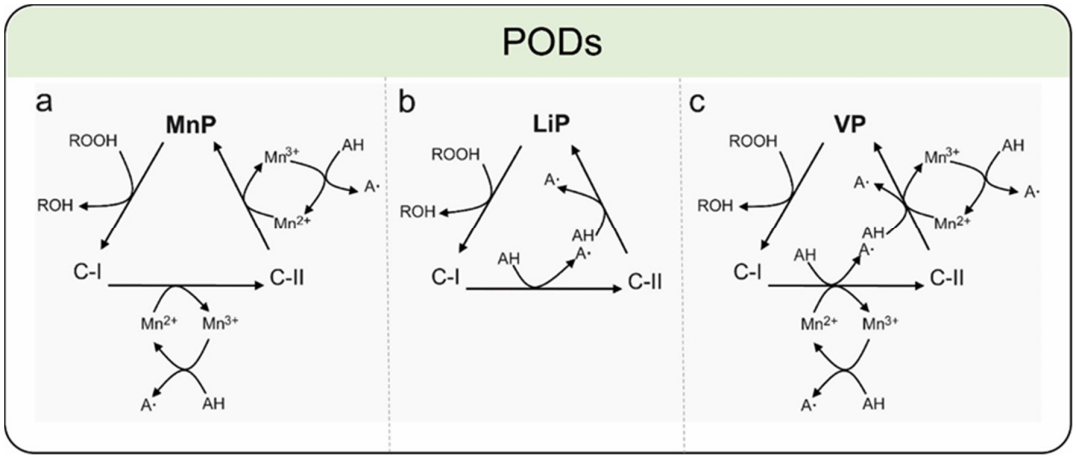

Fig. 1.10: Catalytic cycles of class II peroxidases: (a) manganese peroxidase (MnP), (b) lignin peroxidase (LiP) and (c) versatile peroxidase (VP) (according to Camarero et al. 1999). Abbreviations are explained in the text above.

1.2.2 Dye-decolorizing peroxidase (DyP)

Peroxidases of the DyP-type or shortly DyPs (EC 1.11.1.19) were first reported in 1995 for cultures of *Bjerkandera adusta* (then, described as a strain of *Geotrichum candidum*, Kim et al. 1995, Kim and Shoda 1999). Later, they were recognized as a new family of heme peroxidases, which is found both in fungi and in bacteria. Based on differences in the secondary and tertiary structure, DyPs could not be classified within any of the above mentioned plant, bacterial or fungal peroxidase groups (chap. 1.2). Sequence similarities to the ligninolytic peroxidases are very low (0.5-5%) and the typical heme-binding region, which is conserved among the whole catalase-peroxidase superfamily (chap. 1.2.1), does not contain the distal His (Sugano et al. 1999, 2009, Hofrichter et al. 2010). All DyPs contain a highly conserved GXXDG motif, and the distal His is replaced by an aspartate (Asp) as acid-base catalyst, which is assisted in proton acceptation and charge stabilization by an Arg (Strittmatter et al. 2013b).

After their original discovery, nine fungal DyPs [e.g. from *Mycetinis scorodonius* (*Msc*DyP), Scheibner et al. 2008; *Auricularia auricula-judae* (*Aau*DyP1, *Aau*DyP2), Liers et al. 2010; *Exidia glandulosa* (*Egl*DyP), *Mycena epipterygia* (*Mep*DyP), Liers et al. 2013] and fifteen bacterial enzymes (e.g. from *Thermobifidia fusca*, Rahmanpour et al. 2016; *Rhodococcus jostii*, Roberts et al. 2011) have been described. Among them are eight wild-type proteins and three recombinant enzymes [one from *A. auricula judae* (r*Aau*DyP) and two from *P. ostreatus* (r*Pos*DyP), Fernández-Fueyo et al. 2015]. Wild-type proteins (e.g. *Aau*DyP1 and 2) can be produced in complex plant-based media like diluted tomato juice or soybean meal suspension with or without the addition of 'elicitors' (e.g. guaiacol or β-carotene). Activity levels range from 100 to 8,000 U L^{-1} (corresponding to 0.25 to 20 mg L^{-1} DyP protein, Liers et al. 2010, 2013). Production of recombinant fungal DyPs, e.g. of r*Bad*DyP in *Aspergillus oryzae* or of r*Aau*DyP and r*Pos*DyP in *Escherichia coli*, will facilitate the performance of mutational studies, which will help to understand the relationships between DyP structure and function (Sugano et al. 2007, Linde et al. 2014, 2015; Fernández-Fueyo et al. 2015). So far, only three fungal DyPs (from *B. adusta*, *A. auricula-judae* and *P. ostreatus*) have been thoroughly characterized from the structural and mechanistic point of view (Sugano 2007, Yoshida et al. 2011, 2012; Strittmatter et al. 2013a,b; Linde et al. 2014, 2015; Fernández-Fueyo et al. 2015).

DyPs oxidize a range of substrates (Fig. 1.11), notably recalcitrant azo and anthraquinone dyes (e.g. Reactive Blue5, Kim and Shoda et al. 1999, Liers et al. 2013), phenols (e.g. methoxy- and nitrophenols, Liers et al. 2013, Yoshida et al. 2012), terpenoids (e.g. β–1-carotene, Scheibner et al. 2008), non-phenolic aromatics (e.g. trimethoxybenzene, veratryl alcohol; Liers et al. 2013) and even the lignin model dimer 'adlerol' (chap. 1.1.3.3 and 1.2.1; Liers et al. 2010, 2013; Linde et al. 2015). The oxidation of non-phenolic aromatics and adlerol works best at rather low pH (i.e. pH <3.0; Liers et al. 2010, 2013; Hofrichter et al., 2010). The specific activity of DyP towards adlerol at pH 3.0 was found to be one order of magnitude lower than that of LiP of *P. chrysosporium* but demonstrates its principal capability to oxidize lignin-relevant structures (Liers et al. 2013). Furthermore, a few bacterial DyPs (e.g. *Rjo*DyP; Roberts et al. 2011) and one recombinant fungal DyP (r*Pos*DyP4) could oxidize Mn^{2+} into Mn^{3+}, actually an exclusive catalytic feature of MnPs and VP (chap. 1.1.3.3 and 1.2.1; Hofrichter et al. 2010). Indeed, only for one recombinant bacterial DyP from *Rhodococcus jostii*, it has been shown that respective Mn^{2+} oxidation is involved in the partial breakdown of adlerol (k_{cat} = 7.4 × 10^{-3}; Roberts et al. 2011) – a convincing indication for a possible involvement of DyPs in lignin oxidation.

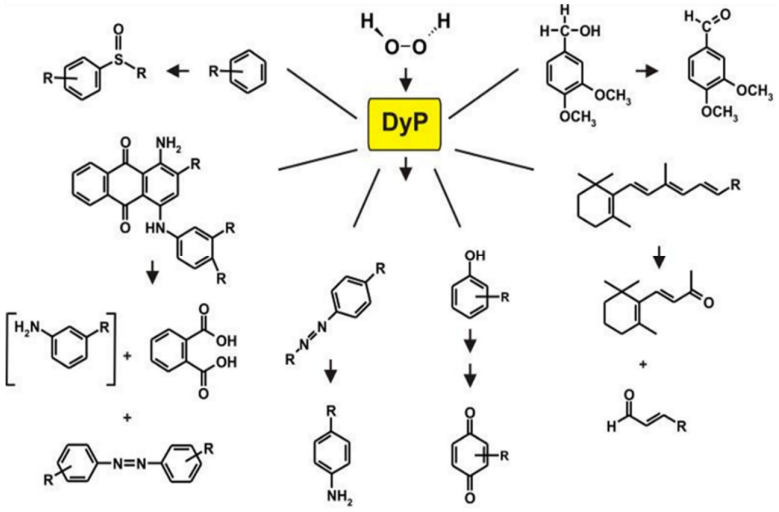

Fig. 1.11: Reactions catalyzed by fungal peroxidases of the DyP-type: sulfoxidation of aromatic sulfides, oxidation of anthraquinone (e.g. Reactive Blue 5) and azo dyes (e.g. Reactive Black 5), phenol oxidation (e.g. *p*-nitrophenol), oxidation of terpenoids (e.g. β-carotene) and the oxidation of non-phenolic aromatics (e.g. veratryl alcohol or β-*O*-4 lignin models) (Hofrichter et al. 2010).

The catalytic DyP cycle shows similarities to those of class II PODs, in which the enzyme reacts with H_2O_2 to form C-I (Fig. 1.10; Hofrichter et al. 2010). C-II formation, however, has not been demonstrated yet and this intermediate seems to be less stable than C-II of classic peroxidases. Nonetheless, it can be assumed that within the overall cycle, the ferryl heme iron (Fe^{4+}) may be reduced back to the resting enzyme (Fe^{3+}) by two one-electron oxidations involving one of the above mentioned substrates (Fig. 1.11).

The physicochemical properties of fungal DyPs resemble those of class II PODs. They are glycosylated proteins (up to 20% sugars) that show a Soret band at 405-407 nm, reflecting the proximal heme-imidazole (His) ligation. Molecular weights of DyPs range between 40 and 67 kDa with isoelectric points (pI) between 3.5 and 4.3 (Hofrichter et al. 2010). According to the InterPro database (http://www.ebi.ac.uk/interpro/), the DyP family currently comprises over 5,019 hypothetical proteins, of which 4,886 are from bacteria, 122 from eukaryotes and 11 from archaea (Mitchell et al., 2015), confirming their ubiquitous distribution but also the dominance of bacterial DyPs. Consequently, van Bloois and colleagues (2009) suggested to rename the DyP family into 'bacterial heme peroxidase' family, however, this was not accepted in the scientific community (Yoshida and Sugano 2015). According to similarities in the primary structure (i.e. sequence homology), DyPs can be phylogenetically categorized in four classes/subfamilies (Zámocký and Obinger 2010). Classes A, B and C correspond to DyPs of prokaryotic origin (e.g. class A – *Thermobifida fusca* DyP, class B – *Schewanella oneidenis* DyP, class C – *Anabaena* and *Amycolatopsis* DyP); fungal DyPs (basidio- and ascomyceteous ones) cluster only within class D that shows 7 to 16% homology to the three bacterial classes (Yoshida and Sugano 2015). To overcome the ambiguity of DyP categorization, especially regrading classes C and D, a new classification has been proposed by Yoshida and Sugano (2015). It distinguishes between primitive (P), intermediate (I) and advanced (V) clades depending on both primary and particularly tertiary structure homologies. The V clade now includes the former classes C and D, since both protein subfamilies appear to be more closely related according to structural homologies (Yoshida and Sugano, 2015).

Although the DyP-catalyzed oxidation of lignin model compounds (adlerol, methoxybenzenes; Liers et al. 2010, 2013) and the assistance of enzymatic straw hydrolysis by *Irpex lacteus* DyP (Salvachúa et al. 2013) have been proven, the natural function of these enzymes remains unclear (Linde et al. 2015). Interestingly, Sugawara et al. (2019) have recently reported that a DyP of *Bjerkandera adusta* is produced and

secreted in response to alizarin, an anti-fungal anthraquinone compound produced by the plant *Rubia tinctorum* (common madder). This indicates that DyPs could be part of the biochemical defence of fungi against toxic plant and microbial metabolites. The widespread occurrence of DyPs in forest soils (which has been shown at the transcript and activity levels) may support this assumption (Kellner et al., 2014).

Their broad substrate spectrum, high stability and interesting physico-chemical properties make DyPs promising candidates for industrial applications, e.g. in the bioremediation field, wastewater treatment (Faraco et al. 2009) or in the pulp and paper sector (Yu et al. 2014). The first commercially available and industrially used DyP is a recombinant protein from *Mycetinis scorodonius* (r*Msc*DyP) traded as MaxiBright™ for whey and milk bleaching by DSM N.V (The Netherlands) (Hofrichter et al., 2010, Scheibner et al., 2008, Colpa et al., 2014).

1.2.3 Unspecific peroxygenases (UPO)

Fungal peroxygenases represent a unique heme-containing, glycosylated enzyme type that efficiently transfers one peroxide-borne oxygen atom to a substrate molecule (Hofrichter et al. 2014a, b). The first fungal peroxygenase activity was reported in 1995 in the agaric mushroom *Agrocybe aegerita* that oxidized veratryl alcohol into veratrylaldehyde at neutral pH[9] (Upadhyay 1995). Later the enzyme was recognized as such and described as a heme-thiolate protein that acts on diverse substrates (e.g. aryl alcohols, halides, simple aromatics like toluene and naphthalene; Ullrich et al. 2004, 2005). The latter findings and the fact that the enzyme turned out to be capable of hydroxylating non-activated C-H bonds led to several renaming and finally to its designation as unspecific peroxygenase (UPO), which was also accepted in the enzyme nomenclature system under EC 1.11.2.1 (Hofrichter et al. 2014a, b).

UPOs belong to a separate superfamily of heme proteins, the so-called heme-thiolate peroxidases (HTP). Members of this superfamily including chloroperoxidase from the ascomycete *Caldariomyces fumago* (*Cfu*CPO; EC 1.11.1.10) contain a proximal cysteine (Cys) as 'trademark' acting as 5th heme ligand (chap. 1.2). This Cys is responsible for the characteristic spectroscopic properties of UPOs that exhibit their Soret band maxima between 417 and 420 nm, which shift in the reduced CO-adduct towards 450 nm as in the

[9] At the time, this reaction was still not recognized as a peroxygenase activity but as the result of an 'alkaline lignin peroxidase' activity (Peter, S. 2013).

case of cytochrome P450 monooxygenases (P450s). Indeed, the catalytic cycle of UPOs combines the pathways of heme peroxidases and P450s, in which C-I and C-II are the key intermediates that catalyze either a two-electron oxidation and oxygen incorporation into one substrate molecule similar to P450s (→ 'mono-peroxygenase route') or two one-electron oxidations resulting in the formation of two substrate radicals as it is known from class II PODs (→ 'peroxidase route') (Hofrichter et al. 2014a, b, 2015 Fig. 1.12).
Meanwhile several spectrophotometric assays are available to specifically measure UPO activities in fungal cultures. The routine assay uses the oxidation of veratryl alcohol to veratraldehyde at pH 7.0 (Ullrich et al. 2004). By using this assay, six wild-type UPOs have been identified over the last decade, five from basidiomycetes [*Agrocybe aegerita* (*Aae*UPO), *Coprinellus radians* (*Cra*UPO), *C. verticillata* (*Cve*UPO), *Marasmius rotula* (*Mro*UPO) and *Marasmius wettsteinii* (*Mwe*UPO); Ullrich et al. 2004, Anh 2008, Gröbe et al. 2011, Ullrich et al. 2018] and one from an ascomycete [*Chaetomium globosum* (*Cgl*UPO); Kiebist et al. 2017, Hofrichter et al. 2019]. In addition, the number of UPOs were increased by two recombinant enzymes from *A. aegerita* (r*Aae*UPO, including mutants such as PaDa-I) and from *Coprinopsis cinerea* (r*Cci*UPO). In both cases, moderate to good protein levels (5 to ~1,000 mg L^{-1}) were achieved in two yeasts and a mold (i.e. in *Saccharomyces cerevisiae* up to 8 mg L^{-1}, in *Pichia pastoris* 217 mg L^{-1} and over 1,000 mg L^{-1} in the industrial host *Aspergillus oryzae* at Novozymes A/S, Denmark) (Babot et al. 2013, Molina-Espeja et al. 2015, Mate et al. 2017).

The production of wild-type UPOs can be carried out in liquid cultures (agitated flasks or stirred-tank bioreactors). Growth media must contain complex plant-based substrates, which are rich in carbon and nitrogen, like soybean meal, peptone, yeast extract or alfalfa pellets. Enzyme secretion starts when the fungus switches from primary to secondary metabolism usually after one to two weeks of cultivation (Hofrichter et al. 2015). The highest yields of wild-type UPO can be obtained with species belonging to the genus *Marasmius*, the pinwheel mushrooms *M. rotula* and *M. wettsteinii* (2,000-40,000 U L^{-1} corresponding to 20-450 mg L^{-1}; Gröbe et al. 2011, R. Ullrich, personal communication 2019). After several steps of protein purification, various UPO isoenzymes and isoforms with different glycosylation patterns (10-40% sugars) can be obtained (Ullrich et al. 2009, Hofrichter et al. 2015). Wild-type UPOs exhibit molecular masses between 32 and 46 kDa and isoelectric points from 3.8 to 6.1 (Hofrichter and Ullrich 2014, Hofrichter et al. 2015).

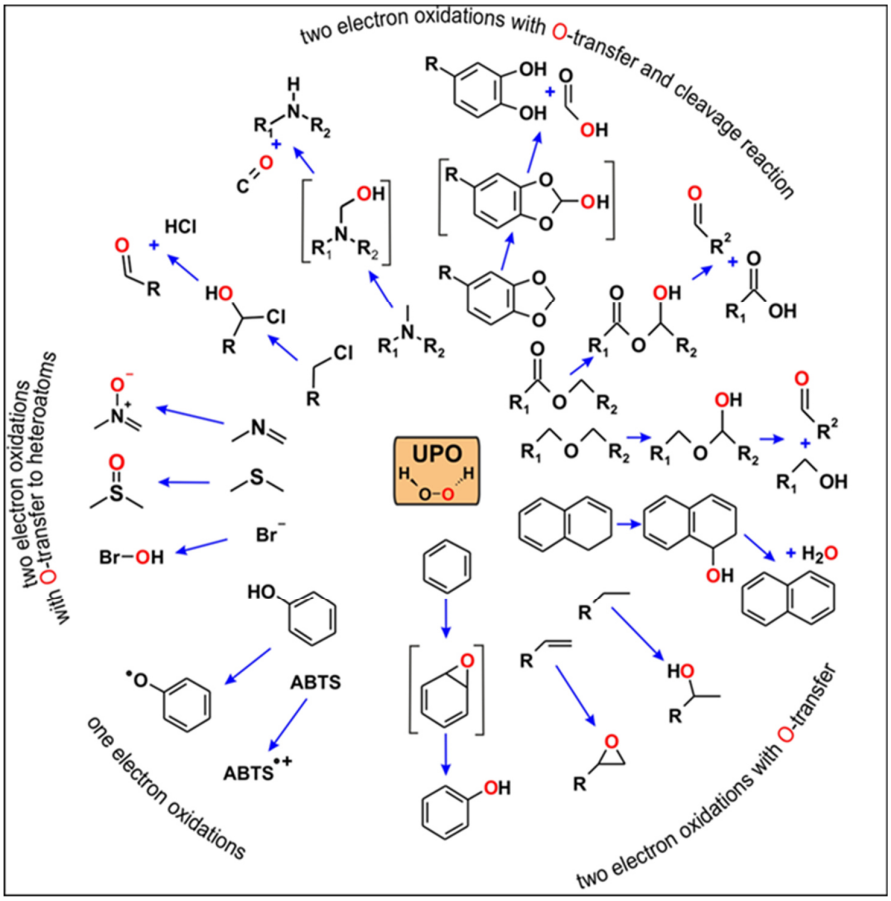

Fig. 1.12: Different oxidation and oxyfunctionalization reactions catalyzed by fungal UPOs: *(i)* two-electron oxidations with *O*-transfer (down right); *(ii)* two-electron oxidations accompanied with *O*-transfer and cleavage reactions (top right and left); *(iii)* two-electron oxidations with *O*-transfer to heteroatoms (middle left) and *(iv)* one-electron oxidations (down left) (Hofrichter et al. 2014a, b, 2015).

Meanwhile over 4,300 putative UPO sequences from over 500 fungal and pseudo-fungal ('oomycetous') species have been found in genetic databases (including JGI), which allows a detailed insight into the vast natural diversity of this enzyme group (Hofrichter et al. 2015, 2019). The phylogenetic tree in Fig. 1.13 includes roughly 2,100 publicly available sequences, most of which belong to 'higher" fungi' (Dikarya) with 1,250 ascomyceteous and 700 basidiomyceteous sequences as well as 150 sequences from basal fungal and pseudo-fungal taxa. Phylogenetic analysis of all available UPO sequences revealed that there are two large groups/clades/families of UPO proteins. They differ, among others, in size and have therefore been divided into 'short' and 'long' UPOs (group/clade/family I and II, respectively; Fig. 1.13) (Pecyna et al. 2009).

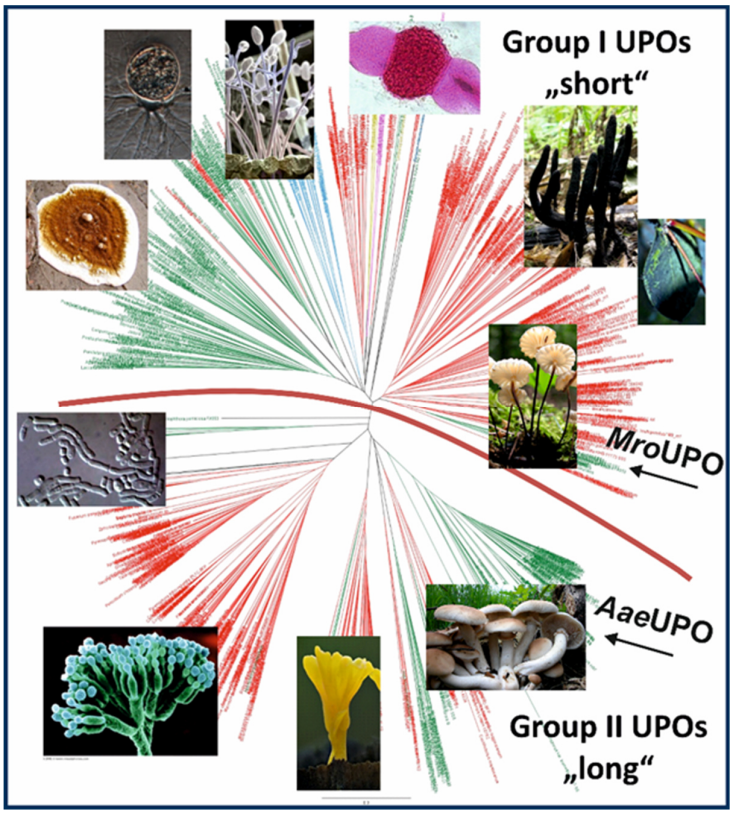

Fig. 1.13: Phylogenetic tree of putative HTP/UPO sequences available from public data bases. It is based on almost 2,100 sequences divided into two groups/clades/families, namely ‘long’ and ‘short’ UPO sequences. Representatives characterized on the protein level from both clades are marked with black arrows. Amino acid sequences were aligned with MAFFT and clustered based on Neighbor-joining algorithm done in Geneious R7.1. Green – Basidiomycota, red – Ascomycota, grey – Glomeromycota, yellow – ‘Zygomycota’ (Mucoromycotina), purple – Chytridiomycota, blue – ‘Oomycota’ (pseudo-fungal Stramenopiles of the order Peronosporales) (modified according to Hofrichter et al. 2019).

Short UPOs of group I have an average molecular mass around 30 kDa and are present in all fungal phyla. Characterized representatives of this group are the UPOs from *Marasmius rotula, Chaetomium globosum* and *Marasmius wettsteinii* (Hofrichter et al., 2015, Ullrich et al., 2018). The group of long UPOs, which the characterized enzymes of *A. aegerita* and *C. radians* belong to, has a mass around 45 kDa and occurs exclusively in Ascomycota and Basidiomycota. Both UPO clades exhibit a highly conserved proximal cysteine (Cys) with two flanking prolines (Pro) within a characteristic PCP motif that guarantees perfect exposition of Cys towards the heme as well as a glutamate (Glu) that acts as acid-base catalyst in peroxide activation. Two further acidic residues and a serine (Ser) form the EXDS-motif that is responsible for binding a stabilizing magnesium ion (Mg^{2+}; Pecyna et al. 2009, Piontek et al. 2013, Hofrichter et al. 2019). Differences in the

active sites of both UPO clades arise from the alkaline amino acid that stabilizes the negative charge of the UPO intermediate 'compound 0'. In short UPOs, this is a His (e.g. His86 in *Mro*UPO) but an Arg in long UPOs (e.g. Arg189 in *Aae*UPO). UPOs may be organized in multigene families with up to 16, 24 or even 50 different sequences present in the genome of one fungus (i.e. in *A. aegerita*, *Agaricus bisporus* or *M. rotula*, respectively), probably also comprising several gene variants (Pecyna 2015, Hofrichter et al. 2014, Hofrichter et al. 2019).

Fungal UPOs represent a unique enzyme type that selectively transfers oxygen from peroxides (H_2O_2, ROOH) to numerous substrates. An overview on UPO-catalyzed reactions is given in Fig. 1.12. They catalyze the hydroxylation of diverse linear, branched and cyclic alkanes, fatty acids and alkyl groups (e.g. attached to aromatic rings). They oxidize alkenes and alkenyls, in which both epoxidation and hydroxylation of the double bond's adjacent carbons (allylic hydroxylation) occurs. Aromatic oxygenation has been studied in detail with naphthalene and benzene as substrates (Kluge et al. 2007, Karich et al. 2013, Kluge et al. 2009). Naphthalene is regioselectively epoxidized by different UPOs to form naphthalene 1,2-oxide that hydrolyzes in the presence of protons (H^+) to 1-naphthol as the major product. Other polycyclic aromatic hydrocarbons such as fluorene, anthracene, phenanthrene, pyrene and dibenzofuran were also found to be subject to UPO-catalyzed oxidation leading to mixtures of mono- and polyhydroxylated products (Aranda et al. 2010). Benzene oxidation proceeds via initial epoxide formation and subsequent re-aromatization to form phenol; further oxygenation is typical and gives mixtures of hydroquinone, catechol and 1,2,4-trihydroxybenzene (Karich et al. 2013). Phenolic products formed can be in turn substrates of the peroxidative activity of UPOs (one-electron oxidation), which can lead to mostly undesired phenoxyl radicals. This can be prevented by adding radical scavengers such as ascorbic acid to the reaction mixture. Re-reduction of phenoxyl radicals is of particular relevance when polyphenolic substrates such as flavonoids are attempted to peroxygenation (Barková et al. 2011).

UPOs catalyze *O*- and *N*-dealkylations of diverse ethers and secondary/tertiary amines, respectively. The mechanism involves, in both cases, initial hydroxylation of one of the heteroatoms' adjacent carbons (e.g. methyl or methylene groups) giving rise to unstable intermediates (e.g. hemiacetals), which spontaneously cleave under release of water (Kinne et al. 2009, Poraj-Kobjelska, 2013). Ether cleavage occurs between aromatic and aliphatic molecule parts in alkyl aryl ethers (e.g. 1,4-dimethoxybenzene) or in alicyclic

and aliphatic ethers (e.g. tetrahydrofuran, di-isopropyl ether). Substantial *N*-dealkylation (~60%) was observed during *N*-methylaniline oxidation by *Aae*UPO (Kinne et al. 2010). UPOs are also capable of transferring oxygen to organic heteroatoms such as sulfur and nitrogen. For example, the heterocycle of dibenzothiophene is oxidized at the sulfur atom to form the corresponding sulfoxide and sulfone (Yarman et al. 2012). In a similar reaction, *Aae*UPO was found to enantioselectively oxidize the side chain of thioanisole into the corresponding (*R*)-sulfoxide with high efficiency (Horn 2009). Pyridine and halo-, nitro- and cyanopyridines are oxidized by *Aae*UPO exclusively at the nitrogen atom to form the respective pyridine *N*-oxides (Ullrich et al. 2008).

*Aae*UPO shows strong bromide (Br^-) oxidation but, in contrast to *Cfu*CPO, only very low chloride oxidation, even though – according to studies of *Aae*UPO C-I – its redox potential is slightly higher than that of *Cfu*CPO (Wang et al. 2013). The oxidation of halides (X^-) is actually also an oxygen transfer reaction yielding reactive hypohalites (OX^-) that in turn can halogenate organic substrates such as phenols (Ullrich et al. 2005, Hofrichter and Ullrich, 2006). In contrast to *Aae*UPO, *Mro*UPO has almost no bromide oxidizing activity, indicating that not all peroxygenases have specific halide binding sites (Gröbe et al. 2011).

The promiscuity of UPOs in oxyfunctionalization reactions becomes evident when oxidation of pharmaceuticals and drugs is examined. All reactions mentioned above have been observed in this context, and more than 60 different pharmaceuticals and a number of illicit drugs were shown to undergo oxidative modification by UPOs (e.g. the painkiller diclofenac, the *beta*-blocker propranolol, or the antiviral drug oseltamivir; Poraj-Kobjelska et al. 2011, 2013). Furthermore, the oxidative conversion of 5-hydroxymethylfurfural (HMF) that is biotechnologically relevant for the synthesis of renewable (lignocellulose-based) platform chemicals, such as 2,5-furandicarboxylic acid (FDCA), was demonstrated by a UPO-based enzyme cascade reaction. In the presence of different peroxide-generating fungal oxidases (such as AAO and GAO, chap. 1.1.3.3), UPO contributes to the formation of substantial amounts of the target product FDCA with a yield of up to 80% (Karich et al. 2018).

Besides differences in the molecular mass, the two UPO families also differ in their molecular architecture and thus in their catalytic ‘behavior’. This becomes evident from the crystal structure-based 3D-models of long *Aae*UPO and short *Mro*UPO (Piontek et al. 2013, Ullrich et al. 2018). *Mro*UPO has a rather open and symmetric frustum-like heme

access channel whereas that of *Aae*UPO is narrower and 'carafe-shaped'; the channel of *Mro*UPO is about 4 Å shorter and up to 5 Å wider than that of *Aae*UPO (Fig. 1.14). Furthermore, the hydrophobic amino acid residues lining the channels are different. While *Aae*UPO contains nine rigid Phe and one Tyr, *Mro*UPO's heme channel comprises only one Phe but ten more flexible aliphatic amino acids (one Ala, two Leu, seven Ile) (Kiebist et al. 2019). These structural differences may explain, why short UPOs are capable of converting bulky substrates such as steroids (e.g. *Mro*UPO and *Cgl*UPO) whereas *Aae*UPO cannot. Thus testosterone epoxidation represents a special reaction that has been so far only observed for *Cgl*UPO with up to 90% regioselectivity for the 4,5-epoxide (Kiebist et al., 2017).

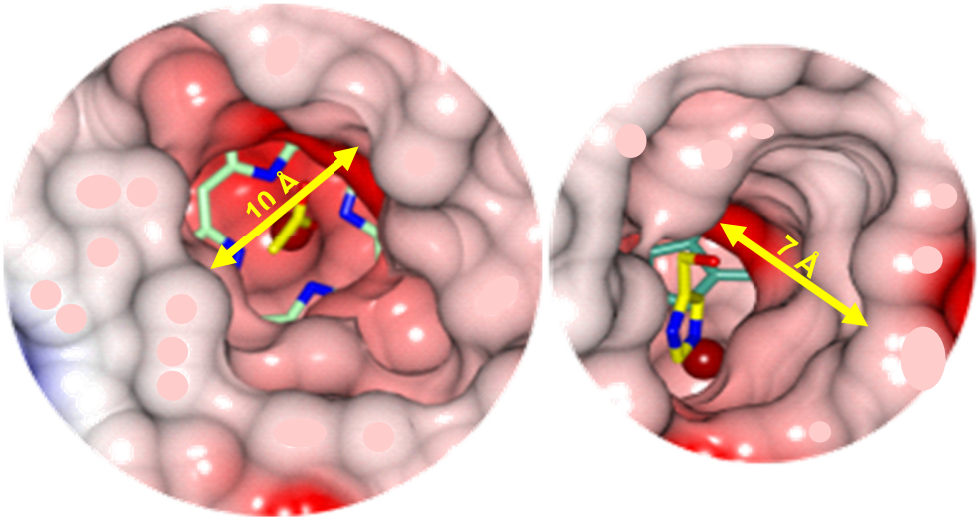

Fig. 1.14: Heme-access channel of *Mro*UPO (left) and *Aae*UPO (right). Hydrophobic amino acids are shown in red (according to Piontek et al. 2013, Piontek et al. 2017, Ullrich et al. 2018).

Although 'etherase' activity (*O*-dealkylation) of *Aae*UPO was proven by scission of different lignin model compounds and its presence has been demonstrated in solid-state wood cultures, the final proof of UPO involvement in ligninolysis or lignin-modification under physiological conditions is still pending. Conclusively, it is noteworthy to mention again that almost nothing is known about the natural function of UPOs in fungi and hence their possible ecological and environmental implications (Karich et al. 2017). Their widespread occurrence in the fungal kingdom and their molecular organization – existing and lacking signal peptides indicate both extracellular and intracellular representatives – suggest different functions in dependence of fungal life style, taxonomic affiliation and environmental conditions. Not least due to their catalytic promiscuity, reflected by more

than 300 substrates whose conversion is of certain industrial interest, and due to the fact that this versatility is reasoned in structural differences, the discovery of further representatives will lead to new UPO types with biotechnological relevance.

1.3 Lignocellulose-degrading fungi from tropical regions

By far the largest part of our current understanding of fungi-based decomposition of lignocellulosic materials (coarse woody debris, deadwood, soil and grassland litter) is based on the investigation of fungi originating from temperate or boreal forests in Europe North America or Japan. By comparison, the diversity of wood-rot and litter-decomposing fungi from tropical regions is still rather unexplored and scientifically underrepresented. On the other hand, it is well-known that especially the tropics (rainforests) harbor the largest 'biodiversity resources' including myriads of fungal species (Arnold et al. 2000, Hawksworth 2001).

Pointing (1999) described a quantitative method to determine lignocellulolytic enzyme production by tropical fungi. Systematic studies and screenings of tropical fungi for bioactive compounds were reported by Hyde (1997). From a Malaysian forest, 36 wood-inhabiting basidiomycets and 15 ascomycetes were isolated and their degradation potential towards wood of Malaysian trees and bamboo (*Blumeodendron tokbrai*, *Hevea brasilliensis* - rubberwood, Bambuseae) was tested, but the authors did not report anything on the secreted lignocellulolytic enzymes (Ujang et al. 2007). The mechanism of soft rot (type I and II) was also studied using Malaysian ascomycetes (e.g. *Xylaria multiplex*) in an electron microscopic approach (Lee 2000). A survey of lignocellulytic enzymes from indigenous wood-rot and litter-decomposing fungi from tropical evergreen dry forests in Tamil Nadu (India) gave maximum Lac and POD levels of 258 U L^{-1} and 288 U L^{-1}, respectively, secreted by the basidiomycetes *Trametes gibbosa* and *Tricholomopsis* sp. (Sudarson et al. 2014). The isolation of freshwater fungi growing on submerged wood was reported from South China, but also in this study, merely the weight loss of inoculated wood (e.g. *Ophioceras dolichostomum*, *Nais aquatica*) was reported (Yuen et al. 1999).

The diversity of tropical fungi and bacteria was subject of a study dealing with the gut microbiome of larvae from wood-feeding Coleoptera in Costa Rica. Fungal isolates could be assigned to three phyla, 16 orders, 24 families, and 40 genera; molds of the opportunistic genus *Trichoderma* were the most abundant fungi detected in all beetle

families studied and on all sites. Fungal isolates belonged to eight genera, among them white-rot *Phlebia* and ascomycetous *Paecilomyces* being able to decolorize the recalcitrant dye Remazol Brilliant Blue R during the growth on solid media. This finding was interpreted as a 'certain ligninolytic potential' of the isolates (Rojas-Jiménez and Hernández 2015). A large study on the fungal diversity of wood-inhabiting species was performed against the background of biomass decomposition with isolates from tropical forests in French Guyana. Overall, 29 basidiomycetous and six ascomycetous fungi were obtained belonging to the Polyporaceae, Ganodermataceae, Fomitopsidaceae, and Hymenochaetaceae as well as to the Nectriaceae, respectively. Enzyme cocktails (concentrated culture liquid) based on the secretome of 13 of these tropical isolates were successfully used for plant biomass hydrolysis and saccharification (Berrin et al. 2012).

Isolation of fungi from African regions were reported from the camphor tree (*Ocotea usambarensis*, 24 strains/species; Nsolomo & Venn 2000) in East Africa and from planted *Eucalyptus* and *Pinus* in South Africa (almost 600 strains; de Koker et al. 2000) as well as from not further characterized, decaying Acacia wood in Ethiopia (Bekele et al. 2015); but in none of these studies, enzyme-related tests were performed. The secretion of enzymes (mainly Lac and one LiP) associated with the degradation of mahogany (*Khaya ivorensis*) and obeche (African whitewood - *Triplochiton scleroxylon*) was reported for the BRF *Gloeophyllum sepiarium* and the WRF *Pleurotus ostreatus*, both causing significant weight loss (Ejechi et al. 1996). Further information on lignocellulolytic fungi from East Africa can be found in the reports of Mtui (2007), Nsolomo et al. (2000), Osano et al. (2004) and Masalu (2016) but they mainly focused on taxonomic and ecological aspects paying only little attention to enzymatic aspects. Against this weak research background, it will be an interesting and promising task to establish a fungal collection of African wood-dwelling fungi with the further goal to identify new species producing biotechnologically relevant enzymes such as DyPs and/or UPOs.

1.4 Relatives of fungal isolates

1.4.1 The genus *Psathyrella*

Psathyrella is one of ten genera (*Psathyrella*, *Coprinellus* and *Coprinopsis*, *Cystoagaricus*, *Lacrymaria*, *Parasola*, *Homophron* and *Mythicomyces*, as well as *Kauffmania* and *Typhrasa*) within the family Psathyrellaceae (Agaricomycetes, Basidiomycota) consisting of small agaric mushroom species that are closely related to

the genus *Coprinellus* (Smith, 1972). More than 400 species of that genus – mostly from Europe and North America but also some from Africa, India and Australia – have been described so far (Larsson and Örstadius, 2008, Padamsee et al., 2008, Vašutová, 2006). Most *Psathyrella* species are saprotrophs living either as primary or secondary decomposers (Padamsee et al., 2008, Smith, 1972). They typically grow on decaying wood, humus, soil litter or dung. Few species like *Psathyrella epimyces* were reported to be parasitic growing on other fungi, e.g. on the ink-cap *Coprinus comatus* (Padamsee et al., 2008).

Fig. 1.15: *Psathyrella* cf. *spadiceogrisea* (Photo: Rene Ullrich 2011).

The genus is characterized by brown to black spores that discolor in sulfuric acid and they have fragile caps, which is quite divergent from the other closely-related genera within the Agaricales (Padamsee et al., 2008). The fragile caps reflect the genus name, which is derived from Old Greek: *psathyros* (πσαθυρος), the word for fragile (Fig. 1.15). A phylogenetic study suggested that the genus is not monophyletic but rather paraphyletic (Hopple Jr and Vilgalys, 1999), which was supported by a second study by Padamsee et al. (2008) on various *Psathyrella* species and the closely related genera *Coprinopsis*, *Coprinellus* and *Parasola*.

Some species have been shown to exhibit antimicrobial activities, while others like *Psathyrella* cf. *hymenocephala* and *Psathyrella velutina* are used as food spices or in the synthesis of lectins, respectively (Paul and Akers, 2000, Ueda et al., 2002, Padamsee et al., 2008).

1.4.2 The genus *Xylaria*

Xylaria (ex Schrank) is the largest and the first described genus of the family Xylariaceae. They belong to the class Pyrenomycetes (Ascomycota), which means they produce meiospores in asci that are embedded in tiny pockets called perithecia. The asci take turns when growing into the narrow opening of the pocket so that they can shoot spores away from the ascocarp into the surrounding air. Species of *Xylaria* are mostly club- or finger-shaped decomposers of wood or plant debris that become black and hard by maturity (melanization), reminiscent of carbon or charcoal (Fig. 1.16). The genus contains more than 300 characterized species that are widely distributed in many geographical regions both in tropical and temperate climate zones (Kirk et al., 2008, Lee et al., 2000, Fournier et al., 2011).

Fig. 1.16: Ascocarps of *Xylaria longipes* growing on a hornbeam log (*Carpinus betulus*; Photo: Rene Ullrich 2017)

However, identification of the species based on morphological features of the stromata, asci and spores (size, color and at times the shape) is difficult as species greatly differ depending on the particular developmental stage (immature, mature and senescent) (Lee et al., 2000, Whalley, 1996). Most species of the genus are of saprotrophic nature and may cause soft-rot of wood (usually type 2; e.g. *Xylaria polymorpha*, *X. hypoxylon*, *X. longipes*; Liers et al. 2006, Liers 2007). They belong to the best investigated species of this type of wood-rot (Liers 2007, Shary et al. 2007, Büttner et al. 2018). Other *Xylaria* species may occur as endophytes in living plants or as pathogens like *X. mali* and *X. arbuscula* (Petrini 1995, Fournier et al. 2011, Sharma et al. 2018). Furthermore, it has been assumed that some species, such as *X. nigripes* and *X. furcata*, developed symbiotic

relationships with termites in a similar way as basidiomycetous fungi of the genus *Termitomyces* (Rogers et al. 2005, Visser et al. 2009). Many species in the genus were reported to be important sources of secondary metabolites like antibiotics, therapeutic agents and bio-pesticides. For instance, *X. grammica* produces grammicin that has nematicidal properties (Macías-Rubalcava and Sánchez-Fernández, 2017, Song et al. 2014, Okane et al., 2008, Kim et al., 2018).

1.5 Objectives of the study

Main objective of the PhD project has been the identification, isolation and biochemical characterization of novel extracellular peroxidases (mainly UPOs and/or DyPs) by exploring the fungal biodiversity of wood- and litter-dwelling Kenyan fungi (basidio-, asco- and zygomycetes) isolated from tropical and coastal forests. A second objective has been the identification of the corresponding enzyme-encoding genes by a next-generation sequencing approach. The knowledge on the distribution of genes encoding for CAZy enzymes would allow to classify the fungi to any of the known eco-physiological groups of wood-rot fungi. The following hypotheses/tasks supported by previous investigations and literature data have been made/defined in connection with the present dissertation:

- Wood- and litter-inhabiting fungi isolated from Kenyan biodiversity hotspots may harbor new, so far unknown fungal species, among them representatives of biotechnological interest secreting relevant oxidoreductases (e.g. UPO, DyP, PODs, laccase, etc.),
- Some of these interesting enzymes can be produced at large scale, purified and characterized,
- Their biochemical properties may be of eco-physiological relevance for the producing fungus and they may also be of interest for applications, e.g. in biomass conversion or organic synthesis,
- Enzyme-producers obtained possess the genes encoding the most important CAZy enzymes required to substantially decompose lignocellulosic materials,
- The determined distribution of CAZy-encoding genes in the genomes of the chosen enzyme producers facilitates their classification within any of the known groups of wood-rot fungi (i.e. WRF, LDF, BRF, SRF, URF, DDF; chap. 1.1.2).

2 MATERIAL AND METHODS

2.1 Collection sites of Kenyan fungi

Fruiting bodies of Basidiomycota and Ascomycota growing on trees, dead-wood, leaf-litter or in soil were collected in the three regions of KAKAMEGA FOREST (K), ABERDARES FOREST (AB) and ARABUKO SOKOKE FOREST (AS) in Kenya (Fig. 2.1). Fungal fruiting bodies were sampled in the months April and May 2016; they were photographed, labeled and categorized in a small culture collection. Geographical, climatic and botanical data as well as some specific biodiversity-related features of the collection areas are summarized in Tab. 2.1.

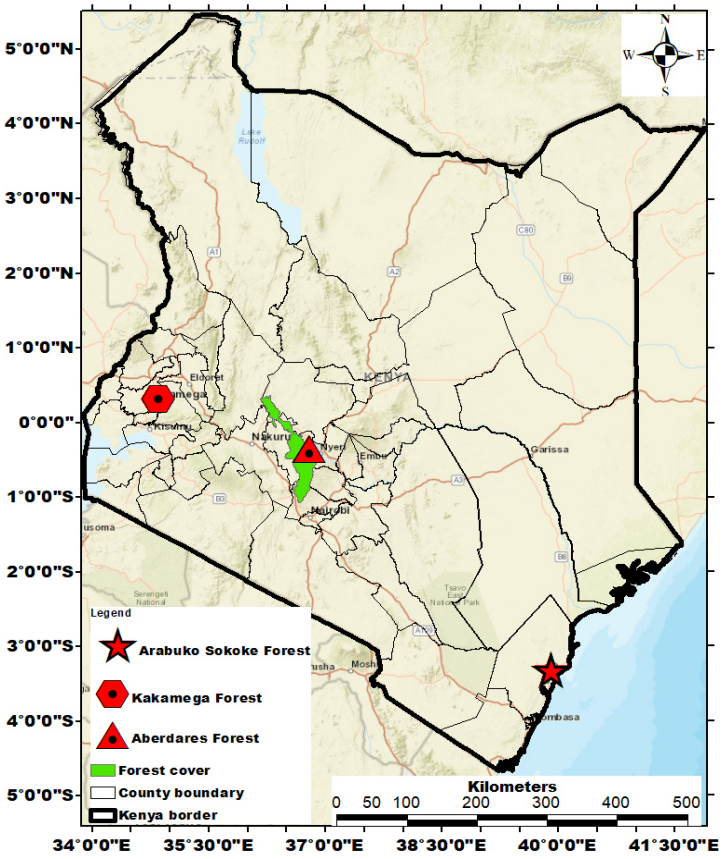

Fig. 2.1: Map of Kenya showing the different sampling sites where the fungal strains studied in the present thesis were collected; Sources: Esri, HERE, DeLorme, USGS, Intermap, INCREMENT P, NRCan, Esri Japan, METI, Esri China (Hongkong), Esri Korea, Esri (Thailand), MapmyIndia, NGCC, (©OpenStreetMap contributors, and the GIS User Community).

Tab. 2.1: Some characteristics of KAKAMEGA FOREST (K), ABERDARES FOREST (AB) and ARABUKO SOKOKE FOREST (AS).

	KAKAMEGA FOREST	ABERDARES FOREST	ARABUKO SOKOKE
Type of forest	Rainforest	Mountain Forest	Coastal Forest
Habitat	Remnant of the Guineo-Congolian rainforest #	Kenyas third highest mountain; canopy forest belt, bamboo zone, sub-alpine and alpine areas§§	Largest coastal forest in East Africa; canopy forest, *Cynometra webberi* [4], *Brachystegia* Forest *Cynometra* Forest
Area	240 km² ##	125 km² §§	416 km² [4]
Geographical location	36N 0707177 UTM 0039613	37N 0264933 UTM 9959613	37M 0601989 UTM 9633236
Annual rainfall	1200-1700 mm, April and May (long rains), August to September (short rains)	940-3,200 mm April and May (long rains), October to November (short rains) [1]	1,000–1,100 mm [4], April and June (long rains), November to December (short rains)
Altitude	1,500 to 1,700 m *	4,000 and 3,900 m §§	60–210 m [4]
Temperature	11-27°C **	Yearly average 18°C [2]	25°C [4]
Biodiversity	At least 400 vascular plants species*, L'Hoest's monkey (*Cercopithecus lhoesti*), 400 butterflies §	Important bird sanctuary (IBA) with 52 of Kenya's 67 afrotropical highland species, six restricted range species [1], critically endangered antilope *Tragelaphus euryceros*, (IUCN SSC, 2008), 778 plant species [3]	More than 230 bird species incl. two endemics: Sokoke scops owl (*Otus irenea*) and Clarks weaver (*Ploceus golandi)* [5]

(Kokwaro 1988, Schmitt 1991), ## (Fashing and Mwangi Gathua 2004), * (Althof 2005), ** (Tsingalia 1990), § (Peltorinne 2004), §§ (Paron et al. 2013), [1] (Lambrechts et al. 2003), [2] (Estes et al. 2008), [3] (Schmitt 1991), [4] (Glenday 2008), [5] (Peltorinne 2004).

2.2 Media and fungal cultivation conditions

Agar media as well as liquid and solid growth media were prepared for the isolation and maintenance/storage as well as for laboratory cultivation of the isolated Kenyan fungi, respectively. After supplementation with indicator substrates, the former media were also used for screening the secretion of oxidative enzyme activities of interest (i.e. peroxidases and laccases). All inoculations were carried out under sterile conditions in a laminar flow hood using disinfected (by heat or 70% ethanol) instruments (ThermoFisher Scientific, Massachusetts, USA).

2.2.1 Malt extract agar media (MA media)

MA media were routinely used to isolate and pre-culture fungal strains. The basic MA medium consisted of the following components (concentration per 1 Liter A. dest.):

Malt extract	20 g
Agar-agar	22 g

The isolation of fungal pure cultures was performed using an MA medium supplemented with antibiotics (MAA medium) that were appropriate to favor growth of basidiomycetous fungi (chloramphenicol 50 mg L^{-1}, penicillin 50 g L^{-1} and streptomycin 50 g L^{-1} – against g^+ and g^- bacteria, nystatin 40 mg L^{-1} – against yeasts, benomyl 50 mg L^{-1} – against molds) or ascomycetous fungi (same composition but without benomyl; MAA-wB). The antibiotics (dissolved in 70% v/v ethanol) were added to the autoclaved but still liquid agar media after cooling down to about 50°C.

2.2.2 Isolation of Kenyan fungi

For the isolation of basidiomycetous pure cultures (e.g. *Psathyrella* spp.), the stipe of the fruiting bodies was cut-off with a sterilized scalpel to expose the low-germ inner mycelium (plectenchyme). From there, a small piece of the plectenchyme was removed and transferred onto plates (Petri dishes) containing MAA (chap. 2.2.1). Ascomycetous strains (e.g. *Xylaria* spp.) were obtained from fruiting bodies, the surface of which had been desinfected with 70% ethanol. This disinfected material was transferred onto Petri dishes containing MAA-wB (chap. 2.2.1). Developing mycelia were visually checked for purity and transferred to fresh MA plates. Pure cultures of successfully isolated strains were routinely grown on the above-mentioned MA plates at 23°C until their mycelia had overgrown the whole agar surface. For long-term storage, stock cultures were prepared in slanted agar tubes (10-mL culture slants), and maintained in the dark at 4°C. Wherever possible, remaining fragments of the fungal fruiting bodies were dried and stored for later molecular identification or microscopic evaluation (chap. 2.10).

2.2.3 Liquid cultivation

For production of peroxidases, liquid cultivation was performed using a glucose-peptone medium (SPM; glucose 28 g L^{-1}, malt extract 3 g L^{-1}, soy-peptone 12 g L^{-1}, yeast extract 3 g L^{-1}), which is known to stimulate the secretion of certain fungal enzymes (Gröbe et al. 2011, Kiebist et al. 2017). A complete fungal pre-culture grown on a MA was homogenized in a 100-mL Erlenmeyer flask containing 80 mL sterile water using an

Ultra-Turax™ device; 9 mL of this homogenized suspension were transferred with a sterile pipette to 500-mL culture flasks containing 200 mL of the SPM. After inoculation, the cultures were agitated on a rotary shaker at 100 rpm and 23°C. Enzyme activities (laccase, peroxygenase/UPO or peroxidase/DyP) and pH were determined every 2-3 days (chap. 2.3.2 and 2.3.3) over a total cultivation period of three weeks.

2.2.4 Agar plate screening for extracellular oxidoreductase activities

Pre-cultures were prepared by transferring an agar plug (1 cm ID) from a stock culture onto a fresh MA plate that was then incubated at 23°C; usually, three-week old pre-cultures were ready for further use (e.g. inoculation of fresh plates or liquid cultures). Fungal isolates were screened for activities of peroxidases and laccases based on their ability to oxidize ABTS [2,2'-azino-*bis*(3-ethylbenzthiazoline-6-sulphonic acid], manganese(II) ions (Mn^{2+}) or humic acids (HA) (Hofrichter et al. 1998, Steffen et al. 2002). To promote fungal growth and enzyme secretion, a complex plant-based soybean meal agar (SMA; Anh 2008) and a modified KIRK-medium agar (KMA; Kirk et al. 1978) were used in the screening, respectively. KMA consisted of the following components (concentration per 1 Liter A. dest.):

Glucose	10 g
2,2-dimethyl succinate	2.2 g
KH_2PO_4	2.0 g
$MgSO_4 \times H_2O$	0.5 g
$CaCL_2$	0.1 g
di-Ammonium tartrate	0.25 g
Yeast extract	0.1 g
Agar agar	22 g

SMA contained the following components (concentration per 1 Liter A. dest.):

Soybean meal	30 g
Agar agar	22 g

The indicator substances were added to the agar either before (Mn^{2+} as $MnCl_2$, 200 mg L^{-1}) or after autoclaving (ABTS, 250 mg L^{-1}; humic acids, 500 mg L^{-1} in 70% ethanol).

Under sterile conditions, an agar plug (1 cm ID) per fungus was cut and transferred onto the KMA or SMA plates containing one of the three indicator substances (ABTS-SMA, ABTS-KMA, Mn^{2+}-SMA, Mn^{2+}-KMA, HA-SMA, HA-KMA). After one to six weeks growth at 23°C, the plates were examined for characteristic color changes that can be described as follows: from colorless to dark blue-green or violet – ABTS-KMA and ABTS-SMA (formation of $ABTS^{\bullet+}$ or its following product), respectively; from colorless to dark-brown (MnO_2 formation) – Mn^{2+} plates; from dark-brown to yellowish (HA 'bleaching') – HA plates. These color reactions are indicative for the presence of secreted fungal oxidoreductases, i.e. laccases and/or peroxidases (Steffen et al. 2002, Hofrichter et al. 1998).

2.3 Enzyme assays

During fungal cultivation, activities of heme peroxidases (MnP, UPO, DyP) and laccase were measured to select the most active strains and to determine the most appropriate time for harvesting the cultures. All activity measurements were performed, after removing the fungal mycelium by centrifugation, in 1-mL cuvettes at room temperature using a Cary 50 UV/Vis spectrophotometer (VARIAN, Darmstadt, Deutschland), and the enzymatic activities were calculated in units. One unit is defined as that amount of enzyme that catalyzes the conversion or formation of 1 µmol substrate or product, respectively, per minute (µmol min^{-1}). In a second approach, a rapid enzyme screening was performed in 96-well microtiter plates using UPO- and DyP-specific enzyme assays (Poraj-Kobielska et al. 2012, Liers et al. 2010).

2.3.1 Rapid screening for oxidoreductases in microtiter plates

A rapid screening for UPO and DyP activities was performed in 96-well microtiter plates using specific enzyme assays. UPO activity was determined by the hydroxylation and demethylenation of 5-nitro-1,3-benzodioxole (NBD; 50 mM in 70% ACN) in phosphate buffer (50 mM, pH 7.0). The reaction was started by adding culture liquid and co-substrate (1.0 mM H_2O_2) almost concomitantly. NBD oxidation was followed by the formation of yellow-colored 4-nitrocatechol at 425 nm (ε_{425} = 9.7 mM^{-1} cm^{-1}). Product formation was verified by a characteristic color shift from yellow to red at pH 12 after addition of 1 M NaOH (Poraj-Kobielska et al. 2012). UPO positive samples were also measured using a second assay based on the oxidation of veratryl alcohol (chap. 2.3.3).

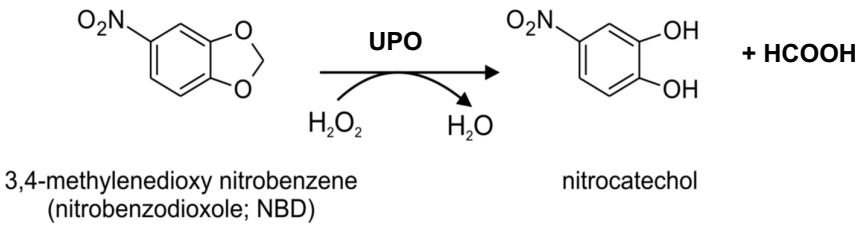

Fig. 2.2: Specific reaction of UPO with 5-nitro-1,3-benzodioxole (NBD). The reaction proceeds via hydroxylation of the methylene group forming an unstable hemiacetal that spontaneously decomposes to 4-nitrocatechol and formic acid (Poraj-Kobielska et al. 2012).

2.3.2 ABTS oxidation

ABTS (0.3 mM final concentration) oxidation was followed in 50 mM sodium citrate buffer (pH 4.5) in the absence (for laccase) or presence of H_2O_2 (0.1 mM for peroxidases/DyP). Formation of the product, the bluegreen colored ABTS cation radical ($ABTS^{\bullet+}$), was monitored by the initial increase in absorbance at 420 nm (ε_{420}= 36 mM^{-1} cm^{-1}) over an appropriate time interval ranging from 10 to 60 seconds (Liers et al. 2010, Wolfenden and Willson 1982).

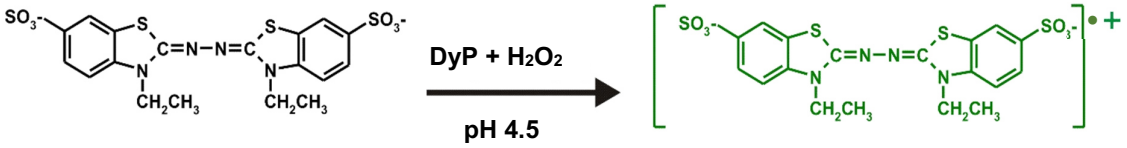

Fig. 2.3: Oxidation of 2,2'-azino-*bis*(3-ethylbenzthiazonline-6-sulphonate - ABTS) to the bluegreen-colored ABTS cation radical ($ABTS^{\bullet+}$). The reaction is catalyzed by peroxidases (shown here) and laccases in the presence or absences of H_2O_2.

2.3.3 Veratryl alcohol oxidation

The oxidation of veratryl alcohol (3,4-dimethoxybenzyl alcohol, VA; 5 mM final concentration) to veratraldehyde (3,4-dimethoxybenzaldehyde) allows to measure UPO activity (Fig. 2.4; Ullrich et al. 2004)) and was routinely used here to detect UPO activities during the screenings in liquid culture (chap. 2.2.3) and in the course of UPO production and purification (chap.2.4.1). The formation of veratraldehyde was detected in 50 mM potassium phosphate buffer (pH 7.0) by following the initial increase in absorbance at 310 nm (ε_{310} = 9.3 mM^{-1} cm^{-1}) over appropriate time intervals ranging between 10 and 60 seconds, after addition of H_2O_2 (1.0 mM final concentration).

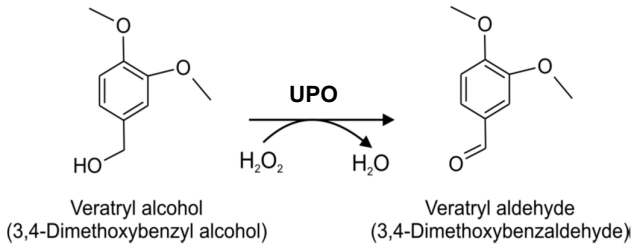

Fig. 2.4: Oxidation of veratryl alcohol to veratraldehyde by UPO at pH 7.0 (Ullrich et al. 2004, Poraj-Kobielska 2013).

2.3.4 Manganese oxidation

The oxidation of Mn^{2+} to Mn^{3+} was used to determine the activity of manganese-oxidizing peroxidases[10] (MnP, Wariishi et al. 1992) in the culture liquid of basidiomycetous isolates (chap. 2.2.3). The formation of Mn^{3+}-malonate complexes was monitored in the presence of $MnCl_2$ (0.5 mM final concentration) in 50 mM sodium malonate buffer (pH 4.5) by measuring the initial increase in absorbance at 270 nm (ε_{270} = 11.5 mM^{-1} cm^{-1}) over an appropriate time interval from 10 to 60 seconds, after addition of H_2O_2 (0.1 mM final concentration).

2.4 Production of peroxidases

For subsequent enzyme purification and characterization, the most promising fungal candidates, secreting high levels of desired enzyme activities (UPO or DyP), were chosen for an up-scaling of enzyme production (chap. 2.2.3). The highest UPO activity was detected for the basidiomycete *Psathyrella aberdarensis*. *Xylaria grammica* was found to produce sufficient amounts of a DyP, which was the first proof for the secretion of that enzyme type by an ascomycetous fungus.

2.4.1 Production of the UPO from *P. aberdarensis* (*Pab*UPO)

For large-scale UPO production, *P. aberdarensis* was cultivated in a 30-L stirred-tank bioreactor (BIOSTAT®, Sartorius GmbH, Göttingen, Germany) containing 15 L of SPM. Inoculation occurred with 1 L of homogenized mycelium of *P. aberdarensis* pre-cultured as described above in SPM (5 × 200 mL medium). Fermentation was carried out under

[10] Manganese-oxidizing activities in fungal cultures are mainly due to MnP (EC 1.11.1.13) but may be also caused by VP (EC 1.11.1.16).

the following conditions: stirring rate 100 rpm, aeration rate 4 L min^{-1}, temperature 28°C; pH was not regulated.

2.4.2 Production of the DyP from *X. grammica* (*Xgr*DyP)

Production of DyP from *X. grammica* was performed at lab-scale in 500- and 1000-mL flasks containing 200 or 1,000 mL of the SPM medium, respectively. Inoculation and incubation was carried out as described above (chap. 2.2.3).

Fig. 2.4: Above – Production of DyP from *Xylaria grammica* (left) and UPO from *Psathyrella aberdarensis* (right) in glucose-peptone medium (SPM) at laboratory-scale. Below – UPO production by *P. aberdarensis* at larger scale in an aerated 30-L stirred-tank bioreactor (stainless steel) in SPM.

Peroxidase/DyP activity (with ABTS) and pH were determined every 2 to 3 days (chap. 2.3.2 and 2.3.3) during a total cultivation period of approximately three weeks. For that, 1-ml samples were taken and analyzed after centrifugation.

2.5 Enzyme purification

2.5.1 Preparation of enzyme crude extract

After reaching maximal activities, the culture liquids were harvested. The fungal mycelium was removed by filtration and the crude liquid was frozen at -20°C prior to purification to remove polysaccharides by precipitation. After thawing, the crude enzyme liquid was again filtrated at 11°C (GF6, SARTORIOUS GmbH, Göttingen, Deutschland) followed by an ultrafiltration and dialysis step using a tangential flow cassette (Vivaflow 200, cut-off 10 kDa; SARTORIUS, Göttingen, Germany).

2.5.2 Fast protein liquid chromatography (FPLC)

Crude enzyme preparations were purified by using anion exchange chromatography (AEX, Q-Sepharose™ FF and MonoQ™; GE HEALTHCARE Europe GmbH, Freiburg, Germany) as well as size exclusion chromatography (SEC, HiLoad™ Superdex™; GE HEALTHCARE). All chromatographic steps were performed with ÄKTA™ AVANT FPLC systems (GE Healthcare). Absorbing material eluting from the columns was simultaneously monitored at 280 nm (to detect total protein) and at 420 and 405 nm to follow the heme proteins of UPO (heme-thiolate) and DyP (heme-imidazole), respectively.

2.5.2.1 Purification of the UPO from *P. aberdarensis (PabUPO*)

Commencing with AEX in 10 mM sodium acetate buffer (pH 6.25), *P. aberdarensis* UPO (*Pab*UPO) was stepwisely separated on Q-Sepharose (26 × 200 mm) and MonoQ (10 × 100 mm) columns with NaCl gradients of 0-1.5 and 0-0.6 M, respectively. Fractions of 12 and 2 mL were collected at flow rates of 13 and 6 mL min^{-1}, respectively. A third purification step (SEC) was performed on a HiLoad 26/600 Superdex 75 PG with 100 mM NaCl in 50 mM sodium acetate buffer at pH 6.75. Fractions of 2 mL were collected at a flow rate of 2.5 mL min^{-1}. The two separated fractions were again loaded onto a MonoQ column (5 × 50 mm); elution of UPO proteins was achieved with a NaCl gradient from 0 to 0.4 M in 10 mM sodium acetate buffer (pH 5.0). The fraction size was 0.8 mL at a flow rate of 6 mL min^{-1}. The fifth and last purification step was a re-chromatography of the three UPO fractions obtained in the previous AEX steps. The NaCl gradient run from 0 to 0.4 M in 10 mM sodium acetate (pH 5.0) with a fraction size of

0.5 mL at a flow rate of 6 mL min^{-1}. Fractions containing UPO activity were pooled, concentrated and washed with 10 mM sodium acetate buffer (pH 6.5).

2.5.2.2 Purification of the DyP-type peroxidase from *X. grammica* (*Xgr*DyP)

Crude peroxidase preparation of *X. grammica* was purified by four steps of FPLC using AEX and SEC separation. In the first step, the concentrated crude enzyme was applied to a Q-Sepharose (26 × 100 mm) column and eluted with a linear gradient of 0-1.0 M NaCl in 10 mM sodium acetate buffer (pH 6.0) at a flow rate of 13 mL min^{-1} and with a fraction size of 7.0 mL. Peroxidase-positive fractions were loaded onto a SEC column HiLoad 26/600 Superdex 75 PG equilibrated with 50 mM sodium acetate buffer (pH 6.75) containing 0.1 M NaCl. Enzyme protein was eluted with the same buffer at a flow rate of 2.5 mL min^{-1}. The third step was performed on a MonoQ column (5 × 50 mm) with a NaCl gradient of 0-0.4 M in 10 mM sodium acetate (pH 6.0) and with a fraction size of 1.5 mL at a flow rate of 6 mL min^{-1}. The last step was a re-chromatograhic elution of the peroxidase-positive fractions originating from the previous AEX separations. The parameter were the same as already described, except that the loading and elution buffers were adjusted to pH 5.8 and 6.0, respectively. Fractions containing *Xgr*DyP activity were pooled, concentrated and washed with 10 mM sodium acetate buffer (pH 6.5).

2.6 Enzyme characterization

2.6.1 Protein determination

Total protein of crude extracts and and of each purification step was determined and carried out according to the dye-binding procedure of Bradford (1976) with a Roti® - Nanoquant Kit (ROTH, Karlsruhe, Germany) and bovine serum albumin (BSA) as protein standards. Samples were pipetted into a 96-well microtiter plate in triplicate and the absorbance was measured at 590/450 nm with a microplate reader (Infinite 200, TECAN, Switzerland).

2.6.2 Protein electrophoresis

2.6.2.1 Sodium dodecyl sulfate polyacrylamide gel electrophoresis (SDS-PAGE)

SDS-PAGE was performed according to the protocol described in (Laemmli, 1970) with a vertical electrophoresis system (XCell *SureLock*™ Mini-Cell, Invitrogen, Carlsbad,

USA) and Novex®NuPAGE® 12% Bis-Tris Gels (INVITROGEN). This electrophoresis method was applied to check the protein purity under denaturing conditions and to determine the molecular weight of the purified enzymes (chap. 2.5.2). A low-M_W protein mixture was used as standard (MBI FERMENTAS, St. Leon-Rot, Germany). Electrophoretically separated proteins were visualized by using a Colloidal Blue Staining Kit (INVITROGEN).

2.6.2.2 Native isoelectric focusing (IEF)

The above-mentioned electrophoresis system was also used to separate proteins according to their isoelectric points (pIs). Electrophoresis was performed according to the manufacturer's protocol with Novex® Vertical IEF Gels (pH gradient 3-7; INVITROGEN) and a Liquid Mix IEF Marker (pH 3.0-10.0; SERVA, Heidelberg, Germany) as reference. Protein bands in the vertical polyacrylamide gel were afterwards visualized by using a Colloidal Blue Staining Kit (INVITROGEN).

2.6.3 Determination of pH-optima and stability

2.6.3.1 pH-Optima and stability of the UPOs from *P. aberdarensis* (*Pab*UPO)

The pH-optima for the oxidation of VA and 5-formyl-2-furancarboxylic acid (FFCA) were evaluated for the purified *Pab*UPO preparationss. The former substrate was applied as already described under 2.3.3. Reactions were performed in 1.5-mL Eppendorf tubes within a pH range from 2.0 to 9.0 in potassium phosphate buffer (50 mM). The reaction mixtures for the FFCA oxidation (total 500 µL in 2-mL HPLC vials) consisted of 50 mM potassium phosphate buffer (50 mM) at varying pH from 3.0 to 9.0 with 2 mM FFCA as substrate and 1.0 U mL^{-1} (VA units) of the respective *Pab*UPO (corresponding to 0.34, 0.21 and 0.25 nmol). Reaction was started by the addition of H_2O_2 (1 mM) to the mixture followed by constant stirring at room temperature for 5 min and reaction termination with 1 mM sodium azide. Substrate conversion and product formation was analyzed as described in under 2.8.6.

The influence of temperature and pH on the activity of purified *Pab*UPOs was tested by exposing the enzyme preparations for different times under respective conditions. Reaction mixtures were prepared in 1.5-mL Eppendorf tubes in triplicate. Aliquots of the enzyme samples were taken after 20 and 40 min as well as 1, 2, 4, 6, 7 and 8 hours of

incubation. In case of temperature stability, enzyme solutions were prepared in potassium phosphate buffer (100 mM, pH 7.0) and incubated at 25, 40 and 60°C; pH-stability was determined in 50 mM phosphate buffer (at 25°C) adjusted to 3.0, 7.0 and 10.0. Samples taken were used for the determination of residual activity towards the assay substrate VA (chap. 2.3.3).

2.6.3.2 pH-Optima of the DyP from *X. grammica* (*Xgr*DyP)

The pH-optimum of *Xgr*DyP was determined for the oxidation of 2,6-dimethoxyphenol (DMP), Reactive Blue 5 (RBlue5) and Mn^{2+}-ions at pH values ranging from 2.0 to 7.0 in either sodium citrate buffer for DMP and RBlue5 or in sodium malonate buffer (50 mM) for the oxidation of Mn^{2+} ions. The later was specifically assayed in the presence of $MnCl_2$ (0.5 mM) by monitoring the formation of Mn^{3+}-malonate complexes at 270 nm (ε_{270} = 11.3 mM^{-1} cm^{-1}; Wariishi et al. 1992). The conversion of DMP (5 mM) was detected at 469 nm (ε_{469} = 27.5 cm^{-1} mM^{-1}; Bollag et al. 1979) and that of RBlue5 (0.1 mM) at 598 nm (ε_{598} = 8.0 cm^{-1} mM^{-1}; Shimokawa et al. 2008). All reactions were started by the addition of H_2O_2 (0.1 mM) and followed spectrophotometrically (Cary 50 UV/Vis spectrophotometer) over appropriate time intervals between10 and 60 seconds.

2.6.4 Kinetic parameters

Apparent Michaelis-Menten (K_m) and catalytic constants (k_{cat}) of the purified *Pab*UPOs and *Xgr*DyP were determined spectrophotometrically for the substrates ABTS (chap. 2.3.2) and DMP (chap. 2.6.3.2) for both enzyme types and for VA (chap. 2.3.3) or RBlue5 and Mn^{2+} (chap. 2.6.3.2) for *Pab*UPOs and *Xgr*DyP, respectively. LINEWEAVER-BURK plots were made from the initial rates obtained at varying substrate concentrations while the concentration of the co-substrate was held constant. The oxidation of RBlue5, DMP and Mn^{2+} ions was monitored at pH 4.5.

2.7 Peptide sequencing

To identify the enzyme-encoding genes from the corresponding genomic data of the seleceted fungi, analysis of internal peptides ('peptide mapping') of purified proteins (*Xgr*DyP and *Pab*UPOs) was performed in collaboration with N. Jehmlich at the Helmholtz Center for Environmental Research – UFZ (Department of Molecular Systems Biology, Leipzig, Germany). Proteins were digested from a Coomassie-stained SDS gel

by trypsin (chap. 2.6.2.1) and the peptide lysates were analyzed by nano-LC-MS/MS as described in the Appendix (A5).

2.8 Substrate conversion by *Pab*UPO

2.8.1 Halogenation of phenol

The *Pab*UPO-catalyzed halogenation was tested by the bromination and chlorination of phenol. The reaction mixtures (total 500 µL in 2-mL HPLC vials) contained 20 mM potassium phosphate buffer at pH 3.0, 0.5 mM phenol, 2 mM H_2O_2 and 10 mM KBr or KCl, respectively. The reaction was started by the addition of a mixture of phenol, KBr and H_2O_2. Bromination was performed with 0.2 U mL^{-1} *Pab*UPO, the chlorination with 0.2 or 0.5 U mL^{-1} of the respective *Pab*UPO and additionally with 5.0 U mL^{-1} exclusively for *Pab*UPO I. For comparison, *Aae*UPO and *Mro*UPO were used under identical conditions with 0.5 U mL^{-1} enzyme. Reaction mixtures were stirred for 10 min at room temperature and then analyzed for the corresponding reactions products (i.e. halogenated phenols, chap. 2.9.1.1) (Anh et al. 2007).

2.8.2 Hydroxylation of naphthalene

Oxygenation of less activated aromatic compounds by purified *Pab*UPOs was proven by the oxidation of naphthalene. The reaction mixtures (total 500 µL in 2-mL HPLC vials) consisted of 20 mM potassium phosphate buffer (pH 7.0), 1.0 mM naphthalene in 20% ACN, 0.5 U mL^{-1} of the respective *Pab*UPO and 1.0 mM H_2O_2. Reaction was started by adding the enzyme to a mixture comprising buffer, substrate and (already) H_2O_2. Reaction was constantly stirred for 10 min at room temperature and then analyzed for the corresponding reactions products (i.e. naphthols and naphthoquinone, chap. 2.9.1.1).

2.8.3 Hydroxylation of anisole (methoxybenzene)

Oxyfunctionalization of methoxylated benzenes by the purified *Pab*UPOs was proven by the example of anisole oxidation. The reaction mixtures (total 250 µL in 2-mL HPLC vials) contained 20 mM potassium phosphate buffer (pH 7.0), 1.0 mM anisole in 2.5% ACN, 5.0 mM ascorbic acid[11], 0.5 U mL^{-1} of the respective *Pab*UPO and 1.0 mM H_2O_2. The reaction was started by the addition of enzyme to the reaction mixture comprising

[11] Ascorbic acid prevents the oxidative coupling and polymerization of phenols formed in the course of the reaction via reduction of phenoxyl radicals (Kinne et al. 2008; Kinne et al. 2009).

buffer, substrate, ascorbic acid and H_2O_2. The reaction was constantly stirred at room temperature for 10 min and then analyzed for the corresponding reactions products (hydroxylated and/or *O*-dealkylated anisole derivatives, chap. 2.9.1.2).

2.8.4 Conversion of toluene (methylbenzene)

Toluene was converted by the purified *Pab*UPOs in a reaction mixture (total 250 µL in 2-mL HPLC vials) consisting of 20 mM potassium phosphate buffer (pH 7.0), 1.0 mM toluene in 5.0% ACN, 5.0 mM ascorbic acid, 0.5 U mL^{-1} of the respective *Pab*UPO and 1.0 mM H_2O_2. The reaction was started by the addition of enzyme to the reaction mixture containing buffer, substrate, ascorbic acid and H_2O_2. The reaction was constantly stirred at room temperature for 10 min and then analyzed for the corresponding reactions products (chap. 2.9.1.2).

2.8.5 Conversion of oseltamivir

Oxidative ester-cleavage within the pharmaceutically relevant molecule of oseltamivir[12], a special case of *O*-dealkylation, was so far only shown for the UPO of the ink-cap *Coprinellus radians* (*Cra*UPO; Poraj-Kobielska et al. 2011). The reaction was carried out with purified *Pab*UPOs in a reaction mixture (total 250 µL in 2-mL HPLC vials) consisting of 25 mM potassium phosphate buffer (pH 7.0), 0.5 mM oseltamivir [ethyl (3*R*,4*R*,5*S*)-4-acetamido-5-amino-3-pentan-3-yloxycyclohexene-1-carboxylate], 1.0 U mL^{-1} of the respective *Pab*UPO and 1.0 mM H_2O_2. The reaction was started by adding the enzyme to the reaction mixture comprising buffer, substrate and H_2O_2. The reaction was stirred at room temperature for 10 min and then analyzed for the corresponding reactions products (i.e. ester fission products, chap. 2.9.1.3). For comparison, several wild-type UPOs (*Cra*UPO, *Aae*UPO, *Mro*UPO) and a recombinant UPO (r*Cci*UPO) were tested under identical conditions.

2.8.6 Oxidation of 5-formyl-2-furancarboxylic acid (FFCA)

The oxidation of FFCA, a precursor of PET-analogous plastics[13], was tested by purified *Pab*UPOs. The reaction mixture (total 500 µL in 2-mL HPLC vials) consisted of 50 mM potassium phosphate buffer (pH 6.0), 2.0 mM FFCA, 1.0 U mL^{-1} of the respective

[12] The shikimic derivative oseltamivir (brand name Tamilflu®) is an antiviral medication used to treat/prevent influenza.
[13] PET – polyethylene terephthalate

*Pab*UPOs (or *Aae*UPO as a positive control) and 1.0 mM H_2O_2. The reaction was started by the addition of H_2O_2, which was pumped constantly via a syringe pump over a total reaction time of 2.0 hours. The pH-optimum for this reaction was determined as already described under 2.6.3.1.

2.9 High performance liquid chromatography (HPLC)

Quantification of substrates and products obtained after the enzymatic reactions was performed by high performance liquid chromatography (HPLC) using an AGILENT Series 1200 instrument equipped with diode array (DAD) and mass detectors (AGILENT TECHNOLOGIES Deutschland GmbH, Böblingen, Germany). Substrate or product identification and quantification occurred using authentic standards based on their retention times, UV-Vis spectra as well as on their mass spectral data obtained by a electrospray ionization mass spectrometer (ESI-MS) (AGILENT TECHNOLOGIES Deutschland GmbH, Böblingen, Germany).

2.9.1 Reversed phase high performance liquid chromatography (RP-HPLC)

2.9.1.1 Halogenation of phenol and oxygenation of naphthalene

To analyze the reaction products formed during the enzymatic halogenation of phenol and the conversion of naphthalene, a KINETEX® 2.6 µm Phenyl-Hexyl column (75 × 2.1 mm, 100 Å, PHENOMENEX, Aschaffenburg, Germany) was used. The elution occurred at 40°C with a flow rate of 0.6 mL min^{-1}. The solvent consisting of H_3PO_4 (0.1%, v/v) and ACN (17% and 30% for phenol and naphthalene, respectively) was used under isocratic conditions with a running time of 5 min and 6 min, respectively. Products of phenol oxidation and halogenation were identified and quantified using authentic 1,4-benzoquinone, 2-bromophenol and 4-bromophenol as well as 2-chlorophenol and 4-chlorophenol as standards. In the case of naphthalene oxidation and oxygenation, 1,4-naphthoquinone, 1-naphthol and 2-naphthol were used as standards.

2.9.1.2 Oxygenation of anisole and toluene

For product identification and quantification, after enzymatic oxygenation of anisole and toluene, a Kinetex 2.6 µm F5 column (50 x 2.1 mm, 100Å, PHENOMENEX) was used. Anisole was eluted from the column at 40°C and a flow rate of 0.6 mL min^{-1}; the solvent was a mixture of aqueous H_3PO_4 (0.1%, v/v) and ACN applied via following program:

100:0 for 4 min, followed by a 8-min linear gradient to 15% ACN and a 2-min linear gradient to 95% ACN, which was held for 1 min. Toluene analysis was performed with a mixture of aqueous H_3PO_4 (0.1%) and ACN using following program: 95:5 for 0.5 min, followed by a 8-min linear gradient to 70% ACN, which was held for 1 min. 4-Hydroxyanisole, hydroquinone and 1,4-benzoquinone were used as standards of anisole conversion and benzyl alcohol, benzaldehyde, benzoic acid, *p*-cresol and *o*-cresol as well as methylhydroquinone for analyzing enzymatic toluene oxidation.

2.9.1.3 Conversion of oseltamivir

Oseltamivir conversion was followed by using a LUNA 5 µm C18 column (150 × 2 mm, PHENOMENEX). The column was eluted at a flow rate of 0.35 mL min^{-1} and 40°C with aqueous ammonium formate (0.01% v/v; pH 3.5) and ACN in a ratio of 95:5 for 5 min, followed by a 25-min linear gradient to 100% ACN. Product formation was followed by mass spectroscopic determination in the positive ESI mode in the mass range from 70 to 500, step size 0.1, at drying gas temperature of 350°C and capillary voltage of 4,000 V.

2.9.1.4 Conversion of 5-formyl-2-furancarboxylic acid (FFCA)

To analyze the reaction products formed during the enzymatic oxidation of FFCA, a RESEX column [ROA-Organic acid H^+ (8%), PHENOMENEX] was used. The column was eluted at 50°C with a flow rate of 0.75 mL min^{-1} and 0.05 N H_2SO_4 as eluent under isocratic conditions. Authentic 2,5-furandicarboxylic acid (FDCA) was used as standard.

2.9.2 Size exclusion chromatography - high performance liquid chromatography (SEC-HPLC)

To prove homogeneity of the purified proteins and to determine their molecular size under native conditions, size exclusion chromatography (SEC) was performed in combination with an HPLC system (chap. 2.7) fitted with a YARRA™ 3 µm column SEC-2000 (300 × 7.8 mm, PHENOMENEX) under isocratic conditions. The mobile phase consisted of 100 mM sodium acetate, 100 mM NaCl (pH 6.8) and elution was achieved at a flow rate of 1 mL min^{-1}. The Gel Filtration LMW Calibration Kit of GE HEALTHCARE was used as protein reference material.

2.10 Molecular work

2.10.1 Identification of isolated fungi

Identification of the isolated fungi (chap. 2.2.2) was carried out in two ways; firstly by examining the morphology and microscopic features of dried fruiting bodies including basidiospores (in cooperation with A. Melzer, a worldwide leading expert in the family of Psathyrellaceae), and secondly, by using molecular methods, i.e. ITS sequencing.

2.10.2 ITS sequencing

The complete internal transcribed spacer (ITS) region including the 5.8S rRNA gene sequence was analyzed to taxonomically identify the collected Kenyan fungal strains. For this purpose, the isolates were grown on MA medium and genomic DNA was extracted from 100 mg of the respective fungal biomass using the peqGOLD Fungal DNA mini Kit (VWR, Darmstadt, Germany) according to manufacturer's directions. PCR amplification was carried out in a total volume of 25 µL consisting of 12.5 µL Taq Green Master Mix 2x, 1.0 µL template, 10.5 µL nuclease-free H_2O and 0.5 µL ITS4 and ITS5 primers (each 10 mM; White et al. 1990) under following cycling conditions: initial denaturation step at 94°C for 2 min, followed by 35 cycles of a 30 sec denaturation step at 94°C, a 30 seconds annealing step at 55°C and a 1 min elongation step at 72°C. A 10 min elongation step at 72°C followed by a termination at 4°C. Then the amplified amplicons were sent to LGC Genomics and sequenced using the SANGER method, and the obtained sequences were blasted (blastn) against known sequences in the NCBI database to achieve the species or in some cases only the genus identification.

2.10.3 DNA isolation and genome sequencing

Genomic DNA from *P. aberdarensis* and *X. grammica* was obtained after cultivation of both fungi in liquid MA medium (20 g L^{-1} MA in A. dest., 200 mL; chap. 2.2.1) in round flasks (500 mL) at 23°C on a rotary shaker (chap. 2.2.3). The harvested mycelium was freeze-dried and the genomic DNA was extracted using the cetyltrimethylammonium bromide (CTAB) protocol (Lee et al. 1988). The genomic DNA obtained was fragmented using a focused ultra sonicator (Covaris S2, Woburn, MA, USA) to generate a 200-bp fragment library with the Ion Plus fragment library kit (THERMOFISHER, Darmstadt, Germany). The fragmented gDNA was purified with AGENCOURT® AMPure® XP

(BECKMAN, Krefeld, Germany) and the fragment size was analyzed using an AGILENT 2100 Bioanalyzer (AGILENT, Santa Clara, CA, USA). Adapters were ligated and blunt-end nick-repaired with the Ion Plus Fragment Library Kit. The ligated DNA was again purified as described above. Afterwards, 300 bp fragments were selected and collected on a SizeSelect agarose E-Gel® (THERMOFISHER SCIENTIFIC, Waltham, MA, USA). The obtained fragments were further amplified and later quantified. The ion sphere particles (ISPs) were prepared as directed, and the enriched template-positive ISPs were sequenced using an ION TORRENT® Personal Genome Machine (PGM) (LIFE TECHNOLOGIES, Grand Island, NY, USA) with a 316™v2 chip according to the manufacturer's protocols.

2.10.4 Assembly and genome annotation

The initial assembly of obtained reads was carried out using MIRA 4.0 (Chevreux et al. 1999) integrated into GENEIOUS R10 (Kearse et al. 2012). A second assembly step using the GENEIOUS R10 assembler on a high sensitivity setting was then performed to filter duplicate contigs and join ends of the 1st assembly step. The quality of the obtained assembly was analyzed using BUSCO (Simão et al. 2015), while QUAST was used to evaluate the genome statistics (Gurevich et al. 2013). The protein-coding genes were predicted using AUGUSTUS and the predictors *Coprinus cinerea* and *Aspergillus nidulans* for the *P. aberdarensis* and *X. grammica* genomes, respectively (Stanke et al. 2004). After identification of the protein coding sequences, Blast2GO was used to annotate the proteins and to identify genes of interest (mainly lignocellulolytic enzymes; Riley et al. 2014) in the respective genomes. CAZy enzymes in the two genomes were determined using the web interface dbCAN (Yin et al. 2012). To identify the putative signal sequences and N-glycosylation sites in the identified UPO and DyP genes in the genomes of *P. aberdarensis* and *X. grammica*, the predictive algorithm signal P and the NetNglyc 1.0 server were used, respectively (Nielsen et al. 1997, Gupta et al. 2004). The raw data and genome assembly of *P. aberdarensis* and *X. grammica* are accessible at National Center for Biotechnology Information under the accession numbers SDEE01000000 and RYZI00000000 in the case of *P. aberdarensis* and *X.* grammica, respectively under the following Bioprojects: PRJNA516162 and PRJNA510724.

2.11 Phylogenetic analysis

A phylogenetic analysis of 43 Kenyan fungal isolates (Basidiomycota, Ascomycota and Mucoromycotina) was carried out using the ITS regions of the ribosomal DNA (chap. 2.10.2). Sequences were aligned using MAFFT 7.388 (Katoh et al. 2002). The phylogenetic neighbor-joining tree based on the Jukes-Cantor distance estimation model and on the MAFFT alignment was constructed using GENEIOUS R10 software.

A total of 77 (fungal) and 26 (fungal and bacterial) UPO and DyP amino acid sequences, respectively, were used to analyze the identities and similarities of the 48 UPO and three DyP sequences identified in the genomes of *P. aberdarensis* and *X. grammica*. Comparative sequences were obtained from NCBI (National Centre for Biotechnology Information).

2.12 Homology modelling

Homology modeling of protein 3D-structures was performed based on the amino acid sequences of *Pab*UPO genes *g7491* and *g8283* as well of *Xgr*DyP gene 488 using the webserver I-TASSER (Zhang 2008). As templates, crystal structures of *Aae*UPO (PDB structure ID, 2YOR; ~61 and 56% identity as well as ~ 77 and 83% similarity to *Pab*UPO I and II), *Mro*UPO (PDB 5FUJ) and *Bad*DyP (PDB structure ID, 2D3Q_A; ~43 and 56% identity and similarity to *Xgr*DyP) were used. The resulting protein models were superimposed and adjusted using PyMOL (The PyMOL Molecular Graphics System, Version 2.2.0 Schrödinger, LLC; http://pymol.org/) with the above mentioned template sequences.

3 RESULTS

3.1 Isolation and identification of fungal strains

In this study, 43 fungal strains were collected (from 21 families) in three natural forests (protected areas) in Kenya: KAKAMEGA, ABERDARES, and ARABUKO SOKOKE. Based on sequencing of the ITS region including the 5.8S rRNA (chap. 2.10.2), these fungi could be grouped into three major divisions (phyla) of the true fungi (Eumycota): Basidiomycota, Ascomycota, and 'Zygomycota' (subphylum Mucoromycotina). Among the 17 basidiomyceteous isolates, six are belonging to the family Polyporaceae (*Fomitopsis meliae, Lentinus squarrosulus, Lentinus tigrinus, Microporus subaffinis, Trametes gibbosa* and an undetermined polyporous species - strain AS024a), three to the Psathyrellaceae (*Coprinellus micaceus, Psathyrella candolleana* and a *Psathyrella* sp.), and one species each to the families Physalacriaceae (*Cribbea* sp.), Omphalotaceae (*Gymnopus brunneigracilis*), Peniophoraceae (*Peniophora* sp.), Phanerochaetaceae (*Phanerochaete australis*), Meruliaceae (*Phlebia subserialis*), Hymenogastraceae (*Psilocybe ovoideocystidiata*), Schizophyllaceae (*Schizophyllum* sp.) and Strophariaceae (*Stropharia rugosoannulata*) (Tab. 3.1 and Tab. 3.3). Of the 20 ascomyceteous isolates, six species were identified as *Fusarium* spp. (*F. equiseti, F. equiseti, F. solani* and three not further identifiable *Fusarium* spp.*)* belonging to the family Nectriaceae; the species *Clonostachys buxi* and *Clonostachys rosea* are members of the Bionectriaceae and two *Cochliobolus* species belong to the Pleosporaceae. The families of Didmellaceae and Pestalotiopsidaceae are represented by two *Epicoccum* spp. and two *Pestalotiopsis* spp., respectively. Furthermore, two species of the family Xylariaceae, *Xylaria grammica* and *X. ophiopoda*, were identified as well as *Pseudallescheria boydii* (family Microascaceae) and a *Phialocephala* sp. in the family Vibrisseaceae. *Stagonosporopsis cucurbitacearum* (two strains) is a species of uncertain family affiliation (*incertae sedis*) (Tab. 3.4). The six Mucoromycotina species were found to belong to four representatives of the Mucoraceae (*Mucor* sp.), *Umbelopsis isabellina* (family Umbelopsidaceae) and *Gongronella* sp. (family Cunninghamellaceae) (Tab. 3.4).

Tab. 3.1: Kenyan fungi isolated in this study and identified by ITS sequencing. *Phialocephala* sp. is not included.

Fungal taxonomy	Isolate label	GenBank match (ITS-5.8S)		
		Reference taxa (RT)	Accession no. of RT	Identity %
Agaricomycetes	AS011	*Fomitopsis meliae*	KC585351.1	98%
Agaricomycetes	K057	*Lentinus squarrosulus*	KM267727.1	81%
Agaricomycetes	K027	*Lentinus tigrinus*	AF516518.1	94%
Agaricomycetes	AS010	*Microporus subaffinis*	KU055646.1	88%
Agaricomycetes	AS024a	*Polyporales* sp.	JQ312137.1	94%
Agaricomycetes	AS015	*Trametes gibbosa*	KT804577.1	99%
Agaricomycetes	AB040	*Coprinellus micaceus*	EU551214.1	99%
Agaricomycetes	AB011	*Psathyrella candolleana*	KF281384.1	96%
Agaricomycetes	AB031	*Psathyrella aberdarensis*	MH880928.1	100%
Agaricomycetes	AB025(2)	*Cribbea* sp.	DQ328156.1	92%
Agaricomycetes	AS007	*Gymnopus brunneigracilis*	AY263434.1	97%
Agaricomycetes	AB007	*Peniophora* sp.	KJ654577.1	96%
Agaricomycetes	K010	*Phanerochaete australis*	KP135075.1	99%
Agaricomycetes	K031	*Phlebia subserialis*	KR093857.1	100%
Agaricomycetes	K054	*Psilocybe ovoideocystidiata*	HE994451.1	94%
Agaricomycetes	AB045	*Schizophyllum* sp.	FJ196608.1	99%
Agaricomycetes	AB024	*Stropharia rugosoannulata*	MH860190.1	98%
Sordariomycetes	K059	*Clonostachys buxi*	KM231840.1	99%
Sordariomycetes	K006	*Clonostachys rosea*	KP760058.1	99%
Sordariomycetes	AS006	*Pestalotiopsis photiniae*	AY682944.1	99%
Sordariomycetes	K002	*Pestalotiopsis* sp.	MH368111.1	99%
Sordariomycetes	K065	*Pseudallescheria boydii*	KJ415569.1	99%
Sordariomycetes	K043	*Xylaria grammica*	JQ341087.1	99%
Sordariomycetes	K046	*Xylaria ophiopoda*	GU322461.1	88%
Sordariomycetes	AB022	*Fusarium equiseti*	KX196808.1	99%
Sordariomycetes	AB049	*Fusarium equiseti*	MH128127.1	99%
Sordariomycetes	K038	*Fusarium solani*	KU382502.1	99%
Sordariomycetes	AS023a	*Fusarium* sp.	JX914476.1	99%
Sordariomycetes	AB041	*Fusarium* sp.	MH605341.1	98%
Sordariomycetes	K042(1)	*Fusarium* sp.	FJ210627.1	99%
Dothideomycetes	AB017	*Cochliobolus miyabeanus*	JQ753706.1	93%
Dothideomycetes	AB039	*Cochliobolus* sp.	KT199720.1	98%
Dothideomycetes	AB044	*Epicoccum nigrum*	KM246284.1	99%
Dothideomycetes	K013	*Epicoccum* sp.	KC178651.1	99%
Dothideomycetes	AB025	*Stagonosporopsis cucurbitacearum*	KX866895.1	99%

Dothideomycetes	AB038	*Stagonosporopsis cucurbitacearum*	KM246252.1	99%
Incerte sedis	AB013	*Mucor fragilis*	KX421451.1	99%
Incerte sedis	K033	*Mucor nederlandicus*	JN206176.1	98%
Incerte sedis	AB047	*Mucor* sp.	KY992878.1	97%
Incerte sedis	AB053a	*Mucor* sp.	KF158220.1	99%
Incerte sedis	K049	*Umbelopsis isabellina*	MG098308.1	99%
Mucoromycetes	AB036	*Gongronella* sp.	MH267954.1	98%

3.2 *Psathyrella aberdarensis*: a new species of Psathyrellaceae

3.2.1 Diagnosis of *Psathyrella aberdarensis*

Interestingly, one of the two isolated *Psathyrella* species could not be properly identified using BLAST analysis (Fig 3.1). Upon additional microscopic and morphologic examination, this fungus was found to be a new *Psathyrella* species that has not been described so far. In cooperation with a renowned *Psathyrella* specialist, Andreas Melzer, the 'first description' of this new species was carried out and the fungus named according to its collection site '*Psathyrella* cf. *aberdarensis*' (Melzer et al. 2018). It turned out that the fungus is closely related to the species complex around *P. candolleana*. These Psathyrellae are characterized by the presence of a gill edge predominantly composed of utriform to sub-cylindrical marginal cells and the absence of pleurocystidia (Smith 1972). With the exception of *P. typhae*, *P. leucotephra* and *P. aberdarensis*, the complex comprises several morphologically hardly distinguishable species (Fig 3.1).

3.2.2 Description of *Psathyrella aberdarensis*

Pileus: Up to 10 mm broad, at first conical to campanulate, later flattening, old with an up-rolled margin, reddish brown to brown (about $Y_{50}M_{50}C_{20}$ to $Y_{50}M_{70}C_{30}$), center darker (about $Y_{50}M_{99}C_{60}$). Parts of the universal veil are well recognizable and quite persistent as patches.

Lamellae: Somewhat distant, adnate and brown with white edge.

Stipe: Up to 15 × 1 mm, cylindrical, in the upper part white, in the lower part brownish, base strikingly white tomentose.

Spores: 7.5-8 (-8.8) × 4.4-5 µm, on the average 7.8 × 4.6 µm, Q=1,60-1,75, $Q_{av.}$=1,70. In front view ellipsoid, in side view adaxially slightly flattened, often somewhat

phaseoliform, apiculus tiny, germ pore not visible. In water and ammonia solution pale yellowish brown, in KOH nearly hyaline.

Basidia: 15-16.5 × 6.8-8 µm, 4-spored, clavate to sphaeropedunculate.

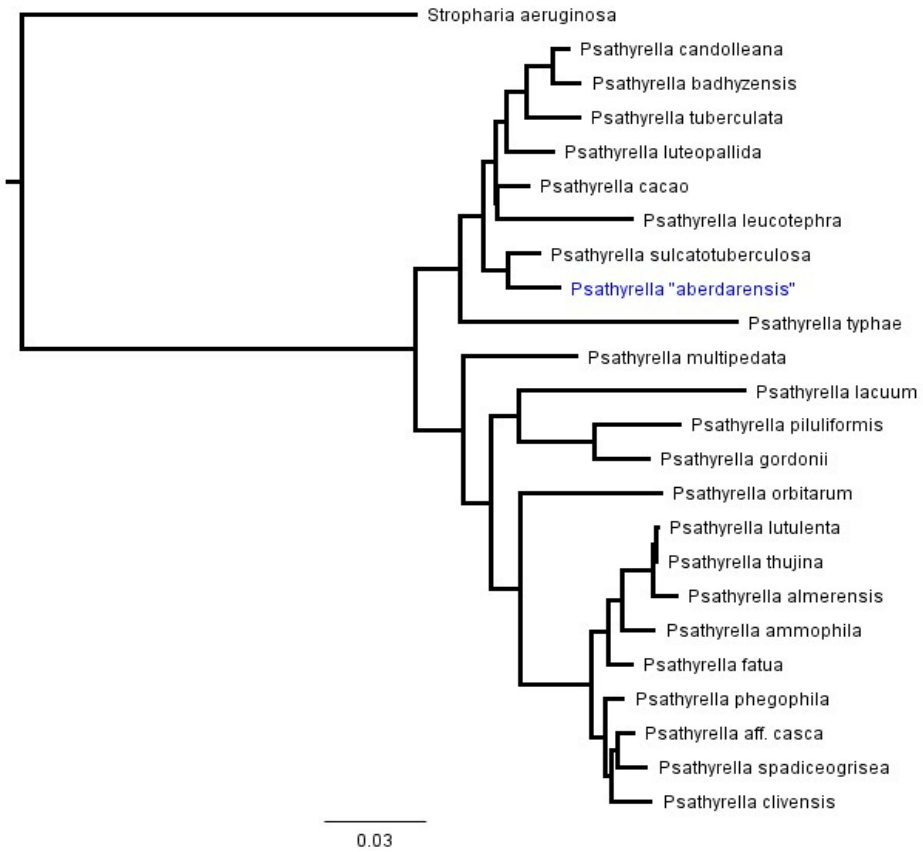

Fig. 3.1: Phylogenetic tree (based on ITS seqq.) showing the distance between different *Psathyrella* species (with an evolutionary distance of 0.03). The tree is rooted with *Stropharia aeruginosa* as outgroup.

Cheilocystidia: 19-33 × 8-12.3 µm, predominantly utriform, rarely lageniform, numerous but moderately crowded, sometimes with small golden-brown deposits. Intermixed with various frequent clavate and sphaeropedunculate cells (paracystidia), 16.5-27 × 9.5-19 µm. All marginal cells thin-walled and colorless.

Pleurocystidia: Absent.

Caulocystidia: 24.5-43.7 × 12.3-16.5 µm, utriform, scattered; sphaeropedunculate and clavate cells are also present, these 19-33 × 11-24.5 µm.

Veil: Made mainly of strongly branched, slightly diverticulate, often thick-walled and brownish pigmented cells, 13.7-50 × 4-11 µm, beside globose elements, these 16.5-30 µm in diameter. All cells appear often slightly to strongly encrusted.

Clamps: Present (e.g. in the mycelium and the veil).

Habitat: Gregarious on dead wood (coarse woody debris, fallen twigs).

Fig. 3.2: Fruiting bodies of *Psathyrella aberdarensis* (Photo: Karich 2017)

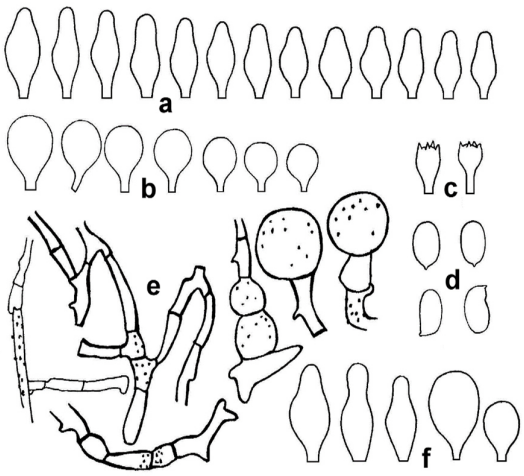

Fig. 3.3: Microcharacters of *Psathyrella aberdarensis*; (a) cheilocystidia, (b) paracystidia, (c) basidia, (d) spores, (e) veil elements, (f) caulocystidia (drawn by Andreas Melzer 2017, Melzer et al. 2018).

3.3 Enzyme screening and strain selection

The main objective of the present PhD project has been the identification of Kenyan fungal isolates that are capable of producing biotechnologically relevant, extracellular oxidoreductases, specifically peroxygenases, peroxidases and/or laccases. To achieve this, a comprehensive enzyme screening was performed by culturing the fungal isolates on synthetic and complex agar media supplemented with ABTS, Mn^{2+}-ions or humic acids as indicator substances (chap. 2.2.4; ABTS-SMA, ABTS-KMA; Mn^{2+}-SMA, Mn^{2+}-KMA, HA-SMA, HA-KMA). In a second screening step, fungi were cultured in a complex liquid, peptone-containing medium that is known to stimulate the production of oxidative enzymes. Enzymatic activities were followed by specific enzyme measurements with NBD and ABTS (chap. 2.3).

Almost all basidiomyceteous strains tested showed positive reactions in the agar plate screening (Fig. 3.4 and Tab. 3.3). ABTS oxidation that is a strong indication for the presence of extracellular oxidoreductases (i.e. laccases and all types of peroxidases) was observed for all isolates, except *Fomitopsis meliae* that is a brown-rot fungus (BRF) and *Schizophyllum* sp. causing an unspecific wood-rot (URF).

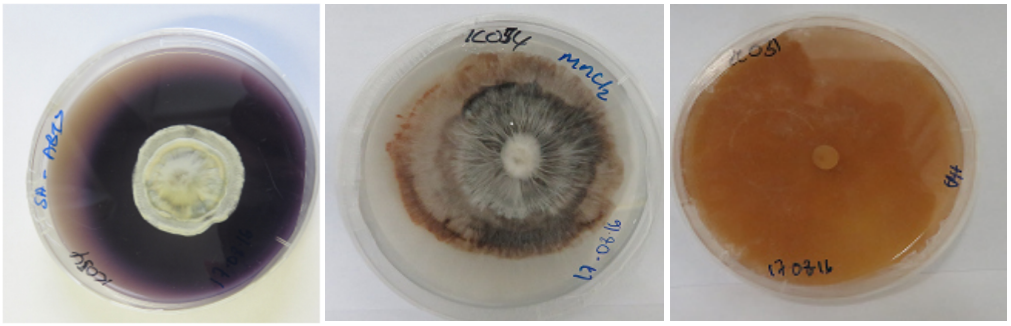

Fig. 3.4: Examples of positive agar plate reactions caused by the enzymatic oxidation of ABTS into a coupling product (left; formation of a violet colored dye), by Mn^{2+} oxidation into Mn^{4+} (MnO_2, middle) and by bleaching of humic acids to form yellowish fulvic acids (right). Color changes were observed in fungal agar plates containing either synthetic KIRK- or complex soybean medium.

The oxidation of Mn^{2+} ions via Mn^{3+} into dark-brown Mn^{4+} (in form of MnO_2, pyrolusite)[14] and the bleaching of humic acids were accomplished in different ways and to different extents by the basidiomycetous isolates. Some of them oxidized both indicator substrates like the four Polyporaceae *Trametes gibbosa*, *Microporus subaffinis, Phlebia*

[14] MnO_2 formation is the result of Mn^{3+} disproportionation: $2\ Mn^{3+} \rightarrow Mn^{4+} + Mn^{2+}$

subseriales and polyporous strain AS024a as well as the agaric *Stropharia rugosoannulata*. Others acted on just one of the indicator substrates such as *Coprinellus micaceus* that oxidized only Mn^{2+} ions or the both *Lentinus* spp. that bleached only humic acids.

Positive reactions of ascomycetous and zygomycetous isolates in the agar plate screening were much less pronounced than those of basidiomycetes (Tab. 3.4). The oxidation of ABTS was only caused by eight isolates among them mainly phytopathogenic representatives like *Fusarium* spp., *Cochliobolus* sp. *Pestalotiopsis* sp. and one of the *Stagonosporopsis curcurbitacearum* strains. The only zygomycetous isolate that caused a positive ABTS reaction was *Mucor fragilis*.

In the second screening approach, all fungal isolates were grown as agitated cultures in a plant-based complex medium (chap. 2.2.3) and every third or fourth day samples were taken for enzyme activity detection (chap. 2.2.3). Two chromogenic substrates absorbing in the visible range were chosen, which allowed rapid evaluation of relevant activities with a plate reader. On one hand, NBD was used as a UPO-specific substrate, on the other hand ABTS was applied, which permits the detection of laccase, manganese-dependent and manganese-independent peroxidases in simple sequential assays (chap. 2.3.). Using the NBD assay, four basidiomycetous species (*Coprinellus micaceus, Trametes gibbosa*, *Psathyrella candolleana* and *P. aberdarensis*) showed a positive reaction due to 4-nitrocatechol formation, i.e. yellow color at pH 7.0 and deep red color after alkalization (pH ~14.0) (Tab 3.3). When using ABTS as substrate, some laccase and DyP activities were found in the absence and presence of H_2O_2, respectively. Interestingly, the latter enzymatic activity was not only found in two basidiomycetes (*Cribbea* sp. and *G. brunneigracilis*; Tab. 3.3) but also in ascomycete *X. grammica* (Tab. 3.4); a low but reproducible UPO activity was also observed for the ascomycetous mold *F. solani*.

UPO and DyP activities observed for the six basidiomycetes and two ascomycetes were confirmed and quantified by the VA and ABTS oxidation assays in cuvette tests in an appropriate spectrophotometer. The three basidiomycetes, *C. micaceus*, *T. gibbosa* and *P. candolleana*, showed relatively low UPO activities <100 U L^{-1} (Fig. 3.5 A-C); the fourth candidate (*P. aberdarensis*), however, secreted a relatively high UPO level of more than 800 U L^{-1} during growth in SPM medium (Fig. 3.5 D). As previously reported for other UPO-producers (e.g. *Agrocybe aegerita*), the increase in UPO activity was accompanied by an alkalization of the medium (from pH 5.5 to pH 8.0). In the case of

P. aberdarensis, this process started on day 12 and lasted until the final day of cultivation (day 24). The low UPO activity of *F. solani* towards NBD detected in the microplate assay could not be verified in the spectrophotometer test. The fungal isolate with the highest UPO activity, *P. aberdarensis*, was used for detailed further studies with regard to production, purification and characterization of the enzyme.

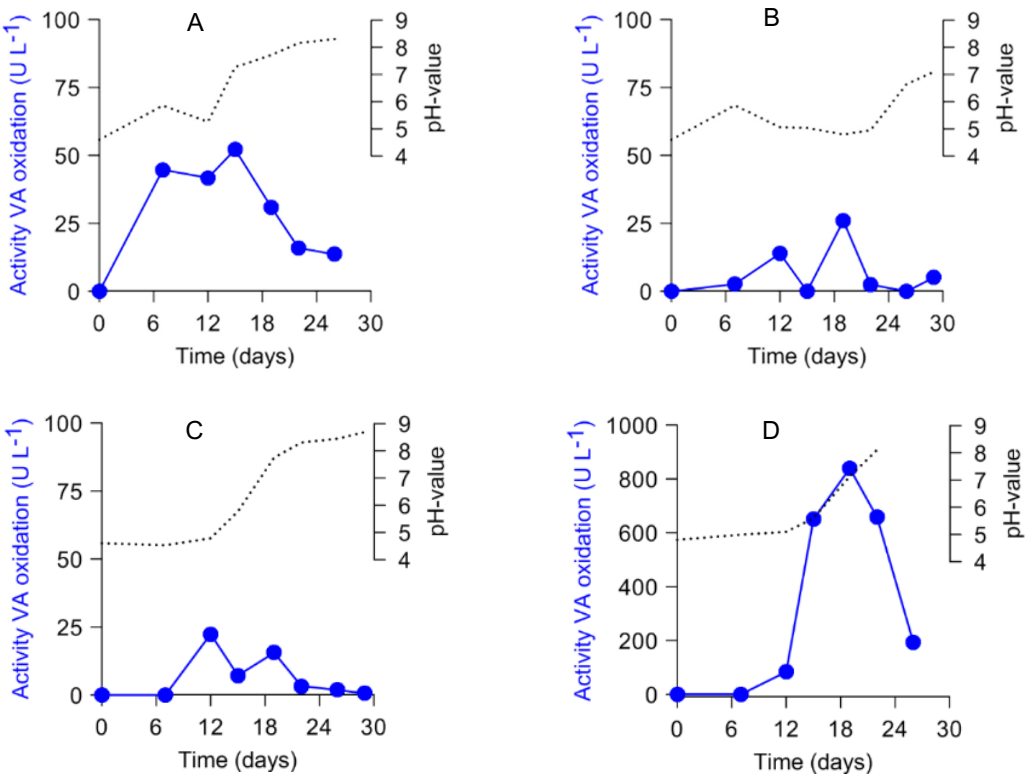

Fig 3.5: Time course of UPO activity (blue circles) in liquid cultures (soybean-peptone medium, SPM) of *Coprinellus micaceus* (A), *Trametes gibbosa* (B), *Psathyrella candolleana* (C) and *P. aberdarensis* (D). Activity was measured with VA, dotted lines mark the time course of pH.

DyP production was highest in cultures of the ascomycete *X. grammica* that secreted up to 750 U L^{-1}, while the basidiomycetes *Cribbea* sp. and *G. brunneigracilis* produced lower levels around 300 U L^{-1} (Fig. 3.6 A-C). Enzyme secretion was again accompanied by alkalization of the medium in all three cases. Particularly, in cultures of *X. grammica*, the pH increased considerably from pH 5.0 on day 12 to 8.9 on day 20; in parallel, the peroxidase activity (DyP) increased from 80 to 750 U L^{-1}. (Fig. 3.6 A). It should be noted that 'true' extracellular peroxidase activity (neither of DyP nor of any other heme peroxidase) has been described so far for an ascomycetous fungus. Therefore, *Xylaria grammica* was chosen for further studies regarding enzyme production, purification and protein characterization.

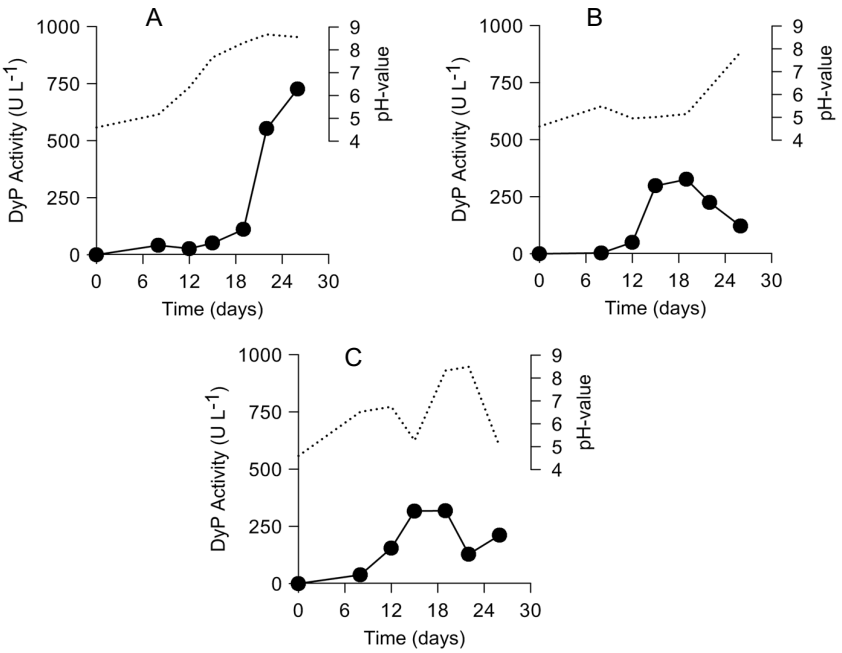

Fig 3.6: Time course of DyP production (black circles) by *Xylaria grammica* (A), *Cribbea* sp. (B) and *Gymnopus brunneigracilis* (C) in SPM medium; activity was measured with ABTS and H_2O_2, dotted lines – pH- value.

Furthermore, the secretion of MnP via the formation of Mn^{3+}-malonate complexes was evidenced for seven fungi belonging to the order Polyporales and Agaricales (maximum activity of ~6,000 U L^{-1} for *S. rugosoannulata* and minimum activity of ~15 and 40 U L^{-1} for *M. subaffinis* and *T. gibbosa*, respectively; Tab. 3.2 and Fig. A.1).

Tab. 3.2: Maximum MnP activities detected by the oxidation of Mn^{2+} into Mn^{3+} for seven basidiomycetous isolates from Kenyan forests. Measurements were carried out in sodium malonate buffer at pH 4.5.

Species	max. MnP activity (U L^{-1})
Cribbea sp.	47
Gymnopus brunneigracilis	683
Microporus subaffinis	14
Stropharia rugosoannulata	6,049
Trametes gibbosa	39
Phlebia subserialis	2,726
Polyporales sp.	4,829

Tab. 3.3: Screening of Kenyan basidiomycetous isolates for secretion of extracellular oxidoreductases.

			Agar plate test[§]				Microplate reader[§§]	
Fungal Strains	Strain Number	Family	ABTS oxidation[a]	Mn^{2+} oxidation[b]	Humic acid bleaching[c]	NBD oxidation[d]	ABTS oxidation	pH of the medium after 26 days
Fomitopsis meliae	AS011	Polyporaceae	-	-	-	-	-	2.18
Lentinus squarrosulus	K057	Polyporaceae	+	-	+	-	+[2]	7.42
Lentinus tigrinus	K027	Polyporaceae	+	-	+	-	+[2]	5.01
Microporus subaffinis	AS010	Polyporaceae	+	+	+	-	-	4.39
Polyporales sp.	AS024a	Polyporaceae	+	+	+	-	-	5.66
Trametes gibbosa	AS015	Polyporaceae	+	+	+	+	+[2]	6.65
Coprinellus micaceus	AB040	Psathyrellaceae	+	+	-	+	+[2]	8.31
Psathyrella candolleana	AB011	Psathyrellaceae	+	-	-	+	+[2]	8.45
Psathyrella aberdarensis	AB031	Psathyrellaceae	+	-	-	+	+[2]	8.40
Cribbea sp.	AB025(2)	Physalacriaceae	+	+	-	-	+[2]	7.87
Gymnopus brunneigracilis	AS007	Omphalotaceae	+	-	-	-	+[2]	5.22
Peniophora sp.	AB007	Peniophoraceae	+	-	-	-	-	5.00
Phanerochaete australis	K010	Phanerochaetaceae	+	-	-	-	-	4.74
Phlebia subserialis	K031	Meruliaceae	+	+	+	-	+[1]	7.38
Psilocybe ovoideocystidiata	K054	Hymenogastraceae	+	+	-	-	-	7.73
Schizophyllum sp.	AB045	Schizophyllaceae	-	-	-	-	+[1]	8.42
Stropharia rugosoannulata	AB024	Strophariaceae	+	+	+	-	+[2]	5.09

[§]Agar plate screening was performed with pure cultures of the fungal isolates: [a] Formation of dark violet zones of oxidized ABTS ($ABTS^{2+}$, dication) around and below the fungal mycelium, [b] Development of brown spots of MnO_2, [c] Decolorization of dark brown humic acids under formation of yellowish fulvic acids; (+) positive reaction, (-) no reaction, -* negative on ABTS-SMA but positive on ABTS-KMA plates. [§]Microtiter plate screening was performed analogously to the enzyme assays but in smaller volumes: [d] Colour change of NBD via hydroxylation and demethylenation to the yellow and red modifications of 4-nitrocatechol, without and after addition of sodium hydroxide, respectively; formation of the darkgreen ABTS cation radical ($ABTS^{+\bullet}$) in the [1] absence or [2] presence of H_2O_2 (100 µM). ND - not determined.

Tab. 3.4: Screening of Kenyan ascomycetous and zygomycetous isolates for secretion of extracellular oxidoreductases.

			Agar plate§		Microplate§§			
Fungal Strains	Strain Number	Family	ABTS oxidation[a]	Mn^{2+} oxidation[b]	Humic acid bleaching[c]	NBD oxidation[d]	ABTS oxidation	pH of the medium after 26 days
Clonostachys buxi	K059	Bionectriaceae	-	ND	ND	-	-	9.12
Clonostachys rosea	K006	Bionectriaceae	-	ND	ND	-	-	8.67
Cochliobolus miyabeanus	AB017	Pleosporaceae	+	ND	ND	-	-	8.27
Cochliobolus sp.	AB039	Pleosporaceae	+	ND	ND	-	-	8.67
Fusarium equiseti	AB022	Nectriaceae	-	ND	ND	-	-	8.49
Fusarium equiseti	AB049	Nectriaceae	+	ND	ND	-	-	9.06
Fusarium solani	K038	Nectriaceae	-*	ND	ND	+[2]	-	8.85
Fusarium sp.	AS023a	Nectriaceae	-	ND	ND	-	-	8.86
Fusarium sp.	AB041	Nectriaceae	-	ND	ND	-	-	8.61
Fusarium sp.	K042(1)	Nectriaceae	+	ND	ND	-	-	8.69
Epicoccum nigrum	AB044	Didymellaceae	-	ND	ND	-	-	9.03
Epicoccum sp.	K013	Didymellaceae	-	ND	ND	-	-	7.12
Mucor fragilis	AB013	Mucoraceae	+	ND	ND	-	-	8.12
Mucor nederlandicus	K033	Mucoraceae	-	ND	ND	-	-	8.19
Mucor sp.	AB047	Mucoraceae	-	ND	ND	-	-	8.74
Mucor sp.	AB053a	Mucoraceae	-	ND	ND	-	-	8.62
Gongronella sp.	AB036	Cunninghamellaceae	-	ND	ND	-	-	8.49

Pestalotiopsis photiniae	AS006	Pestalotiopsidaceae	-	ND	ND	-	-	8.23
Pestalotiopsis sp.	K002	Pestalotiopsidaceae	+	ND	ND	-	-	8.04
Phialocephala sp.	K023	Vibrisseaceae	-	ND	ND	-	-	8.67
Pseudallescheria boydii	K065	Microascaceae	+	ND	ND	-	-	8.87
Stagonosporopsis cucurbitacearum	AB025	Incertae sedis	-*	ND	ND	-	-	8.82
Stagonosporopsis cucurbitacearum	AB038	Incertae sedis	+	ND	ND	-	-	8.94
Umbelopsis isabellina	K049	Umbelopsidaceae	-	ND	ND	-	-	4.03
Xylaria grammica	K043	Xylariaceae	-*	ND	ND	-	+[2]	8.56
Xylaria ophiopoda	K046	Xylariaceae	-*	ND	ND	-	-	8.66

§Agar plate screening was performed with pure cultures of the fungal isolates: [a] Formation of dark violet zones of oxidized ABTS ($ABTS^{2+}$, dication) around and below the fungal mycelium, [b] Development of brown spots of MnO_2, [c] decolorization of dark brown humic acids under formation of yellowish fulvic acids; (+) positive reaction, (-) no reaction, -* negative on ABTS-SMA but positive on ABTS-KMA plates.§§ Microtiter plate screening was performed analogously to the enzyme assays but in smaller volumes: [d] Colour change of NBD via hydroxylation and demethylenation to the yellow and red modifications of 4-nitrocatechol, without and after addition of sodium hydroxide, respectively; formation of the darkgreen ABTS cation radical ($ABTS^{+\bullet}$) in the [1] absence or [2] presence of H_2O_2 (100 µM). ND - not determined.

3.4 Optimization of UPO production by *Psathyrella aberdarensis*

To obtain sufficient amounts of the UPO from *P. aberdarensis* (*Pab*UPO) for its purification and characterization, the possibility of producing the enzyme at larger scale was tested in a 30-L-stirred tank bioreactor in SPM (chap. 2.2.3 and 2.4). After seven culture days, the activity started to increase up to a maximum of approx. 280 U L^{-1} on day 17 (Fig. 3.7). The activity increase was at first accompanied with a slight decrease in pH from 6.0 to 5.2 over seven days followed by a pronounced pH increase to 8.0. The same phenomenon was already reported for other UPO-producing fungi and observed as well for *P. aberdarensis* within the screening described above (chap. 3.3). In addition to UPO activities, low and fluctuating levels of laccase were detected starting on day six and reaching 50 U L^{-1} on day 17 (Fig. 3.7). After UPO activity had reached its maximum of 2,750 total units (detected with VA, chap. 2.3.3), the culture liquid (about eleven liters in total) was harvested. The up-scaling of *Pab*UPO production by using the 30-L fermentation device led to an approx. three-fold lower volume activity compared to lab-scale production (~800 U L^{-1}) in 500-mL flasks.

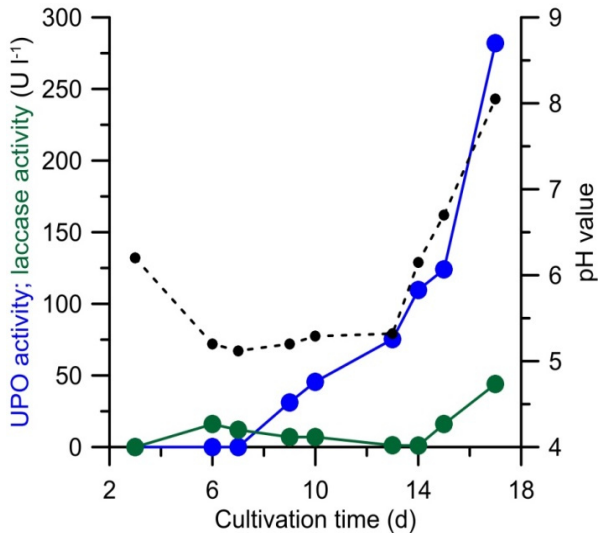

Fig. 3.7: Time course of UPO activity (blue circles) of *P. aberdarensis* in a 30-L stirred tank bioreactor in soy-peptone medium (SPM); green circles – laccase activity, dotted line – pH.

3.5 Purification of *Psathyrella aberdarensis* UPO (*Pab*UPO)

The culture liquid of *P. aberdarensis* harvested from the bioreactor was filtered to separate the enzyme-containing crude extract from the fungal biomass; the liquid obtained was frozen and stored at -20 °C until enzyme purification. The freezing and thawing step led to the partial removal of slime polysaccharides by precipitation and was accompanied by an activity loss of 4% (100 total units, i.e. 2,650 units remained). After centrifugation, the crude extract was concentrated and dialyzed by ultrafiltration and diafiltration, and then applied to a five-step purification approach using an FPLC system fitted with anion exchange (Q-Sepharose, MonoQ) as well as size exclusion chromatography (SEC) columns. The first purification step on an anion exchanger removed the dark-colored material obviously originating from soy-peptone ingredients in the culture medium (Fig. 3.8).

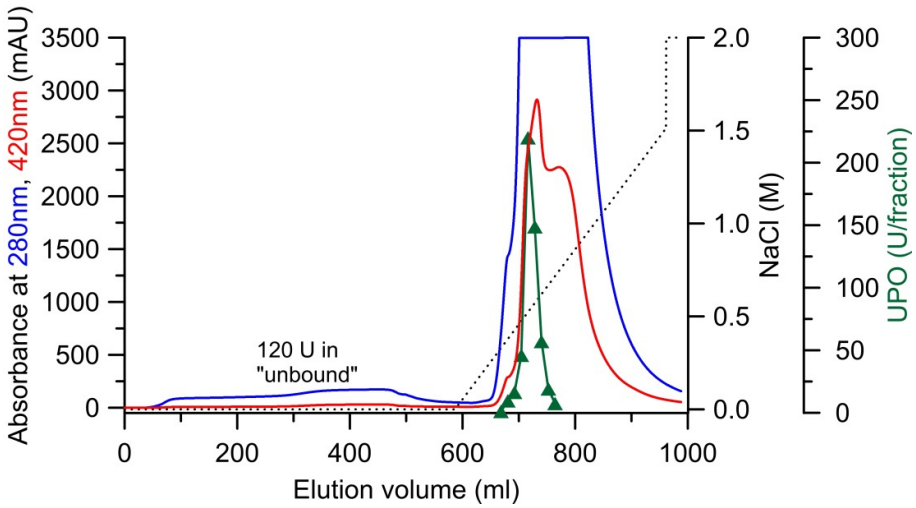

Fig. 3.8: FPLC elution profile of the first purification step of *Pab*UPO on a Q-Sepharose column. Absorption (in mAU) of total protein at 280 nm (blue) and of heme 420 nm (red), UPO activity measured with VA (green), NaCl gradient (dashed line).

By using Q-Sepharose as first purification matrix, a fair enzyme recovery was achieved with approx. 90% of the initial UPO activity bound to the column. That way two UPO fractions were obtained while just a low amount of enzyme (4.5%, 120 total units) was recovered in the unbound fraction (Fig. 3.9). Subsequently, purification to apparent homogeneity was accomplished with MonoQ and SEC columns resulting in three *Pab*UPO isoforms designated as *Pab*UPO I, II and III (Fig. 3.9 & 3.11).

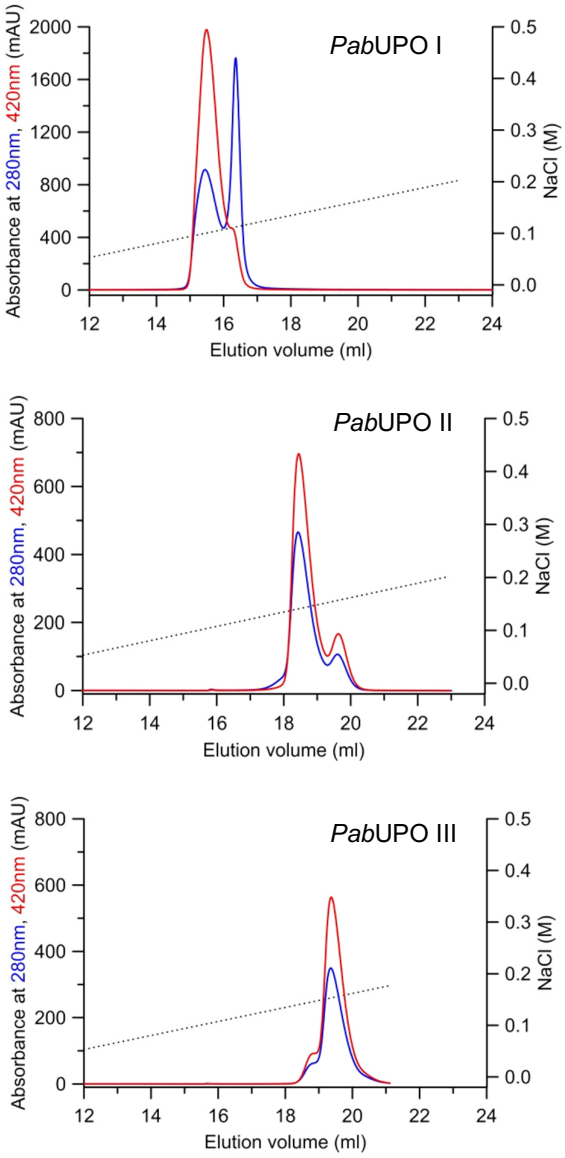

Fig. 3.9: FPLC elution profiles of the 5th and 6th (last) purification step of the three UPO isoforms from *P. aberdarensis* (*Pab*UPO I, II and III) using a MonoQ column (5×50 mm). Absorption (mAU) at 280 nm (blue, total protein) and 420 nm (red, heme), NaCl gradient (dashed line).

The purified protein fractions exhibited specific activities (VA) between 74 and 117 U mg^{-1} with purification factors from 31 to 49 (Tab. 3.5). Final activities obtained ranged between 58 and 198 total units, which corresponds to 1-3 mg total protein.

Tab. 3.5: Purification of three UPO isoforms from *P. aberdarensis* (*Pab*UPO I, II and III).

Purification step	Total Activity (U)	Specific activity (U mg^{-1})	Total protein (mg)	Yield (%)	Purification (x-fold)
Culture filtrate	2,772	2.4	1161	-	-
Ultrafiltrate (10 kDa)	2,717	2.7	1022	98	1.1
Q-Sepharose bound	2,584	9.9	261	93	4.1
MonoQ 10/100-1	421	20.2	21	15	8.5
MonoQ 10/100-2	981	27.8	35	35	11.7
SEC I	347	28.6	12	13	12.0
SEC II	513	137.8	4	19	57.7
MonoQ 5/50-1 I	198	73.7	3	7	30.8
MonoQ 5/50-2 II	90	116.8	1	3	48.9
MonoQ 5/50-2 III	58	97.5	1	2	40.8
Q-Sepharose unbound	1,093	8.9	123	39	3.7
MonoQ *unbound*	60	0.5	133	2	0.2

3.6 UV-visible spectra of the *P. aberdarensis* UPOs

The three UPO isoforms displayed the typical UV-Vis spectrum of resting-state heme thiolate proteins with the Soret bands between 416 and 420 nm (as an example, the spectrum of *Pab*UPO I is given in Fig. 3.10).

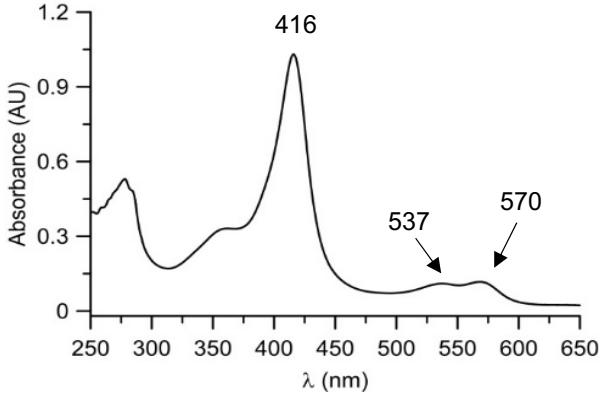

Fig. 3.10: UV-Vis absorption spectrum of purified *Pab*UPO I (resting state enzyme with Soret band as well as α- and β-bands at 416, 570 and 537 nm).

Further characteristic local maxima, representing the α- and β-bands, were observed at 570/575/574 nm and 537/541/541 nm for *Pab*UPO I, II and III, respectively. '*Reinheitszahl*' values ($RZ_{420/280}$) of the three proteins were calculated to be 1.95, 1.45 and 1.56.

3.7 Electrophoretic analyses of the *P. aberdarensis* UPOs

Homogeneity (purity), molecular mass and isoelectric points (p*I*s) of the three purified proteins (*Pab*UPO 1, II, III) were checked by SDS-PAGE and IEF (chap. 2.6.2). As shown in Fig. 3.11, the almost homogeneous preparations had molecular masses of 40.0, 40.4 and 41.3 kDa and p*I*s of 4.2, 4.0 and 3.8, respectively.

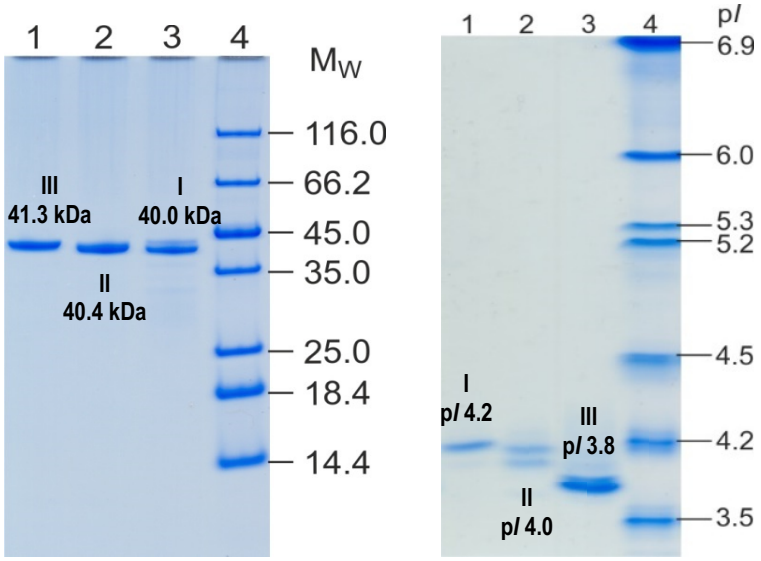

Fig. 3.11: SDS-PAGE gel (left) and IEF gel (right) of the three purified *P. aberdarensis* UPOs (*Pab*UPO I, II and III).

3.8 pH Optima and stabilities of the *P. aberdarensis* UPOs

The three purified *Pab*UPOs were found to oxidize typical peroxidase substrates like ABTS and DMP as well as characteristic UPO substrates like VA and naphthalene. The pH dependency of VA oxidation by the three UPOs is shown in Fig. 3.12. VA oxidation by *Pab*UPO I occurred in a broad pH range between 3.0 and 8.0, and the flat activity maximum appeared between pH 4.5 and 6.0. Optimal pH of VA oxidation by *Pab*UPO II and III showed a narrower maximum at slightly acidic pH (between 5.5 and 6.5). Interestingly, the three *Pab*UPOs exhibited still 60% of their relative activity at rather drastic pH values of 2.0 and 9.0.

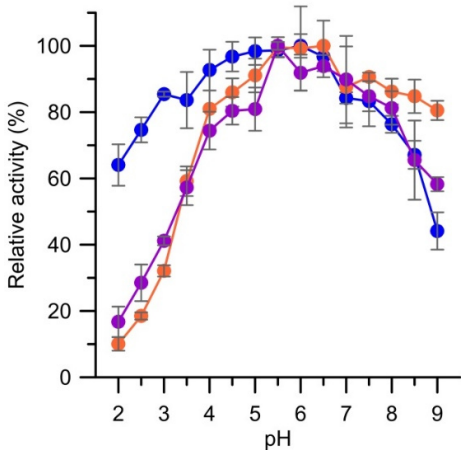

Fig. 3.12: pH-Optima for the oxidation of VA by (**A**) the three UPOs of *P. aberdarensis*: *Pab*UPO I (blue), *Pab*UPO II (orange), *Pab*UPO III (purple).

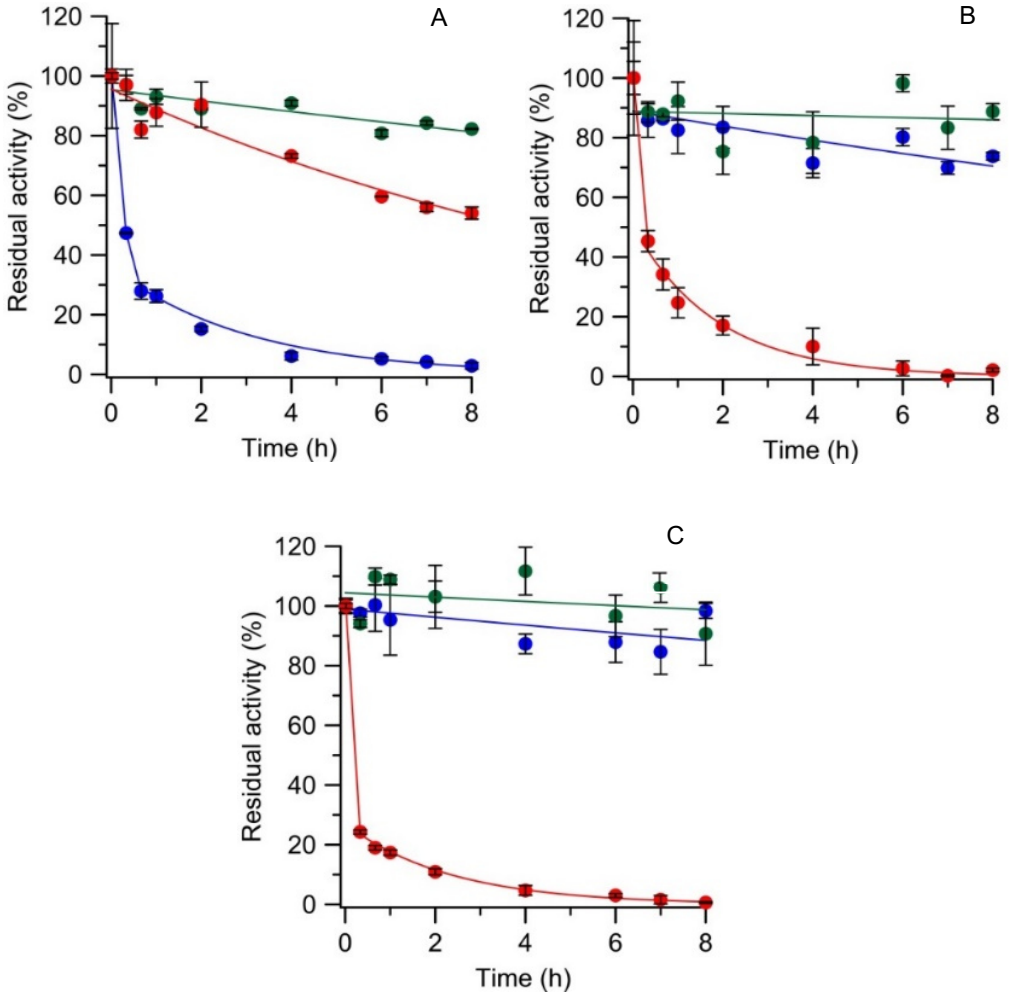

Fig. 3.13: Stability of the three UPOs from *P. aberdarensis*, *Pab*UPO I (**A**), *Pab*UPO II (**B**), *Pab*UPO III (**C**) at pH 3.0 (red), 7.0 (green) and 10.0 (blue) at 25°C.

All three *Pab*UPOs turned out to be relatively stable at neutral pH with 85-90% remaining activity after eight hours of incubation at pH 7.0. While *Pab*UPO II and III retained over 75% of their activity upon exposure to pH 10.0, *Pab*UPO I rapidly lost its activity at this pH, but retained 60% activity at pH 3.0 (a pH at which the other two UPOs lost their activity within minutes) (Fig. 3.13).

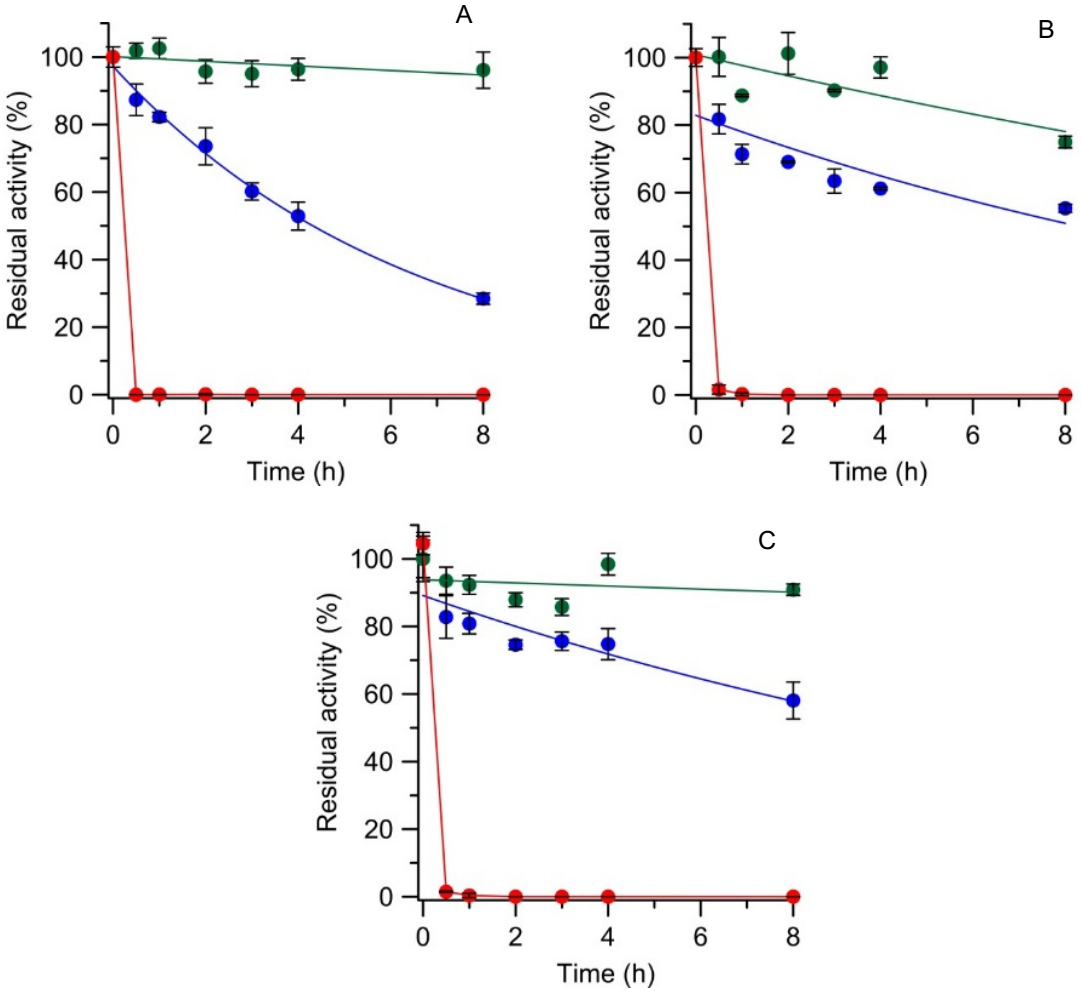

Fig. 3.14: Stability of the three UPOs from *P. aberdarensis*, *Pab*UPO I (**A**), *Pab*UPO II (**B**), *Pab*UPO III (**C**) at 60°C (red), 40°C (blue) and 25°C (green).

Temperature stability was not much pronounced. As expected, the highest stability of the three *Pab*UPOs was observed at 25°C, at which temperature the enzymes remained 75-95% of their initial activity after eight hours of incubation (Fig. 3.14). However, already at 40°C, differences were observed between the three enzymes. *Pab*UPO I retained only 35% of its initial activity whereas *Pab*UPO II and III retained 60%. At 60°C, all three enzymes showed a similar 'behavior' and lost almost their total activity within 30 min.

3.9 Kinetic parameters of purified UPOs from *P. aberdarensis*

The apparent[15] Michaelis-Menten constants (K_M), turnover numbers (k_{cat}) as well as catalytic efficiencies (k_{cat} /K_M) of the purified *P. aberdarensis* UPOs towards 'classic' peroxidase substrates are summarized in Tab. 3.6. The K_M values of the three enzymes for ABTS and DMP ranged between 105 and 656 µM indicating relatively high affinity to these substrates, while those for VA[16] were higher (K_M = 856 to 1,291 µM) suggesting lower affinity. The turnover numbers (k_{cat}) were in the same order of magnitude and ranged between 20 s^{-1} and 137 s^{-1} for ABTS, 23 s^{-1} and 70 s^{-1} for DMP as well as 20 s^{-1} and 122 s^{-1} for VA. The aromatic *N*-heteroatom of ABTS was oxidized with the highest catalytic efficiency by all three enzymes (k_{cat}/K_M = 1.91 to 9.42 × 10^5 s^{-1} M^{-1}) and *Pab*UPO III turned out to be the most powerful of them with efficiencies of 1.35 to 9.42 × 10^5 s^{-1} M^{-1}.

Tab. 3.6: Apparent kinetic data (K_M, k_{cat} and k_{cat}/K_M) of *Pab*UPOs for veratryl alcohol (VA), 2,6-dimethoxyphenol (DMP) determined at a constant H_2O_2 concentration of 1,000 µM.

Enzyme	Substrate	k_{cat} (s^{-1})	K_M (µM)	k_{cat}/K_M (s^{-1} M^{-1})	pH
*Pab*UPO III		122	904	1.35 × 10^5	
*Pab*UPO II	VA	104	1,291	8.02 × 10^4	7.0
*Pab*UPO I		20	856	2.36 × 10^4	
*Pab*UPO III		70	129	5.45 × 10^5	
*Pab*UPO II	DMP	50	143	3.52 × 10^5	7.0
*Pab*UPO I		23	656	3.52 × 10^4	
*Pab*UPO III		137	145	9.42 × 10^5	
*Pab*UPO II	ABTS	85	128	6.64 × 10^5	4.5
*Pab*UPO I		20	105	1.91 × 10^5	

[15] Steady state kinetics of UPOs are apparent, since these enzymes have two substrates (the actual 'target' compound and H_2O_2). Usually, the data are determined at constant concentration of one substrate while the other substrate's concentration is being varied. In consequence, UPOs (and all peroxidases) do not operate by classic Michaelis-Menten kinetics (Ullrich et al. 2004).

[16] VA is substrate both of peroxidases such as LiP or VP and of peroxygenases (Hofrichter et al. 2010).

3.10 Peroxygenase-specific reactions catalyzed by *Pab*UPOs

Despite their catalytic versatility regarding substrates and reaction types (e.g. epoxidation, hydroxylation, *O*-demethylenation, *N*-oxidation; Hofrichter et al. 2010), the substrate specificities of individual UPOs may differ in dependence of their protein structure (e.g. size and design of the heme entrance channel; Piontek et al. 2013, Hofrichter et al. 2015, Ullrich et al. 2018). For that reason, a selection of substrates that are characteristic of different UPO reaction types were tested to evaluate the catalytic specificities of the three purified *Pab*UPO proteins (chap. 2.8).

3.10.1 Halogenation of phenol

As observed for other fungal UPOs, the chlorination of phenol was catalyzed by *Pab*UPOs to just moderate extent (Tab. 3.7 and Fig. 3.15). Rather, the oxidation of phenol to 1,4-benzoquinone was the preferred reaction. Thus *Pab*UPOs II and III (0.5 U mL^{-1}) caused the formation of 128 and 193 µM of this product (when applying 500 µM phenol), which is more than the comparison enzymes, *Aae*UPO and *Mro*UPO, formed (29 and 61 µM, respectively).

Tab. 3.7: Average concentrations (three measurements with standard deviation, ±SD) of products formed by *Pab*UPOs and the comparison enzymes *Aae*UPO and *Mro*UPO in the course of phenol conversion (500 µM) in the presence of chloride (10 mM KCl).

Enzyme	Residual phenol (µM)	±	1,4-Benzo-quinone (µM)	±	2-Chloro-phenol (µM)	±	4-Chloro-phenol (µM)	±	Sum* (µM)
*Pab*UPO I [a)]	486.1	0.1	2.5	0.1	1.0	0.0	1.1	0.1	490.7
*Pab*UPO I [b)]	466.7	1.8	6.4	1.2	1.8	0.1	1.6	0.0	476.4
*Pab*UPO I [c)]	306.5	0.3	35.6	18.6	3.3	0.1	2.3	0.0	347.7
*Pab*UPO II [a)]	424.5	2.0	41.8	1.7	1.2	0.1	1.3	0.1	468.7
*Pab*UPO II [b)]	328.5	3.5	128.4	4.9	1.9	0.2	2.0	0.0	460.9
*Pab*UPO III [a)]	375.7	1.8	90.6	1.5	1.9	0.0	2.0	0.0	470.2
*Pab*UPO III [b)]	251.7	1.0	193.0	1.2	2.8	0.1	2.6	0.0	450.1
*Aae*UPO [b)]	269.1	1.9	29.3	13.3	1.6	0.2	1.3	0.0	301.3
*Mro*UPO [b)]	379.1	0.4	61.3	0.0	0.0	0.0	0.0	0.0	440.4

*sum of products, [a)] 0.2 U mL^{-1} *Pab*UPOs, [b)] 0.5 U mL^{-1} *Pab*UPOs or *Aae/Mro*UPOs, [c)] 5.0 U mL^{-1} *Pab*UPOI

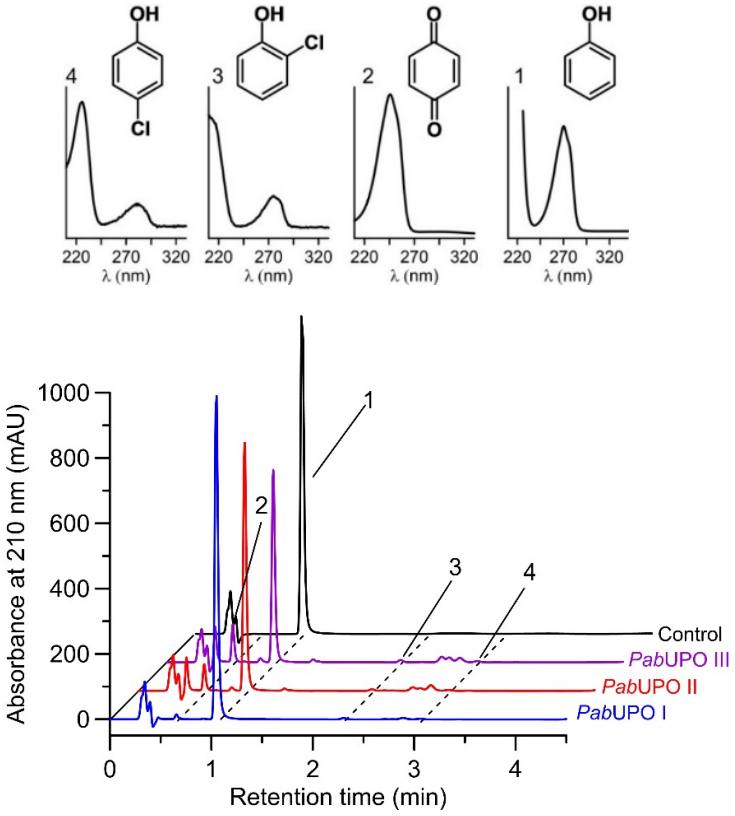

Fig. 3.15: Chlorination of phenol by *Pab*UPO I,II, III (0.2 U mL^{-1}); above: UV-Vis spectra of the key products; below: HPLC elution profiles recorded at 210 nm, (**1**) phenol, (**2**) 1,4-benzoquinone, (**3**) 2-chlorophenol and (**4**) 4-chlorophenol.

Tab. 3.8: Average concentrations (three measurements with standard deviation, ±SD) of products formed by *Pab*UPO isoforms in the course of phenol conversion (500 µM) in the presence of bromide (10 mM KBr).

Enzyme	Residual phenol (µM)	±SD	1,4-Benzo-quinone (µM)	±SD	2-Bromo-phenol (µM)	±SD	4-Bromo-phenol (µM)	±SD	Sum* (µM)
*Pab*UPO I	463.0	1.9	4.8	0.2	5.4	0.0	13.8	0.4	24.0
*Pab*UPO II	280.6	15.1	74.3	4.0	31.5	0.8	94.5	5.2	200.3
*Pab*UPO III	232.7	0.4	83.0	0.3	33.1	0.2	111.1	1.0	227.3
control	498.7	0.7	-	-	-	-	-	-	-

*sum of products formed (without 1,4-bromobenzoquinone that was not available as authentic standard)

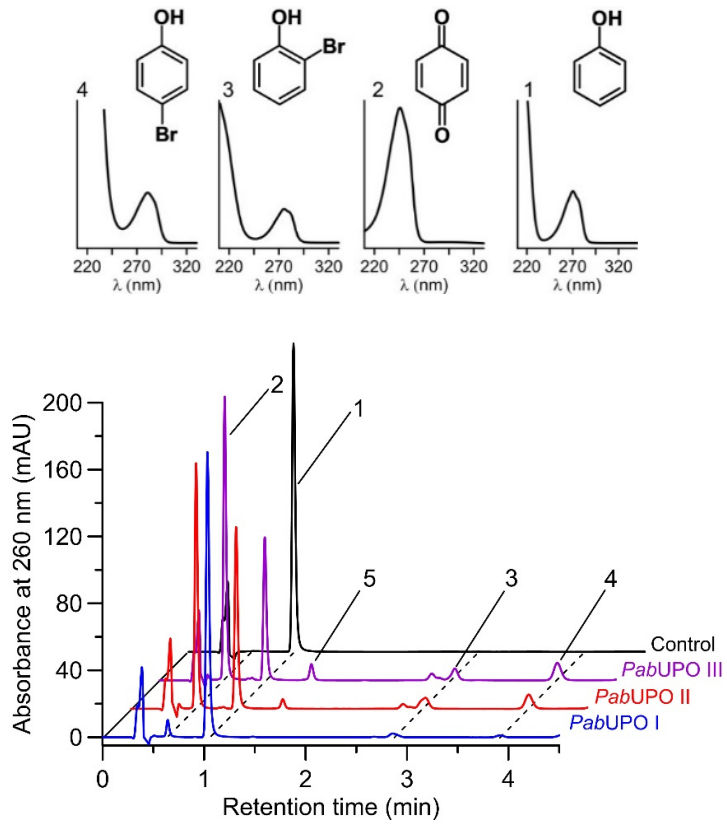

Fig. 3.16: Bromination of phenol by *Pab*UPO I, II and III (0.2 U mL^{-1}); above: UV-Vis spectra of the key product (without bromobenzoquinone); below: HPLC elution profiles at 260 nm, (**1**) phenol, (**2**) 1,4-benzoquinone, (**3**) 2-bromophenol, (**4**) 4-bromophenol and (**5**) bromo-1,4-benzoquinone.

On the contrary, the oxidation of chloride to hypochlorite (OCl^-) by UPOs and the subsequent chlorination of phenol resulted only in trace amounts of 2- and 4-chlorophenol (maximum 5.5 µM chlorphenols formed by *Pab*UPO I and for comparison, 2.9 µM by *Aae*UPO). *Mro*UPO, a representative of the 'short' basidiomycetous UPOs, did not oxidize any chloride and thus only 1,4-benzoquinone was found as product.

Significant bromination was catalysed by *Pab*UPO II and III (and moderately by *Pab*UPO I). The former two enzymes converted about 50% of the phenol supplied (500 µM) and formed 4-bromophenol as major (19-22% yield) and 2-bromophenol (6-7%) and 1,4-benzoquinone (15-17%) as minor products (Tab. 3.8, Fig. 3.16). Both brominated phenols were formed at the ratio of 1:3 in all three cases. In addition to the mentioned products, indication of the formation of traces of bromo-1,4-benzoquinone (inferred from the characteristic UV spectrum) were found in the HPLC profiles.

3.10.3 Hydroxylation of naphthalene

The HPLC elution profiles of the oxygenation experiment with the three *Pab*UPOs and naphthalene showed the formation of substantial amounts of 1-naphthol (20-27% respectively) and traces of 2-naphthol (0.1-0.25%; Tab. 3.9 and Fig. 3.17). This reaction demonstrates the ability of the *Pab*UPOs to catalyze regio-selective aromatic hydroxylation, probably via formation of an epoxide intermediate that decays by spontaneous rearrangement to 1-napthtol and 2-naphthol as major and minor products, respectively.

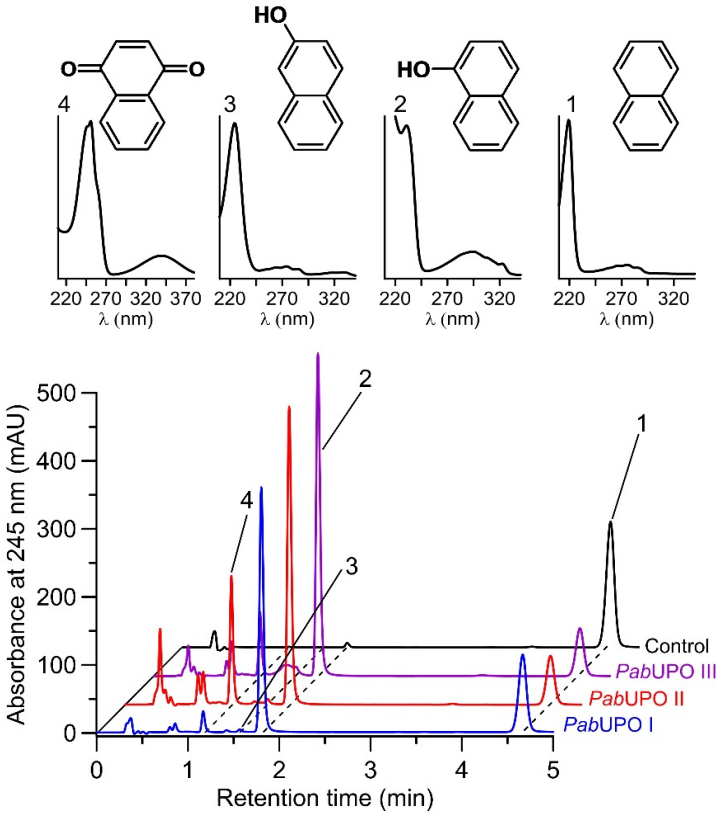

Fig. 3.17: Hydroxylation (via epoxidation) of naphthalene by *Pab*UPOs I–III (0.5 U mL^{-1}); above: UV-Vis spectra relating to the major peaks; below: HPLC elution profiles recorded at 245 nm, (**1**) naphthalene, (**2**) 1-naphthol, (**3**) 2-naphthol, (**4**) 1,4-naphthoquinone.

Tab. 3.9: Average concentrations of products formed in the course of naphthalene oxygenation (1000 µM) by three purified *Pab*UPOs.

Enzyme	1-Naphthol (µM)	±	2-Naphthol (µM)	±	2-OH* (%)	Naphtho-quinone (mAU*s)	±
*Pab*UPO I	195.1	2.0	1.0	0.0	0.5	75.6	5.6
*Pab*UPO II	247.0	0.6	2.5	0.5	1.0	459.9	2.5
*Pab*UPO III	269.0	2.1	1.7	0.3	0.6	238.4	14.1
control	<0.1	-	<0.1	-	<0.1	<0.1	-

* percentage of both naphthols

In addition to naphthols, 1,4-naphthoquinone was also formed during the reaction (the highest amount by *Pab*UPO II). Due to the volatility of naphthalene in aqueous solution, the remaining amounts of naphthalene (including controls) could not be reliably quantified.

3.10.4 Hydroxylation of anisole

In the case of anisole (methoxybenzene) oxidation, 4-hydroxyanisole (*p*-methoxyphenol) was identified as the major product for all three enzymes, while hydroquinone was only observed for *Pab*UPO II and III (that had higher specific activities than *Pab*UPO I). Formation of 1,4-benzoquinone, which would have been expected, was not observed due to the presence of ascorbic acid that reduced radical intermediates. The highest amount of 4-hydroxyanisole (354 µM) was detected in reactions with *Pab*UPO II.

Tab. 3.10: Average concentrations of residual anisole and products formed in the course of anisole hydroxylation (1000 µM) by three purified *Pab*UPOs.

Enzyme	residual anisole (µM)	±	4-OH-anisole (µM)	±	hydro-quinone (µM)	±
*Pab*UPO I	761	15	163	4	0	0
*Pab*UPO II	485	0	354	3	41	1
*Pab*UPO III	477	30	320	25	36	1
control	921	38	0	0	0	0

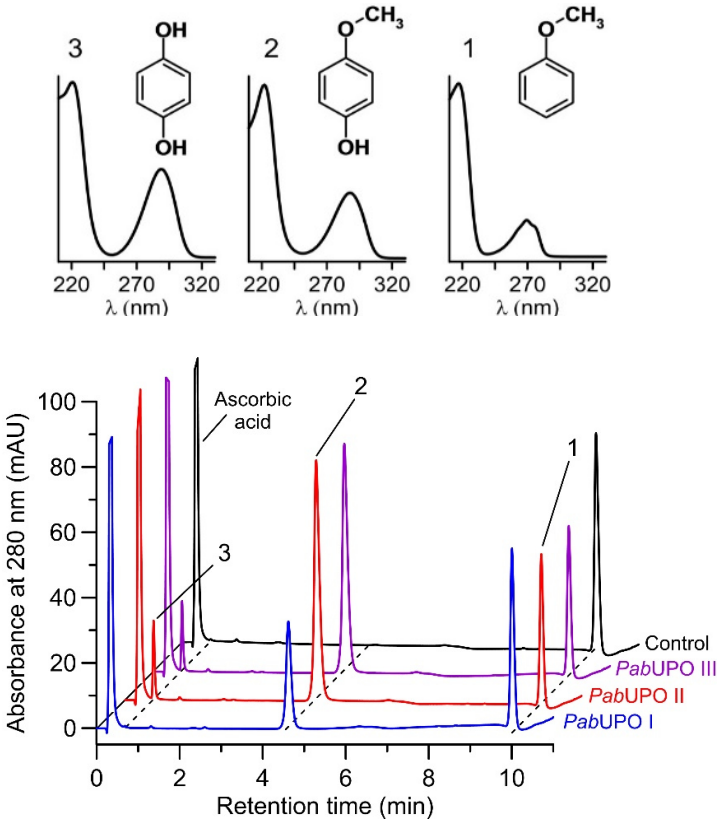

Fig. 3.18: Hydroxylation and *O*-dealkylation (ether cleavage) of anisole by *Pab*UPOs I–III (0.5 U mL^{-1}); above: UV-Vis spectra relating to the major peaks; below: HPLC elution profiles recorded at 280 nm, (**1**) anisole, (**2**) 4-OH-anisole, (**3**) hydroquinone.

3.10.5 Conversion of toluene

The toluene molecule can be subject of two UPO-specific reactions: aromatic oxygenation (hydroxylation via epoxidation) and side chain (alkyl) hydroxylation (Ullrich and Hofrichter 2005). Indeed, specific products of both routes were found for all three enzymes but with different ratios (Tab. 3.11 and 3.12). The respective product ratios (aromatic hydroxylation *versus* total products) demonstrate that *Pab*UPO I preferred side chain hydroxylation (20%; products: benzyl alcohol, benzaldehyde and benzoic acid) over ring hydroxylation, while *Pab*UPO II and III catalyzed both reactions to almost the same extent (52%; products: methylhydroquinone, *p*-cresol and *o*-cresol). After 24 hours, treatment of toluene with *Pab*UPO II and III resulted in the appearance of a yellowish color caused by the high concentration of methylhydroquinone (that tends to disproportionate to the corresponding colored methylbenzoquinone or couple to polymerization products after intermediate semiquinone formation, which are colored as well).

Tab. 3.11: Conversion of toluene (1000 µM) by the three purified *Pab*UPOs via alkyl hydroxylation.

Enzyme	Benzyl alcohol (µM)	±	Benz-aldehyde (µM)	±	Benzoic acid (µM)	±	Σ Alkyl hydroxylation (µM)	±
*Pab*UPO I	58.2	0.8	35.4	2.3	2.1	0.5	**95.8**	3.6
*Pab*UPO II	79.9	2.3	5.8	0.0	0.3	0.1	**86.0**	2.4
*Pab*UPO III	79.5	0.8	5.7	0.1	0.2	0.1	**85.4**	1.0
control	<0.1	-	<0.1	-	<0.1	-	<0.1	-

Tab. 3.12: Conversion of toluene (1000 µM) by the three purified *Pab*UPOs via aromatic hydroxylation.

Enzyme	*p*-Cresol (µM)	±	*o*-Cresol (µM)	±	Methyl-HQ (µM)	±	Σ Aromatic (µM)	±	Aromatic *vs.* total hydroxylation* (%)
*Pab*UPO I	1.5	0	6.1	0.6	15.6	0.8	**23.1**	1.5	**19.5**
*Pab*UPO II	7.6	0.4	4.5	0.2	82.0	1.4	**94.1**	2.0	**52.3**
*Pab*UPO III	7.7	0.1	4.4	0	81.4	0	**93.6**	0.1	**52.3**
control	0	0	0	0	0	0	**0**	0	

* Percentage of aromatic hydroxylation *vs.* all products quantified

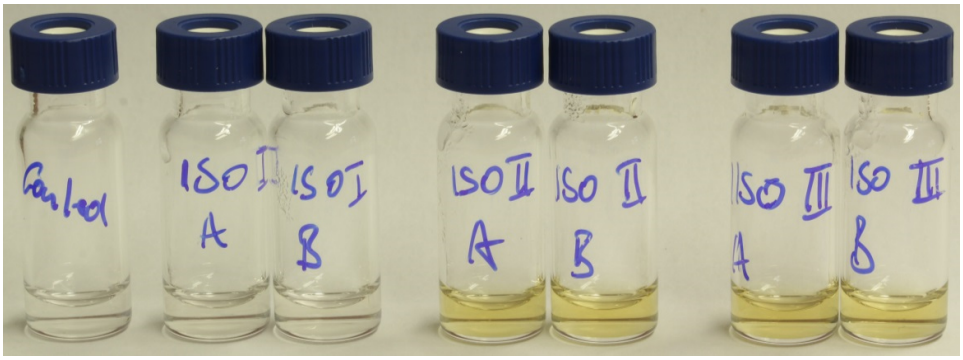

Fig. 3.20: Toluene reaction solutions after 24 hours (Photo: Alexander Karich 2017).

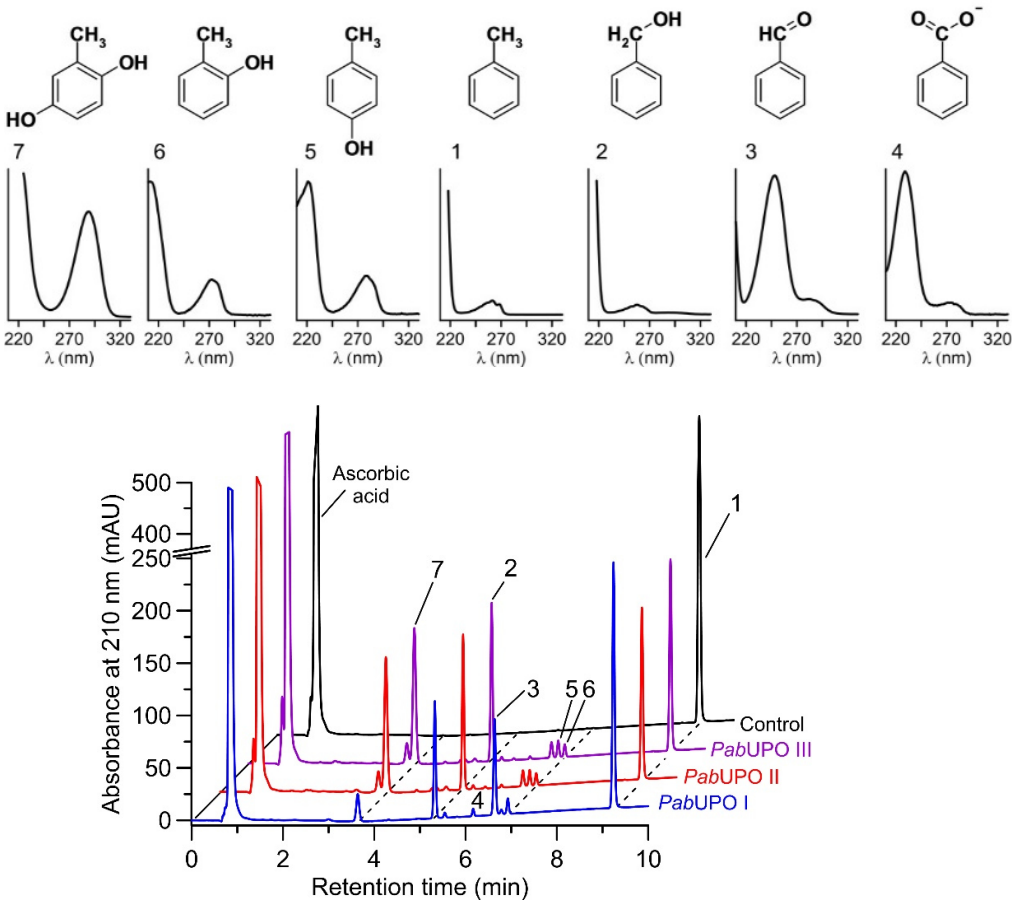

Fig. 3.19: Hydroxylation of toluene by *Pab*UPOs I–III (0.5 U mL^{-1}); above: UV-Vis spectra relating to the major peaks; below: HPLC elution profiles recorded at 280 nm, (**1**) toluene, (**2**) benzyl alcohol, (**3**) benzaldehyde, (**4**) benzoic acid, (**5**) *p*-cresol, (**6**) *o*-cresol, (**7**) methyl-hydroquinone.

3.10.6 Conversion of oseltamivir

The peroxygenative conversion of the antiviral pharmaceutical oseltamivir (brand name 'Tamiflu') via 'atypical' ester cleavage has been reported for one UPO of *Coprinellus radians* (*Cra*UPO; (Poraj-Kobielska et al. 2011, Poraj-Kobielska 2013). Oseltamivir carboxylate, the actually active form of the drug, was identified as the main metabolite. Contrary to that, all *Pab*UPOs including acid-tolerant *Pab*UPO I were unable to attack oseltamivir and no reaction product was detectable (data not shown).

3.10.7 *O*-Demethylenation of nitrobenzodioxole

The ability of *Pab*UPOs to catalyze *o*-demethylenation, a special case of *o*-dealkylation (ethers scission) was demonstrated using 5-nitro-1,3-benzodioxole (NBD) as the substrate. The compound, that contains a methylene group (-CH_2-) between two ether

oxygens (-O-) in a 5-ring system as characteristic functionality (dioxolane), had already been used in the rapid microplate-screening assay (chap. 2.3.1). Thus, it was not surprising that also the three purified *Pab*UPOs were able to oxidize NBD into the yellow colored reaction product 4-nitrocatechol, which was spectrophotometrically analyzed resulting in specific activities of 1.0, 3.2 and 5.2 U mg^{-1} for *Pab*UPO I, II and III, respectively. Formic acid (HCOOH) originating from the peroxygenation of the methylene group was formed as the second cleavage product.

3.10.8 Conversion of FFCA into FDCA

The oxidation of formylfuran carboxylic acid (FFCA) into 5-furandicarboxylic acid (FDCA) is another interesting reaction that might be catalyzed via peroxygenation. The product (FDCA) is a desired renewable building block for the production of bio-based polyesters (substitute for terephthalic acid in PET plastics[17]). All three *Pab*UPOs catalyzed the predicted reaction and the isoforms II and III turned out to be the most efficient ones (Fig. 3.21). They yielded higher FDCA levels (38 and 40%, respectively) than determined with the model enzyme *Aae*UPO (15%; data not shown) or *Pab*UPO I (4%) over a reaction time of 120 min and under H_2O_2 supply with by a syringe pump (chap. 2.8.6). The pH profiles (obtained in the course of 5-min measurements after one-time addition of H_2O_2; chap. 2.6.3.1) of FFCA oxidation by the three enzymes are given in Fig. 3.22.

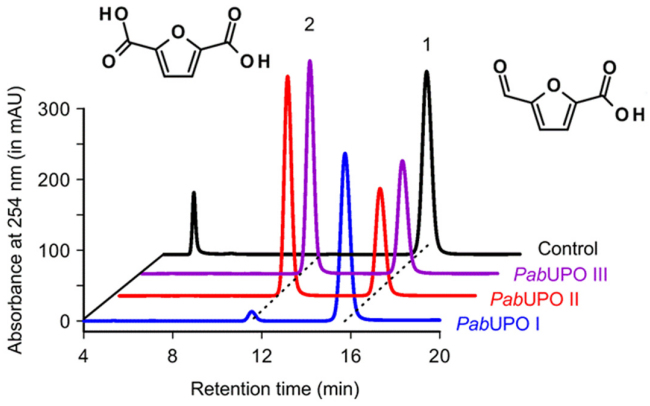

Fig. 3.21: FDCA (**2**) formation from FFCA (**1**) at pH 6.0 catalyzed by three *Pab*UPOs.

[17] PET – polyethylene terephthalate; crude-oil based polymer used, for example, for the production of plastic bottles.

Again, the highest product yields were observed for *Pab*UPO II and III (0.15 and 0.17 mM FDCA) with pH-optima ranging between 5.0 and 6.0 as well as 5.5 and 6.0, respectively. *Pab*UPO I catalysed the breakdown of FFCA at a steady low rate (<0.01 mM min^{-1}) over the whole pH-range tested (pH 3.0-9.0) without distinct pH-optimum.

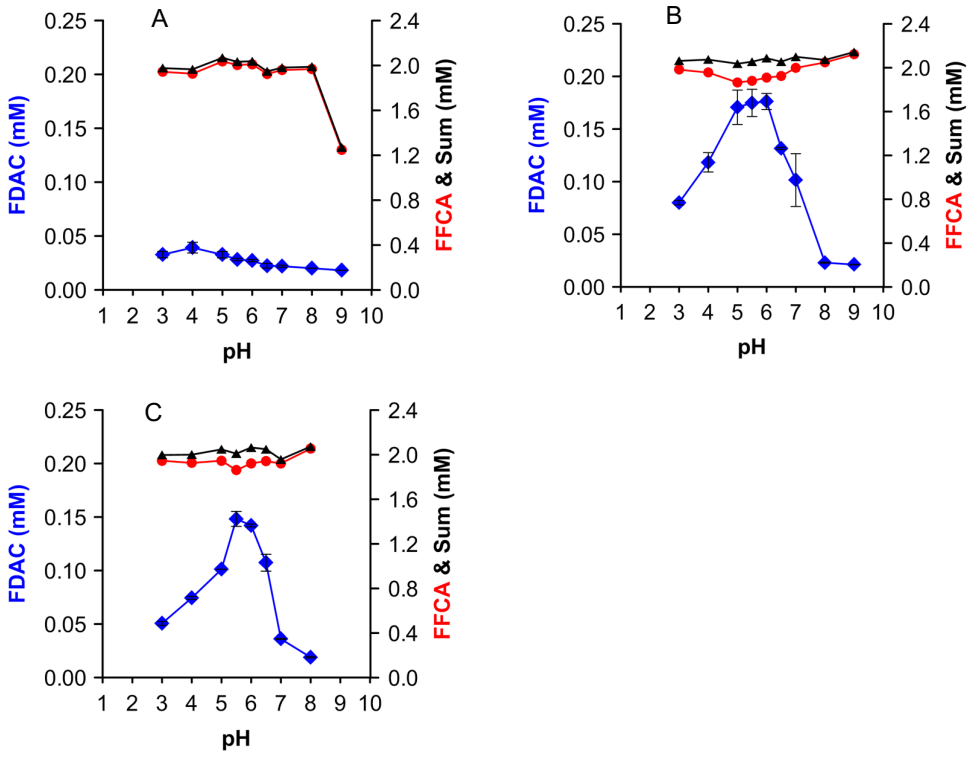

Fig. 3.22: pH-Dependencies of FFCA oxidation to FDCA catalyzed by the three purified *Pab*UPOs: I (A), II (B) and III (C).

3.11 The *Psathyrella aberdarensis* genome

3.11.1 Assembly and quality assessment of *P. aberdarensis* draft genome

The genome of *P. aberdarensis* was assembled from 5.5 million reads obtained from an ION TORRENT® PGM System. Before that, all the reads obtained from polyclonal and low quality ISPs, were excluded. The average fragment size was 215 bp and a final 60.6 Mbp-sized draft genome organized in 2,303 contigs (largest contig 354,805 bp) was obtained after the assemblies using MIRA and Geneious R8 (Tab. 3.13). The GC content was 50.28 and the N50 value 57,370. The empirical average 'depth-of-coverage' (number of reads * read length / assembly size) was 19.5x.

Tab. 3.13: Statistical assembly of the *P. aberdarensis* genome.

Assembly and annotation statistics	
Total genome length	60,615,474
Number of contigs	2,303
Largest contig length	354,805
GC%	50.28
N50	57,370
N75	25,971
L50	297
L75	691
N's per 100 kbp	84.04

3.11.2 *Pab*UPO encoding genes and their deduced protein sequences

A custom blast search using *A. aegerita* UPO as a reference proved the presence of as much as 48 UPO encoding genes in the *P. aberdarensis* genome (Fig. 3.23). The properties of all genes (e.g. ORF and the number of introns) and their deduced putative protein sequences (protein length, molecular mass, etc.) are summarized in Tab. 3.14. With the exception of *g4882* (silent gene), in all *Pab*UPO genes, the typical conserved amino acid motif **PCP**, which includes the proximal heme-binding ligand cysteine was identified. Additionally, the two characteristic motifs that are indicative for either 'long' (**EGD**) or 'short' (**EHD**) UPOs (Hofrichter et al. 2015) were found in 46 and 2 corresponding genes, respectively (data not shown).

De-novo peptide sequencing of the three purified *Pab*UPOs (chap.2.7) revealed that they are products of just two different genes: '*Pab*UPO I' belongs to the UPO gene *g7491* and '*Pab*UPO II and III' to *g8283*. Thus, '*Pab*UPO I' can be regarded as a true isoenzyme expressed from one gene, while the other two UPOs may be isoforms of the same gene that underwent different post-translational modification (e.g. glycosylation; Fig. A.2).

The phylogenetic tree shown in Fig. 3.23 comprises 77 selected sequences of 'long' and 'short' UPOs and demonstrates that most of the putative UPOs of *P. aberdarensis* (including the purified enzymes) belong to the former clade (46 out of 48 *Pab*UPO sequences). The model UPO of *A. aegerita* and the first recombinant peroxygenase from *C. cinerea* (r*Cci*UPO) are also members of this clade that possibly represents their own protein family (or at least a subfamily).

Tab. 3.14: Summary of the properties of all genes encoding for UPOs identified in the *P. aberdarensis* genome. Bold letters mark the two genes of the three purified *Pab*UPOs, dark-grey highlighted white letters the two putative 'short' UPOs.

Gene	ORF	Introns	Protein	M_w (kDa)	pI	Signal peptide	Glycosylation sites
735	1,402	4	385	42.0	6.91	+	3
732	1,408	4	386	42.0	6.91	+	2
2962	862	1	266	29.8	7.26	-	0
4882	1,227	2	330	36.1	7.66	-	1
4987	1,116	3	298	32.8	5.45	-	1
5176	1,189	2	324	35.4	6.03	+	2
7269	1,336	4	367	40.4	6.44	-	4
7489	1,374	4	378	40.6	6.40	+	4
7495	1,379	4	380	41.8	6.95	+	4
7491	**1,514**	**4**	**379**	**41.3**	**4.80**	**+**	**4**
7926	1,360	4	378	42.2	5.22	+	3
8236	1,380	4	383	41.9	5.81	+	3
8238	**1,402**	**4**	**386**	**41.9**	**4.92**	**+**	**3**
8303	746	4	183	19.1	7.73	+	0
8304	1,307	5	331	36.0	5.74	+	3
8310	1,440	2	379	41.5	5.94	+	3
8858	1,385	4	383	42.1	8.10	+	2
8859	1,385	4	383	42.0	7.34	+	2
9049	1,336	4	367	40.6	7.15	-	4
9346	1,362	4	377	41.5	4.83	+	3
9479	1,427	4	390	42.0	6.28	+	3
9684	1,500	4	376	41.4	6.91	+	5
10111	1,442	4	379	41.6	5.31	+	4
10113	1,387	4	383	42.0	6.88	+	3
10114	1,413	4	388	42.1	7.30	+	3
10137	1,387	4	383	42.5	7.19	+	2
10138	1,448	4	323	35.5	7.12	-	3
10129	1,408	4	387	41.8	6.59	+	2
10231	1,387	4	383	42.1	7.69	+	3
10815	1,381	4	383	41.9	5.56	+	2
10976	1,393	4	386	42.7	7.62	+	4
10979	1,263	2	376	41.4	6.67	-	3
11073	1,480	6	368	40.1	8.56	+	3
11190	1,360	4	380	41.9	8.10	+	3
11331	1,381	4	383	42.1	8.11	+	2
11332	1,382	4	383	41.9	7.71	+	3
11430	827	3	264	28.4	6.51	+	2
11608	1,371	2	379	41.6	6.51	+	2
11607	1,418	4	385	41.5	7.07	+	3
11752	1,412	4	387	41.7	6.72	+	3
12537	1,039	3	258	27.8	6.51	+	1
12786	1,494	5	384	42.4	8.56	+	3
13107	1,427	4	390	42.1	6.35	+	4
13381	1,364	4	377	41.6	4.86	+	3

Gene	ORF	Introns	Protein	M_w (kDa)	pI	Signal peptide	Glycosylation sites
13382	1,368	4	377	41.5	4.69	+	3
13383	1,374	4	380	42.3	6.52	+	3
13395	1,378	4	380	41.8	4.94	+	3
14459	704	2	188	20.2	9.44	+	0

+…signal peptide is present, **-**…signal peptide is lacking

The putative two 'short' UPOs of *P. aberdarensis* (*g2962* and *g4987*) are found in the same cluster as basidiomycetous *Mro*UPO and the UPO of the ascomycete *Chaetomium globosum* (*Cgl*UPO). Interestingly, chloroperoxidase from *Caldariomyces (Leptoxyphium) fumago* (*Lfu*CPO) also matches within that group (Fig. 3.23). The deduced proteins of the two expressed 'long' UPO genes (*g8238* and *g7491*) comprise 379 and 386 amino acids, respectively, which gives hypothetical molecular weights of 41.3 and 41.9 kDa (as well as a pIs of 4.80 and 4.92). As it could be calculated on the basis of the amino acid sequences, the hypothetical size of the 'short' UPOs is only 266 and 298 amino acids for *g2962* and *g4987*, respectively. Most of the 48 *Pab*UPOs were found to exhibit a signal peptide, except seven representatives among them the two 'short' UPOs of *P. aberdarensis*. Remarkably, one of these proteins (*g2962*) does not even have a glycosylation site (which points to its intracellular nature).

Sequence comparison of the two 'long' *Pab*UPO genes *g8238* and *g7491* (belonging to the characterized proteins) to those of the two putative 'short' ones, *Lfu*CPO (AAA33025.1), *Mro*UPO (5FUJ_A) and *Aae*UPO (2YOR_A) demonstrates their highest identities and similarities to each other and to the model enzyme *Aae*UPO (Tab. 3.15). Thus both genes show 60% sequence homology as well as 61% (*g7491*) and 56% (*g8238*) to *Aae*UPO. The lowest identity (merely 14%) of the 'long' *Pab*UPOs were found to one of the 'short' ones (*g2962*). The latter putative protein exhibited the highest identity (26%) to *g4987*; both 'short' *Pab*UPOs are to 21% identical (and to 49-51% similar) to the 'short' model UPO from *M. rotula*.

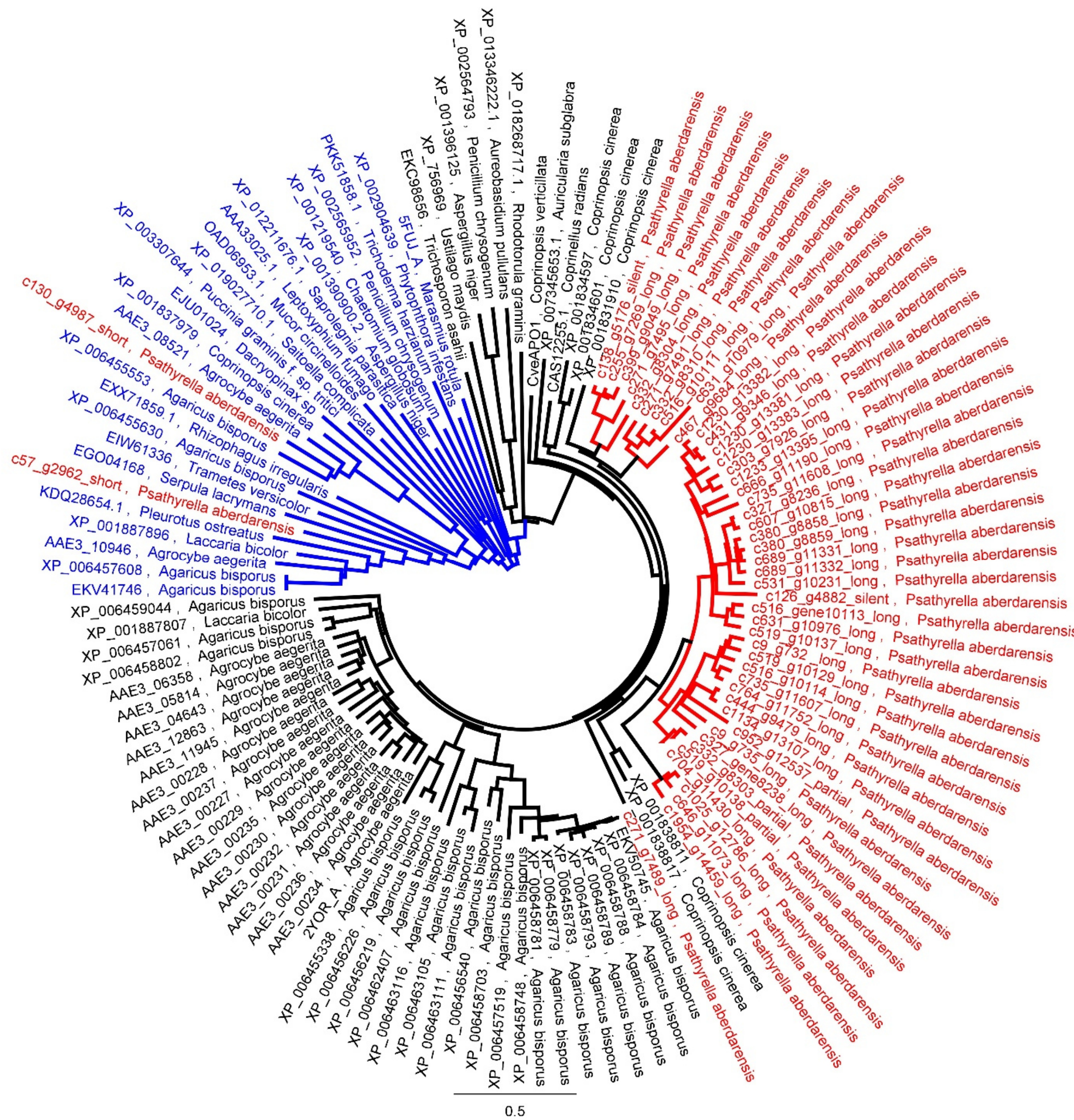

Fig. 3.23: Phylogenetic tree of selected unspecific peroxygenases (UPOs); black: 'long' UPOs, blue: 'short' UPOs, red: UPOs from *P. aberdarensis*. The tree was built using GENEIOUS R10, the jukes cantor model and the neighbor joining method; alignment was carried out using MAFFT.

Tab. 3.15: Identity and similarity matrix of the two genes encoding the three purified UPOs from *Psathyrella aberdarensis* (*Pab*UPOs, red) and the two putative 'short' *Pab*UPOs (blue) in comparison to respective enzymes from *Agrocybe aegerita* (*Aae*UPO) and *Marasmius rotula* (*Mro*UPO) as well as chloroperoxidase (CPO) from *Leptoxyphium fumago* (*Lfu*CPO).

	*Lfu*CPO	g4987	g2962	*Mro*UPO	*Aae*UPO	g8238	g7491
*Lfu*CPO		15.5	16.3	15.2	14.4	14.8	15.6
g4987	38.5		25.9	21.0	12.7	14.7	15.9
g2962	37.8	49.8		21.2	14.7	14.0	13.9
*Mro*UPO	39.3	49.2	50.5		21.6	18.6	18.9
*Aae*UPO	38.8	38.9	39.3	41.9		55.6	60.7
g8238	37.7	38.1	34.4	39.7	77.1		59.4
g7491	40.2	40.9	37.5	41.5	83.6	82.4	

Similarity (%)

Identity (%)

3.11.3 Classification of the lignocellulytic enzymes in the *Psathyrella* genome

Based on the 250 BUSCO eukaryotic subset, 1,308 (98%) complete and twelve (0.9%) fragmented proteins sequences (data not shown) were found. Annotation using AUGUSTUS (species parameter according to the basidiomycetous ink-cap *Coprinopsis cinerea*) predicted a total of 14,704 protein-coding sequences. An assignment of these sequences to the main CAZy classes using dbcan identified 664 carbohydrate-related enzymes, including 138 enzymes with auxiliary activities (AAs), 99 carbohydrate esterases (CEs), 224 glycoside hydrolases (GHs), 80 glycosyltransferaces (GTs), 14 polysaccharide lyases (PLs) and 109 carbohydrate-binding modules (CBMs).

3.11.3.1 Glycoside Hydrolases

The most abundant GHs found in the *Psathyrella aberdarensis* genome (36 and 38 sequences, respectively) belong to the CAZy families GH16 and GH5. Other GH families present with large numbers of genes encode for cellulolytic (e.g. GH6, GH7), hemicellulolytic (e.g. GH10, GH11, GH30) and pectinolytic (e.g. GH43, GH28, GH53) enzyme proteins (Tab. 3.16).

Fig. 3.24: A representation of the *P. aberdarensis* genome according to CAZy gene classification. Yellow (AA, auxiliary activities), grey (PL, polysaccharide lyases), orange (CE, carbohydrate esterases), light blue (GH, glycoside hydrolyses), green (GT, glycoside transferases) and dark blue (CBM, carbohydrate-binding modules).

Genes encoding for enzymes acting on compact amorphous cellulose (endoglucanases of families GH 6 and 7) are characteristic for WRF genomes (Riley et al. 2014). In that context, *P. aberdarensis* belongs to the 'upper group' of lignocellulose degraders with five copies of GH6 endoglucanases, while other WRF were reported to have between one to four copies of this family (e.g. *Phanerochaete chrysosporium* or *A. aegerita*). The number of GH7 genes in the *Psathyrella* genome (five copies) is also comparable to that of typical WRF (e.g. three and five genes in the genomes of *Ceriporiopsis subvermispora* and *Bjerkandera adusta*, respectively as well as eleven in *A. aegerita*).

A remarkably high number of CBMs (50 genes), coding protein domains that efficiently bind plant cell-wall carbohydrates and being necessary for diverse carbohydrate-active enzymes (e.g. cellulases, xylanases, chitinases), were found in the *Psathyrella* genome. They are distributed across 17 different CBM families (e.g. CBM1, 13, 18, 67). CEs that can hydrolytically cleave various types of ester bonds within the lignocellulosic complex accounted for 15% of the predicted CAZy gene models. Putative pectinolytic enzymes found in the families CE4, 7, 9 and 15 were among them, along with diverse members of the CE10 family containing carboxyl and aryl esterases; with 44 predicted genes, the latter enzymes represented the largest group of CEs.

3.11.3.2 Oxidoreductases

Oxidoreductases derived from the predicted gene models of the *P. aberdarensis* genome are listed in Tab. 3.16. Among them are typical biocatalysts (AAs) involved in oxidative lignocellulose breakdown and modification by wood-rot fungi.

First, it is remarkable that no sequence encoding for ligninolytic class II POD (i.e. MnP, LiP or VP, AA2 CAZy group) – the presence of which is indicative for WRF – was found in the *P. aberdarensis* genome; the only sequence belonging to the AA2 family was a generic peroxidase (GP). The respective protein sequence contained neither the typical Mn binding residues (e.g. E35, E39 and D175 in MnP of *P. chrysosporium*) nor the LiP-characteristic Trp (e.g. at position W171). On the other hand, a noticeably high number (48 sqq.) of UPO sequences was predicted in the genome of *P. aberdarensis,* which represents the highest number of published UPO genes in one fungus reported so far[18].

Further AA representatives (AA3-9) predicted in the *Psathyrella* genome belong to biocatalysts helping or interacting with enzymes that modify carbohydrates (e.g. GMCs, CDH, LPMOs) or lignin and aromatics (e.g. UPOs or DyPs). Some of them are peroxide-producing proteins like most members of the AA3_2 and A3_3 group (e.g. alcohol oxidases and aryl alcohol oxidases) or pyranose oxidases (AA3_4), which are present with two genes. It is interesting that the GMCs (A3_2) occur with a remarkably high abundance in the *Psathyrella* genome (52 genes). Only one CDH gene (*g8702*) of the AA3_1 group was found, encoding an enzyme that is probably involved in FENTON-based chemistry and LPMO activation. For the latter group of enzymes, which are thought to be involved in the oxidative attack of crystalline cellulose by WRF and BRF, a comparably high number of genes (33 genes) was identified. Another group of oxidoreductases containing benzoquinone reductases (AA6) was present in the *Psathyrella* genome with two genes. They encode for proteins involved in FENTON-based attack of lignocelluloses, a mechanism that is thought to contribute to wood degradation by both BRF and WRF (Gómez-Toribio et al. 2009). Last but not least, the *P. aberdarenis* genome was found to possess several copper-containing oxidoreductases, namely six genes of copper-radical oxidases (CRO; AA5_1) and 19 laccases. The latter number is in the upper range that has been reported for typical WRF (e.g. seven in *Trametes versicolor* or eleven in *Pleurotus ostreatus*).

[18] There are indications that around 60 peroxygenases may be present in the genome of *Marasmius rotula* but the respective data have not been published yet (H. Kellner, unpublished result 2019).

Tab. 3.16: Lignocellulose-degrading enzymes in different basidiomycetous wood-decay fungi (modified according to Riley et al. 2014; published data from JGI and NCBI, yellow – WRF (white-rot fungi), grey – BRF (brown-rot fungi), blue – URF (unresolved/unspecific wood-rot fungi):

Order		Po								Au	Hy	Co	Ru		Ag									Ag	Ja	Ca	Po			Da	Gl	Bo			
		Bjead	Cersu	Dicsq	Phaca	Phchr	Phlbr	Pycci	Trave	Aursu	Fomme	Punst	Hetan	Stehi	Agabi	Agrae	Armme	Copci	Galma	Mycch	Pleos	Psaab	Volvo	Schco	Jaaar	Botbo	Fompi	Pospl	Wolco	Dacsp	Glotr	Conpu	Serla		
Crystalline cellulose		32	16	17	27	30	28	20	23	48	6	21	17	17	17	30	11	39	54	25	33	50	56	5	24	28	0	0	0	1	1	2	8	CBM1	Carbohydrate-binding module family 1
		1	1	1	1	1	1	1	1	2	2	1	1	1	1	4	2	5	3	1	3	5	5	1	3	3	0	0	0	0	0	2	1	GH6	Glycoside hydrolase family 6
		5	3	4	5	8	4	3	4	6	2	5	1	3	1	11	4	6	8	6	16	5	11	2	5	7	0	0	0	0	0	2	0	GH7	Glycoside hydrolase family 7
		28	9	15	11	15	12	17	18	19	13	14	10	16	11	21	25	34	19	12	29	33	31	22	15	32	4	2	2	0	4	10	5	AA9	Lytic polysaccharide monooxygenase
Lignin		20	17	12	11	15	15	11	26	19	17	11	8	6	2	4	10	1	10	11	9	1	7	0	1!	0	1*	1*	1*	0	0	0	0	AA2	Class II peroxidase
		30	17	27	32	31	32	20	17	38	23	18	29	40	31	25	52	35	32	2	36	52	27	18	17	19	16	15	8	8	20	14	8	AA3_2	GMC oxidoreductase
		7	3	9	6	7	8	7	9	9	4	9	5	8	9	8	7	6	15	10	16	6	4	2	4	5	4	2	4	3	2	6	3	AA5_1	Copper radical oxidase
		0	7	11	0	0	8	5	7	0	10	12	14	15	12	14	24	17	8	13	11	19	11	2	1	0	5	4	3	0	4	6	4	AA1_1	Laccase
		7	4	4	4	3	6	2	4	7	3	4	3	7	5	3	8	2	6	18	4	5	5	4	2	3	5	1	6	1	2	5	5	AA3_3	Alcohol oxidase
		4	0	4	0	0	0	0	0	2	0	1	2	3	3	2	3	2	9	2	3	19	2	4	1	5	5	0	0	3	0	0	0	AA7	Glucooligosaccharide oxidase
		2	1	1	1	1	2	1	2	0	1	1	1	2	1	1	3	0	1	0	1	1	0	0	1	1	1	1	1	3	1	1	1	AA1_2	Ferroxidase
		1	1	1	1	1	1	1	1	1	1	1	1	1	1	0	3	1	1	1	1	1	1	1	1	3	0	0	0	0	1	2	2	AA3_1	Cellobiose dehydrogenase
		5	0	0	0	1	1	2	1	3	0	1	0	0	0	0	4	0	0	0	0	2	0	0	1	2	0	0	0	0	1	0	0	AA3_4	Pyranose oxidase
		0	0	0	0	4	0	0	0	0	1	0	1	3	1	0	1	0	0	0	0	0	0	4	0	0	0	0	0	2	0	1	0	AA1_dist	Multicopper oxidase
		4	0	1	3	4	4	1	1	4	3	2	1	1	4	3	3	3	3	0	2	2	2	4	3	1	1	0	1	1	3	2	2	AA6	Benzoquinone reductase
		1	2	2	2	2	2	2	2	1	1	1	2	2	1	1	2	6	1	1	1	3	1	3	2	2	0	0	0	0	0	4	4	AA8	Iron reductase domain
		0	0	0	0	0	0	0	0	0	0	0	0	0	0	0	0	0	0	0	0	1	0	0	2	0	0	0	0	2	3	0	0	AA4	Vanillyl alcohol oxidase
		9	0	1	3	0	3	0	2	11	3	5	1	2	2	3	2	4	5	1	5	1	1	1	1	3	0	2	0	0	0	0	0	DyPs	DyP-type peroxidase
		4	9	4	2	5	2	3	3	15	3	8	4	9	22	18	4	7	21	3	4	48	3	3	8	7	5	5	5	6	6	2	3	HTP	Heme-thiolate peroxidases

Agabi, *Agaricus bisporus*; Agrae, *Agrocybe aegerita* (Gupta et al. 2018); Armme, *Armillaria mellea*; Aursu, *Auricularia subglabrata*; Bjead, *Bjerkandera adusta*; Botbo, *Botryobasidium botryosum*; Cersu, *Ceriporiopsis subvermispora*; Conpu, *Coniophora puteana*; Copci, *Coprinopsis cinereus*; Dacsp, *Dacryopinax sp.*; Dicsq, *Dichomitus squalens*; Fomme, *Fomitiporia mediterranea*; Fompi, *Fomitopsis pinicola*; Galma, *Galerina marginata*; Glotr, *Gloeophyllum trabeum*; Hetan, *Heterobasidion annosum*; Jaaar, *Jaapia argillacea*; Mycch, *Mycena chlorophos* (Tanaka et al. 2014); Phaca, *Phanerochaete carnosa*; Phchr, *Phanerochaete chrysosporium*; Phlbr, *Phlebia brevispora*; Pleos, *Pleurotus ostreatus*; Pospl, *Postia placenta*; Psaab, *Psathyrella aberdarensis*; Punst, *Punctularia strigosozonata*; Pycci, *Pycnoporus cinnabarinus*; Schco, *Schizophyllum commune*; Serla, *Serpula lacrymans*; Stehi, *Stereum hirsutum*; Trave, *Trametes versicolor*; Volvo, *Volvariella volvacea* and Wolco, *Wolfiporia cocos*.

3.12 Production and purification of a DyP from *Xylaria grammica*

Production of the manganese-independent peroxidase of *X. grammica* (*Xgr*DyP) was performed in a liquid complex SPM in 500-mL flasks as described in chapter 2.4.2. After reaching a sufficient *Xgr*DyP level (up to 2,028 U L^{-1} overall activity at culture day 26; data not shown), the culture liquid was harvested, filtrated, frozen and stored at -20 °C until enzyme purification. The freezing and thawing step led to the removal of precipitated polysaccharides that were separated by a second filtration step (chap. 2.5.1). After concentration of the crude enzyme obtained, *Xgr*DyP was purified by five steps of FPLC using AEX and SEC techniques.

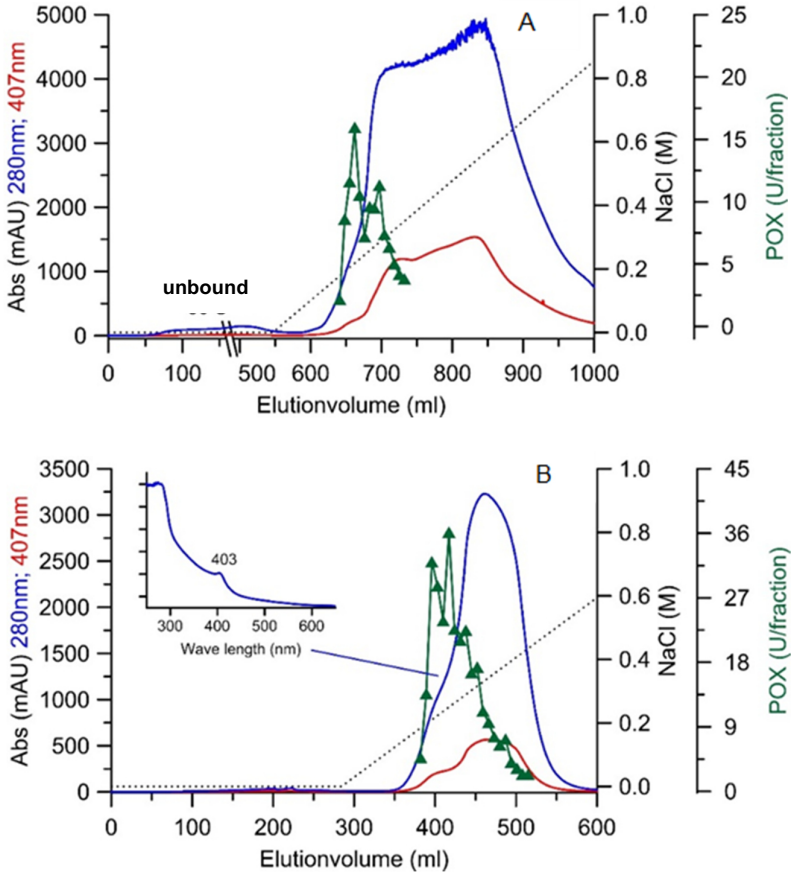

Fig. 3.25: *Xgr*DyP purification: FPLC elution profiles of the first (**A**) and second chromatographic steps (**B**; re-chromatography of A, inset – UV-Vis spectrum of the fraction with the highest peroxidase activity) on a Q-Sepharose column. Absorption (mAU) was recorded at 280 nm (blue → protein) and 407 nm (red → heme), DyP activity (green), NaCl gradient (dashed line).

By using Q-Sepharose as first separation medium, nearly half of the peroxidase activity applied was found in the unbound fraction (Fig. 3.25 A). The bound peroxidase fraction

was re-chromatographed under the same conditions and thus, almost 100% enzyme recovery could be achieved (Fig. 3.25 B).

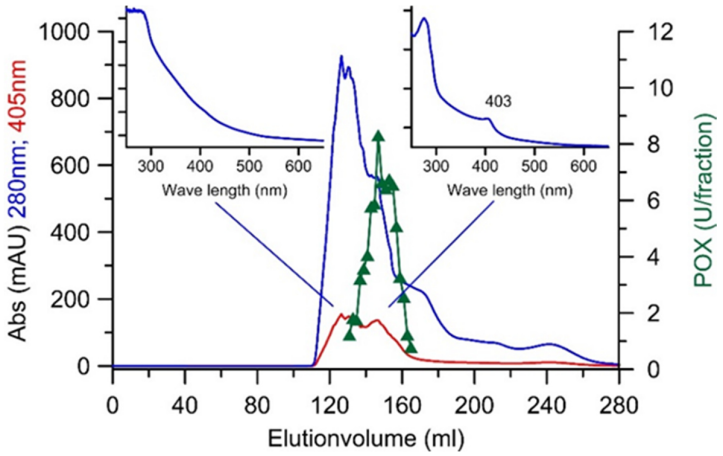

Fig. 3.26: Third purification step of *Xgr*DyP using SEC after Q-Sepharose [insets: UV-Vis spectrum of the fraction with the highest peroxidase activities (right) and of pooled active fractions (left)]. Absorption (mAU) at 280 nm (blue → protein) and 405 nm (red → heme), DyP activity (green).

In the next step, the fraction with the highest peroxidase activity was loaded to a SEC column (Fig. 3.26). Thereby further protein material was separated from the target protein (*Xgr*DyP) without noticeable activity loss, which led to an increase in specific activity from 4.6 to 10.9 U mg^{-1} (purification factor increased from 1.4 to 3.2; Tab. 3.17). By using a MonoQ column, the active SEC fraction was divided into two peaks (Fig. 3.27 A), which was accompanied with an activity loss of approx. 44% in relation to the preceding step and with a further increase in specific activity (→ 14 U mg^{-1}). Immediately following, the fraction with the highest activity was purified to apparent homogeneity by a re-chromatographic step on a MonoQ column under almost identical conditions (except that the pH was slightly reduced from 6.0 to 5.8; chap. 2.5.2.2). Finally, a 15-fold purification was achieved along with moderate activity recovery of 6% for the homogeneous *Xgr*DyP protein preparation. The final specific activity was 51.0 U mg^{-1}, the Reinheitszahl 1.10 and the residual activity amounted to 120 total units corresponding to approx. 2.4 mg total protein (Tab. 3.17).

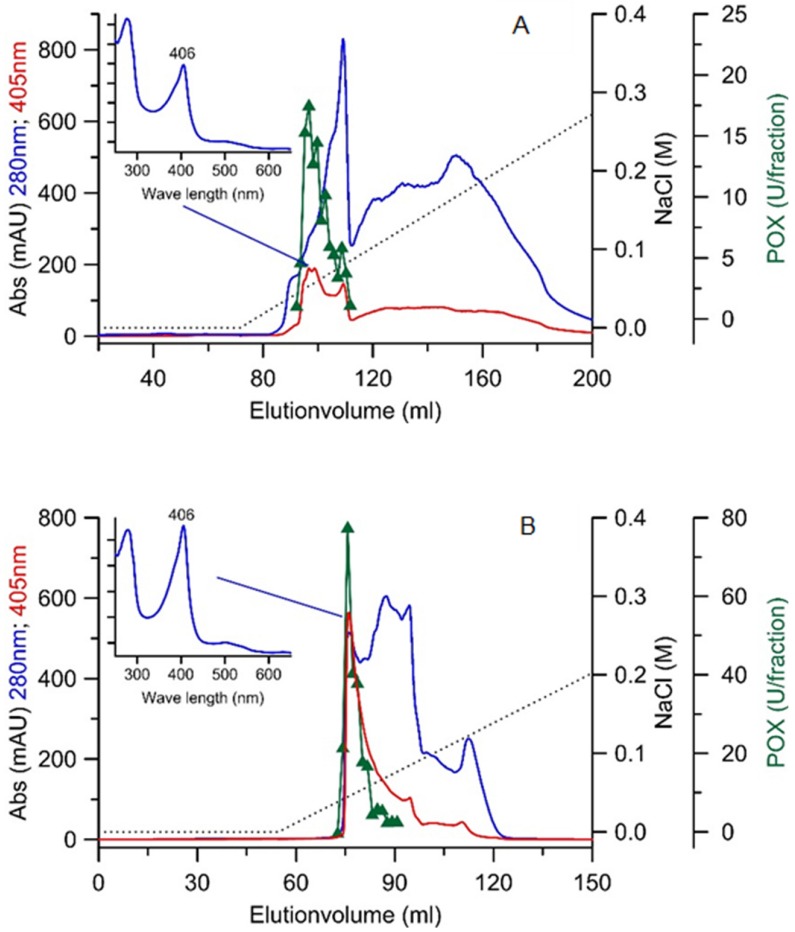

Fig. 3.27: FPLC elution profiles of the fourth and fifth purification step of *Xgr*DyP using a MonoQ column (10 × 100 mm). Absorption (mAU) at 280 nm (blue → protein) and 405 nm (red → heme), DyP activity (green), NaCl gradient (dashed line).

Tab. 3.17: Purification of the extracellular peroxidase from *Xylaria grammica* (*Xgr*DyP).

Purification step	Activity (U)	Specific activity (U mg^{-1})	Protein amount (mg)	Yield (%)	Purification (x-fold)
Culture filtrate	2,028	3.4	595.7	100	-
Ultrafiltrate 10 kDa	1,923	3.3	584.0	95	1.0
Q-Sepharose	1,160	4.6	254.4	57	1.4
SEC	1,301	10.9	119.9	64	3.2
MonoQ_I	568	13.8	41.1	28	4.1
MonoQ_II	120	51.0	2.4	6	15.0

3.13 Characterization of the *X. grammica* DyP

Purified *Xgr*DyP exhibited the characteristic reddish color of heme-containing enzymes and had absorption maxima at 406, 501, and 630 nm (Fig. 3.28). The protein appeared as single protein band with a molecular mass of 49 kDa in the SDS-PAGE gel indicating its monomeric nature (Fig. 3.29).

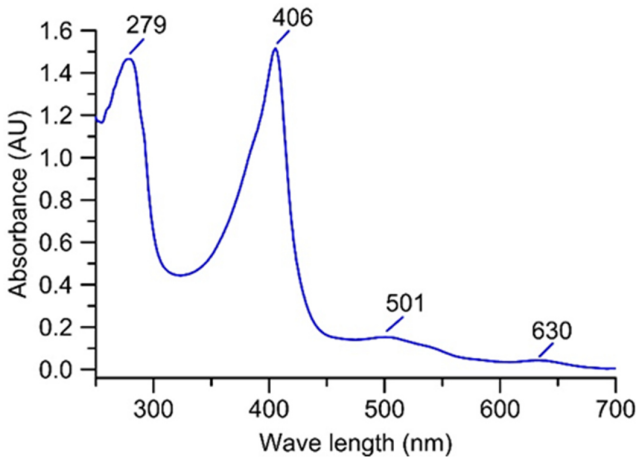

Fig. 3.28 UV-Vis absorption spectrum of the purified *Xgr*DyP in its resting state with the Soret band at 406 nm and additional bands at 279, 501 and 630 nm representing the δ-, β- and α-bands, respectively.

Besides typical peroxidase substrates like heterocyclic ABTS and phenolic DMP, *Xgr*DyP oxidized also non-phenolic VA (data not shown) and Mn^{2+} ions. To my best knowledge, the oxidation of the latter substrate has been reported neither for any wild-type DyP so far nor for any ascomyceteous peroxidase. Against this background, the pH dependencies of *Xgr*DyP for the oxidation of the classic peroxidase substrate DMP, the specific DyP substrate RBlue5 as well as of the untypical DyP substrate Mn^{2+} were determined (chap. 2.6.3.2). The oxidation of the phenolic substrate (DMP) occurred with a distinct pH maximum at 3.5, and at pH 3.0 and 4.0, approx. 95% and 90% of the maximum activity, respectively, was still detectable (Fig. 3.30). Above pH 4.0, however, DMP oxidation dropped rapidly to 20% at pH 5.0 and to almost zero at pH 6.0; on the

other hand, over 40% activity remained at pH 2.0. The pH optimum of RBlue5 oxidation formed a sharper maximum at pH 4.0 but otherwise resembled the DMP curve.

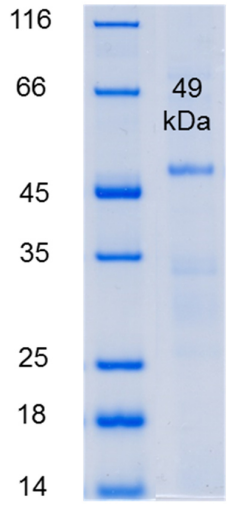

Fig. 3.29: SDS-PAGE of the purified *X. grammica* DyP (*Xgr*DyP).

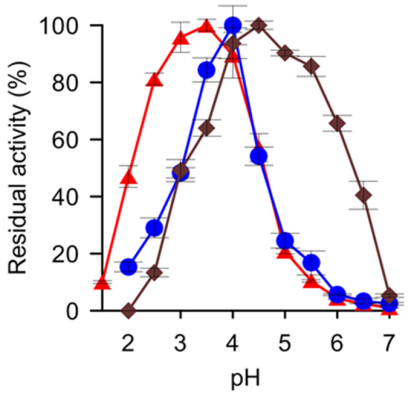

Fig. 3.30: pH-Optima for the oxidation of 2,6-dimethoxyphenol (DMP, red triangles), Reactive Blue 5 (RB5, blue circles) and Mn^{2+} ions (brown squares) by the purified *Xgr*DyP.

The curve for the oxidation of Mn^{2+} showed a maximum at pH 4.5 and appreciable activities down to pH 4.0 and up to pH 5.5 (80-90% in relation to the maximal activity). Interestingly, Mn^{2+}-oxidizing activities were still detectable at less optimal pH above 5.5.

3.14 Kinetic parameters of the purified *X. grammica* DyP

The Michaelis-Menten constants (K_M) for ABTS, DMP and RBlue5 were calculated to be 41, 12 and 41 µM, which is in the range of those of the DyP from *Auricularia auricula-judae* (*Aau*DyP, Liers et al. 2010). The enzyme showed the highest affinity (K_m = 12 µM) to and catalytic efficiency (k_{cat}/K_M = 2,499 s^{-1} mM^{-1}) for the phenolic substrate DMP. The K_M-value for the oxidation of Mn^{2+} ions (49 µM) was relatively low (suggesting high affinity to the substrate) compared to recombinant DyPs from *Pleurotus ostreatus* and interestingly ranged in the same order of magnitude as those of true MnPs and VPs of *Pleurotus* spp. and other WRF (Fernandez-Fueyo et al. 2015). On the other hand, the catalytic efficiency and turnover number of *Xgr*DyP for Mn^{2+} ions (k_{cat}/K_M = 7.0 s^{-1} mM^{-1} and k_{cat} = 0.4 s^{-1}) were many times lower than the respective data for typical Mn-oxidizing peroxidases from basidiomycetous fungi (Tab. 3.18).

Tab. 3.18: Apparent kinetic constants (K_M, k_{cat} and k_{cat}/K_M) of purified *Xgr*DyP for the substrates ABTS, DMP, RBlue5 and Mn^{2+}.

Substrate	k_{cat} (s^{-1})	K_M (µM)	k_{cat}/K_M (s^{-1} mM^{-1})
ABTS	12	41	287
2,6-DMP	29	12	2,499
RBlue5	20	41	495
Mn^{2+}	0.4	49	7

3.15 The *Xylaria grammica* genome

3.15.1 Assembly and quality assessment of the *X. grammica* draft genome

The genome of *X. grammica* was assembled from 6.6 million reads obtained from the ION TORRENT® PGM System. Beforehand, all reads obtained from polyclonal and low quality ISPs were excluded. The average fragment size was 251 bp and a final 47.0 Mbp-sized draft genome organized in 1,053 contigs (largest contig 494,172 bp) was obtained after the assemblies using MIRA and GENEIOUS R10 (Tab. 3.19). The GC content was 48.08 and the N50 value 82,670. The empirical average 'depth-of-coverage' (number of reads * read length / assembly size) was 35.2x.

Tab. 3.19: Statistical assembly of the *X. grammica* genome.

Assembly and annotation statistics	
Total genome length	47,039,132
Number of contigs	1,053
Largest contig length	494172
GC%	48.08
N50	82,670
N75	41,207
L50	172
L75	372
N's per 100 kbp	34.28

3.15.2 *Xgr*DyP encoding genes and their deduced protein sequences

A custom blast search using reference sequences from *Bjerkandera adusta* and *Pseudomonas aeruginosa* DyPs proved the presence of three DyP-encoding genes (*g488*, *g9177* and *g1956*) in the *X. grammica* genome (Fig. 3.31). The properties of the three genes (e.g. ORF and the number of introns) and their deduced putative protein sequences (protein length, molecular weight, etc.) are given in Tab. 3.20. The two genes *g9177* and *g488* had the typical conserved heme binding motif **G-**X-X**-D-G** (Hofrichter et al. 2010; data not shown, Fig. A.3 and A.4); in contrast, *g1956* had an unusual **G-**X-X**-D-H** motif. By peptide *de-novo* sequencing it turned out that the purified *Xgr*DyP (chap. 2.7) is a product of *g488* (Fig. 3.31). The deduced protein from DyP *g488* contained 493 amino acids, it had a hypothetical molecular mass of 53.9 kDa as well as a p*I* of 6.5. No signal peptide was predicted for all three DyP sequences (Tab. 3.20).

Tab. 3.20: Summary of the properties of the three genes encoding DyPs, which were identified in the *X. grammica* genome; bold letters indicate the gene belonging to the purified *Xgr*DyP.

Gene	ORF	Introns	Protein	Mw (kDa)	pI	Signal peptide	Glycosylation sites
488	**1,888**	**6**	**493**	**53.9**	**6.45**	**-**	**2**
1956	3,642	1	1,196	133.0	5.16	-	2
9177	1,095	0	364	40.4	6.73	-	3

The phylogenetic tree (Fig. 3.31) contains sequences from 29 selected fungal and bacterial DyPs. It demonstrates that the *Xgr*DyPs encoded by three genes belong to different clades. For instance, the gene encoding the purified protein *g488* matches within group 'D', in which all so far characterized basidiomyceteous DyPs (e.g. DyPs from *B. adusta*, *Bad*DyP and *A. auricula-judae*, *Aau*DyP) can be grouped (Zámocký and Obinger 2010) or the new group 'V' according to Yoshida and Sugano (2015).

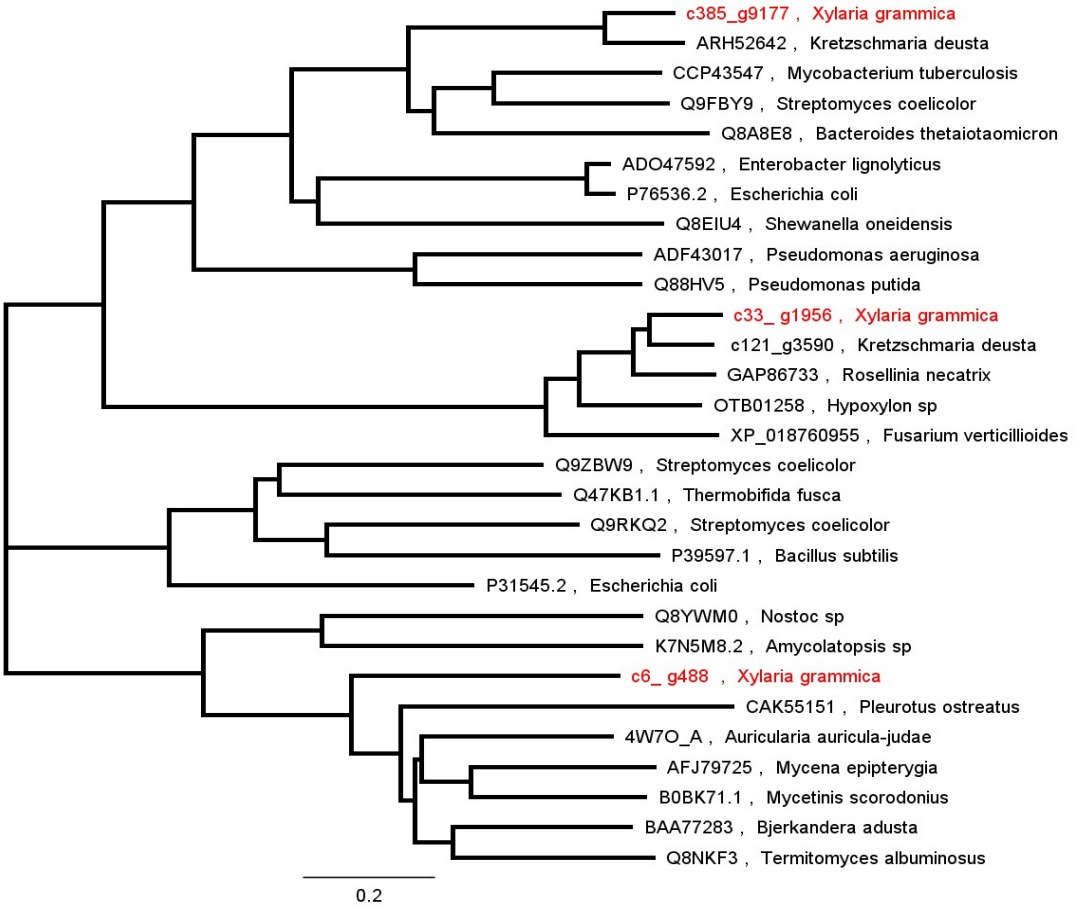

Fig 3.31: Phylogenetic tree of sequences from 29 bacterial and fungal peroxidases of the DyP-type; *X. grammica* DyPs (red). Tree building was done using GENEIOUS 10, the jukes cantor model and the neighbor joining method. The tree was built after MAFFT alignment.

The theoretical protein encoded by *g488* showed the highest homology (identities and similarities) to a *Bad*DyP (42.8 and 55.6%, respectively) and an *Aau*DyP (39.3 and 54.8%, respectively; Tab. 3.21). Gene *g9177* could be assigned to group 'B' (Zámocký and Obinger 2010) or the new group 'P' according to Yoshida and Sugano (2015), which mainly contains bacterial DyPs or encapsulin encoding sequences and a putative DyP from the wood-dwelling ascomycete *Kretzschmaria deusta* (*Kde*DyP). With the latter, *g9177* shares 77.5% and 85.2% identity and similarity, respectively. *G1956*, however,

proved to be an unusual gene encoding probably for both a DyP and a pyruvate-formate lyase-like domain[19] (similar genes are deposited in NCBI under GAW13804.1 and GAP86733.1). Moreover, it groups within a cluster of four putative DyPs from *K. deusta, Rosellina necatrix, Hypoxylon* sp. *and Fusarium vericilloides* (Fig. 3.31). Highest homology (19% and 18%) were found to the hypothetical DyP proteins of the bacterium *Bacteroides thetaiotaomicron* (*Bth*DyP), *Kde*DyP and *g9177* and the highest similarity (~35%) to *g9177* and *Bth*DyP.

Tab. 3.21: Identity and similarity matrix of the gene encoding the purified *XgrDyP* (*g488*; red) and two putative *Xgr*DyP*s* (*g9177* and *g1956;* red) in comparison to enzymes from *A. auricula-judae* (*Aau*DyP, 4W7O_A),), *B. adusta* (*Bad*DyP, BAA77283) as well as hypothetical proteins from *K. deusta (Kde*DyP, ARH52642*), Rhodococcus jostii* (*Rjo*DyP, Q0SE24) and *Bacteroides thetaiotaomicron* (*Bth*DyP, Q8A8E8).

	*Aau*DyP	*Bad*DyP	g488	*Kde*DyP	g9177	*Rjo*DyP	*Bth*DyP	g1956
*Aau*DyP		52.7	39.3	12.4	12.9	11.5	12.0	6.5
*Bad*DyP	67.3		42.8	11.6	12.8	10.9	11.0	6.0
g488	54.8	55.6		10.0	9.9	10.3	10.1	4.1
*Kde*DyP	26.9	25.3	21.1		77.5	42.5	37.2	18.0
g9177	28.2	27.1	22.4	85.2		42.9	36.1	17.6
*Rjo*DyP	24.1	21.9	20.1	57.3	56.6		46.3	6.8
*Bth*DyP	25.9	23.2	20.9	51.7	52.5	59.1		19.1
g1956	12.8	12.8	9.3	34.3	35.4	12.3	34.9	

Identity (%)

Similarity (%)

3.15.3 Classification of lignocellulytic enzymes in the *X. grammica* genome

Based on the 250 BUSCO eukaryotic subset, 1,231 (93.7%) complete and 35 (2.7%) fragmented proteins sequences were found (data not shown). Annotation using AUGUSTUS (species parameter according to *Aspergillus nidulans*, an ascomycetous mold) predicted a total of 12,126 protein-coding sequences. An assignment of these sequences

[19] Pyruvate formate lyase (*syn.* formate C-acetyltransferase, EC 2.3.1.54) is an enzyme that uses radical non-redox chemistry to catalyze the reversible conversion of pyruvate and coenzyme A into formate and acetyl coenzyme A. It is involved in the anaerobic glucose metabolism in *E. coli*.

to main enzyme classes of the CAZy classification using dbcan identified 753 carbohydrate related enzymes, including 165 enzymes with auxiliary activities (AAs), 117 carbohydrate esterases (CEs), 295 glycoside hydrolases (GHs), 97 glycosyl transferases (GTs), 18 polysaccharide lyases (PLs) and 61 carbohydrate-binding modules (CBMs) (Fig. 3.32).

Fig. 3.32: A representation of the *X. grammica* genome according to CAZy gene classification. Yellow (AA, auxiliary activities), grey (PL, polysaccharide lyases), orange (CE, carbohydrate esterases), light blue (GH, glycoside hydrolyses), green (GT, glycoside transferases) and dark blue (CBM, carbohydrate-binding modules).yellow (AA), grey (PL), orange (CE), light blue (GH), green (GT) and dark blue (CB).

3.15.3.1 Glycoside Hydrolases

Most abundant GHs in genome of the soft-rot fungus (SRF) *Xylaria grammica* belong – with 16, 22 and 17 sequences –to the functionally diverse CAZy families GH16, GH18 and GH3, respectively. Additionally, a few gene sets from GH families encoding cellulolytic (e.g. GH6, GH7), hemicellulolytic (e.g. GH10, GH11, GH27, GH35) and pectinolytic (e.g. GH43, GH28, GH53) proteins were found to be present in the *Xylaria* genome (data not shown). Not least, various CBM genes were identified belonging to 15 different CAZy families (e.g. CBM1 - exclusively present in fungi as well as CBM13, 18 and 67). They may be part of polysaccharide hydrolyzing enzymes and facilitate binding of respective enzymes to cellulose and xylans. Approximately 16% of the predicted CAZy

gene models with hydrolytic activities encoded CEs. Among them, were pectinolytic representatives like CE4, 7, 9 and 15, and members of the CE family 10 (containing carboxyl and aryl esterases); the latter was the largest family with a total of 50 predicted genes.

Interesting differences became evident between SRF, WRF, BRF and URF ('unresolved' wood-rot fungi), when comparing genes that encode proteins acting on cellulose (Tab. 3.22; e.g. CBMs, GHs). Thus, CBM, GH6 and GH7 genes are rather rare in BRF. In contrast to this, WRF, SRF and even URT possess a relatively high number of these enzymes including respective 'helper' enzymes/domains. Their number may range from ten to fifty with regard to CBMs, and from one to nine with respect to GHs in WRF and SRF.

3.15.3.2 Oxidoreductases

Lignocellulytic oxidoreductases (grouped in CAZy among AAs) deduced from predicted gene models of the *X. grammica* genome are listed in Tab. 3.22 and again, there were considerable differences observed among the three major eco-physiological groups of wood-degrading fungi (i.e. SRF, WRF and BRF). So a remarkably high number of AA9 genes encoding LPMOs was found in the *Xylaria* genome (23 genes), which ranges among the highest numbers known from WRF (e.g. 20 for *Auricularia dedicata* and 28 for *B. adusta*). Although, AA3 encoding genes (AA3_2, GMC oxidoreductases; AA3_3, alcohol oxidases) were present in the *Xylaria* genome, AA3_4 genes (pyranose oxidase) were lacking and in other SRF as well, they have been only rarely found (and if so <2). On the other hand, *X. grammica* ranges, with three CDH genes (AA3_1), within the 'top group' compared to other fungi (e.g. five genes in *Magnaporthe oryzae* or three genes in *Botryobasidium botryosum*) and particularly, it has more of these enzymes than WRF have (typically just one CDH gene). Furthermore, *X. grammica* exhibits the highest number of genes (62 copies) encoding AA7 oxidases, that are thought to be involved in the oxidative attack on gluco-oligosaccharides. The number of these genes in SRF is generally high (for example, 29 to 52 in *Podospora anserina* and *Xylaria longipes*, respectively), while they are present in small number (up to five) or lacking in WRF (e.g. in *Trametes versicolor* or *Pycnoporus cinnabarinus*, respectively).

None of the ascomycetous fungi mentioned here, irrespective whether it is a SRF, soil dweller, opportunistic saprotroph or plant pathogen, has any gene encoding for an AA2 protein (class-II peroxidases such as MnP, VP, LiP or GP). However, the high number of

laccase (AA1_1) genes (13) implicates that possibly ‘alternative’ enzyme systems could replace the ligninolytic class-II peroxidases of WRF (that may possess up to 25 of the respective AA2 genes). Moreover, other groups of peroxidases, namely the above described DyPs (chap. 3.10-3.12) as well as UPOs, could be part of such ‘alternative’ enzyme systems in ascomycetes (e.g. there are three DyP and five UPO/HTP genes present in *X. grammic*a). Finally, numerous peroxide-producing proteins (e.g. from CAZy families AA3 and AA5) as well as enzymes associated with FENTON-chemistry (such as benzoquinone reductases, AA6) were also predicted in the *Xylaria* genome.

Tab. 3.22: Lignocellulose-degrading enzymes in different basidiomycetous and ascomyceteous wood-decay fungi (supplemented and modified according to Riley et al. 2014), light yellow – white-rot fungi (WRF, Basidiomycota), grey – brown rot fungi (BRF, Basidiomycota), light blue – unresolved wood-rot fungi (URF, Basidiomycota), green – ectomycorrhizal fungi (Basidiomycota), blue – plant pathogens/ parasitic fungi (Basdiomycota and Ascomycota), yellow – oportunistic saprotrophs (e.g. *Aspergillus* spp., Ascomycota), orange – soft-rot fungi (SRF, Ascomycota):

		Basidiomycetes																		Ascomycetes														
	Order	URT			BRF							WRF						ECM		PPP			AP						SRF						
		Schco	Jaaar	Botbo	Fompi	Pospl	Wolco	Dacsp.	Glotr	Conpu	Serla	Aursu	Bjead	Phach	Phlbr	Pycci	Trave	Lacbi	Pirin	Mella	Pucgr	Ustma	Magor	Colgl	Gaetr	Chagl	Aspfu	Aspnid	Aspnig	Aspor	Xylgr	Xyllo	Krede	Scyll	Podan		
Crystalline cellulose		5	24	28	0	0	0	1	1	2	8	48	32	27	28	20	23	1	47	0	0	0	25	19	18	34	14	6	5	0	12	12	14	19	30	CBM1	Carbohydrate-binding module family 1
		1	3	3	0	0	0	0	0	2	1	2	1	1	1	1	1	0	2	0	0	0	3	4	5	4	1	2	2	1	3	3	2	1	4	GH6	Glycoside hydrolase family 6
		2	5	7	0	0	0	0	0	2	0	6	5	5	4	3	4	0	1	8	8	0	5	7	6	6	4	3	2	3	5	6	5	4	7	GH7	Glycoside hydrolase family 7
		22	15	32	4	2	2	0	4	10	5	19	28	11	12	17	18	13	25	4	3	0	23	28	25	45	7	9	8	8	23	29	21	5	33	AA9	Lytic polysaccharide monooxygenase
Lignin		0	1!	0	1*	1*	1*	0	0	0	0	19	20	11	15	11	26	0	0	0	0	0	0	0	0	0	0	0	0	0	0	0	0	0	0	AA2	Class II peroxidase
		18	17	19	16	15	8	8	20	14	8	38	30	32	32	20	17	4	8	4	5	9	9	29	8	8	8	8	22	22	16	15	12	15	14	AA3_2	GMC oxidoreductase
		2	4	5	4	2	4	3	2	6	3	9	7	6	8	7	9	4	5	4	4	3	1	0	1	1	0	0	0	0	2	2	3	1	1	AA5_1	Copper radical oxidase
		2	1	0	5	4	3	0	4	6	4	0	0	0	8	5	7	11	3	16	1	1	13	18	11	7	5	8	13	8	13	11	9	21	13	AA1_1	Laccase
		4	2	3	5	1	6	1	2	5	5	7	7	4	6	2	4	0	0	0	0	0	2	4	3	2	0	1	1	1	6	3	5	5	2	AA3_3	Alcohol oxidase
		4	1	5	5	0	0	3	0	0	0	2	4	0	0	0	0	1	3	14	5	3	33	77	32	35	1	2	2	5	62	52	50	29	29	AA7	Glucooligosaccharide oxidase
		0	1	1	1	1	1	3	1	1	1	0	2	1	2	1	2	2	0	0	1	0	2	4	1	2	2	0	2	2	2	3	3	3	2	AA1_2	Ferroxidase
		1	1	3	0	0	0	0	1	2	2	1	1	1	1	1	1	0	2	0	0	0	5	4	2	1	2	2	2	2	3	1	2	1	2	AA3_1	Cellobiose dehydrogenase
		0	1	2	0	0	0	0	1	0	0	3	5	0	1	2	1	0	0	0	0	0	0	1	1	0	0	0	0	0	0	2	0	0	1	AA3_4	Pyranose oxidase
		4	0	0	0	0	0	2	0	1	0	0	0	0	0	0	0	0	0	0	0	0	0	0	0	0	0	0	0	0	0	0	0	0	0	AA1_dist	Multicopper oxidase
		4	3	1	1	0	1	1	3	2	2	4	4	3	4	1	1	2	4	1	1	1	1	2	1	1	2	1	1	2	3	2	1	1	1	AA6	Benzoquinone reductase
		3	2	2	0	0	0	0	0	4	4	1	1	2	2	2	2	0	2	0	0	0	2	1	1	2	3	1	1	4	1	3	1	1	2	AA8	Iron reductase domain
		0	2	0	0	0	0	2	3	0	0	0	0	0	0	0	0	1	0	0	0	0	1	7	3	2	0	2	1	0	3	4	3	5	7	AA4	Vanillyl alcohol oxidase
		1	1	3	0	2	0	0	0	0	0	11	9	3	3	0	2	2	2	2	7	0	0	1	0	0	2	0	0	9	3	4	2	1	0	DyPs	DyP-type peroxidase
		3	8	7	5	5	5	6	6	2	3	15	4	2	2	3	3	5	2	11	3	2	3	8	5	3	8	5	5	7	5	4	3	2	4	HTP	Heme-thiolate peroxidases

Aspfu, *Aspergillus fumigates;*Aspnid, *Aspergillus nidulans*; Aspnig, *Aspergillus niger*; Aspor, *Aspergillus oryzae*; Aursu, *Auricularia subglabrata*; Bjead, *Bjerkandera adusta*; Botbo, *Botryobasidium botryosum*; Chagl, *Chaetomium globosum*; Colgl, *Colletotrichum gloeosporioides*; Conpu, *Coniophora puteana*; Dacsp, *Dacryopinax sp.*; Fompi, *Fomitopsis pinicola*; Gaetr, *Gaeumannomyces tritici*; Glotr, *Gloeophyllum trabeum*; Jaaar, *Jaapia argillacea*; Krede, *Kretzschmaria deusta* Lacbi, *Laccaria bicolor*; Magor*, Magnaporthe oryzae*; Mella, *Melampsora laricis-populina*; Phach, *Phanerochaete chrysosporium*; Phlbr, *Phlebia brevispora*; Podan, *Podospora anserine*; Pospl, Postia placenta; Pucgr, *Puccinia graminis*; Pycci, *Pycnoporus cinnabarinus*; Pirin, *Piriformospora indica*; Schco, *Schizophyllum commune*; Serla, *Serpula lacrymans*; Scyli, *Scytalidium lignicola*; Trave, *Trametes versicolor*; Ustma, *Ustilago maydis*; Wolco, *Wolfiporia cocos*; Xglgr, *Xylaria grammica*; Xyllo *Xylaria longipes*

4 DISCUSSION

4.1 Setting up a culture collection of Kenyan fungi

In the present study, 43 new fungal isolates were successfully isolated from three different Kenyan forest types and biodiversity hotspots (KAKAMEGA as a tropical rainforest from the Guineo-Congolina type; the ABERDARE mountain range and the ARABUKO SOKOKE as the largest fragments of East African coastal forests; Kenya Wildlife Service). The isolates correspond to 21 families of the (sub)phyla Basidiomycota, Ascomycota and Mucoromycotina, and represent 38 different species, which is indicative for the high diversity of Kenyan forests. Most of the basidiomycetous isolates belong to the eco-physiological groups of white-rot fungi (WRF) and litter-decomposing fungi (LDF) causing the degradation of lignocellulosic materials (e.g. from the families Polyporaceae as well as Psathyrellaceae and Strophariceae, respectively). They were isolated from coarse woody debris (trunks, branches, stumps), soil litter (leaves, twigs, grass remains) or animal droppings (dung of herbivores). The only brown-rot isolate was the polyporous fungus *Fomitopsis*[20] *meliae*. Among the saprotrophic ascomycetes, two members of the family Xylariaceae, which harbors various soft-rot fungi, were isolated from coarse woody debris. The other ascomycetous families include unspecific saprotrophs living on organic soil materials (such as *Fusarium solani* as member of the Nectriaceae) or as parasites on plants, other fungi, insects or nematodes (e.g. the family of Pleosporaceae with two *Cochliobolus* species, the Bionectriacea with *Clonostachys rosea* or *Stagonosporopsis cucurbitacearum* as a member of the *incertae sedis*, i.e. 'of uncertain phylogenetic placement'). Further saprotrophs isolated from decaying plant remains turned out to be representatives of the zygomycetous genus *Mucor* (four strains) that contains numerous fast-growing molds (Hesseltine, 1955).

There are only a few studies reporting on the specific isolation of fungi from environmental compartments (i.e. soils, woody debris, water) and biodiversity hotspots in the tropics (e.g. from soil of the Amazon rain forest; Sena et al. 2018). They mainly focus on 'microscopic' fungi (molds) belonging to the Ascomycota (including former 'deuteromycetes') and 'Zygomycota' (Kutateladze et al. 2016, Ahirwar et al. 2017). Two studies describing also the isolation of saprotrophic Basidiomycota were published by

[20] In older publications, the fungus has been also referred to as *Fomes meliae* but the genus *Fomes* is (nowadays) restricted to white-rot fungi such as *Fomes fomentarius* (Tinder fungus; Kim et al. 2007).

Rojas-Jiménez & Hernández (2015) and almost 20 years earlier, by Thorn et al. (1996). In the former article, representatives of 24 fungal families and 40 genera were reported to be present in guts of tropical wood-feeding beetles (Coleoptera), among them three basidiomycetous genera (*Coprinellus* sp., *Trametes* sp. and *Phlebia* sp.). Thorn et al. (1996) specifically isolated 67 basidiomycetous strains from soils of various sampling sites (e.g. a hybrid poplar plantation, conifer forests) by using malt-extract agar supplemented with lignin, the plant ingredient guaiacol and the fungicide benomyl (that reduced the growth of unwanted molds). However, the identification of the fungi was exclusively based on morphological and physiological characteristics and did not include molecular data.

The most comprehensive study on the isolation of tropical fungi and the establishment of a respective culture collection has recently published by Brandt and coworkers (Brandt et al. 2018). They set up a collection of almost 300 fungal strains from nine different habitats and locations in Vietnam (wood, rice straw, shrimp shells, dead insects, etc.), a country with a high organismic diversity and a 'hidden treasure box' of yet unknown microbial species. Of the 295 isolated strains, 164 species were identified to species level (ITS-based) and most of them were also assayed for special enzymatic activities such as cellulase, xylanase, chitinase and lipase in order to find new producer strains and enzymes with biotechnological relevance, e.g. for the conversion of plant waste materials (Brandt et al. 2018). A similar approach has been followed here with setting up a small but focused culture collection of Kenyan fungi from specific forest habitats. In the next step, the isolated fungi were evaluated for their potential to produce and secrete biotechnologically relevant oxidoreductases, in first place heme-peroxidases (DyPs, PODs) and unspecific peroxygenases (UPOs).

4.2 First description of a new *Psathyrella* species

Psathyrella aberdarensis was described as a new species that is characterized by small fruiting bodies, a persistent veil made of polymorphic elements and very pale spores without a recognizable germ pore (Melzer et al. 2018). Some other species without pleurocystidia, the spores of which are also pale and do not have a germ pore, are mentioned below along with species suggesting a closer relationship to the new *Psathyrella* species for other reasons. Since sequences of these species are currently not available from Genbank, distinctions have been made based on morphological and microscopic characteristics that – as a whole – appear to be plausible.

Psathyrella aequatoriae SINGER was described from Ecuador. According to Singer (1978) it is a very small species with a cap diameter of 6-14 mm and without (or not visible) veil. The lamellae are crowded and only pale brownish. *Psathyrella atroumbonata* PEGLER is habitually quite similar but represents a larger species, the veil of which hangs on the margin of the cap and consists of hyaline hyphae. The spores are pale brownish, and the germ pore is small and sometimes indistinct. However, the drawings in Pegler (1966, 1977) show strongly truncate spores.

Psathyrella bivelata CONTU is probably a closely related species due to a similar veil structure (globose elements mixed with branched-cylindrical, slightly thick-walled elements). The spores, however, are larger, darker and have a germ pore. Moreover, the species is currently known only from the Mediterranean region (Contu 1991, Voto 2011, Sammut and Melzer 2012).

Psathyrella pallidispora DENNIS has spores with the dimensions 8-11 × 4-5 µm and a more slender shape, the cheilocystidia are often capitate (see Fig. 9 G in Dennis 1970). No records are known outside South America.

Psathyrella varicosa A. PEARSON is relatively large (fruiting body), the cap up to 60 mm wide, and the stipe up to 120 mm long. A veil is not mentioned (Pearson 1950). The spores have the dimensions (6-) 7-9 × (4-) 4.5-5 µm, are frontally ellipsoid to amygdaloid, laterally phaseoliform, yellowish; the germ pore is absent. The terrestrial (soil-associated) species was described from South Africa (Melzer et al. 2018).

The phylogenetic tree, in which the new taxon, *P. aberdarensis*, clusters, is shown in Fig. 3.1. Its closest relatives are *Psathyrella singeri* A. H. SM., *Psathyrella sulcatotuberculosa* (J. FAVRE) EINHELL, and an unidentified fungal strain. The sequence of the latter (KF800637.1) was deposited by Rittenour et al. (2014), but unfortunately without any morphological description. *P. singeri* was first described from a wetland area in the U.S. (Florida). A veil was not mentioned in Smith (1972) and the lamellae were described as very crowded and strikingly pale. A respective sequence in the NCBI Genbank (MG734718.1) was analyzed using a specimen from China, Jilin, Changbai Mountain National Nature Reserve (Yan and Bau 2018). It is not certain whether this sequence in fact belongs to *P. singeri*; in any case, it does not match with the *P. aberdarensis* sequence and thus surely represent a separate species. On the other hand, a good match was found between *P. aberdarensis* and *P. sulcatotuberculosa*. This species forms also small and fragile fruiting bodies on dead wood, and its spores that are all almost of the same size

appear very pale and do not have a distinct germ pore or – at best – very indistinct germ pores. However, there are also significant differences to *P. aberdarensis*: The cheilocystidia are more polymorphic, the cap surface is heavily rugulose, the veil being pale yellowish and fibrillose does not make patches and is made of subcylindrical to median slightly enlarged, thin-walled cells, some of which are sometimes encrusted. A detailed description is given by Battistin et al. (2014).

In summary, the genus *Psathyrella* (Brittlestems, Germ. *Faserlinge*) is obviously more diverse than originally expected[21] and with the broader use of molecular identification tools, the number of species will certainly increase over the next years, particularly with respect to tropical and subtropical representatives.

4.3 Agar-plate screening of fungal isolates for oxidoreductases

First indications for the production and secretion of oxidative enzymes by larger numbers of fungal strains and isolates can be inferred from rather simple agar-plate screenings introduced by Hofrichter and Fritsche (1997) and further developed by Steffen et al. (2000). These screenings are appropriate for the rapid assessment of fungal activities related to the oxidation of aromatics including lignin and are based on color changes of indicator substrates (usually ABTS, Mn^{2+} and sodium humates) added to synthetic or complex agar media (chap. 2.2.4).

Color changes of colorless ABTS molecules to form blue-green cation radicals ($ABTS^{+\bullet}$) or purple-to-violet colored dications ($ABTS^{2+}$) are strongly indicative for the presence of extracellular oxidoreductases catalyzing one-electron oxidations (Gramss 2017); at least one of these reactions was observed for most of the basidiomycetous strains tested (Tab. 3.3). One should keep in mind, however, that the oxidation of ABTS is rather unspecific and realized by both 'true' ligninolytic class II PODs (including LiP, MnP and VP) as well as by generic peroxidases, UPOs, DyPs and laccases. In any case, BRF are lacking class II PODs in their genomes (Riley et al. 2014, Sipos et al. 2017) and it has been proposed that they may have evolved from WRF, in the course of which they lost the respective genetic information (Rytioja et al. 2014, Floudas et al. 2012). On the other hand, this assumption applies only to ligninolytic peroxidases as a few reports showed the presence of laccase genes in the genomes of BRF such as *Gloeophyllum trabeum*, *Postia placenta*, *Wolfiporia cocos*, *Merilus lacryman*, and *Coniophora puteana* (Lee et

[21] The 'Dictionary of the Fungi' (10th ed.) from 2008 mentioned already about 400 *Psathyrella* species.

al. 2004, D'Souza et al. 1996). *F. meliae*, the only BRF isolated and tested here, did not cause any color change of ABTS indicating the absence of laccase. Similar is valid for a *Schizophyllum* sp. that did not oxidize ABTS in agar plates as well; it can be assumed that it is related to *Schizophyllum commune*, a wood-dwelling fungus that causes a weak 'unresolved' type of wood-rot (Floudas *et* al., 2012).

The oxidation of Mn^{2+} into Mn^{4+} (MnO_2) in agar plates is a specific reaction of certain ligninolytic peroxidases (MnPs, VP) and the result of the disproportionation of incipiently formed Mn^{3+} in aqueous solution in the absence of sufficient amounts of chelators (Steffen 2003).

$$2\ Mn^{3+} \rightarrow Mn^{2+} + Mn^{4+}$$

$$Mn^{4+} + O_2 \rightarrow MnO_2$$

MnO_2 formation in form of dark-brown to black spots and rings was less frequently observed than ABTS oxidation. Positive reactions were typically brought about by WRF and LDF belonging to the basidiomycetous orders Polyporales and Agaricales such as *Trametes gibbosa*, *Phlebia subseriales* and *Stropharia rugosoannulata*. Meanwhile, numerous genomes of polyporous and agaric fungi (69 and 103 species, respectively[22]) have been sequenced and deposited, for example, those of *Bjerkandera adusta*, *Ganoderma* sp. and *Phlebia brevispora*, (Binder et al. 2013), *Trametes versicolor* (Floudas et al. 2012), *Coprinopsis cinerea* (Stajich et al. 2010), *Pleurotus ostreatus* (Riley et al. 2014), and *Lentinula edodes* (Chen et al. 2016). It turned out that all WRF sequenced so far contain one or more genes encoding for manganese-oxidizing class II PODs (i.e. MnP and/or VP; Riley et al. 2014, Sipos et al. 2017). The physiology and biochemistry of some of these and related enzymes have been known for a long time, and respective proteins were purified and characterized regarding their substrate spectra and potential roles in lignin and humus degradation (Hofrichter 2002; *Psilocybe cubensis*, Steffen et al. 2000; *S. rugusoanulata* and *Phlebia radiata*, Liers et al. 2011, *B. adusta*, Heinfling et al. 1998; *P. radiata*, van Aken et al. 1999; *Lentinus sajor-caju*, Martinez et al. 1996; *T. versicolor*, Carabajal et al. 2013).

Since ascomycetes and zygomycetes are lacking MnP and VP sequences in their genomes[3] (e.g. *Scytalidium lignicola,* Büttner et al. 2018; *Lecythophora hoffmannii*, Leonhardt et al. 2018; *Rhizomucor pusillus*, Hüttner et al. 2018; *Kretzschmaria deusta*,

[22] https://genome.jgi.doe.gov; Status: 05.11.2018

Büttner et al. 2017; *Chaetomium globosum*, Berka et al. 2011), just the oxidation of ABTS in agar plates was followed in these cases. Positive reactions – theoretically indicative for UPO, DyP or laccase activities – were merely observed for twelve species. Some of them belong to genera that are known to secrete laccases, e.g. *Cochliobolus* (Sumathi et al. 2016), *Fusarium* (Kwiatos et al. 2015), *Pestalotiopsis* (Naranjo-Briceño et al. 2013; Chen et al. 2011) and *Xylaria* (Liers et al. 2006, 2007). In the other cases, such knowledge is missing and it is ambiguous whether they have laccase genes in their genomes. For example, *Mucor circinelloides* (CBS277.49v2) possesses seven AA1 genes that can be classified as multicopper oxidases (three ferroxidases and four oxidases distantly related to laccases), however, the presence of 'true' laccase genes (AA1_1) has not been reported so far. Furthermore, *M. circinelloides* was found to contain putative UPO genes but no DyP encoding gene (Zámocký et al. 2015). Genome data of the ascomycetous genera *Pseudallescharia* and *Stagonosporopsis* are not available from the JGI portal.

4.4 Production of oxidoreductases by Kenyan isolates in liquid culture

A further screening test was performed in liquid cultures of the fungi using a plant-based complex medium (soy-peptone) that has been shown to stimulate the production of extracellular oxidoreductases (UPO, DyP, MnP, laccase) both in basidiomycetes and ascomycetes (Ullrich et al. 2004, Liers et al. 2006, Anh et al. 2007, Gröbe et al. 2011, Pecyna 2015). That way seven new producer strains were identified: four basidiomycetes that secreted UPO activities (measured with veratryl alcohol; Fig. 3.5) and three fungi that realized Mn-independent peroxidase activities of the DyP-type (Fig. 3.6). Interestingly, among the latter fungi was an ascomycete. Three of the four UPO producing strains were members of the family Psathyrellaceae (*Coprinellus micaceus*, *Psathyrella candolleana, P. aberdarensis*). Anh et al. (2007) already demonstrated that two members of this family, *Coprinellus radians* and *Coprinopsis verticillata*, produced UPOs in a soybean-glucose medium.

Generally, UPO and DyP genes are widely distributed in the whole fungal kingdom including some pseudo-fungal protists. Over 4,300 putative UPO sequences and 2,500 DyP sequences from over 500 species can be found in public databases (Hofrichter et al. 2015, 2019; H. Kellner and M. Pecyna 2019, personal communication). UPOs occur in the genomes of most true fungi (Eumycota) as well as in fungus-like 'Oomycota' (actually stramenopiles of the class Peronosporomycetes). The majority of UPO sequences is present in the subkingdom of Dikarya ('higher' fungi) with over 2,500 ascomycetous and

1,500 basidiomycetous sequences (Hofrichter et al. 2015, 2019, H. Kellner, personal communication). Fungal DyPs can be found in more than 100 basidiomycetous and ascomycetous species with about 400 and 200 individual sequences, respectively. Though thousands of putative UPO sequences are meanwhile known, just eleven proteins of heme-thiolate peroxidases (CPO as well as eight wild-type and two recombinant UPOs) from eight organisms (*Caldariomyces fumago*, Shaw et al. 1959, Manoj and Hager 2008; *Agrocybe aegerita*, Ullrich et al. 2004, 2009, Molina-Espeja et al. 2014; *C. radians*, *C. verticillata*, Anh et al. 2007; *Marasmius rotula*; Gröbe et al. 2011; *C. cinerea*, Babot et al. 2013; *C. globosum,* Kiebist et al. 2017; *Marasmius wettsteinii*, Ullrich et al. 2018) have been characterized so far. In the case of fungal DyPs, nine proteins from seven organism have been reported (*B. adusta*, *Mycetinis scorodonius*, *Termitomyces albuminosus*, *Auricularia auricula-judae*, *Exidia glandulosa*, *Mycena epipterygia*, *Irpex lacteus*; Pecyna, 2015); moreover there are numerous reports on intracellular bacterial DyPs, which, however, considerably differ from their fungal counterparts (Yoshida and Sugano 2015).

The conditions under which UPOs and DyPs are expressed and secreted are not fully understood yet (Hofrichter et al. 2015; Pecyna 2015). This applies also to the physiological functions of both enzyme types, which appear more or less nebulous. The induction of UPOs and DyPs under lab-scale conditions is usually accomplished by using complex plant-based growth media. In the case of UPOs, that are nitrogen-rich legume media with a low content of phenolics such as soybean meal suspension (Ullrich et al. 2004), glucose-peptone media or alfalfa pellets (Gröbe et al. 2011), diluted soymilk or crushed tofu (Pecyna 2015). Furthermore, M. Pecyna (2015) reported in his dissertation that – at least in the case of *A. aegerita* – there are indications for the proteinaceous nature of UPO-inducing components in soybeans (probably related to peptides of the storage proteins β-conglycinin and glycinin).

Not least, due to the exceptional catalytic properties and biotechnological relevance of UPOs, the search for new UPO producers and UPO-inducing growth media remains an attractive item. This especially applies to ‘unusual’ UPOs from ‘lower’ fungi or protists, of which merely putative sequences having little homology with known UPO sequences in databases, for example, from endomycorrhiza-forming Glomeromycota (e.g. *Rhizophagus*), from representatives of the basal phylum Chytridiomycota (*Gonapodya, Spizellomyces*) or from the diatom *Thalassiosira*.

The fungal DyPs that have been characterized so far (only nine representatives are known) can also be produced in complex plant-based media, e.g. in soybean meal suspension or in diluted 'organic tomato juice' supplemented with 'elicitors' like phenols or terpenoids (as shown for the DyPs or *M. epipterygia* and *E. glandulosa*; Liers et al. 2013). Stimulating effects of such media on fungal growth and enzyme secretion were reported in several studies and can be attributed to low-molecular mass secondary metabolites (e.g. phenolic compounds) always present in plant materials (Ullrich et al. 2004; Liers et al. 2013). In this context, the stimulation of DyP secretion by guaiacol, a natural phenolic ingredient of beech trees (*Fagus sylvatica*; Bollag and Leonowicz 1984, Liers et al. 2007) or by β-carotene, a ubiquitous tetraterpene known to be oxidized by DyPs of *M. scorodonius* (Scheibner et al. 2008), strongly supports this assumption.

For subsequent protein purification and characterization studies, the most interesting fungal candidates were those with the highest activity levels of UPO (*P. aberdarensis* with >800 U L^{-1}; chap. 4.3) or DyP (*X. grammica* with ~750 U L^{-1}). Notably, the latter fungus has been the first ascomycete that produces a wild-type DyP. The enzyme titers secreted by both fungi correspond to medium activity levels mentioned for other fungi. Several fungi have been reported to secrete low amounts of UPO or DyP (<100 U L^{-1}), which are sometimes difficult to verify and too low to serve as starting point for purification studies (e.g. UPOs: *Agrocybe pediades*, *Aspergillus nidulans*, *Mycena galopus*; Pecyna 2016 or DyPs: *Mycena haematopus*, *S. rugosoannulata*; Liers et al. 2011). On the other hand, there are only some 'rare' fungal species/strains that produce high-enough enzyme titers making laborious purification and subsequent characterization and application studies worthwhile, like *M. rotula* (with ~41,000 U L^{-1} UPO corresponding to 445 mg L^{-1}, Gröbe et al. 2011) or *A. auricula-judae* (with ~8,000 U L^{-1} DyP, Liers et al. 2010).

While larger amounts of the DyP of *X. grammica* (*Xgr*DyP) were produced in agitated 500 or 2,000-mL Erlenmeyer flasks (containing 200 or 1,000 mL culture medium; chap. 2.4.2), UPO production by *P. aberdarensis* (*Pab*UPO) occurred, in a single step, on a larger scale in a 30-L bioreactor with 15 L medium (chap. 2.4.1). Though this cultivation strategy was accompanied with an activity loss of up to 800 U L^{-1}, the advantage lay in the simple 'one-pot fermentation step' and the production of large volumes of crude enzyme broth. On the other hand, it is known that only a small number of fungi are suitable for an upscaling from flask cultivation to reactor-scale at 5 to 30 L (Ullrich et al.

2005; Gröbe et al. 2011). The reason for that may be altered culture conditions like increased shear stress and reduced supply of dissolved dioxygen.

4.5 Comparison of *Pab*UPOs with other fungal peroxygenases

4.5.1 General aspects

The purification of *Pab*UPO was carried out with an FPLC device (via AEC and SEC, chap. 2.5.2) and resulted in three different protein fractions. Similar methods were successfully applied for the purification of other UPOs, e.g. from *C. radians* and *C. verticillata* (Anh, 2008) or *M. rotula* (Gröbe et al. 2011). Table 4.1 compares properties of the three *P. aberdarensis* unspecific peroxygenases (*Pab*UPOs) with those of five other UPOs and CPO from *C. fumago*. The specific activities (74 to 117 U mg^{-1}), molecular masses (40-41 kDa) and isoelectric points (p*I*s 3.8 to 4.2) of *Pab*UPOs are in a similar range as those of the related enzymes belonging to the protein family of 'long' UPOs (along with *Aae*UPO, *Cra*UPO and *Cve*UPO with 30 to 197 U mg^{-1}, 40 to 46 kDa and p*I*s 3.8 to 5.2). Contrary, proteins of the family of 'short' UPOs are known to form dimers and in its monomeric forms have just molecular masses between 32 and 36 kDa. The presence of different isoforms and isoenzymes of the same enzyme (according to its catalyzed reaction) has also been described for other heme-thiolate proteins, e.g. for CPO (Hashimoto and Pickard 1984), *Cra*UPO and *Cve*UPO (Anh 2008) as well as for *Aae*UPO (Ullrich et al. 2009) and particularly for *Mro*UPO (Gröbe et al. 2011); the *Mro*UPO cluster seemingly forms a multigene family with as much as 60 different UPO genes (Hofrichter et al. 2019). In addition to true isoenzymes encoded by different genes and allelic UPO forms (due to the dikaryotic nature of most basidiomycetes), UPO diversity can be the result of different glycosylation patterns (Hofrichter and Ullrich 2006, Sae and Cunningham 1979). Thus, the UPO isoforms of *A. aegerita* were found to have the same molecular mass but slightly differing isoelectric points, which led to an incomplete protein separation by ion exchange chromatography. The only method to purify these differently glycosylated *Aae*UPO forms with almost identical physicochemical and catalytic properties turned out to be highly pH-sensitive chromatofocusing (Ullrich et al. 2009).

Tab. 4.1 Comparison of the three purified peroxygenases from *Psathyrella aberdarensis* (*Pab*UPOs) with other UPOs characterized so far ('short' UPOs are highlighted in grey).

Organisms	Enzyme	Mw (kDa)	(p*I*/s)	Spec. activity U mg^{-1}
P. aberdarensis	*Pab*UPO I	40.0	4.2	74
P. aberdarensis	*Pab*UPO II	40.4	4.0	117
P. aberdarensis	*Pab*UPO III	41.3	3.8	98
A. aegerita[1]	*Aae*UPO	46	4.9-5.7	165
C. radians[2]	*Cra*UPO	43-45	3.8-4.5	30-60
C. verticillata[2]	*Cve*UPO	40	4.5-5.2	197
M. rotula[3]	*Mro*UPO	32 (58[#])	5.0-5.3	77
M. wettsteinii[4]	*Mwe*UPO	32-33 (62[#])	n.d.	38
C. globusum[5]	*Cgl*UPO	36	5.6*	191-292
C. fumago[6]	CPO	40 - 46	4.0	n.d.

*calculated theoretical pI according to the *Cgl*UPO gene, [#]dimeric form, n.d. not determined; [1]Ullrich et al. (2004), [2]Ahn et al. (2008), [3]Gröbe et al. (2011), [4]Ullrich et al. (2018), [5]Kiebist et al. (2017), [6]Hollenberg and Hager (1973)

The absorption maxima of the three *Pab*UPOs (soret bands between 416 and 420 nm, α-bands at 570 and 575 nm, β-bands at 537 and 541 nm; chap. 3.6) clearly indicate their affiliation to the superfamily of heme-thiolate proteins that comprises besides UPOs the highly diverse protein superfamily of cytochrome P450 enzymes (Hofrichter et al. 2010, Omura 2005).

4.5.1 Physicochemical optima and stabilities of *Pab*UPOs

The pH optima of the purified *Pab*UPOs were determined for two substrates, i.e. the routinely used veratryl alcohol (chap. 3.8, Ullrich et al. 2004) and 5-formylfuran-2-carboxylic acid (FFCA). *Pab*UPO I was found to exhibit an unusually broad pH-optimum for the oxidation of veratryl alcohol and showed still ~60% of its maximum activity at pH 2.0. This finding differs from those of the UPOs from *M. rotula* (*Mro*UPO) and *A. aegerita* (*Aae*UPO), which maintained merely 20% or even no activity at that pH (Fig. 4.1; Gröbe et al. 2011, Ullrich et al. 2004). As expected, the pH optima of the isoforms *Pab*UPO II and III differed just slightly among each other but to some extent from that of isoenzyme I. The profiles rather resemble those of *Mro*UPO and *Aae*UPO but with a

more distinct pH maximum between pH 5.5 and 7.0. However, in contrast to those enzymes, *Pab*UPO II and III showed a relatively high activity (80% and 60%, respectively) still at pH 9.0. The same is true for the oxidation of FFCA, which was only studied using the proteins II and III (in contrast, *Pab*UPO I showed just a negligible reaction with FFCA as substrate over the whole pH-range). The different pH optima of the three *Pab*UPOs for both substrates support the assumption that *Pab*UPO I is an isoenzyme and *Pab*UPO II and III represent isoforms of the same gene (chap. 3.8). The pH profiles and optima of *Pab*UPO II and III resemble those determined for *Aae*UPO (pH 6.0; Karich et al., 2018), the only peroxygenase able to efficiently oxidize FFCA.

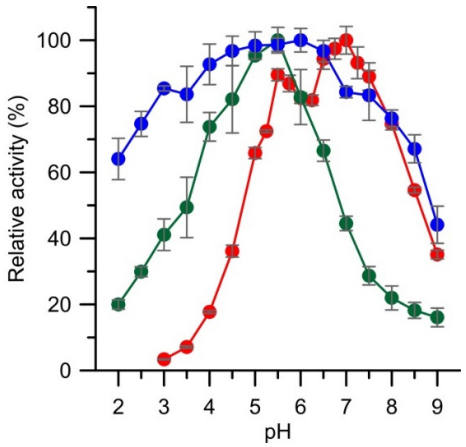

Fig. 4.1: pH-Profiles and optima for the oxidation of veratryl alcohol by *Pab*UPO I (blue) in comparison to the UPOs from *M. rotula* (*Mro*UPO, green; Gröbe et al. 2011) and *A. aegerita* (*Aae*UPO III, red; Ullrich et al. 2004).

This assumption was further supported by the pH stability tests (chap. 3.8). All three proteins turned out to be relatively stable at neutral pH, but the isoenzyme *Pab*UPO I was rather stable under acidic pH conditions, while the two other isoforms were stable in an alkaline environment. Maybe such different physicochemical properties of secreted UPO isoforms and isoenzymes reflect adaptations to rapidly changing conditions in the fungal habitat. To sum up, all three *Pab*UPOs exhibited notable pH stabilities at pH-values where they acted with optimal activity. So far, similar findings have not been reported for any other characterized UPO.

The *Pab*UPOs were relatively stable at 25°C (e.g. *Pab*UPO II and II retained 80-90% activity after eight hours, respectively; chap. 3.8) but rapidly lost their activity at elevated temperatures above 40°C. The UPOs from *A. aegerita* and *C. radians* showed a similar behavior and remained also 80% of their initial activity after eight hours at 25°C (Ullrich

et al. 2005, Anh et al. 2007). The most stable enzyme of *P. aberdarensis* was *Pab*UPO I, which still showed over 90% residual activity after the same incubation time. Similar as described for *Cra*UPO (>60% remaining activity after eight hours; Anh et al. 2007), the stability of the *Pab*UPOs II and III at 60°C (~60%; Fig. 3.14) was relatively high when comparing these data with those of the model enzyme *Aae*UPO (<10% remaining activity after eight hours at 60°C; Ullrich et al. 2008).

The higher temperature stability of the two isoforms *Pab*UPO II and III as well as the interesting 'behavior' of all three *Pab*UPOs under varying pH conditions make them interesting candidates for synthetic applications, e.g. in enzyme cocktails that cover a broad pH range.

4.5.2 Catalytic properties of *P. aberdarensis* UPOs

Comparison of the apparent kinetic data of *Pab*UPOs with those of other UPOs revealed that they exhibit relatively low affinities (K_M = 856 to 1,291 µM) towards veratryl alcohol, which represent medium values compared to the lowest and the highest K_M values determined so far (for *Cra*UPO and *Cve*UPO: 88 and 3,013 µM, respectively). It is worth noting that, the corresponding k_{cat} of *Pab*UPOs III and II (122 and 104 s^{-1}, respectively) are the highest values ever reported for this substrate, whereas that of *Pab*UPO I (k_{cat} = 20 s^{-1}) is among the lowest ones so far evidenced for any UPO (Tab. 4.2).

Tab. 4.2: Apparent kinetic data (K_M, k_{cat} and k_{cat}/K_M) of *Pab*UPOs for veratryl alcohol as substrate in comparison with data of other wild-type UPOs. [a] Ahn et al. 2007, *Cra*UPO – *Coprinellus radians* UPO; [b] Gröbe et al. 2011, *Mra*UPO – *Marasmius rotula* UPO; [c] Ullrich et al. 2004, *Aae*UPO – *Agrocybe aegerita* UPO; [d] Ahn 2008, *Cve*UPO – *Coprinopsis verticillata* UPO; [e] Kiebist et al. 2017, *Cgl*UPO – *Chaetomium globosum* UPO.

Enzyme	k_{cat} (s^{-1})	K_M (µM)	k_{cat}/K_M (s^{-1} M^{-1})	pH
*Pab*UPO III	122	904	1.35 x 10^5	7.0
*Pab*UPO II	104	1,291	8.02 x 10^4	7.0
*Aae*UPO [c]	85	2,367	3.58 x 10^4	7.0
*Mro*UPO [b]	49	279	1.76 x 10^5	5.5
*Cra*UPO [a]	34	88	3.86 x 10^5	7.0
*Cve*UPO [d]	33	3,013	1.09 x 10^4	7.0
*Pab*UPO I	20	856	2.36 x 10^4	7.0
*Cgl*UPO [e]	19	346	5.49 x 10^5	7.0

For the phenolic substrate 2,6-dimethoxyphenol (DMP), *Pab*UPO II and III (K_M = 143 and 129 µM, respectively) were found to have higher affinities, which are comparable to that determined for *Mro*UPO (K_M = 133 µM). Indeed, *Pab*UPO I had the lowest affinity to this substrate (K_M = 656 µM) compared to all other characterized UPOs. The affinities to ABTS (K_M = 105 to 145 µM), the second one-electron-oxidation substrate, ranged in the middle of those reported for the other UPOs (K_M = 37 to 423 µM of *Aae*UPO and *Cve*UPO, respectively).

Tab. 4.3: Apparent kinetic data (K_M, k_{cat} and k_{cat}/K_M) of *Pab*UPOs for vertryl alcohol, 2,6-dimethoxyphenol (DMP) and ABTS in comparison to data obtained for other wild-type UPOs ([a]Ahn et al. 2007, *Cra*UPO – *Coprinellus radians* UPO; [b] Gröbe et al. 2011, *Mra*UPO – *Marasmius rotula* UPO; [c] Ullrich et al. 2004, *Aae*UPO – *Agrocybe aegerita* UPO; [d] Ahn 2008, *Cve*UPO – *Coprinopsis verticillata* UPO; [e] Kiebist et al. 2017, *Cgl*UPO – *Chaetomium globosum* UPO).

Enzyme	K_M (µM)		
	VA	2,6-DMP	ABTS
*Pab*UPO III	904	129	145
*Pab*UPO II	1,291	143	128
*Pab*UPO I	856	656	105
*Aae*UPO [c]	2,367	298	37
*Mro*UPO [b]	279	133	71
*Cra*UPO [a]	88	342	49
*Cve*UPO [d]	3,013	284	423
*Cgl*UPO [e]	346	205	106

In addition to ‘classic’ peroxidase substrates such as ABTS, DMP and veratryl alcohol, substrates specificities of the three *Pab*UPOs towards typical peroxygenase substrates such as aromatic ethers and esters, alkyl aromatics and halides were also tested (chap. 3.9 and 3.10).

Tab. 4.4: Overview on the conversion of peroxygenase-specific substrates by *Pab*UPOs in comparison to other wild-type UPOs (*Aae*UPO – *Agrocybe aegerita* UPO, *Cra*UPO – *Coprinellus radians* UPO, *Mra*UPO – *Marasmius rotula* UPO); ++ - effective conversion, + **-** moderate conversion, **(+)** conversion of traces, 0 – no conversion.

Substrate	*Pab*UPO I	*Pab*UPO II	*Pab*UPO III	*Aae*UPO	*Cra*UPO	*Mro*UPO
Anisole	+	++	++	+	+	+
Toluene	+	+	+	+	+	+
Naphthalene	+	+	+	+	+	+
Bromination of phenol	(+)	+	+	+	+	0
Chlorination of phenol	(+)	(+)	(+)	(+)	(+)	0
4-Nitrobenzodioxole	+	+	+	+	+	+
Oseltamivir	0	0	0	0	+	0

In accordance to most characterized UPOs, *O*-dealkylation of anisole (ether cleavage), aromatic epoxidation/hydroxylation (naphthalene), combined aromatic and aliphatic hydroxylation (toluene), demethylenation (nitrobenzodioxole) and to some extent halide peroxygenation and subsequent halogenation (chlorination and bromination of phenol) were evidenced for the three *Pab*UPOs (Tab. 4.4).

Overall, the substrate spectra of *Pab*UPOs confirm their affiliation to the 'long' UPO clade, to which also *Aae*UPO, *Cr*aUPO and *Cve*UPO belong (Hofrichter et al. 2015). It is unlikely that *Pab*UPOs catalyze the conversion of bulky substrates, a catalytic feature that is seemingly a specific feature of 'short' UPOs like *Cgl*UPO or *Mro*UPO and *Mwe*UPO and includes, for example, the conversion of steroids such as testosterone (Kiebist et al. 2017) or cortisone (Ullrich et al. 2018). 'Short' UPOs are phylogenetically older and have a wider and flatter heme channel compared with 'long' UPOs (thus the channel of 'short' *Mro*UPO is about 4 Å shorter and up to 5 Å wider than that of *Aae*UPO). Furthermore, the flanking amino acids at the entrance of and within the heme channels differ in 'short' and 'long' UPOs; in the former, they are mostly less hydrophobic, more flexible and aliphatic (Ullrich et al. 2018).

Indeed, when the same activity in terms of veratryl-alcohol-oxidizing units (0.5 U mL^{-1}) was used in certain enzymatic reactions, the amount of reaction products differed among the three *Pab*UPOs. Thus, just the isoforms *Pab*UPO II and III formed hydroquinone as reaction product from anisole (chap. 3.10.4) or catalyzed the bromination of phenol (chap. 3.10.1), and only *Pab*UPO I preferred side-chain hydroxylation over aromatic ring hydroxylation during toluene conversion, whereas the two other proteins performed side-

chain and ring hydroxylation to the same extent (chap. 3.10.5). These differences may originate from structural differences of the three proteins, e.g. in size and molecular architecture of the heme channels and the enzymes' active sites. This finding further strengthens the assumption that the three enzymes are different gene products. Thus, genomic and proteomic studies demonstrated that *Pab*UPO II and III originate from one gene (*g8238*) and are therefore isoforms with a similar protein structure (and probably just modified glycosylation pattern). Contrary, the isoenzyme *Pab*UPO I is the product of another gene (*g7491*) and thus has a clearly different protein structure compared to the other two enzyms.

4.5.3 Structural aspects of the *Pab*UPOs

By molecular modelling of the amino acid sequences deduced from the two *Pab*UPO genes *g7491* and *g8238* (chap. 2.12), hypothetical protein structures were obtained that showed structural similarities to *Aae*UPO, the first solved peroxygenase structure (Piontek et al. 2013), for which also the highest identities and similarities were ascertained on the sequence level (chap. 3.11.2). The UPO-specific proximal cysteine (Cys36 and Cys32) and distal glutamate (Glu196 and Glu192) are apparently at appropriate position and in correct distances to the heme center (Fig. 4.2). The distal glutamate is also in close neighborhood to an arginine residue (Arg189 and Arg185) that acts as charge stabilizer of the acid-base pair glutamic acid/glutamate via an H-bonding network, which is required for heterolytic peroxide cleavage during formation of the reactive intermediate UPO Compound I (Piontek et al. 2013).

Slight differences between *Pab*UPOs and *Aae*UPO were found with respect to the dimensions and amino acid composition of the heme channels. The properties of the latter have been reported to be essential for the catalytic performance and substrate specificities of UPOs (Piontek et al. 2013, Hofrichter et al. 2015, Ullrich et al. 2018). The heme access channels had following dimensions in the models of *Pab*UPO I and *Pab*UPO II/III: length 15.3 and 15.7 Å as well as widths of 5.2 and 6.4 Å, respectively (Fig. 4.3). Thus, these channels are somewhat narrower than those described for the crystal structures of *Aae*UPO (between 8.5 and 10 Å, Piontek et al. 2013) and *Mro*UPO (between 8.5 and 18 Å, Piontek 2017, personal communication; Ullrich et al. 2018) as well as that calculated for the model of *Cgl*UPO (between 8.5 and 13 Å, Kiebist 2018).

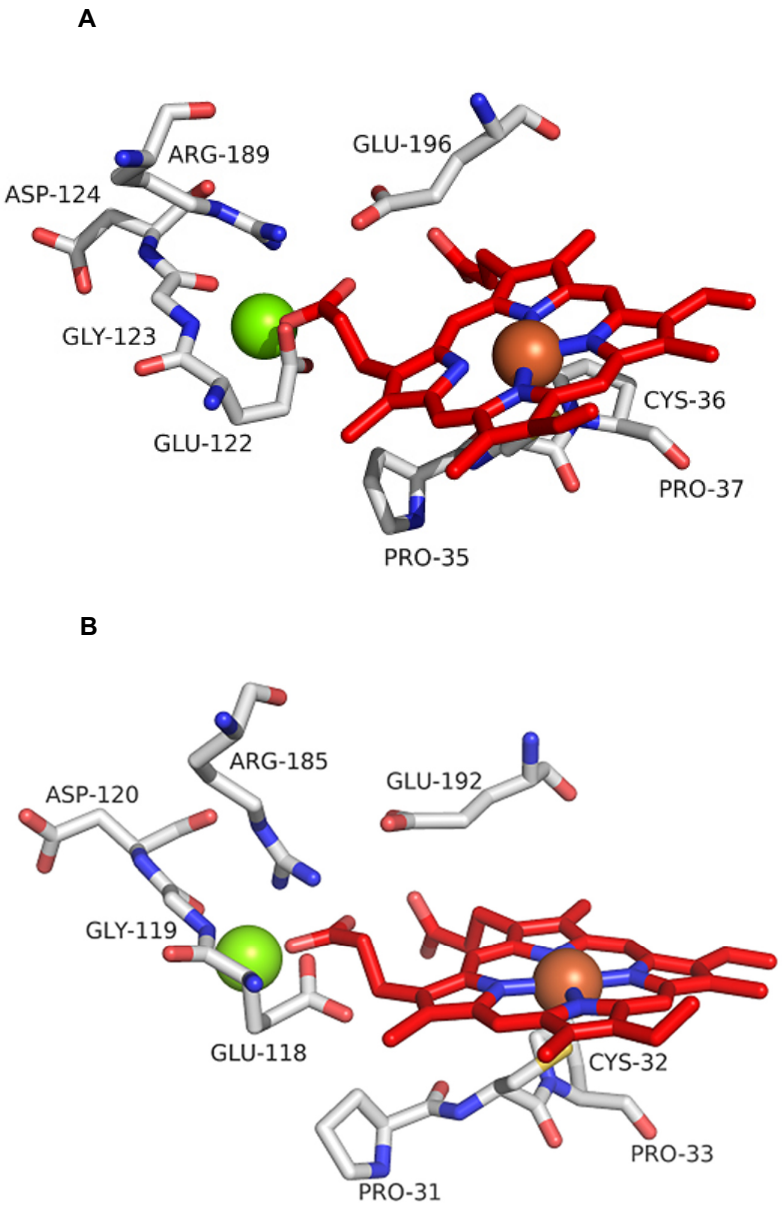

Fig. 4.2: Hypothetical heme environment of the *Pab*UPOs deduced from *g7491* (*Pab*UPO I, **A**) and *g8238* (*Pab*UPO II & III, **B**) indicating the key amino acids involved in the enzymes' catalysis. The red-brown and green spheres represent iron (Fe^{3+}) and magnesium (Mg^{2+}), respectively.

Mainly hydrophobic rigid phenylalanines flank the entrances of the heme channel of both *Pab*UPOs (i.e. Phe76/121/199 for *g7491* and Phe65/117/195 for *g8238*), which is again similar to *Aae*UPO, the entrance of which comprises an 'aromatic triad' of three phenylalanines (Phe69/121/199; Piontek et al. 2013).

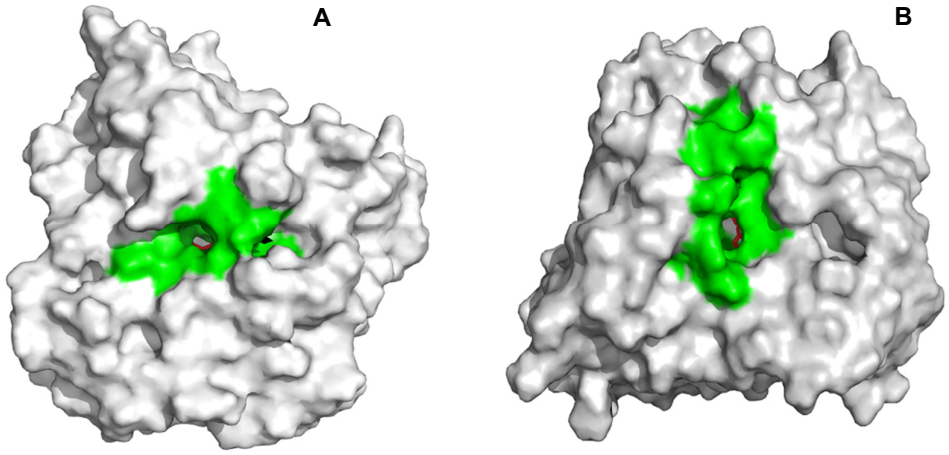

Fig. 4.3: Hypothetical protein models of the *Pab*UPOs deduced from *g7491* (*Pab*UPO I, **A**) and *g8238* (*Pab*UPOs II & III, **B)** obtained by using the I-TASSER server (Zhang et al. 2008); the entrance to the heme channel is highlighted in green.

These structural characteristics of the heme channels of *Pab*UPOs may explain their catalytic properties (substrate spectrum), which are rather similar to those of the *Aae*UPO and *Cra*UPO. Thus, the relatively narrow heme channel entrance is certainly responsible for the inability of *Pab*UPOs to convert bulky substrates such as corticosteroids and testosterone, which is a characteristic feature of *Mro*UPO and *Cgl*UPO, respectively; both enzymes belong to the 'short' UPOs and have relatively wide and flat heme access channels (Kiebist 2018, Ullrich et al. 2018). *Pab*UPOs are also not able to oxidize and cleave oseltamivir, a polar pharmaceutical known to be an exclusive substrate of *Cra*UPO (Poraj-Kobjelska 2013). To summarize, as it has already been postulated for the other so far characterized UPOs, the molecular architecture of the heme access channels, guiding the substrates towards the active site heme iron, determines – at least to some extent – the catalytic properties and particularly the substrate spectrum of *Pab*UPOs (Piontek et al. 2013, Kiebist 2018, Ullrich et al. 2018). More precise predictions and structure-function analyses will only be possible, after the crystal structures of the three *Pab*UPOs have been solved.

4.6 Comparison of *Xgr*DyP with other fungal DyP-type peroxidases

4.6.1 General aspects

The DyP of *X. grammica* was purified with similar FPLC methods (AEC and SEC; chap. 2.5.2) that had already been successfully used to prepare other fungal wild-type DyPs (e.g. from *A. auricula-judae*, *M. epipterygia* and *E. glandulosa*; Liers et al. 2010, 2013). Finally, one homogeneous *Xgr*DyP fraction was obtained that could be used for enzyme characterization. Table 4.5 compares several physical properties of *Xgr*DyP with those of all fungal DyPs characterized so far.

Tab. 4.5: Comparison of physical characteristics of *Xgr*DyP and other fungal DyPs.

Organism	Enzyme	M_w (kDa)	pH-optimum		Spec. activity
			2,6-DMP	Mn^{2+}	U mg^{-1}
X. grammica	***Xgr*DyP**	**49**	**3.5**	**4.5**	**51**
B. adusta[#,1]	*Bad*DyP	60	4.5	0	57
T. albuminosus[2]	*Tal*DyP	67	n.d.	0	1
A. auricula-judae[3]	*Aau*DyP1	51	4.5	0	469
A. auricula-judae[3]	*Aau*DyP2	43	4.5	0	375
M. epiterygia[4]	*Mep*DyP	61	4.0	0	384
E. glandulosa[4]	*Egl*DyP	56	4.5	0	174
*M. scorodonius**[,5]	r*Msc*DyP	69	3.5	0	0.1
*P. ostreatus**[,6]	r*Pos*DyP1	55	3.0	4.5	n.d.
*P. ostreatus**[,6]	r*Pos*DyP4	55	3.0	4.5	n.d.
I. lacteus[7]	*Ila*DyP	57	3.0	n.d.	38

*recombinant protein; [#]first described as *Geotrichum candidum*, [1] Kim and Shoda 1999; [2] Johjima et al. 2003; [3] Liers et al. 2010; [4] Liers et al. 2013; [5] Scheibner et al. 2008; [6] Fernández-Fueyo et al. 2015; [7] Salvachúa et al. 2013; n.d. not detected

All purified and characterized reference DyPs are of basidiomycetous origin and as of yet, there is no other ascomycetous enzyme of this type available. The specific activity (51 U mg^{-1} with ABTS as substrate), molecular mass (49 kDa) and spectroscopic absorbance maxima (with the characteristic Soret band at 406 nm) of this first ascomycetous DyP are in similar ranges as the data reported for the basidiomycetous counterparts (up to 469 U mg^{-1}, 43 to 69 kDa, Soret bands between 405 and 407 nm; Liers et al. 2013, Tab. 4.5).

4.6.2 Catalytic properties of *X. grammica* DyP

The substrate spectrum of *Xgr*DyP is strongly indicative of its affiliation to the protein family of DyP-type peroxidases (Sugano et al. 2009). Particularly, the oxidation of the recalcitrant substrate RBlue5[23], a high-redox potential anthraquinone dye that cannot be oxidized by other peroxidases (including LiP, VP and MnP), is a specific catalytic feature of fungal DyPs (Liers et al. 2010, Hofrichter et al. 2010). The affinity of *Xgr*DyP to this substrate (K_M = 41 µM) is in the range of values reported for other DyPs (e.g. K_M = 15 and 23 µM for *Aau*DyP1 and 2, respectively; Liers et al. 2013 and K_M = 54 µM for *Bad*DyP, Kim and Shoda 1999). Also the catalytic efficiency (k_{cat}/K_M) for the conversion of RBlue5 by *Xgr*DyP (0.5×10^6 s^{-1} M^{-1}) is in the characteristic range of basidiomycetous DyPs (1.7×10^7 s^{-1} M^{-1} to 5.0×10^6 s^{-1} M^{-1}; Kim and Shoda 1999, Liers et al. 2010). Remarkably, the catalytic constants for other substrates indicate that *Xgr*DyP shares characteristics of both DyP-type peroxidases and high-redox potential class II PODs like VP and MnP (e.g. from *Pleurotus eryngii*, *P. ostreatus* or *B. adusta*) or LiP (e.g. from *Phanerochaete chrysosporium*). So the K_M-values (affinities) for the oxidation of typical peroxidase substrates like ABTS and 2,6-DMP by *Xgr*DyP are in the same range as the values reported for two *Aau*DyPs (Liers et al. 2010) and the oxidation of the non-phenolic aromatic substrate veratryl alcohol turned out to proceed in the same acidic pH-range (pH<3.0) as reported for *Aau*DyPs (Liers et al. 2013). Furthermore, *Xgr*DyP's affinities to these 'classic' peroxidase substrates were higher than those described for *Pos*MnP3 and *Pos*MnP6[24] (K_M = 778 and 1,020 µM, respectively for ABTS and K_M = 59,000 and 117,000 µM, respectively for DMP). Also the recombinant DyPs from *P. ostreatus* (r*Pos*DyP1 and 4) had much lower affinities for these typical peroxidase substrates (K_M = 779 and 787 µM, respectively for ABTS and K_M = 31,100 and 126 µM, respectively for DMP) (Fernández-Fueyo et al. 2015).

Interestingly, the ascomycetous DyP belongs – from the biochemically point of view – to the small group of Mn^{2+}-oxidizing DyPs, of which only five representatives are so far known. Among them are a few bacterial representatives (from *Pseudomonas fluorescens*, *Rhodococcus jostii*, and *Amycolatopsis* sp.; Roberts et al. 2011, Brown et al. 2012, Rahmanpour and Bugg 2015) and only two recombinant basidiomycetous proteins from

[23] Indeed, according to the EC classification, a DyP is a 'Reactive-Blue-5 : hydrogen-peroxide oxidoreductase' (EC 1.11.1.19; https://www.qmul.ac.uk/sbcs/iubmb/enzyme/EC1/11/1/19.html)

[24] Two short hybrid-type manganese peroxidases (hMnPs) that oxidize, in addition to Mn^{2+}, also phenolics and ABTS (Hofrichter et al. 2010).

P. osteratus (r*Pos*DyP1 and 4) expressed in *E. coli* (Fernández-Fueyo et al. 2015). The affinity of *Xgr*DyP for Mn^{2+} ions (K_M = 49 µM) is in the typical range of 'classic' MnPs (e.g. from *P. chrysosporium*, 4-9 µM, Pease et al. 1992; *Agrocybe praecox* and *Stropharia coronilla*, 17 and 12 µM, respectively, Steffen et al. 2002; *P. ostreatus*, 10 µM, Sarkar et al. 1997) as well as for VPs (e.g. from *P. eryngii*, 12-20 µM; Martinez et al. 1996). On the other hand, the turnover numbers (k_{cat}) accomplished by 'true' MnPs are (with >100 s^{-1}; e.g. 150 s^{-1} for *B. adusta*, Wang et al. 2002 or 218 s^{-1} for *P. chrysosporium*, Giardina et al. 2000) two orders of magnitude higher than the k_{cat} values determined for the ascomycetous DyP (k_{cat} = 0.4 s^{-1}). The MICHAELIS-MENTEN constants of the so far only known Mn^{2+}-oxidizing fungal DyPs (*Pos*DyP1 and 4) are much higher (K_M = 2,780 and 286 µM, respectively) than that of *Xgr*DyP, but the catalytic efficiency, at least of *Pos*DyP4, is about one magnitude higher (196 s^{-1} mM^{-1}) than that calculated for the *Xgr*DyP (7 s^{-1} mM^{-1}). All these findings indicate that Mn^{2+} ions bind with high affinity to the *Xgr*DyP protein (very probably at suitable acidic amino acid, i.e. aspartates and glutamates) but their subsequent oxidation into reactive Mn^{3+} may proceed with much lower efficiency compared to MnPs and VPs.

Generally, the ability to efficiently oxidize Mn^{2+} ions is a specific catalytic property of certain class II PODs (MnP, hMnP and VP). These enzyme-types are exclusively found in Basidiomycota (e.g. in the families Polyporaceae, Corticiaceae, Pleurotaceae, Agaricaceae or Strophariaceae) causing white-rot or accomplishing soil-litter decomposition (Ruiz-Dueñas et al. 2009, Hofrichter et al. 2010,). Not least, due to the high abundance of these peroxidases among saprotrophic basidiomycetes and their ubiquitous presence in natural deadwood, it is meanwhile well accepted that the oxidation of manganese ($Mn^{2+} \rightarrow Mn^{3+}$) is one (if not 'the') key step in lignin decomposition (Hofrichter 2002, Hofrichter et al. 2010, Arnstadt et al. 2016, Noll et al. 2016). Chelated Mn^{3+}-ions act as a diffusible reactive oxidant infiltrating the tight lignocellulosic complex, oxidizing phenolic lignin moieties directly and initiating radical chain reactions such as lipid peroxidation. These radical-mediated processes lead to the subsequent destabilization of lignin (Hofrichter et al. 2001, 2010). In contrast, according to comprehensive genomic data, wood-inhabiting ascomycetes (e.g. Xylariaceae) are obviously lacking MnPs and other high-redox potential class II PODs (Büttner et al. 2017, 2018, 2019). In this context, the finding of an Mn-oxidizing ascomycetous DyP is remarkable, since it could explain why some of these fungi (e.g. *X. grammica* or *Xylaria polymorpha*) can nevertheless degrade and mineralize lignin, at least to some

extent (Liers et al. 2006). In other words, certain DyPs may fulfill the 'job' of MnPs/VP in some ascomycetous fungi, for example, in those species causing a strong soft-rot (Fernández-Fueyo et al. 2015). But whether this catalytic property of *Xgr*DyP has really physiological implications for wood and lignin degradation by *Xylaria* spp., remains unclear. Maybe 'DyP-knock-out mutants' of *X. grammica* (that could be obtained using modern techniques of gene-editing like CRISPR/Cas) will help to answer this interesting question in the future.

Besides MnPs, VP and certain DyPs, some UPOs are also known to have moderate Mn-oxidizing activity and they are present in ascomyceteous genomes (oral communication, R. Ullrich, 2019, Hofrichter et al. 2019). Furthermore, DyPs and UPOs are able to convert – though by different mechanisms – hardly oxidizable non-phenolic lignin dimers (i.e. β-*O*-4 dimers such as adlerol; Kinne et al. 2009, Kinne et al. 2011, Liers et al. 2010, Salvachúa et al. 2013, Hofrichter et al. 2015) and should therefore also belong to the high-redox potential peroxidases, which include all 'classic' ligninolytic peroxidases (MnPs, VP, LiP). Thus, altogether, DyPs and UPOs may overlap in their physiological roles with 'classic' ligninolytic peroxidases both with respect to manganese oxidation and the cleavage of recalcitrant ether structures (Salvachúa et al. 2013; Reina et al. 2019). Again, just suitable mutant studies with ascomycetous strains where DyPs and/or UPOs will be knocked-out may unambiguously prove or refute this assumption.

Mn^{2+} oxidation by *Xgr*DyP proceeded most effectively under acidic pH conditions (chap. 3.13), which is also a characteristic feature of all 'classic' MnPs and comparable to the respective activities of certain recombinant DyPs from *P. ostreatus* (e.g. at pH 4.5; Fernández-Fueyo et al. 2015). The reason for the acidic pH-optima of all these enzymes is based on the higher stability of Mn^{3+}-complexes below pH 5.0 and on the conserved, solvent exposed Mn^{2+}-binding sites in the vicinity of one of the two heme propionates comprising three acidic amino acid residues, e.g. two glutamates (Glu35 and Glu39) and one aspartate (Asp179) in the MnP of *P. chrysosporium* (Sundaramoorthy et al. 1997, Hofrichter et al. 2010). It can be assumed that such an acidic Mn^{2+}-binding region is also present in the protein structure of *Xgr*DyP.

The gene encoding *Xgr*DyP (*g488*) eventually proved its affiliation to the clade 'D' of DyP-type peroxidases (Zámocký and Obinger 2010), in which also the characterized DyPs from the basidiomycetes *B. adusta*, *M scorodonius*, *M. epipterygia*, *E. glandulosa* and *A. auricula-judae* have been classified. However, none of the latter peroxidases has

been reported to be capable of oxidizing Mn^{2+} ions (Liers et al. 2013) and none of the putative ascomycetous DyPs of this and other subfamilies has been purified or characterized so far (neither in homologous nor in heterologous form). This is the reason why their substrate specificities, possible physiological functions and potential biotechnological relevance have remained fully unclear until now (Zámocký and Obinger 2010). The other two DyP genes of *X. grammica*, *g9177* and *g1956*, surprisingly cluster within the DyP clades that mainly comprise bacterial DyPs (actinobacteria and proteobacteria, e.g. of *Streptomyces* spp., *Mycobacterium* spp. and *E. coli*). It has been proposed that DyPs of clade 'B', for example, were introduced into ascomycetous genomes via horizontal gene transfer from various bacteria (Zámocký et al. 2016). However, it should be noted that most of the putative bacterial DyPs of clade 'B', in which also ten ascomycetous homologous are classified, have been predicted as cytoplasmic (i.e. intracellular) enzymes that may have totally different functions than their extracellular counterparts (Hofrichter et al. 2010).

All three DyP genes identified in the *X. grammica* genome encode proteins with conserved DyP-specific amino acid motifs representing the proximal and distal heme regions. Putative glycosylation sites have been predicted as well, but similar as described for the r*Pos*DyP4 (Fernández-Fueyo et al. 2015), all three *Xgr*DyP genes do not contain a signal peptide. Such findings regarding obviously secreted enzymes without signal peptides are rare but have been reported for a number of extracellular bacterial proteins (e.g. a lipase of *Serratia marcescens*, Akatsuka et al. 1994 and hemolysin of *Escherichia coli*, Felmlee et al. 1985) and for few fungal enzymes; such as hydrolases of the ascomycetes *Cochliobolus carbonum* (Wegener et al. 1999) and *X. polymorpha* (Nghi et al. 2012). Moreover, in numerous hypothetical DyP sequences from basidiomycetes (e.g. from *A. aegerita*, *A. pediades*, *Galerina marginata* or *Hebeloma cylindrisporum*), which apparently form an own subfamily within the DyP clade "D" (or formerly 'superfamily 1' or 'fungal DyP-type peroxidase clade'; Hofrichter et al. 2010), no signal peptides have been predicted (Pecyna 2015). Nonetheless, to explain their extracellular presence, it can be assumed that the three *Xgr*DyPs are released to the outside by alternative 'unconventional' pathways (UPS), which may be triggered by special physiological conditions, e.g. by different kinds of stress (Rabouille 2017). Thus, due to the late appearance of DyP activities in the liquid culture of *X. grammica* (Fig. 3.6 C), it is plausible that the *Xgr*DyP encoded by *g488* may be released as cytosolic or membrane-bound protein during the process of hyphal autolysis.

Generally, there is no 'logic' phylogenetic or ecophysiological distribution of DyP sequences within the Dikarya fungi (Pecyna 2015). They occur both in some white-rot, brown-rot and soft-rot fungi, but all of these groups include also species that do not have DyP sequences in their genomes (e.g. *Pycnoporus cinnabarinus*, *G. trabeum* and *Serpula lacrymans* or *Podospora anserina*, respectively). Within the ecological group of ectomycorrhizal fungi, merely a few basidiomycetous species contain DyPs in their genomes, ascomycetes do not (Pecyna 2015).

4.6.3 Structural aspects of the DyP of *X. grammica* (*Xgr*DyP)

To identify and compare catalytically relevant structural elements in *Xgr*DyP, a hypothetical protein model was created using the gene *g488* and the web-server I-Tasser (chap. 2.12). Pairing the *Xgr*DyP structure with the respective protein structure of the phylogenetically most related DyP (of *B. adusta*, *Bad*DyP) revealed that both proteins are rather similar in their tertiary structure and overall shape as well as in their dimensions (Fig. 4.4 A). As other peroxidases of this type, *Xgr*DyP has a characteristic heme environment comparable with that of some characterized basidiomycetous DyPs (*Aau*DyP1, Strittmatter et al., 2013a, b; r*Pos*DyP4, Fernández-Fueyo et al. 2018).

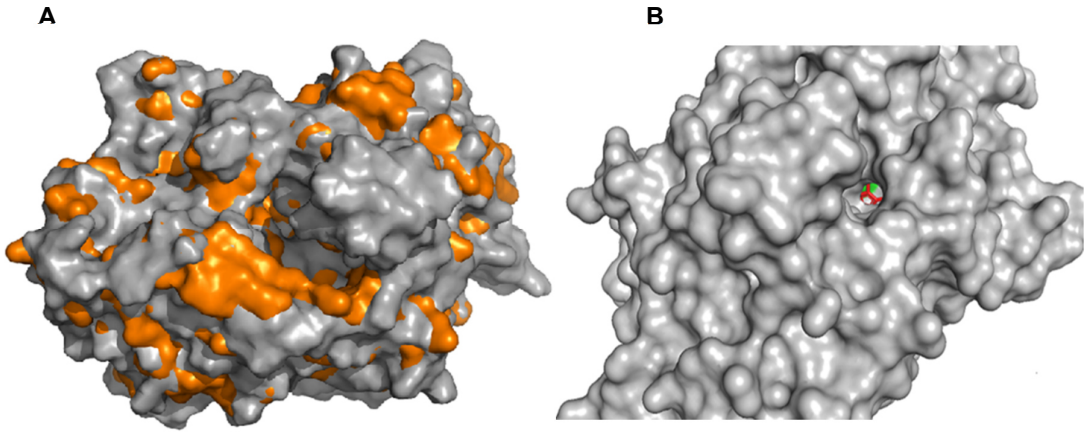

Fig. 4.4 (**A**) Comparison of the super-imposed hypothetical structures of *Xgr*DyP (grey; *g488*) and *Bad*DyP (orange; PDB structure ID 2D3Q_A) and (**B**) hypothetical entrance to the heme channel of *Xgr*DyP that guides H_2O_2 towards the catalytically active heme (red).

It contains a proximal histidine (His336), which is structurally homologous to His361 and His334 in r*Pos*DyP1 and 4, respectively (Fernández-Fueyo et al. 2015) as well as to

His306 and His304 in *Bad*DyP and *Aau*DyP, respectively (Strittmatter et al., 2013a). These histidine residues are linking the heme to an α-helix of the apoprotein and are found in all heme peroxidases, with the exception of UPOs and catalases (that bear a cysteine or tyrosine at the respective position) (Torres and Ayala, 2010).

The distal heme environment of *Xgr*DyP *g488* exhibits also conserved amino acids that act as proton acceptor (aspartate, Asp 192) and charge stabilizer (arginine, Arg 359; Hofrichter et al. 2010, Strittmatter et al. 2013a) as well as the co-substrate binding/guiding residues (phenylalanine/Phe390 and leucine/Leu388; Pecyna 2015). The hypothetical *Xgr*DyP protein encoded by *g9177* shows remarkable differences to this picture regarding the conserved amino acids. Threonine residues (Thr280 and 308) seemingly replace the proximal His336 and the distal Leu388 (Appendix Fig A.6 & A.7). Since such a threonine as proximal heme ligand has not been reported yet for any heme-containing enzyme, it is, however, questionable whether the *g9177* encoded protein has a catalytic function or not. In the other putative DyP from *X. grammica* (encoded by *g1956*), the distal leucine (Leu388 of *g488*) is replaced by an isoleucine (Ile258); as both amino acids (Leu, Ile) have very similar physico-chemical properties, this replacement should not be of any catalytic relevance. Unusual amino acids, in the distal heme environment, were also observed for a hypothetical DyP structure of the basidiomycete *A. aegerita* (*Aae*DyP2), which was proposed to contain a glycine instead of the aspartate as acid-base catalyst and a phenylalanine as substitute of a hydrophobic valine (Pecyna 2015).

The entrance to the heme channel of *Xgr*DyP (*g488*) has a hypothetical width between 2.1 and 2.6 Å and a putative length of 2.5-2.7 Å (Fig. 4.4 B); the access channel in the 3D-crystal structure of *Aau*DyP1 was found to be somewhat wider with 3 to 3.5 Å. It has been speculated that the width of this narrow entrance to the heme channel can be altered by the molecular movement of an appropriate amino acid residue, which would act then as a 'gatekeeper' (e.g. Asp168 in the case of *Aau*DyP1; Strittmatter et al. 2013a). Furthermore, it is imaginable that *Xgr*DyP oxidizes bulkier substrates such as RBlue5 by a long-range electron transfer (LRET), starting from a catalytically active tyrosine or tryptophan at the protein surface and leading via other aromatic amino acids towards the heme, similarly as it was previously reported for *Aau*DyP1 and r*Pos*DyP4 (Liers et al. 2013, Fernandez-Fueyo et al., 2018).

In analogy to the Mn^{2+}-binding amino acids in MnP (e.g. from *P. chrysosporium*, *Pch*MnP), a similar binding site can be proposed within the hypothetical *Xgr*DyP

structure (Fig. 4.5). It should be located close to the heme and could be based on the presence of the carboxylic groups of two glutamates (Glu212/ 319) and one aspartate (Asp192) with distances of 4.4, 5.8 and 6.9 Å, respectively, as well as of a heme propionate. A differing hypothetical coordination sphere was identified in *Bad*DyP, and includes one acidic and two polar residues (Asp171, Asn289, Tyr293); in this case, substantial Mn^{2+} oxidation has not been observed (Liers et al. 2013). In *Pch*MnP, the Mn^{2+}-binding site consists of three acidic amino acid residues (Glu35/ 39 and Asp179) and a heme propionate, which have much lower distances (2.1-2.4 Å) to the Mn^{2+} ion to be complexed compared to *Xgr*DyP; this might be the reason for the two-orders of magnitude higher efficiency of *Pch*MnP regarding Mn^{2+} oxidation.

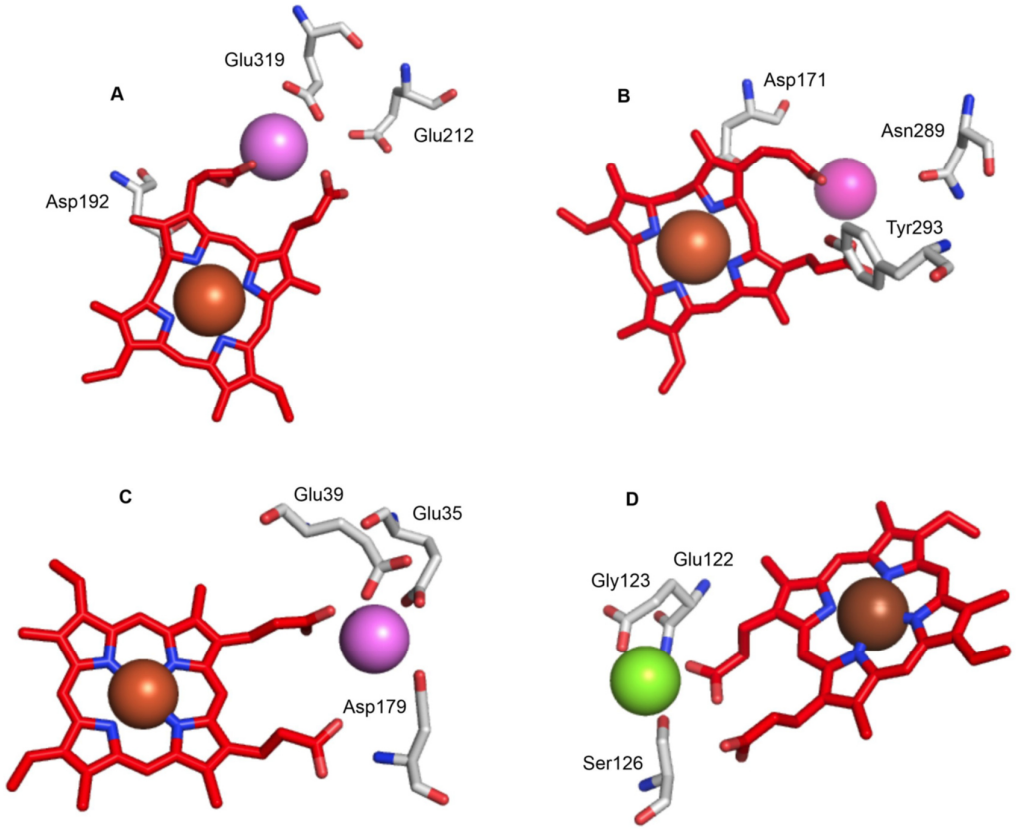

Fig. 4.5: Putative Mn^{2+}-binding sites of *Xgr*DyP (**A**) and *Bad*DyP (**B**) in comparison to the Mn^{2+}-coordination sphere in *Pch*MnP (**C**) and the Mg^{2+}-binding region in *Aae*UPO[25] (**D**). Fe^{3+} – red-brown spheres, Mn^{2+} - pink spheres, Mg^{2+} - green sphere.

[25] There are indications that the Mg^{2+} in UPOs can be replaced by Mn^{2+}, which is then oxidized (Hofrichter et al. 2019).

Comparative structure studies on a designed Mn^{2+}-oxidizing cytochrome c peroxidase (MnC*c*P, 'artificial' MnP) and a native MnP (from *P. eryngii*) indicated that differences in the geometry and distances between the metal ion and its ligands may cause differences in Mn^{2+}-binding affinity and MnP activity (i.e. Mn^{2+}-oxidation efficacy; Hosseinzadeh et al. 2016).

Another type of a coordination sphere for a bivalent cation (Me^{2+}) near the enzyme's active heme was observed in the crystal structure of the peroxygenase from *A. aegerita* (*Aae*UPO; Piontek et al. 2013). In this case, aspartate (Asp124), glutamate (Glu122), serine (Ser126) and a heme propionate coordinate an Mg^{2+} ion that has a ring-stabilizing function for the porphyrin ring system embedded within the protein. Interestingly, this particular molecular arrangement resembles the manganese oxidation site of an 'untypical' MnP from the litter-decomposing fungus *A. praecox*; its Mn-binding site comprises a heme propionate, glutamate (Glu36), aspartate (Asp176) and serine (Ser40) (Hildén et al. 2014). This molecular convergence of UPO and MnP is supported by the finding that Mg^{2+} can be replaced by Mn^{2+} in certain UPOs. Thus *Aae*UPO and r*Cci*UPOs were found to have moderate Mn^{2+}-oxidizing activities with K_M and k_{cat} values between 35 and 111 µM as well as 0.4 and 1.0 s^{-1}, respectively (Saß 2010, Hofrichter et al. 2019).

Contrary to MnPs and UPOs, the Mn^{2+}-binding site of the recently described r*Pos*DyP4 is located on the surface of the protein and consists of three aspartates (Asp352/ 354/ 215) and one glutamate (Glu345; Fernandez-Fueyo et al., 2018). This enzyme obviously uses an electron transfer mechanism from the glutamate (Glu345) to the heme via an aromatic residue (Tyr339; Fernandez-Fueyo et al 2018). In the case of *Xgr*DyP, a similar surface exposed Mn^{2+} oxidation site was identified within the hypothetical structure model, which consists of two glutamates (Glu212/ 353) and one aspartate (Asp347), however, these potentially coordinating carboxylates do not show a distinct orientation towards the protein surface (data not shown). Four aromatic amino acids (being predestined to act as partners for an electron transfer) were found in close vicinity to that region, i.e. a phenylalanine (Phe349) that is located between Glu353 and Asp347, two further phenylalanines (Phe321/ 323) converging Asp347 along with a tyrosine (Tyr352; data not shown).

Finally, it should be mentioned again that the substrate oxidation site of *Xgr*DyP is putative and that the orientation and distances between the involved ligands and metal ions may alter during binding and/or catalysis (Fig 4.5). Definite clarification of these

points can be only achieved, if the crystal structure of *Xgr*DyP (encoded by *g488*) will be solved and the respective molecular architecture will be analyzed regarding the Mn^{2+}-coordination sphere.

4.6.4 Eco-physiological classification of *P. aberdarensis* and *X. grammica*

The genomic data sets of lignocellulolytic enzymes obtained for both fungi were summarized and analyzed according to Riley et al. (2014) (chap. 3.11.3 and 3.15.3). Such a summary, the so-called 'RILEY table', allows to classify fungi with respect to their eco-physiological affiliation to the saprotrophic litter-decomposers, wood-degraders (including rot-type) or dung-dwellers. *P. aberdarensis* and *X. grammica* possess diverse hydrolases and oxidoreductases in their genomes, which may be involved in the degradation and modification of lignocelluloses. All these enzymes are characteristic for saprotrophic fungi (and are lacking, for example, in mycorrhizal fungi). In the case of *P. aberdarensis*, it should be noted that some of these enzymes are highly abundant such as CBM1, LPMOs, laccases and AA3_2. Furthermore, only one class II POD that belongs to the group of low-redox potential, so-called generic peroxidases (GPs) was identified in the *P. aberdarensis* genome. This enzyme does not belong to the ligninolytic peroxidases so that the fungus must follow an alternative strategy to accomplish wood and particularly lignin degradation (at least to some extent). Similar findings were made for other agaric fungi, such as 'atypical' wood-rotters, litter-decomposers or dung-dwellers (Gupta et al. 2018, Morin et al. 2012). They either contain only few ligninolytic peroxidases (mostly MnPs) such as wood-colonizing *A. aegerita* (with merely one 'long' MnP and three short MnP genes while LiP or VP genes are lacking) and compost-dwelling *Agaricus bisporus* (with several 'long' and 'short' MnP genes but no LiP or VP gene) or they are even lacking MnPs like coprophilic *Coprinopsis cinerea* that has merely GP genes (as *P. aberdarensis* does). *M. rotula* has also just two class II POD genes in its genome, one of an MnP and one of a GP (H. Kellner, personal communication 2019). On the other hand, all these agaric fungi including *P. aberdarensis* contain numerous genes encoding for DyPs and UPOs/HTPs, which are also high-redox potential peroxidases though they do not belong to the canonical ligninolytic enzymes (Hofrichter et al. 2015). Both peroxidase types were shown to oxidize and cleave non-phenolic lignin model compounds (e.g. veratryl alcohol, adlerol) so that it can be assumed that they substitute ligninolytic class II peroxidases to some extent. This assumption is supported by the fact that some of these agaric fungi including *P. aberdarensis*, *M. rotula*, *A. bisporus* and *A. aegerita* contain the

highest numbers of UPO genes reported so far (48, 52, 22 and 18 UPO genes, respectively; H. Kellner, personal communication 2019, Morin et al. 2012, Gupta et al. 2018). According to the principal component analysis (PCA), *P. aberdarensis* does not cluster within any group of wood-rot fungi, neither within the white-rot nor the brown-rot fungi (like *P. chrysosporium*, *P. ostreatus* or *G. trabeum*) and it does also not group within the unresolved (unspecific or atypical) wood-rot fungi (like *S. commune*) (Fig.4.6). On the other hand, *P. aberdarensis* contains a core set of enzymes (UPOs, DyPs, H_2O_2-generating oxidases, LPMO, benzoquinone reductase, endocellulases and xylanases) required for wood degradation and partial ligninolysis/lignin-modification. Hence we suggest *P. aberdarensis* to be grouped among the agaric litter-decomposers with some relation to white-rot fungi (similar as *C. cinerea*).

The genomic dataset of lignocellulolytic enzymes of *X. grammica* clearly differs from those of white-rot or brown-rot fungi belonging exclusively to the Basidiomycota (Fig. 4.7). The former group contains the key enzymes of ligninolysis, i.e. the high-redox potential class II PODs (MnP, hMnP, VP, LiP), which are generally lacking in all Ascomycota, irrespective whether they are following saprotrophic or parasitic life styles (Büttner et al. 2017, 2018). Moreover, white-rot fungi possess a higher number of copper-radical oxidase and laccase encoding genes. As distinguished from the genomes of white-rot fungi, ascomycetous fungi, among them soft-rot fungi of the genus *Xylaria* and parasitic fungi like *Colletotrichum gloeosporioides* or *Gaeumannomyces tritici*, contain a remarkably higher number of glucooligosaccharide oxidase and CDH genes (Kracher et al. 2016) as well as often several DyP genes. The PCA groups *X. grammica* close to the two so far sequenced wood-colonizing soft-rot fungi, *Xylaria longipes* and *K. deusta*. Due to differences in the number of glucooligosaccharide oxidases, DyPs and copper radical oxidases/laccases, two other sequenced ascomycetes with some relation to the soft-rot group, *Scytalidium lignicola* and *Podospora anserina*, do not match well with *X. grammica*. Thus, due to this clustering, we suggest *X. grammica* to be a typical representative of the wood-dwelling soft-rot ascomycetes.

5 CONCLUSION AND OUTLOOK

Up to now, mycological research in tropical regions has been rather under-represented in comparison to temperate regions in Europe or the United States. On the other hand, tropical forests and landscapes as found in Kenya harbor an enormous pool of microbial biodiversity with special emphasis on saprotrophic basidiomycetous and ascomycetous fungi. The here performed sampling of various litter-decomposing, wood-rot and dung-dwelling fungi enabled the establishment of a small but specific culture collection of Kenyan saprotrophic fungi. Based on this collection, it was possible to discover a new basidiomycetous species (*Psathyrella aberdarensis*), to physiologically characterize a so far ignored ascomycetous species (*Xylaria grammica*) and to identify several novel enzymes (unspecific peroxygenases and a DyP-type peroxidase) with interesting molecular, biochemical and catalytic properties, and biotechnological relevance. Besides the genes of the purified and characterized UPOs and DyP, genes encoding for the most important CAZy enzymes involved in lignocellulose degradation were identified in the course of genome sequencing of both fungi. Not least, due to the absence of classic ligninolytic class II peroxidases in genomes of both fungi, the characterized heme peroxidases may be of eco-physiological relevance for alternative pathways degrading woody materials and leaf-litter. Based on the core set of lignocellulolytic CAZy enzymes, *P. aberdarensis* and *X. grammica* can be classified within the groups of litter-decomposing white-rot and wood-colonizing soft-rot fungi, respectively.

In continuation of the present Ph.D. work, recombinant expression studies will be a promising and challenging task, which will facilitate improved production of the target heme peroxidases. This in turn would be an important prerequisite for comprehensive protein structure-function and molecular engineering studies. Both approaches may help to identify catalytically relevant amino acids (e.g. for the binding and oxidation of Mn^{2+} by *Xgr*DyP). Furthermore, testing lignocellulose degrading activities of both characterized peroxidases will help to answer the interesting ecological and physiological question as to whether they are actually involved in ligninolysis. Especially the evidence for a DyP/Mn^{3+} based depolymerization of lignin could demonstrate the involvement of this exceptional degradation principle for an ascomycete for the first time. In addition, the lignocellulolytic potential of both fungi could be directly tested in appropriate solid-state cultures (wood microcosms) using different types of wood, straw or soil-litter materials. These physiological studies should be combined with proteomic/secretomic

approaches (focusing on CAZy enzymes), which will give insight into the degradative machinery that is really used by the two fungi. Last but not least, comparative genomics focusing on the repertoire of most important CAZy enzyme-encoding genes could help to identify gene doubling or loss events for some of these genes (e.g. for UPOs or GMC oxidoreductases in *P. aberdarensis* or for LPMOs, glucooligosaccharide oxidase and cellobiose dehydrogenases in *X. grammica*), which in turn may help to better understand the evolution of white-rot, brown-rot and soft-rot fungi.

Fig. 4.6: Principal component analysis (PCA) of main CAZy lignocellulolytic gene content in the analyzed genomes (published data from JGI and NCBI) and in the *P. aberdarensis* genome. A variance-covariance matrix of the values in (Tab. 1.16) were used; symbols: white rot fungi (green diamonds), brown rot (blue squares) and unresolved (unspecific) wood-rot fungi (black circles).

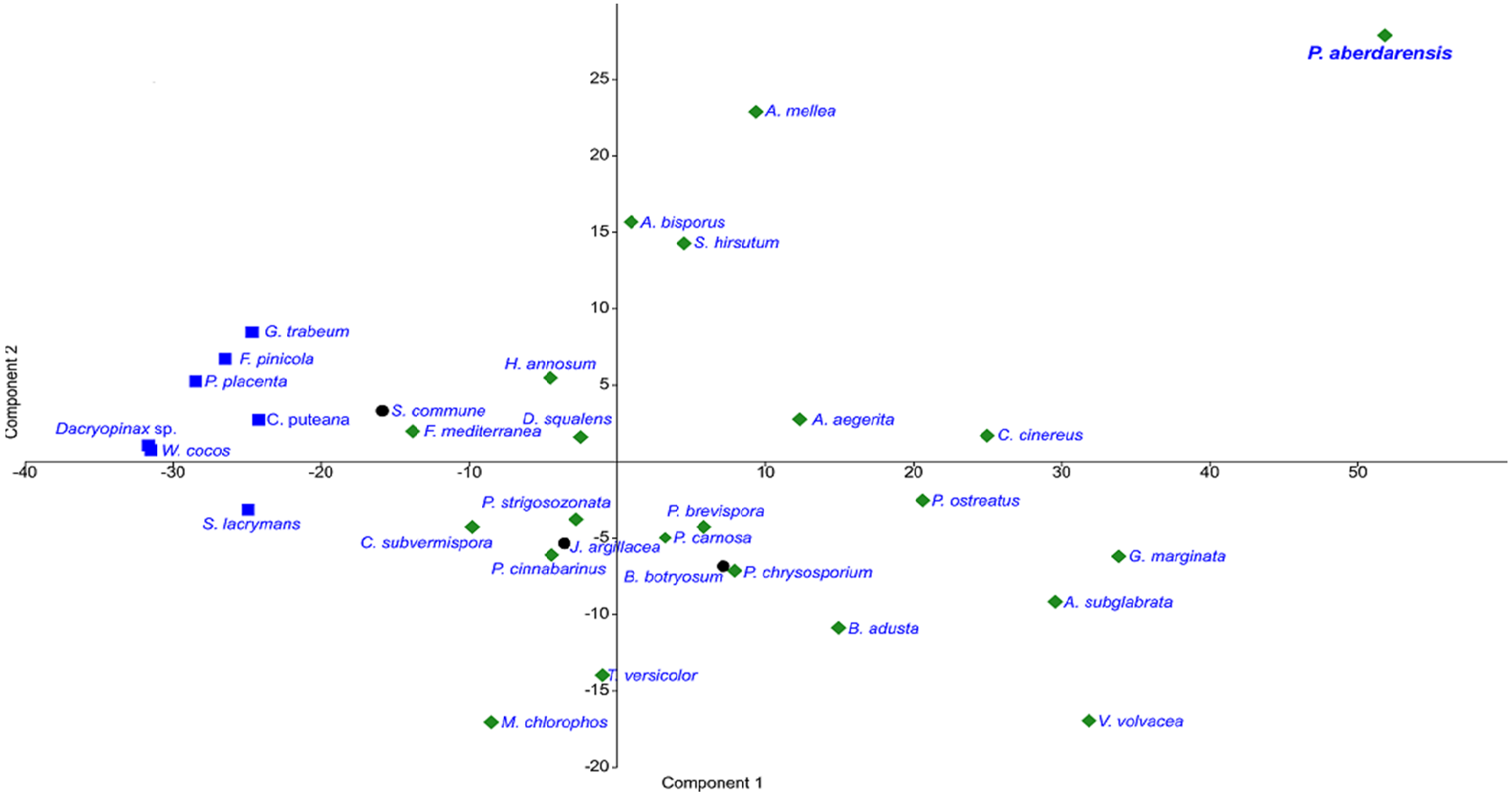

Fig. 4.7: Principal component analysis (PCA) of main CAZy lignocellulolytic gene content in the analyzed genomes (published data from JGI and NCBI) and in the *X. grammica* genome. A variance-covariance matrix of the values in (Tab. 1.16) were used; symbols: white rot fungi (purple diamonds), brown rot (brown diamonds), unresolved (unspecific) wood-rot fungi (light blue diamonds), opportunistic saprotrophs (blue diamonds), *Aspergillus*-type molds (orange squares), ectomycorrhizal fungi (green diamonds), soft rot (brown squares), plant pathogenic/parasitic fungi (Basidio- and Ascomycota; blue squares).

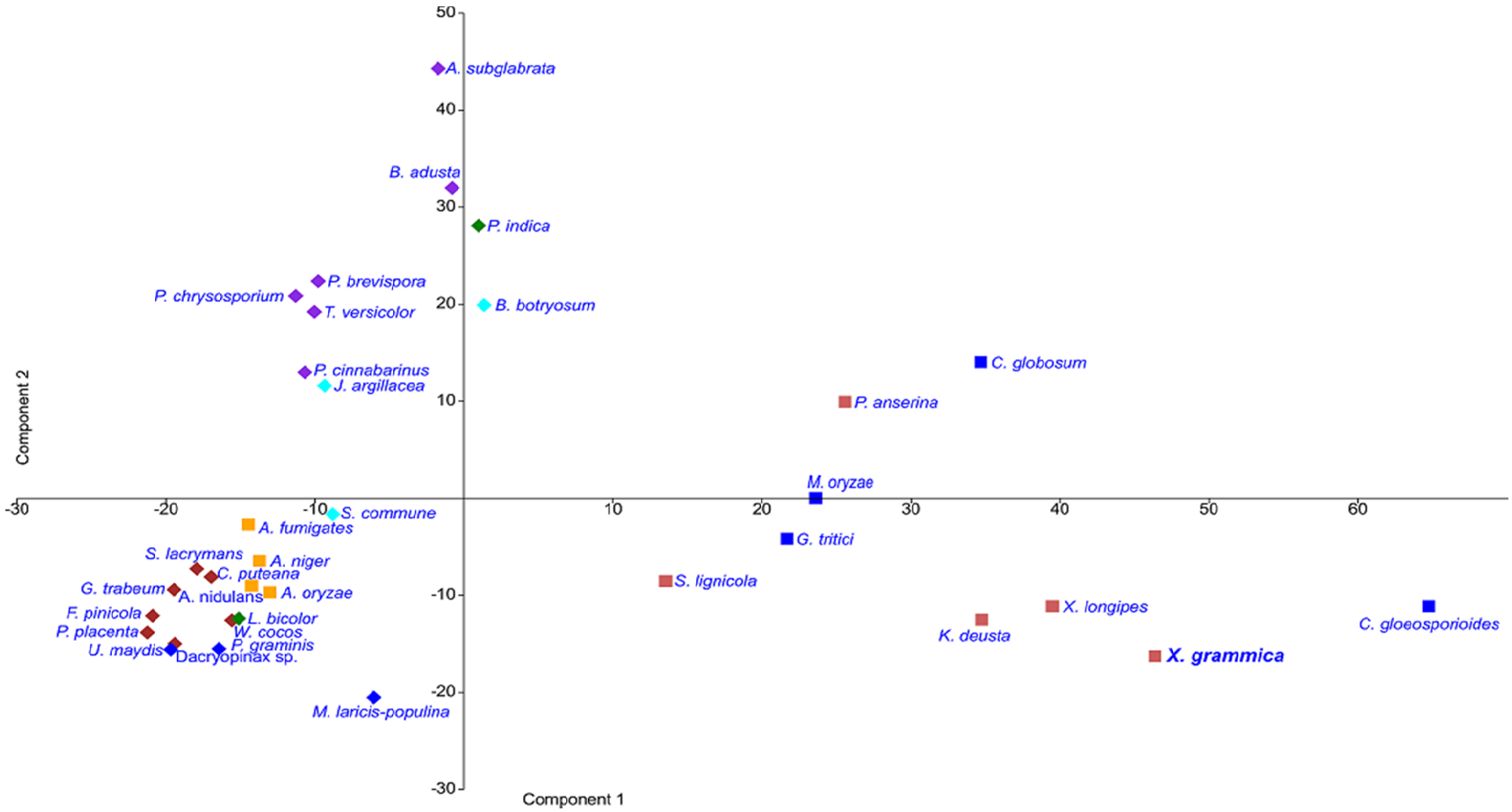

6 REFERENCES

ADLER, E. 1977. Lignin chemistry—past, present and future. *Wood science and technology,* 11**,** 169-218.

AHIRWAR, S., SONI, H., PRAJAPATI, B. P. & KANGO, N. 2017. Isolation and screening of thermophilic and thermotolerant fungi for production of hemicellulases from heated environments. *Mycology,* 8**,** 125-134.

AKATSUKA, H., KAWAI, E., OMORI, K., KOMATSUBARA, S., SHIBATANI, T. & TOSA, T. 1994. The lipA gene of *Serratia marcescens* which encodes an extracellular lipase having no N-terminal signal peptide. *Journal of Bacteriology,* 176(7)**,** 1949-1956.

ALTHOF, A. 2005. *Human impact on flora and vegetation of Kakamega Forest, Kenya. Structure, distribution and disturbance of plant communities in an East African rainforest.* Doctoral dissertation, University of Koblenz-Landau, Germany.

ANAGNOST, S. E. 1998. Light microscopic diagnosis of wood decay. *Iawa Journal,* 19(2)**,** 141-167.

ANH, D. H. 2008. *Novel extracellular haloperoxidase-peroxygenases from the coprophilous fungi Coprinus radians and Coprinus verticillatus: production, purification and biochemical characterization.* Doctoral dissertation, Internationales Hochschulinstitutes Zittau, Germany.

ANH, D. H., ULLRICH, R., BENNDORF, D., SVATOŚ, A., MUCK, A. & HOFRICHTER, M. 2007. The coprophilous mushroom *Coprinus radians* secretes a haloperoxidase that catalyzes aromatic peroxygenation. *Applied and Environmental Microbiology,* 73**,** 5477-5485.

ARANDA, E., ULLRICH, R. & HOFRICHTER, M. 2010. Conversion of polycyclic aromatic hydrocarbons, methyl naphthalenes and dibenzofuran by two fungal peroxygenases. *Biodegradation,* 21(2)**,** 267-281.

ARANTES, V., JELLISON, J. & GOODELL, B. 2012. Peculiarities of brown-rot fungi and biochemical Fenton reaction with regard to their potential as a model for bioprocessing biomass. *Applied Microbiology and Biotechnology,* 94(2)**,** 323-338.

ARNOLD, A. E., MAYNARD, Z., GILBERT, G. S., COLEY, P. D. & KURSAR, T. A. 2000. Are tropical fungal endophytes hyperdiverse? *Ecology Letters,* 3**,** 267-274.

ARNSTADT, T., HOPPE, B., KAHL, T., KELLNER, H., KRÜGER, D., BÄSSLER, C., BAUHUS, J. & HOFRICHTER, M. 2016. Patterns of laccase and peroxidases in coarse woody debris of *Fagus sylvatica, Picea abies* and *Pinus sylvestris* and their relation to different wood parameters *European Journal of Forest Research,* 135(1)**,** 109-124.

BABOT, E. D., DEL RÍO, J. C., KALUM, L., MARTÍNEZ, A. T. & GUTIÉRREZ, A. 2013. Oxyfunctionalization of aliphatic compounds by a recombinant peroxygenase from *Coprinopsis cinerea*. *Biotechnology and Bioengineering,* 110(9)**,** 2323-2332.

BARKOVÁ, K., KINNE, M., ULLRICH, R., HENNIG, L., FUCHS, A. & HOFRICHTER, M. 2011. Regioselective hydroxylation of diverse flavonoids by an aromatic peroxygenase. *Tetrahedron Letters***,** 4874–4878.

BARRASA, J. M., BLANCO, M. N., ESTEVE-RAVENTÓS, F., ALTÉS, A., CHECA, J., MARTÍNEZ, A. T. & RUIZ-DUEÑAS, F. J. 2014. Wood and humus decay strategies by white-rot basidiomycetes correlate with two different dye decolorization and enzyme secretion patterns on agar plates. *Fungal Genetics and Biology,* 72**,** 106-114.

BATTISTIN, E., CHIARELLO, O., VIZZINI, A., ÖRSTADIUS, L. & LARSSON, E. 2014. Morphological characterisation and phylogenetic placement of the very rare species *Psathyrella sulcatotuberculosa*. *Sydowia,* 66(2)**,** 171–181.

BEKELE, A., ABENA, T., HABTEYOHANNES, A., NUGISSIE, A., GUDETA, F., GETIE, T., KELEL, M. & BERHANU, A. 2015. Isolation and characterization of efficient cellulolytic fungi from degraded wood and industrial samples. *African Journal of Biotechnology,* 14(48)**,** 3228-3234.

BERKA, R. M., GRIGORIEV, I. V., OTILLAR, R., SALAMOV, A., GRIMWOOD, J., REID, I., ISHMAEL, N., JOHN, T., DARMOND, C., MOISAN, M. C. & HENRISSAT, B.

2011. Comparative genomic analysis of the thermophilic biomass-degrading fungi *Myceliophthora thermophila* and *Thielavia terrestris*. *Nature Biotechnology,* 29(10)**,** 922.

BERRIN, J. G., NAVARRO, D., COUTURIER, M., OLIVÉ, C., GRISEL, S., HAON, M., TAUSSAC, S., LECHAT, C., COURTECUISSE, R., FAVEL, A. & COUTINHO, P. M. 2012. Exploring the natural fungal biodiversity of tropical and temperate forests toward improvement of biomass conversion. *Applied and Environmental Microbiology,* 78(18)**,** 6483-6490.

BIDLACK, J., MALONE, M. & BENSON, R. 1992. Molecular structure and component integration of secondary cell walls in plants. *In Proceedings of the Oklahoma Academy of Science* 72**,** 51-56.

BINDER, M., JUSTO, A., RILEY, R., SALAMOV, A., LOPEZ-GIRALDEZ, F., SJÖKVIST, E., COPELAND, A., FOSTER, B., SUN, H., LARSSON, E. & LARSSON, K. H. 2013. Phylogenetic and phylogenomic overview of the Polyporales. *Mycologia,* 105(6)**,** 1350-1373.

BLANCHETTE, R. A. 1995. Degradation of the lignocellulose complex in wood. *Canadian Journal of Botany,* 73(S1)**,** 999-1010.

BLANCHETTE, R. A., HELD, B. W., JURGENS, J. A., MCNEW, D. L., HARRINGTON, T. C., DUNCAN, S. M. & FARRELL, R. L. 2004. Wood-destroying soft rot fungi in the historic expedition huts of Antarctica. *Applied and Environmental Microbiology,* 70(3)**,** 1328-1335.

BLANCHETTE, R. A., NILSSON, T., DANIEL, G. & ABAD, A. 1990. Biological degradation of wood. *In:* ROWELL, R. M., BARBOUR, R.J ADVANCES IN CHEMISTRY SERIES (ed.) *Archaeological Wood: Properties, Chemistry, and Preservation.* American Chemical Society,Washington, DC.

BODDY, L. 2001. Fungal community ecology and wood decomposition processes in angiosperms: from standing tree to complete decay of coarse woody debris. *Ecological Bulletins***,** 43-56.

BOERJAN, W., RALPH, J. & BAUCHER, M. 2003. Lignin biosynthesis. *Annual Review of Plant Biology,* 54**,** 519-546.

BOLLAG, J.-M. & LEONOWICZ, A. 1984. Comparative studies of extracellular fungal laccases. *Applied and Environmental Microbiology,* 48**,** 849-854.

BOLLAG, J.-M., SJOBLAD, R. D. & LIU, S.-Y. 1979. Characterization of an enzyme from *Rhizoctonia praticola* which polymerizes phenolic compounds. *Canadian Journal of Microbiology,* 25**,** 229-233.

BOURBONNAIS, R. & PAICE, M. G. 1990. Oxidation of non-phenolic substrates. *FEBS Letters,* 267(1)**,** 99-102.

BRADFORD, M. M. 1976. A rapid and sensitive method for the quantitation of microgram quantities of protein utilizing the principle of protein-dye binding. *Analytical Biochemistry,* 72**,** 248-254.

BRANDT, S. C., ELLINGER, B., VAN NGUYEN, T., THI, Q. D., VAN NGUYEN, G., BASCHIEN, C., YURKOV, A., HAHNKE, R. L., SCHÄFER, W. & GAND, M. 2018. A unique fungal strain collection from Vietnam characterized for high performance degraders of bioecological important biopolymers and lipids. *PloS One,* 13**,** e0202695.

BRINK, D. P., RAVI, K., LIDÉN, G. & GORWA-GRAUSLUND, M. F. 2019. Mapping the diversity of microbial lignin catabolism: experiences from the eLignin database. *Applied Microbiology and Biotechnology,* 103(10)**,** 1-24.

BROWN, M. E., BARROS, T. & CHANG, M. C. 2012. Identification and characterization of a multifunctional dye peroxidase from a lignin-reactive bacterium. *ACS Chemical Biology,* 7(12)**,** 2074-2081.

BROWN, R. M. 2004. Cellulose structure and biosynthesis: what is in store for the 21st century? *Journal of Polymer Science Part A: Polymer Chemistry,* 42**,** 487-495.

BURANOV, A. U. & MAZZA, G. 2008. Lignin in straw of herbaceous crops. *Industrial crops and products,* 28**,** 237-259.

BUSCH, R., HIRTH, T., LIESE, A., NORDHOFF, S., PULS, J., PULZ, O., SELL, D., SYLDATK, C. & ULBER, R. 2006. The utilization of renewable resources in German

industrial production. *Biotechnology Journal: Healthcare Nutrition Technology,* 1**,** 770-776.

BÜTTNER, E., GEBAUER, A. M., HOFRICHTER, M., LIERS, C. & KELLNER, H. 2017. Draft Genome Sequence of the Wood-Degrading *Ascomycete Kretzschmaria* deusta DSM 104547. *Genome announcements,* 5**,** e01076-17.

BÜTTNER, E., GEBAUER, A. M., HOFRICHTER, M., LIERS, C. & KELLNER, H. 2018. Draft Genome Sequence of *Scytalidium lignicola* DSM 105466, a Ubiquitous Saprotrophic Fungus. *Microbiology Resource Announcements,* 7(14)**,** e01208-18.

BÜTTNER, E., LIERS, C., GEBAUER, A. M., COLLEMARE, J., NAVARRO-MUÑOZ, J. C., HOFRICHTER, M. & KELLNER, H. 2019. Draft Genome Sequence of the Wood-Staining Ascomycete *Chlorociboria aeruginascens* DSM 107184. *Microbiology Resource Announcements,* 8(17)**,** e00249-19.

CAMARERO, S., CAÑAS, A. I., NOUSIAINEN, P., RECORD, E., LOMASCOLO, A., MARTÍNEZ, M. J. & MARTÍNEZ, Á. T. 2008. *p*-Hydroxycinnamic acids as natural mediators for laccase oxidation of recalcitrant compounds. *Environmental Science & Technology,* 42(17)**,** 6703-6709.

CAMARERO, S., SARKAR, S., RUIZ-DUEÑAS, F. J., MARTíNEZ, M. A. J. & MARTíNEZ, Á. T. 1999. Description of a versatile peroxidase involved in the natural degradation of lignin that has both manganese peroxidase and lignin peroxidase substrate interaction sites. *Journal of Biological Chemistry,* 274**,** 10324-10330.

CARABAJAL, M., KELLNER, H., LEVIN, L., JEHMLICH, N., HOFRICHTER, M. & ULLRICH, R. 2013. The secretome of *Trametes versicolor* grown on tomato juice medium and purification of the secreted oxidoreductases including a versatile peroxidase. *Journal of Biotechnology,* 168**,** 15-23.

CHEN, H. Y., XUE, D. S., FENG, X. Y. & YAO, S. J. 2011. Screening and production of ligninolytic enzyme by a marine-derived fungal *Pestalotiopsis* sp. J63. *Applied Biochemistry and Biotechnology,* 165(7-8)**,** 1754-1769.

CHEN, L., GONG, Y., CAI, Y., LIU, W., ZHOU, Y., XIAO, Y., XU, Z., LIU, Y., LEI, X., WANG, G. & GUO, M. 2016. Genome sequence of the edible cultivated mushroom *Lentinula edodes* (Shiitake) reveals insights into lignocellulose degradation. *PLoS One,* 11(8)**,** e0160336.

CHEN, Y. R. & SARKANEN, S. 2010. Macromolecular replication during lignin biosynthesis. *Phytochemistry,* 71**,** 453-462.

CHEVREUX, B., WETTER, T. & SUHAI, S. Genome sequence assembly using trace signals and additional sequence information. German conference on bioinformatics, 1999. Hanover, Germany, 45-56.

COLPA, D. I., FRAAIJE, M. W. & VAN BLOOIS, E. 2014. DyP-type peroxidases: a promising and versatile class of enzymes. *Journal of Industrial Microbiology & Biotechnology,* 41**,** 1-7.

CONESA, A., PUNT, P. J. & VAN DEN HONDEL, C. A. 2002. Fungal peroxidases: molecular aspects and applications. *Journal of Biotechnology,* 93(2)**,** 143-158.

CONTU, M. 1991. *Psathyrella bivelata* spec. nov., une nouvelle espèce sarde de la section Cystopsathyra. *Bulletin trimestriel de la Société mycologique de France,* 107**,** 85-89.

CORBETT, N. H. 1965. Micro-morphological studies on the degradation of lignified cell walls by Ascomycetes and Fungi Imperfecti. *Journal of the Institute of Wood Science,* 14**,** 18-29.

COUTURIER, M., TANGTHIRASUNUN, N., NING, X., BRUN, S., GAUTIER, V., BENNATI-GRANIER, C., SILAR, P. & BERRIN, J.-G. 2016. Plant biomass degrading ability of the coprophilic ascomycete fungus *Podospora anserina*. *Biotechnology Advances,* 34**,** 976-983.

D'SOUZA, T. M., BOOMINATHAN, K. & REDDY, C. A. 1996. Isolation of laccase gene-specific sequences from white-rot and brown-rot fungi by PCR. *Applied and Environmental Microbiology,* 62**,** 3739-3744.

DANIEL, G. 2003. Microview of wood under degradation by bacteria and fungi. *Wood Deterioration and Preservation,* 845**,** 34-72.

DANIEL, G. F. & NILSSON, T. 1998. Developments in the study of soft rot and bacterial decay. *In:* PALFREYMANN, A. B. J. W. (ed.) *Forest products biotechnology.* Tayler & Francis Ltd, London.

DE KOKER, T. H., JOHN, Z. H. A. O., ALLSOP, S. F. & JANSE, B. J. 2000. Isolation and enzymic characterisation of South African white-rot fungi. *Mycological Research,* 104(7)**,** 820-824.

DE VRIES, R. P. & VISSER, J. 2001. *Aspergillus* enzymes involved in degradation of plant cell wall polysaccharides. *Microbiology and Molecular Biology Reviews,* 65(4)**,** 497–522.

DENNIS, R. W. G. 1970. Fungus flora of Venezuela and adjacent countries. *Fungus flora of Venezuela and adjacent countries.*

DORADO, J., ALMENDROS, G., CAMARERO, S., MARTíNEZ, A. T., VARES, T. & HATAKKA, A. 1999. Transformation of wheat straw in the course of solid-state fermentation by four ligninolytic basidiomycetes. *Enzyme and Microbial Technology,* 25(7)**,** 605-612.

DUNFORD, H. 1991. Horseradish peroxidase: structure and kinetic properties. *In:* EVERSE J, E. K., GRISHAM MB (ed.) *Peroxidases in chemistry and biology.* CRC Press, Boca Raton, Ann Arbor, Boston.

DUNFORD, H. 1999. *Heme Peroxidases*, Wiley-VCH, New York.

EGGERT, C., TEMP, U., DEAN, J. F. & ERIKSSON, K. E. L. 1996. A fungal metabolite mediates degradation of non-phenolic lignin structures and synthetic lignin by laccase. *Febs Letters,* 391(1-2)**,** 144-148.

EIJSINK, V. G., PETROVIC, D., FORSBERG, Z., MEKASHA, S., RØHR, Å. K., VÁRNAI, A., BISSARO, B. & VAAJE-KOLSTAD, G. 2019. On the functional characterization of lytic polysaccharide monooxygenases (LPMOs). *Biotechnology for Biofuels,* 12(1)**,** 58.

EJECHI, B. O., OBUEKWE, C. O. & OGBIMI, A. O. 1996. Microchemical studies of wood degradation by brown rot and white rot fungi in two tropical timbers. *International Biodeterioration & Biodegradation,* 38(2)**,** 119-122.

ERIKSSON, K., BLANCHETTE, R. & ANDER, P. 1990. Microbial and Enzymatic Degradation of Wood Components. Springer-Verlag, Berlin.

ESTES, L., OKIN, G., MWANGI, A. & SHUGART, H. 2008. Habitat selection by a rare forest antelope: A multi-scale approach combining field data and imagery from three sensors. *Remote Sensing of Environment,* 112**,** 2033-2050.

EVANS, C. S., DUTTON, M. V., GUILLÉN, F. & VENESS, R. G. 1994. Enzymes and small molecular mass agents involved with lignocellulose degradation. *FEMS Microbiology Reviews,* 13**,** 235-239.

FARACO, V., PEZZELLA, C., MIELE, A., GIARDINA, P. & SANNIA, G. 2009. Bio-remediation of colored industrial wastewaters by the white-rot fungi *Phanerochaete chrysosporium* and *Pleurotus ostreatus* and their enzymes. *Biodegradation,* 20(2)**,** 209-220.

FASHING, P. J. & MWANGI GATHUA, J. 2004. Spatial variability in the vegetation structure and composition of an East African rain forest. *African Journal of Ecology,* 42**,** 189-197.

FELMLEE, T., PELLET, S. & WELCH, R. 1985. Nucleotide sequence of an *Escherichia coli* chromosomal hemolysin. *Journal of Bacteriology,* 163**,** 94–105.

FERNÁNDEZ-FUEYO, E., DAVÓ-SIGUERO, I., ALMENDRAL, D., LINDE, D., BARATTO, M. C., POGNI, R., ROMERO, A., GUALLAR, V. & MARTÍNEZ, A. T. 2018. Description of a non-canonical Mn(II)-oxidation site in peroxidases. *ACS Catalysis,* 8(9)**,** 8386-8395.

FERNÁNDEZ-FUEYO, E., LINDE, D., ALMENDRAL, D., LÓPEZ-LUCENDO, M. F., RUIZ-DUEÑAS, F. J. & MARTÍNEZ, A. T. 2015. Description of the first fungal dye-decolorizing peroxidase oxidizing manganese(II). *Applied Microbiology and Biotechnology,* 99**,** 8927-8942.

FINDLAY, W. P. K. 1984. Soft rot of timber—a review. *Journal of the Indian Academy of Wood Science,* 15**,** 1-11.

FLOUDAS, D., BINDER, M., RILEY, R., BARRY, K., BLANCHETTE, R. A., HENRISSAT, B., MARTÍNEZ, A. T., OTILLAR, R., SPATAFORA, J. W. & YADAV, J. S. 2012. The

Paleozoic origin of enzymatic lignin decomposition reconstructed from 31 fungal genomes. *Science,* 336**,** 1715-1719.

FLOUDAS, D., HELD, B. W., RILEY, R., NAGY, L. G., KOEHLER, G., RANSDELL, A. S., YOUNUS, H., CHOW, J., CHINIQUY, J., LIPZEN, A. & TRITT, A. 2015. Evolution of novel wood decay mechanisms in Agaricales revealed by the genome sequences of *Fistulina hepatica* and *Cylindrobasidium torrendii*. *Fungal Genetics and Biology,* 76**,** 78-92.

FOURNIER, J., FLESSA, F., PERŠOH, D. & STADLER, M. 2011. Three new *Xylaria* species from southwestern Europe. *Mycological Progress,* 10**,** 33-52.

FÜLÖP, V., RIDOUT, C. J., GREENWOOD, C. & HAJDU, J. 1995. Crystal structure of the di-haem cytochrome c peroxidase from *Pseudomonas aeruginosa*. *Structure,* 3(11)**,** 1225-1233.

GIARDINA, P., PALMIERI, G., FONTANELLA, B., RIVIECCIO, V. & SANNIA, G. 2000. Manganese peroxidase isoenzymes produced by *Pleurotus ostreatus* grown on wood sawdust. *Archives of Biochemistry and Biophysics,* 376(1)**,** 171-179.

GLENDAY, J. 2008. Carbon storage and emissions offset potential in an African dry forest, the Arabuko-Sokoke Forest, Kenya. *Environmental Monitoring and Assessment,* 142**,** 85-95.

GLENN, J. K., AKILESWARAN, L. & GOLD, M. H. 1986. Mn (II) oxidation is the principal function of the extracellular Mn-peroxidase from *Phanerochaete chrysosporium*. *Archives of Biochemistry and Biophysics,* 251**,** 688-696.

GOBLIRSCH, B., KURKER, R. C., STREIT, B. R., WILMOT, C. M. & DUBOIS, J. L. 2011. Chlorite dismutases, DyPs, and EfeB: 3 microbial heme enzyme families comprise the CDE structural superfamily *Journal of Molecular Biology,* 408(3)**,** 379-398.

GÓMEZ-TORIBIO, V., GARCÍA-MARTÍN, A. B., MARTÍNEZ, M. J., MARTÍNEZ, Á. T. & GUILLÉN, F. 2009. Induction of extracellular hydroxyl radical production by white-rot fungi through quinone redox cycling. *Applied and Environmental Microbiology,* 75**,** 3944-3953.

GRAMSS, G. 2017. Reappraising a controversy: Formation and role of the azodication ($ABTS^{2+}$) in the laccase-ABTS catalyzed breakdown of lignin. *Fermentation,* 3**,** 27.

GRÖBE, G., ULLRICH, R., PECYNA, M. J., KAPTURSKA, D., FRIEDRICH, S., HOFRICHTER, M. & SCHEIBNER, K. 2011. High-yield production of aromatic peroxygenase by the agaric fungus *Marasmius rotula*. *AMB Express,* 1**,** 31.

GUILLÉN, F., MARTINEZ, A. T. & MARTÍNEZ, M. J. 1990. Production of hydrogen peroxide by aryl-alcohol oxidase from the ligninolytic fungus *Pleurotus eryngii*. *Applied Microbiology and Biotechnology,* 32**,** 465-469.

GUPTA, D. K., RÜHL, M., MISHRA, B., KLEOFAS, V., HOFRICHTER, M., HERZOG, R., PECYNA, M. J., SHARMA, R., KELLNER, H., HENNICKE, F. & M, T. 2018. The genome sequence of the commercially cultivated mushroom *Agrocybe aegerita* reveals a conserved repertoire of fruiting-related genes and a versatile suite of biopolymer-degrading enzymes. *BMC Genomics,* 19**,** 48.

GUPTA, R., JUNG, E. & BRUNAK, S. 2004. Predicition of N-glycosylation sites in human proteins. *Center for Biological Sequence Analysis at Technical University of Denmark DTU*.

GUREVICH, A., SAVELIEV, V., VYAHHI, N. & TESLER, G. 2013. QUAST: quality assessment tool for genome assemblies. *Bioinformatics,* 29**,** 1072-1075.

HAMMEL, K. E. & CULLEN, D. 2008. Role of fungal peroxidases in biological ligninolysis. *Current Opinion in Plant Biology,* 11(3)**,** 349-355.

HAMMEL, K. E., JENSEN, K. A., MOZUCH, M. D., LANDUCCI, L. L., TIEN, M. & PEASE, E. A. 1993. Ligninolysis by a purified lignin peroxidase. *Journal of Biological Chemistry,* 268**,** 12274-12281.

HARTLEY, R. D. & FORD, C. W. 1989. Phenolic constituents of plant cell walls and wall biodegradability. *Plant Cell Wall Polymers, Biogenesis and Biodegradation,* 399**,** 137-145.

HASHIMOTO, A. & PICKARD, M. A. 1984. Chloroperoxidases from *Caldariomyces* (= *Leptoxyphium*) cultures: glycoproteins with variable carbohydrate content and isoenzymic forms. *Microbiology,* 130**,** 2051-2058.

HATAKKA, A. 1994. Lignin-modifying enzymes fungi: production and role from selected white-rot in lignin degradation. *FEMS Microbiology Reviews,* 13**,** 125-135.

HATAKKA, A. 2001. Biodegradation of lignin. *In:* HOFRICHTER M, S. A. E. (ed.) *Biopolymers: Biology, Chemistry, Biotechnology, Applications, Vol 1. Lignin, Humic Substances and Coal.* Wiley VCH, Weinheim.

HATAKKA, A. & HAMMEL, K. E. 2010. Fungal biodegradation of lignocelluloses. *In: Industrial Applications.* Springer. Berlin, Heidelberg.

HATAKKA, A. I. & UUSI-RAUVA, A. K. 1983. Degradation of ^{14}C-labelled poplar wood lignin by selected white-rot fungi. *European Journal of Applied Microbiology and Biotechnology,* 17(4)**,** 235-242.

HAWKSWORTH, D. L. 2001. The magnitude of fungal diversity: the 1·5 million species estimate revisited. *Mycological Research,* 105**,** 1422-1432.

HEINFLING, A., MARTINEZ, M., MARTINEZ, A., BERGBAUER, M. & SZEWZYK, U. 1998. Transformation of industrial dyes by manganese peroxidases from *Bjerkandera adusta* and *Pleurotus eryngii* in a manganese-independent reaction. *Applied and Environmental Microbiology,* 64**,** 2788-2793.

HENRIKSSON, G., ZHANG, L., LI, J., LJUNGQUIST, P., REITBERGER, T., PETTERSSON, G. & JOHANSSON, G. 2000. Is cellobiose dehydrogenase from *Phanerochaete chrysosporium* a lignin degrading enzyme? *Biochimica et Biophysica Acta (BBA)-Protein Structure and Molecular Enzymology,* 1480(1-2)**,** 83-91.

HERNÁNDEZ-ORTEGA, A., FERREIRA, P. & MARTÍNEZ, A. T. 2012. Fungal aryl-alcohol oxidase: a peroxide-producing flavoenzyme involved in lignin degradation. *Applied Microbiology and Biotechnology,* 93**,** 1395-1410.

HESSELTINE, C. 1955. Genera of Mucorales with notes on their synonymy. *Mycologia,* 47**,** 344-363.

HIGUCHI, T. 2006. Look back over the studies of lignin biochemistry. *Journal of Wood Science,* 52(1)**,** 2-8.

HILDÉN, K., MÄKELÄ, M. R., STEFFEN, K. T., HOFRICHTER, M., HATAKKA, A., ARCHER, D. B. & LUNDELL, T. K. 2014. Biochemical and molecular characterization of an atypical manganese peroxidase of the litter-decomposing fungus *Agrocybe praecox. Fungal Genetics and Biology,* 72**,** 131-136.

HILDÉN, K. S., BORTFELDT, R., HOFRICHTER, M., HATAKKA, A. & LUNDELL, T. K. 2008. Molecular characterization of the basidiomycete isolate *Nematoloma frowardii* b19 and its manganese peroxidase places the fungus in the corticioid genus *Phlebia*. *Microbiology,* 154(8)**,** 2371-2379.

HINTIKKA, V. 1970. Studies on white-rot humus formed by higher fungi in forest soils. *Communicationes Instituti Forestalis Fenniae* 69(2)**,** 68.

HOFRICHTER, M. 2002. lignin conversion by manganese peroxidase (MnP). *Enzyme and Microbial Technology,* 30**,** 454-466.

HOFRICHTER, M. & FRITSCHE, W. 1997. Depolymerization of low-rank coal by extracellular fungal enzyme systems. II. The ligninolytic enzymes of the coal-humic-acid-depolymerizing fungus *Nematoloma frowardii* b19. *Applied Microbiology and Biotechnology,* 47**,** 419-424.

HOFRICHTER, M., KELLNER, H., HERZOG, R., KARICH, A., LIERS, C., SCHEIBNER, K., KIMANI, V. W. & ULLRICH, R. 2019. Fungal Peroxygenases: A Phylogenetically Old Superfamily of Heme Enzymes with Promiscuity for Oxygen Transfer Reactions Springer, in press.

HOFRICHTER, M., KELLNER, H., PECYNA, M. J. & ULLRICH, R. 2015. Fungal unspecific peroxygenases: heme-thiolate proteins that combine peroxidase and cytochrome P450 properties. *Monooxygenase, peroxidase and Peroxygenase properties and mechanisms of cytochrome P450.* Springer.

HOFRICHTER, M., LUNDELL, T. & HATAKKA, A. 2001. Conversion of milled pine wood by manganese peroxidase from *Phlebia radiata*. *Applied and Environmental Microbiology,* 67(10)**,** 4588-4593.

HOFRICHTER, M., SCHEIBNER, K., SCHNEEGAß, I., ZIEGENHAGEN, D. & FRITSCHE, W. 1998. Mineralization of synthetic humic substances by manganese peroxidase from the white-rot fungus *Nematoloma frowardii*. *Applied Microbiology and Biotechnology,* 49**,** 584-588.

HOFRICHTER, M. & ULLRICH, R. 2006. Heme-thiolate haloperoxidases: versatile biocatalysts with biotechnological and environmental significance. *Applied Microbiology and Biotechnology,* 71**,** 276.

HOFRICHTER, M. & ULLRICH, R. 2014. Oxidations catalyzed by fungal peroxygenases. *Current Opinion in Chemical Biology,* 19**,** 116-125.

HOFRICHTER, M., ULLRICH, R., KELLNER, H., UPADHYAY, R. C. & SCHEIBNER, K. Fungal unspecific peroxygenases: a new generation of oxygen-transferring biocatalysts. *In:* ICMBMP8, ed. In Proceedings of the 8th international conference on Mushroom Biology and Mushroom Products 2014. 172-181.

HOFRICHTER, M., ULLRICH, R., PECYNA, M., KINNE, M., KLUGE, M., ARANDA, E., LIERS, C., PORAJ-KOBIELSKA, M., GRÖBE, G., SCHEIBNER, K., BITTNER, B., PIONTEK, K., SCHUBERT, R. & HAMMEL, K. 2009. Aromatic peroxygenases from mushrooms: extracellular heme-thiolate proteins of a new enzyme sub-subclass? *In:* SHOUN H, O. H. (ed.) *16th International Conference on Cytochrome P450 (Nago, Okinawa, Japan), Medimond (International Proceedings), Bologna, (Italy).*

HOFRICHTER, M., ULLRICH, R., PECYNA, M. J., LIERS, C. & LUNDELL, T. 2010. New and classic families of secreted fungal heme peroxidases. *Applied and Environmental Microbiology,* 87**,** 871-897.

HOFRICHTER, M., VARES, T., KALSI, M., GALKIN, S., SCHEIBNER, K., FRITSCHE, W. & HATAKKA, A. 1999. Production of manganese peroxidase and organic acids and mineralization of ^{14}C-labelled lignin (^{14}C-DHP) during solid-state fermentation of wheat straw with the white rot fungus *Nematoloma frowardii*. *Applied and Environmental Microbiology,* 65(5)**,** 1864-1870.

HOPPLE JR, J. S. & VILGALYS, R. 1999. Phylogenetic relationships in the mushroom genus *Coprinus* and dark-spored allies based on sequence data from the nuclear gene coding for the large ribosomal subunit RNA: divergent domains, outgroups, and monophyly. *Molecular phylogenetics and evolution,* 13**,** 1-19.

HORN, A. 2009. *The use of a novel peroxidase from the basidiomycete Agrocybe aegerita as an example of enatioselective sulfoxidation (Der Einsatz einer neuartigen Peroxidase des Basidiomyceten Agrocybe aegerita am Beispiel der enatioselektiven Sulfoxidation)* Doctoral dissertation, University of Rostock, Germany.

HOSSEINZADEH, P., MIRTS, E. N., PFISTER, T. D., GAO, Y. G., MAYNE, C., ROBINSON, H., TAJKHORSHID, E. & LU, Y. 2016. Enhancing Mn(II)-binding and manganese peroxidase activity in a designed cytochrome c peroxidase through fine-tuning secondary-sphere interactions. *Biochemistry,* 55(10)**,** 1494-1502.

HÜTTNER, S., GRANCHI, Z., NGUYEN, T. T., VAN PELT, S., LARSBRINK, J., THANH, V. N. & OLSSON, L. 2018. Genome sequence of *Rhizomucor pusillus* FCH 5.7, a thermophilic zygomycete involved in plant biomass degradation harbouring putative GH9 endoglucanases. *Biotechnology Reports,* 20**,** e00279.

HYDE, K. D. 1997. *Biodiversity of tropical microfungi*, Hong Kong University Press.

JENSEN, K. A., HOUTMAN, C. J., RYAN, Z. C. & HAMMEL, K. E. 2001. Pathways for extracellular Fenton chemistry in the brown rot basidiomycete *Gloeophyllum trabeum*. *Applied and Environmental Microbiology,* 67**,** 2705-2711.

JOHJIMA, T., OHKUMA, M. & KUDO, T. 2003. Isolation and cDNA cloning of novel hydrogen peroxide-dependent phenol oxidase from the basidiomycete *Termitomyces albuminosus*. *Applied Microbiology and Biotechnology,* 61**,** 220-225.

JØRGENSEN, H., KRISTENSEN, J. B. & FELBY, C. 2007. Enzymatic conversion of lignocellulose into fermentable sugars: challenges and opportunities. *Biofuels, Bioproducts and Biorefining,* 1**,** 119-134.

KÄLL, L., CANTERBURY, J. D., WESTON, J., NOBLE, W. S. & MACCOSS, M. J. 2007. Semi-supervised learning for peptide identification from shotgun proteomics datasets *Nature Methods,* 4**,** 923-925.

KAMM, B. & KAMM, M. 2004. Principles of biorefineries. *Applied Microbiology and Biotechnology,* 64**,** 137-145.

KARICH, A., KLEEBERG, S. B., ULLRICH, R. & HOFRICHTER, M. 2018. Enzymatic preparation of 2,5-furandicarboxylic acid (FDCA)-a substitute of terephthalic acid-by the joined action of three fungal enzymes. *Microorganisms,* 6**,** 5.

KARICH, A., KLUGE, M., ULLRICH, R. & HOFRICHTER, M. 2013. Benzene oxygenation and oxidation by the peroxygenase of *Agrocybe aegerita*. *AMB Express,* 3(1)**,** 5.

KARICH, A., ULLRICH, R., SCHEIBNER, K. & HOFRICHTER, M. 2017. Fungal unspecific peroxygenases oxidize the majority of organic EPA priority pollutants. *Frontiers in Microbiology,* 8**,** 1463.

KATOH, K., MISAWA, K., KUMA, K. I. & MIYATA, T. 2002. MAFFT: a novel method for rapid multiple sequence alignment based on fast Fourier transform. *Nucleic Acids Research,* 30**,** 3059-3066.

KEARSE, M., MOIR, R., WILSON, A., STONES-HAVAS, S., CHEUNG, M., STURROCK, S., BUXTON, S., COOPER, A., MARKOWITZ, S. & DURAN, C. 2012. Geneious Basic: an integrated and extendable desktop software platform for the organization and analysis of sequence data. *Bioinformatics,* 28**,** 1647-1649.

KELLNER, H., LUIS, P., PECYNA, M. J., BARBI, F., KAPTURSKA, D., KRÜGER, D., ZAK, D. R., MARMEISSE, R., VANDENBOL, M. & HOFRICHTER, M. 2014. Widespread occurrence of expressed fungal secretory peroxidases in forest soils. *PLoS One,* 9(4)**,** e95557.

KERSTEN, P. & CULLEN, D. 2007. Extracellular oxidative systems of the lignin-degrading Basidiomycete *Phanerochaete chrysosporium*. *Fungal Genetics and Biology,* 44(2)**,** 77-87.

KERSTEN, P. & CULLEN, D. 2014. Copper radical oxidases and related extracellular oxidoreductases of wood-decay Agaricomycetes. *Fungal Genetics and Biology,* 72**,** 124-130.

KERSTEN, P. J. & KIRK, T. K. 1987. Involvement of a new enzyme, glyoxal oxidase, in extracellular H_2O_2 production by *Phanerochaete chrysosporium*. *Journal of Bacteriology,* 169**,** 2195-2201.

KIEBIST, J. 2018. *Oxyfunktionalisierung pharmazeutisch relevanter Strukturen durch unspezifische Peroxygenasen der Familie I aus Dikarya-Pilzen.* Dissertation PhD, TU Dresden-IHI Zittau, Germany.

KIEBIST, J., HOFRICHTER, M., ZUHSE, R. & SCHEIBNER, K. 2019. Oxyfunctionalization of pharmaceuticals by fungal peroxygenases (accepted). *In:* P, G. (ed.) *Pan Stanford Series on Biocatalysis.* Pan Stanford Publishing.

KIEBIST, J., SCHMIDTKE, K. U., ZIMMERMANN, J., KELLNER, H., JEHMLICH, N., ULLRICH, R., ZÄNDER, D., HOFRICHTER, M. & SCHEIBNER, K. 2017. A peroxygenase from *Chaetomium globosum* catalyzes the selective oxygenation of testosterone. *ChemBioChem,* 18**,** 563-569.

KIM, K. M., LEE, J. S. & JUNG, H. S. 2007. *Fomitopsis incarnatus* sp. nov. based on generic evaluation of *Fomitopsis* and *Rhodofomes*. *Mycologia,* 99(6)**,** 833-841.

KIM, S. J., ISHIKAWA, K., HIRAI, M. & SHODA, M. 1995. Characteristics of a newly isolated fungus, *Geotrichum candidum* Dec 1, which decolorizes various dyes. *Journal of Fermentation and Bioengineering,* 79(6)**,** 601-607.

KIM, S. J. & SHODA, M. 1999. Purification and characterization of a novel peroxidase from *Geotrichum candidum* Dec1 involved in decolorization of dyes. *Applied and Environmental Microbiology,* 65**,** 1029-1035.

KIM, T. Y., JANG, J. Y., YU, N. H., CHI, W. J., BAE, C. H., YEO, J. H., PARK, A. R., HUR, J. S., PARK, H. W. & PARK, J. Y. 2018. Nematicidal activity of grammicin produced by *Xylaria grammica* KCTC 13121BP against *Meloidogyne incognita*. *Pest Management Science,* 74**,** 384-391.

KINNE, M., PORAJ-KOBIELSKA, M., ARANDA, E., ULLRICH, R., HAMMEL, K. E., SCHEIBNER, K. & HOFRICHTER, M. 2009. Regioselective preparation of 5-hydroxypropranolol and 4′-hydroxydiclofenac with a fungal peroxygenase. *Bioorganic & Medicinal Chemistry Letters,* 19**,** 3085-3087.

KINNE, M., PORAJ-KOBIELSKA, M., ULLRICH, R., NOUSIAINEN, P., SIPILÄ, J., SCHEIBNER, K., HAMMEL, K. E. & HOFRICHTER, M. 2011. Oxidative cleavage of non-phenolic β-O-4 lignin model dimers by an extracellular aromatic peroxygenase. *Holzforschung,* 65(5)**,** 673-679.

KINNE, M., ULLRICH, R., HAMMEL, K. E., SCHEIBNER, K. & HOFRICHTER, M. 2008. Regioselective preparation of (R)-2-(4-hydroxyphenoxy) propionic acid with a fungal peroxygenase. *Tetrahedron Letters,* 49**,** 5950-5953.

KINNE, M., ZEISIG, C., ULLRICH, R., KAYSER, G., HAMMEL, K. E. & HOFRICHTER, M. 2010. Stepwise oxygenations of toluene and 4-nitrotoluene by a fungal peroxygenase. *Biochemical and Biophysical Research Communications,* 397**,** 18-21.

KIRK, P., CANNON, P., MINTER, D. & STALPERS, J. 2008. Dictionary of the fungi, 10th edn. CABI Europe. Oxford.

KIRK, T. 1984. Degradation of lignin. *In:* DT, G. (ed.) *Microbial degradation of organic compounds.* Dekker, New York.

KIRK, T., SCHULTZ, E., CONNORS, W., LORENZ, L. & ZEIKUS, J. 1978. Influence of culture parameters on lignin metabolism by *Phanerochaete chrysosporium*. *Archives of Microbiology,* 117**,** 277-285.

KIRK, T. K. & CULLEN, D. 1998. Enzymology and molecular genetics of wood degradation by white-rot fungi. *Environmentally Friendly Technologies For The Pulp and Paper Industry.* Wiley, New York.

KIRK, T. K. & FARRELL, R. L. 1987. Enzymatic" combustion": the microbial degradation of lignin. *Annual Reviews in Microbiology,* 41**,** 465-501.

KLUGE, M., ULLRICH, R., DOLGE, C., SCHEIBNER, K. & HOFRICHTER, M. 2009. Hydroxylation of naphthalene by aromatic peroxygenase from *Agrocybe aegerita* proceeds via oxygen transfer from H_2O_2 and intermediary epoxidation. *Applied Microbiology and Biotechnology,* 81**,** 1071-1076.

KLUGE, M., ULLRICH, R., SCHEIBNER, K. & HOFRICHTER, M. 2007. Spectrophotometric assay for detection of aromatic hydroxylation catalyzed by fungal haloperoxidase-peroxygenase. *Applied Microbiology and Biotechnology,* 75**,** 1473–1478.

KOKWARO, J. 1988. Conservation status of the Kakamega Forest in Kenya: the easternmost relic of the equatorial rain forests of Africa. *Monographs in Systematic Botany of the Missouri Botanical Garden,* 25**,** 471-489.

KOSHIJIMA, T. & WATANABE, T. 2003. *Association between lignin and carbohydrates in wood and other plant tissues*, Springer-Verlag. Berlin Heidelberg.

KRACHER, D., SCHEIBLBRANDNER, S., FELICE, A. K., BRESLMAYR, E., PREIMS, M., LUDWICKA, K., HALTRICH, D., EIJSINK, V. G. & LUDWIG, R. 2016. Extracellular electron transfer systems fuel cellulose oxidative degradation. *Science,* 352(6289)**,** 1098-1101.

KRAH, F. S., BÄSSLER, C., HEIBL, C., SOGHIGIAN, J., SCHAEFER, H. & HIBBETT, D. S. 2018. Evolutionary dynamics of host specialization in wood-decay fungi. *BMC Evolutionary Biology,* 18(1)**,** 119.

KUHAD, R. C., SINGH, A. & ERIKSSON, K. E. L. 1997. Microorganisms and enzymes involved in the degradation of plant fiber cell walls. *In Biotechnology In The Pulp and Paper Industry Advances in Biochemical Engineering/Biotechnology.* Springer. Berlin, Heidelberg.

KUTATELADZE, L., ZAKARIASHVILI, N., JOBAVA, M., BURDULI, T. & SADUNISHVILI, T. 2016. Microscopic fungi spread in different types of soils in Western Georgia. *Annals of Agrarian Science,* 14**,** 227-232.

KUTZ, M. 2005. *Handbook of environmental degradation of materials*, William Andrew, Inc New York.

KWIATOS, N., RYNGAJŁŁO, M. & BIELECKI, S. 2015. Diversity of laccase-coding genes in *Fusarium oxysporum* genomes. *Frontiers in Microbiology,* 6**,** 933.

LAEMMLI, U. K. 1970. Cleavage of structural proteins during the assembly of the head of bacteriophage T4. *Nature,* 227**,** 680.

LAMBRECHTS, C., WOODLEY, B., CHURCH, C. & GACHANJA, M. 2003. Aerial survey of the destruction of the Aberdare Range forests. *Division of Early Warning and Assessment, UNEP*.

LANGSTON, J. A., SHAGHASI, T., ABBATE, E., XU, F., VLASENKO, E. & SWEENEY, M. D. 2011. Oxidoreductive cellulose depolymerization by the enzymes cellobiose dehydrogenase and glycoside hydrolase 61. *Applied and Environmetal Microbiology,* 77(19)**,** 7007-7015.

LANKINEN, P. 2004. *Ligninolytic enzymes of the basidiomycetous fungi Agaricus bisporus and Phlebia radiata on lignocellulose-containing media.* Dissertation, University of Helsinki, Finland.

LARSSON, E. & ÖRSTADIUS, L. 2008. Fourteen coprophilous species of *Psathyrella* identified in the Nordic countries using morphology and nuclear rDNA sequence data. *Mycological Research,* 112**,** 1165-1185.

LEE, J. S., KO, K. S. & JUNG, H. S. 2000. Phylogenetic analysis of *Xylaria* based on nuclear ribosomal ITS1-5.8 S-ITS2 sequences. *FEMS Microbiology Letters,* 187**,** 89-93.

LEE, K. H., WI, S. G., SINGH, A. P. & KIM, Y. S. 2004. Micromorphological characteristics of decayed wood and laccase produced by the brown-rot fungus *Coniophora puteana*. *Journal of Wood Science,* 50**,** 281-284.

LEE, S., MILGROOM, M. & TAYLOR, J. 1988. A rapid, high yield mini-prep method for isolation of total genomic DNA from fungi. *Fungal Genetics Reports,* 35**,** 23.

LEE, Y. S. 2000. Observation of soft-rot wood degradation caused by higher Ascomyceteous fungi. *Mycobiology,* 28(1)**,** 47-50.

LEONHARDT, S., BÜTTNER, E., GEBAUER, A. M., HOFRICHTER, M. & KELLNER, H. 2018. Draft Genome Sequence of the *Sordariomycete Lecythophora* (*Coniochaeta*) *hoffmannii* CBS 245.38. *Genome Announcements,* 6(7)**,** e01510-17.

LEONOWICZ, A., ROGALSKI, J., JASZEK, M., LUTEREK, J., WOJTAS-WASILEWSKA, M., MALARCZYK, E., GINALSKA, G., FINK-BOOTS, M. & CHO, N. S. 1999. Cooperation of fungal laccase and glucose1-oxidase in transformation of Björkman lignin and some phenolic compounds. *Holzforschung,* 53(4)**,** 376-380.

LI, K., HORANYI, P. S., COLLINS, R., PHILLIPS, R. S. & ERIKSSON, K. E. L. 2001. Investigation of the role of 3-hydroxyanthranilic acid in the degradation of lignin by white-rot fungus *Pycnoporus cinnabarinus*. *Enzyme and Microbial Technology,* 28(4-5)**,** 301-307.

LIERS, C. 2007. *Das Lignozellulose abbauende Enzymsystem des holzbesiedelnden Schlauchpilzes Xylaria polymorpha.* Doctoral dissertation, IHI-Zittau, Germany.

LIERS, C., ARANDA, E., STRITTMATTER, E., PIONTEK, K., PLATTNER, D. A., ZORN, H., ULLRICH, R. & HOFRICHTER, M. 2014. Phenol oxidation by DyP-type peroxidases in comparison to fungal and plant peroxidases. *Journal of Molecular Catalysis B: Enzymatic,* 103**,** 41-46.

LIERS, C., ARNSTADT, T., ULLRICH, R. & HOFRICHTER, M. 2011. Patterns of lignin degradation and oxidative enzyme secretion by different wood-and litter-colonizing basidiomycetes and ascomycetes grown on beech-wood. *FEMS Microbiology Ecology,* 78**,** 91-102.

LIERS, C., BOBETH, C., PECYNA, M., ULLRICH, R. & HOFRICHTER, M. 2010. DyP-like peroxidases of the jelly fungus *Auricularia auricula-judae* oxidize nonphenolic lignin

model compounds and high-redox potential dyes. *Applied Microbiology and Biotechnology,* 85**,** 1869-1879.

LIERS, C., PECYNA, M. J., KELLNER, H., WORRICH, A., ZORN, H., STEFFEN, K. T., HOFRICHTER, M. & ULLRICH, R. 2013. Substrate oxidation by dye-decolorizing peroxidases (DyPs) from wood-and litter-degrading agaricomycetes compared to other fungal and plant heme-peroxidases. *Applied Microbiology and Biotechnology,* 97(13)**,** 5839-5849.

LIERS, C., ULLRICH, R., PECYNA, M., SCHLOSSER, D. & HOFRICHTER, M. 2007. Production, purification and partial enzymatic and molecular characterization of a laccase from the wood-rotting ascomycete *Xylaria polymorpha*. *Enzyme and Microbial Technology,* 41**,** 785-793.

LIERS, C., ULLRICH, R., STEFFEN, K. T., HATAKKA, A. & HOFRICHTER, M. 2006. Mineralization of ^{14}C-labelled synthetic lignin and extracellular enzyme activities of the wood-colonizing ascomycetes *Xylaria hypoxylon* and *Xylaria polymorpha*. *Applied Microbiology and Biotechnology,* 69(5)**,** 573-579.

LIESE, W. 1970. Ultrastructural aspects of woody tissue disintegration. *Annual Review of Phytopathology,* 8**,** 231-258.

LINDE, D., COSCOLÍN, C., LIERS, C., HOFRICHTER, M., MARTÍNEZ, A. T. & RUIZ-DUEÑAS, F. J. 2014. Heterologous expression and physicochemical characterization of a fungal dye-decolorizing peroxidase from *Auricularia auricula-judae*. *Protein Expression and Purification,* 103**,** 28-37.

LINDE, D., POGNI, R., CANELLAS, M., LUCAS, F., GUALLAR, V., BARATTO, M. C., SINICROPI, A., SÁEZ-JIMÉNEZ, V., COSCOLÍN, C., ROMERO, A. & MEDRANO, F. J. 2015. Catalytic surface radical in dye-decolorizing peroxidase: a computational, spectroscopic and site-directed mutagenesis study. *Biochemical Journal,* 466(2)**,** 253-262.

LIYAMA, K., LAM, T. B.-T. & STONE, B. A. 1994. Covalent cross-links in the cell wall. *Plant Physiology,* 104**,** 315.

LOMBARD, V., GOLACONDA RAMULU, H., DRULA, E., COUTINHO, P. M. & HENRISSAT, B. 2014. The carbohydrate-active enzymes database (CAZy) in 2013. *Nucleic Acids Research,* 42(D1)**,** D490-D495.

LUDWIG, E. 2001. *Pilzkompendium*, IHW-Verlag, Berchtesgaden.

LUDWIG, R., HARREITHER, W., TASCA, F. & GORTON, L. 2010. Cellobiose dehydrogenase: a versatile catalyst for electrochemical applications. *ChemPhysChem,* 11**,** 2674–2697.

LUNDELL, T., WEVER, R., FLORIS, R., HARVEY, P., HATAKKA, A., BRUNOW, G. & SCHOEMAKER, H. 1993. Lignin peroxidase L3 from *Phlebia radiata.* Pre-steady-state and steady-state studies with veratryl alcohol and a non-phenolic lignin model compound 1-(3,4-dimethoxyphenyl)-2-(2-methoxyphenoxy)propane-1,3-diol. *European Journal of Biochemistry,* 211**,** 391– 402.

LUNDELL, T. K., MÄKELÄ, M. R. & HILDÉN, K. 2010. Lignin-modifying enzymes in filamentous basidiomycetes–ecological, functional and phylogenetic review. *Journal of Basic Microbiology,* 50**,** 5-20.

LYND, L. R., CUSHMAN, J. H., NICHOLS, R. J. & WYMAN, C. E. 1991. Fuel ethanol from cellulosic biomass. *Science,* 251**,** 1318-1323.

MACÍAS-RUBALCAVA, M. L. & SÁNCHEZ-FERNÁNDEZ, R. E. 2017. Secondary metabolites of endophytic *Xylaria* species with potential applications in medicine and agriculture. *World Journal of Microbiology and Biotechnology,* 33**,** 15.

MÄKELÄ, M. R., HILDÉN, K. S. & DE VRIES, R. P. 2014. Degradation and Modification of Plant Biomass by Fungi. *Fungal Genomics.* Springer, Berlin, Heidelberg.

MANOJ, K. M. & HAGER, L. P. 2008. Chloroperoxidase, a janus enzyme. *Biochemistry,* 47(9)**,** 2997-3003.

MAPEMBA, L. D., EPPLIN, F. M., TALIAFERRO, C. M. & HUHNKE, R. L. 2007. Biorefinery feedstock production on conservation reserve program land. *Review of Agricultural Economics,* 29**,** 227-246.

MARTÍNEZ, A., RUIZ-DUEÑAS, F., MARTÍNEZ, M., DEL RIO, J. & GUTIERREZ, A. 2009. Enzymatic delignification of plant cell wall: from nature to mill. *Current Opinion in Biotechnology,* 20**,** 348–357.

MARTÍNEZ, A. T., CAMARERO, S., GUILLÉN, F., GUTIÉRREZ, A., MUÑOZ, C., VARELA, E., MARTÍNEZ, M. J., BARRASA, J. M., RUEL, K. & PELAYO, J. M. 1994. Progress in biopulping of non-woody materials: chemical, enzymatic and ultrastructural aspects of wheat straw delignification with ligninolytic fungi from the genus *Pleurotus*. *FEMS Microbiology Reviews,* 13(2-3)**,** 265-273.

MARTÍNEZ, Á. T., SPERANZA, M., RUIZ-DUEÑAS, F. J., FERREIRA, P., CAMARERO, S., GUILLÉN, F., MARTÍNEZ, M. J., GUTIÉRREZ SUÁREZ, A. & RÍO ANDRADE, J. C. D. 2005. Biodegradation of lignocellulosics: microbial, chemical, and enzymatic aspects of the fungal attack of lignin. *International Microbiology,* 8**,** 195-204.

MARTÍNEZ, M. J., RUIZ-DUEÑAS, F. J., GUILLÉN, F. & MARTÍNEZ, Á. T. 1996. Purification and catalytic properties of two manganese peroxidase isoenzymes from *Pleurotus eryngii*. *European Journal of Biochemistry,* 237**,** 424-432.

MASALU, R. 2016. Ligninolytic enzymes of the fungus isolated from soil contaminated with cow dung. *Tanzania Journal of Science,* 42**,** 85-93.

MATE, D. M., PALOMINO, M. A., MOLINA-ESPEJA, P., MARTIN-DIAZ, J. & ALCALDE, M. 2017. Modification of the peroxygenative: peroxidative activity ratio in the unspecific peroxygenase from *Agrocybe aegerita* by structure-guided evolution. *Protein Engineering, Design and Selection,* 30(3)**,** 191-198.

MATHEWS, S. L., PAWLAK, J. & GRUNDEN, A. M. 2015. Bacterial biodegradation and bioconversion of industrial lignocellulosic streams. *Applied Microbiology and Biotechnology,* 99(7)**,** 2939-2954.

MELZER, A., KIMANI, V. W. & ULLRICH, R. 2018. *Psathyrella aberdarensis*, a new species of *Psathyrella* (Agaricales) from a Kenyan National Park. *Austrian Journal of Mycology***,** 22-30.

MITCHELL, A., CHANG, H. Y., DAUGHERTY, L., FRASER, M., HUNTER, S., LOPEZ, R., MCANULLA, C., MCMENAMIN, C., NUKA, G., PESSEAT, S. & SANGRADOR-VEGAS, A. 2015. The InterPro protein families database: the classification resource after 15 years. *Nucleic Acids Research,* 43**,** 213-221.

MOLINA-ESPEJA, P., GARCIA-RUIZ, E., GONZALEZ-PEREZ, D., ULLRICH, R., HOFRICHTER, M. & ALCALDE, M. 2014. Directed evolution of unspecific peroxygenase from *Agrocybe aegerita*. *Applied and Environmental Microbiology,* 80**,** 3496-3507.

MOLINA-ESPEJA, P., MA, S., MATE, D. M., LUDWIG, R. & ALCALDE, M. 2015. Tandem-yeast expression system for engineering and producing unspecific peroxygenase. *Enzyme and Microbial Technology,* 73**,** 29-33.

MONTIES, B. & FUKUSHIMA, K. 2001. Occurrence, function, and biosynthesis of lignins. In A. Steinbüchel & M. Hofrichter (Eds.), Biopolymers, lignin, humic substances, and coal. Weinheim: Wiley.

MORIN, E., KOHLER, A., BAKER, A. R., FOULONGNE-ORIOL, M., LOMBARD, V., NAGYE, L. G., OHM, R. A., PATYSHAKULIYEVA, A., BRUN, A., AERTS, A. L. & MARTIN, F. 2012. Genome sequence of the button mushroom *Agaricus bisporus* reveals mechanisms governing adaptation to a humic-rich ecological niche. *Proceedings of the National Academy of Sciences,* 109**,** 17501-17506.

MTUI, G. 2007. Characteristics and dyes biodegradation potential of crude lignolytic enzymes from white-rot fungus *Crepidotus variabilis* isolated in coastal Tanzania. *Tanzania Journal of Science,* 33.

MUELLER, G. M., BILLS, G. F. & FOSTER, M. S. 2004. *Biodiversity of Fungi*, Elservier Academic Press, Burlington.

MUNK, L., SITARZ, A. K., KALYANI, D. C., MIKKELSEN, J. D. & MEYER, A. S. 2015. Can laccases catalyze bond cleavage in lignin? *Biotechnology Advances,* 33(1)**,** 13-24.

NARANJO-BRICEÑO, L., PERNÍA, B., GUERRA, M., DEMEY, J. R., DE SISTO, Á., INOJOSA, Y., GONZÁLEZ, M., FUSELLA, E., FREITES, M. & YEGRES, F. 2013.

Potential role of oxidative exoenzymes of the extremophilic fungus *Pestalotiopsis palmarum* BM-04 in biotransformation of extra-heavy crude oil. *Microbial Biotechnology,* 6(6)**,** 720-730.

NGHI, D. H. 2012. *A Novel Extracellular Hydrolase from the Wood Rot Ascomycete Xylaria polymorpha that Combines Glycosidase and Esterase Activities: Production, Purification and Characterization.* Doctoral dissertation, IHI-Zittau, Germany.

NGHI, D. H., BITTNER, B., KELLNER, H., JEHMLICH, N., ULLRICH, R., PECYNA, M. J., NOUSIAINEN, P., SIPILÄ, J., HOFRICHTER, M. & LIERS, C. 2012. The wood-rot ascomycetes *Xylaria polymorpha* produces a novel GH 78 glycoside hydrolase that exhibits α-L-rhamnosidase and feruloyl esterase activity and releases hydroxycinnamic acids from lignocelluloses. *Applied and Environmental Microbiology***,** 4893–4901.

NIELSEN, H., ENGELBRECHT, J., BRUNAK, S. & VON HEIJNE, G. 1997. Identification of prokaryotic and eukaryotic signal peptides and prediction of their cleavage sites. *Protein Engineering,* 10**,** 1-6.

NILSSON, T., DANIEL, G., KIRK, T. K. & OBST, J. R. 1989. Chemistry and microscopy of wood decay by some higher ascomycetes. *Holzforschung,* 43**,** 11-18.

NOLL, L., LEONHARDT, S., ARNSTADT, T., HOPPE, B., POLL, C., MATZNER, E., HOFRICHTER, M. & KELLNER, H. 2016. Fungal biomass and extracellular enzyme activities in coarse woody debris of 13 tree species in the early phase of decomposition *Forest Ecology and Management,* 378**,** 181-192.

NSOLOMO, V. R. & VENN, K. 2000. Capacity of fungi to colonise wood of the East African camphor tree, *Ocotea usambarensis*. *Mycological Research,* 104**,** 1468-1472.

NSOLOMO, V. R., VENN, K. & SOLHEIM, H. 2000. The ability of some fungi to cause decay in the East African camphor tree, *Ocotea usambarensis*. *Mycological Research,* 104**,** 1473-1479.

OKANE, I., TOYAMA, K., NAKAGIRI, A., SUZUKI, K.-I., SRIKITIKULCHAI, P., SIVICHAI, S., HYWEL-JONES, N., POTACHAROEN, W. & LÆSSØE, T. 2008. Study of endophytic Xylariaceae in Thailand: diversity and taxonomy inferred from rDNA sequence analyses with saprobes forming fruit bodies in the field. *Mycoscience,* 49**,** 359-372.

OMURA, T. 2005. Heme–thiolate proteins. *Biochemical and Biophysical Research Communications,* 338**,** 404-409.

OSANO, A., SIBOE, G., OCHANDA, I. & KOKWARO, J. 2004. Biodegradation properties of white rot fungi in Karura Forest, Kenya. *Discovery and Innovation,* 16**,** 76-84.

OSONO, T. 2007. Ecology of ligninolytic fungi associated with leaf litter decomposition. *Ecological Research,* 22(6)**,** 955-974.

PADAMSEE, M., MATHENY, P. B., DENTINGER, B. T. & MCLAUGHLIN, D. J. 2008. The mushroom family Psathyrellaceae: evidence for large-scale polyphyly of the genus Psathyrella. *Molecular Phylogenetics and Evolution,* 46**,** 415-429.

PARON, P., OLAGO, D. O. & OMUTO, C. T. 2013. *Kenya: A Natural Outlook: Geo-Environmental Resources and Hazards*, Newnes.

PAUL, A. & AKERS, B. 2000. Use of *Psathyrella* cf. *hymenocephala* (Coprinaceae) as a spice in Haiti. *Mycologist,* 14**,** 161-164.

PEARSON, A. 1950. Cape agarics and boleti. *Transactions of the British Mycological Society,* 33**,** 276-IN8.

PEASE, E. A. & TIEN, M. I. N. G. 1992. Heterogeneity and regulation of manganese peroxidases from *Phanerochaete chrysosporium*. *Journal of Bacteriology,* 174(11)**,** 3532-3540.

PECYNA, M. 2015. *Molekularbiologische Charakterisierung von Häm-Thiolat-und DyP-type-Peroxidasen ausgewählter Basidiomyceten.* Doctoral dissertation, TU Dresden-IHI Zittau, Germany.

PECYNA, M., ULLRICH, R., BITTNER, B., CLEMENS, A., SCHEIBNER, K., SCHUBERT, R. & HOFRICHTER, M. 2009. Molecular characterization of aromatic peroxygenase from *Agrocybe aegerita*. *Applied Microbiology and Biotechnology* 84**,** 885–897.

PEGLER, D. 1966. Tropical African Agaricales. *Persoonia-Molecular Phylogeny and Evolution of Fungi,* 4**,** 73-124.

PEGLER, D. N. 1977. *A preliminary agaric flora of East Africa*, Her Majesty's Stationery Office.

PELTORINNE, P. 2004. The forest types of Kenya In: Pellikka, P., J. Ylhäisi & B. Clark (eds.) Taita Hills and Kenya, 2004–seminar, reports and journal of a field excursion to Kenya. Expedition reports of the Department of Geography, University of Helsinki 40, 8-13. Helsinki 2004, ISBN 952-10-2077-6, 148 pp.

PÉREZ, J., MUNOZ-DORADO, J., DE LA RUBIA, T. & MARTINEZ, J. 2002. Biodegradation and biological treatments of cellulose, hemicellulose and lignin: an overview. *International Microbiology,* 5**,** 53-63.

PETER, S. 2013. *Oxyfunctionalization of alkanes, alkenes and alkynes by unspecific peroxygenase (EC 1.11. 2.1).* Doctoral dissertation, IHI-Zittau, Germany.

PETERS, D. 2007. Raw materials. *Advances in Biochemical Engineering /Biotechnology,* 105**,** 1-30.

PETRINI, O. 1995. Xylariaceous endophytes: an exercise in biodiversity. *Fitopatologia Brasileira,* 20**,** 531-539.

PIONTEK, K., GLUMOFF, T. & WINTERHALTER, K. 1993. Low pH crystal structure of glycosylated lignin peroxidase from *Phanerochaete chrysosporium* at 2.5 A resolution. *FEBS Letters,* 315**,** 119–124.

PIONTEK, K., STRITTMATTER, E., ULLRICH, R., GRÖBE, G., PECYNA, M. J., KLUGE, M., SCHEIBNER, K., HOFRICHTER, M. & PLATTNER, D. A. 2013. Structural basis of substrate conversion in a new aromatic peroxygenase: P450 functionality with benefits. *Journal of Biological Chemistry***,** 34767–34776.

POINTING, S., PARUNGAO, M. & HYDE, K. 2003. Production of wood-decay enzymes, mass loss and lignin solubilization in wood by tropical Xylariaceae. *Mycological Research* 107**,** 231-235.

POINTING, S. B. 1999. Qualitative methods for the determination of lignocellulolytic enzyme production by tropical fungi. *Fungal Diversity***,** 17-33.

POLIZELI, M., RIZZATTI, A., MONTI, R., TERENZI, H., JORGE, J. & AMORIM, D. 2005. Xylanases from fungi: properties and industrial applications. *Applied Microbiology and Biotechnology,* 67**,** 577–591.

PORAJ-KOBIELSKA, M. 2013. *Conversion of pharmaceuticals and other drugs by fungal peroxygenases.* Doctoral dissertation, TU Dresden-IHI Zittau, Germany.

PORAJ-KOBIELSKA, M., KINNE, M., ULLRICH, R., SCHEIBNER, K. & HOFRICHTER, M. 2012. A spectrophotometric assay for the detection of fungal peroxygenases. *Analytical Biochemistry,* 421**,** 327-329.

PORAJ-KOBIELSKA, M., KINNE, M., ULLRICH, R., SCHEIBNER, K., KAYSER, G., HAMMEL, K. E. & HOFRICHTER, M. 2011. Preparation of human drug metabolites using fungal peroxygenases. *Biochemical Pharmacology,* 82**,** 789-796.

POULOS, T. 1993. Peroxidases. *Current Opinion in Biotechnology,* 4**,** 484–489.

RABOUILLE, C. 2017. Pathways of unconventional protein secretion. *Trends in Cell Biology,* 27(3)**,** 230-240.

RAHMANPOUR, R. & BUGG, T. D. 2015. Characterisation of Dyp-type peroxidases from *Pseudomonas fluorescens* Pf-5: oxidation of Mn(II) and polymeric lignin by Dyp1B. *Archives of Biochemistry and Biophysics,* 574**,** 93-98.

RAHMANPOUR, R., REA, D., JAMSHIDI, S., FÜLÖP, V. & BUGG, T. D. 2016. Structure of *Thermobifida fusca* DyP-type peroxidase and activity towards Kraft lignin and lignin model compounds. *Archives of Biochemistry and Biophysics,* 594**,** 54-60.

REINA, R., KELLNER, H., HESS, J., JEHMLICH, N., GARCÍA-ROMERA, I., ARANDA, E., HOFRICHTER, M. & LIERS, C. 2019. Genome and secretome of *Chondrostereum purpureum* correspond to saprotrophic and phytopathogenic life styles. *PloS One,* 14(3)**,** e0212769.

REINA, R. P. 2016. *Effects of agroindustrial by-products on wood-dwelling agaricomycetes: lignocellulolytic enzyme enhancement and residue transformation.* Doctoral dissertation, Universidad de Granada, Spain.

RILEY, R., SALAMOV, A. A., BROWN, D. W., NAGY, L. G., FLOUDAS, D., HELD, B. W., LEVASSEUR, A., LOMBARD, V., MORIN, E. & OTILLAR, R. 2014. Extensive

sampling of basidiomycete genomes demonstrates inadequacy of the white-rot/brown-rot paradigm for wood decay fungi. *Proceedings of the National Academy of Sciences,* 111**,** 9923-9928.

RITTENOUR, W. R., CIACCIO C. E, BARNES, C. S., KASHON, M. L., LEMONS, A. R., BEEZHOLD, D. H. & BRETT J. GREEN, B. J. 2014. Internal transcribed spacer rRNA gene sequencing analysis of fungal diversity in Kansas City indoor environments. *Environmental Science Process and Impacts* 16(1)**,** 33–43.

ROBERTS, J. N., SINGH, R., GRIGG, J. C., MURPHY, M. E., BUGG, T. D. & ELTIS, L. D. 2011. Characterization of dye-decolorizing peroxidases from *Rhodococcus jostii* RHA1. *Biochemistry,* 50(23)**,** 5108-5119.

ROGERS, J. D., JU, Y. M. & LEHMANN, J. 2005. Some *Xylaria* species on termite nests. *Mycologia,* 97(4)**,** 914-923.

ROJAS-JIMÉNEZ, K. & HERNÁNDEZ, M. 2015. Isolation of fungi and bacteria associated with the guts of tropical wood-feeding Coleoptera and determination of their lignocellulolytic activities. *International Journal of Microbiology***,** 285018.

ROWELL, R. M. 1992. *Opportunities for lignocellulosic materials and composites*, American Chemical Society.

RUBIN, E. M. 2008. Genomics of cellulosic biofuels. *Nature,* 454**,** 841.

RUIZ-DUENAS, F. J., MORALES, M., MATE, M. J., ROMERO, A., MARTÍNEZ, M. J., SMITH, A. T. & MARTÍNEZ, Á. T. 2008. Site-directed mutagenesis of the catalytic tryptophan environment in *Pleurotus eryngii* versatile peroxidase. *Biochemistry,* 47(6)**,** 1685-1695.

RUIZ-DUEÑAS, F. J. & MARTÍNEZ, Á. T. 2009. Microbial degradation of lignin: how a bulky recalcitrant polymer is efficiently recycled in nature and how we can take advantage of this. *Microbial Biotechnology,* 2**,** 164-177.

RUIZ-DUEÑAS, F. J., MARTÍNEZ, M. J. & MARTÍNEZ, A. T. 1999. Molecular characterization of a novel peroxidase isolated from the ligninolytic fungus *Pleurotus eryngii*. *Molecular Microbiology,* 31(1)**,** 223-235.

RYTIOJA, J., HILDÉN, K., YUZON, J., HATAKKA, A., DE VRIES, R. P. & MÄKELÄ, M. R. 2014. Plant-polysaccharide-degrading enzymes from basidiomycetes. *Microbiology and Molecular Biology Reviews,* 78**,** 614-649.

RYVARDEN, L. 1991. Genera of polypores: Nomenclature and taxonomy. *Synopsis Fungorum,* 5**,** 1– 3.

SAE, A. S. & CUNNINGHAM, B. A. 1979. Isolation and properties of chloroperoxidase isozymes. *Phytochemistry,* 18(11)**,** 1785-1787.

SALVACHÚA, D., MARTÍNEZ, A. T., TIEN, M., LÓPEZ-LUCENDO, M. F., GARCÍA, F., DE LOS RÍOS, V., MARTÍNEZ, M. J. & PRIETO, A. 2013. Differential proteomic analysis of the secretome of *Irpex lacteus* and other white-rot fungi during wheat straw pretreatment. *Biotechnology for Biofuels,* 6(1)**,** 115.

SAMMUT, C. & MELZER, A. 2012. Psathyrellaceae from Malta, a preliminary survey. *Micologia e Vegetazione Mediterranea,* 27**,** 33-44.

SÁNCHEZ, C. 2009. Lignocellulosic residues: biodegradation and bioconversion by fungi. *Biotechnology Advances,* 27**,** 185-194.

SARKAR, S., MARTÍNEZ, A. T. & MARTÍNEZ, M. J. 1997. Biochemical and molecular characterization of a manganese peroxidase isoenzyme from *Pleurotus ostreatus*. *Biochimica et Biophysica Acta (BBA)-Protein Structure and Molecular Enzymology,* 1339(1)**,** 23-30.

SARROCCO, S. 2016. Dung-inhabiting fungi: a potential reservoir of novel secondary metabolites for the control of plant pathogens. *Pest Management Science,* 72**,** 643-652.

SAß, A. 2010. *Search for oxidoreductases in Coprinopsis cinerea strains: purification of wild-type enzymes and characterization of a recombinant aromatic peroxygenase (in German).* Bachelor Thesis, University of Applied Sciences Zittau/Görlitz, Zittau, Germany.

SCHEIBNER, M., HÜLSDAU, B., ZELENA, K., NIMTZ, M., DE BOER, L., BERGER, R. G. & ZORN, H. 2008. Novel peroxidases of *Marasmius scorodonius* degrade β-carotene. *Applied Microbiology and Biotechnology,* 77**,** 1241-1250.

SCHMITT, K. 1991. The vegetation of the Aberdare National Park, Kenya. *High Mountain Research,* 8.

SCHWARZE, F. 2007. Wood decay under the microscope. *Fungal Biology Reviews 1***,** 133–170.

SENA, H. H., SANCHES, M. A., ROCHA, D. F. S., SEGUNDO FILHO, W. O. P., DE SOUZA, É. S. & DE SOUZA, J. V. B. 2018. Production of biosurfactants by soil fungi isolated from the Amazon forest. *International Journal of Microbiology***,** 8.

SHARMA, S., ZACCARON, A. Z., RIDENOUR, J. B., ALLEN, T. W., CONNER, K., DOYLE, V. P., PRICE, T., SIKORA, E., SINGH, R. & SPURLOCK, T. 2018. Draft genome sequence of *Xylaria* sp., the causal agent of taproot decline of soybean in the southern United States. *Data in Brief,* 17**,** 129-133.

SHARY, S., RALPH, S. & HAMMEL, K. 2007. New insights into the ligninolytic capability of a wood decay ascomycete. *Applied and Environmental Microbiology,* 73**,** 6691– 6694.

SHAW, P. D. & HAGER, L. P. 1959. Biological chlorination III. β-Ketoadipate chlorinase: a soluble enzyme system. *Journal of Biological Chemistry,* 234**,** 2565-2569.

SHAWN, D. M. 2009. Solutions for dissolution—engineering cell walls for deconstruction. *Current Opinion in Biotechnology,* 20(3)**,** 286-294.

SHIMOKAWA, T., HIRAI, M., SHODA, M. & SUGANO, Y. 2008. Efficient dye decolorization and production of dye decolorizing enzymes by the basidiomycete *Thanatephorus cucumeris* Dec1 in a liquid and solid hybrid culture. *Journal of Bioscience and Bioengineering,* 106**,** 481-487.

SIMÃO, F. A., WATERHOUSE, R. M., IOANNIDIS, P., KRIVENTSEVA, E. V. & ZDOBNOV, E. M. 2015. BUSCO: assessing genome assembly and annotation completeness with single-copy orthologs. *Bioinformatics,* 31**,** 3210-3212.

SINGER, R. 1978. Interesting and new species of Basidiomycetes from Ecuador II. *Nova Hedwigia,* 29**,** 1-98.

SIPOS, G., PRASANNA, A. N., WALTER, M. C., O'CONNOR, E., BÁLINT, B., KRIZSÁN, K., KISS, B., HESS, J., VARGA, T., SLOT, J & RILEY, R. 2017. Genome expansion and lineage-specific genetic innovations in the forest pathogenic fungi *Armillaria. Nature Ecology & Evolution,* 1(12)**,** 1931.

SKREDE, I., ENGH, I. B., BINDER, M., CARLSEN, T., KAUSERUD, H. & BENDIKSBY, M. 2011. Evolutionary history of Serpulaceae (Basidiomycota): molecular phylogeny, historical biogeography and evidence for a single transition of nutritional mode. *BMC Evolutionary Biology,* 11(1)**,** 230.

SMITH, A. H. 1972. North American species of *Psathyrella*. *Mem. New York Bot. Gar d***,** 24.

SONG, F., WU, S. H., ZHAI, Y. Z., XUAN, Q. C. & WANG, T. 2014. Secondary metabolites from the genus *Xylaria* and their bioactivities. *Chemistry & Biodiversity,* 11**,** 673-694.

STAJICH, J. E., WILKE, S. K., AHRÉN, D., AU, C. H., BIRREN, B. W., BORODOVSKY, M., BURNS, C., CANBÄCK, B., CASSELTON, L. A., CHENG, C., J, G. & PUKKILA, P. J. 2010. Insights into evolution of multicellular fungi from the assembled chromosomes of the mushroom *Coprinopsis cinerea* (*Coprinus cinereus*). *Proceedings of the National Academy of Sciences,* 107**,** 11889-11894.

STANKE, M., STEINKAMP, R., WAACK, S. & MORGENSTERN, B. 2004. AUGUSTUS: a web server for gene finding in eukaryotes. *Nucleic Acids Research,* 32**,** W309-W312.

STEFFEN, K., HOFRICHTER, M. & HATAKKA, A. 2000. Mineralisation of ^{14}C-labelled synthetic lignin and ligninolytic enzyme activities of litter-decomposing basidiomycetous fungi. *Applied Microbiology and Biotechnology,* 54**,** 819-825.

STEFFEN, K. T. 2003. *Degradation of recalcitrant biopolymers and polycyclic aromatic hydrocarbons by litter-decomposing basidiomycetous fungi.* Doctoral dissertation, University of Helsinki, Finland.

STEFFEN, K. T., HATAKKA, A. & HOFRICHTER, M. 2002. Degradation of humic acids by the litter-decomposing basidiomycete *Collybia dryophila*. *Applied and Environmental Microbiology,* 68**,** 3442-3448.

STRITTMATTER, E., LIERS, C., ULLRICH, R., WACHTER, S., HOFRICHTER, M., PLATTNER, D. A. & PIONTEK, K. 2013a. First crystal structure of a fungal high-redox potential dye-decolorizing peroxidase substrate interaction sites and long-range electron transfer. *Journal of Biological Chemistry,* 288(6)**,** 4095-4102.

STRITTMATTER, E., WACHTER, S., LIERS, C., ULLRICH, R., HOFRICHTER, M., PLATTNER, D. A. & PIONTEK, K. 2013b. Radical formation on a conserved tyrosine residue is crucial for DyP activity. *Archives of Biochemistry and Biophysics,* 537(2)**,** 161-167.

SUDARSON, J., RAMALINGAM, S., KISHOREKUMAR, P. & VENKATESAN, K. 2014. Expeditious quantification of lignocellulolytic enzymes from indigenous wood rot and litter degrading fungi from tropical dry evergreen forests of Tamil Nadu. *Biotechnology Research International***,** 6.

SUGANO, Y., MATSUSHIMA, Y., TSUCHIYA, K., AOKI, H., HIRAI, M. & SHODA, M. 2009. Degradation pathway of an anthraquinone dye catalyzed by a unique peroxidase DyP from *Thanatephorus cucumeris* Dec 1. *Biodegradation,* 20**,** 433–440.

SUGANO, Y., MURAMATSU, R., ICHIYANAGI, A., SATO, T. & SHODA, M. 2007. DyP, a unique dye-decolorizing peroxidase, represents a novel heme peroxidase family: ASP171 replaces the distal histidine of classical peroxidases. *Journal of Biological Chemistry,* 282**,** 36652–36658.

SUGANO, Y., SASAKI, K. & SHODA, M. 1999. cDNA cloning and genetic analysis of a novel decolorizing enzyme, peroxidase gene dyp from *Geotrichum candidum* Dec 1. *Journal of Bioscience Bioengineering,* 87**,** 411–417.

SUGAWARA, K., IGETA, E., AMANO, Y., HYUGA, M. & SUGANO, Y. 2019. Degradation of antifungal anthraquinone compounds is a probable physiological role of DyP secreted by *Bjerkandera adusta*. *AMB Express,* 9(1)**,** 56.

SUMATHI, T., VISWANATH, B., SRI LAKSHMI, A. & SAIGOPAL, D. V. R. 2016. Production of laccase by *Cochliobolus* sp. isolated from plastic dumped soils and their ability to degrade low molecular weight PVC. *Biochemistry Research International*, 10.

SUNDARAMOORTHY, M., KISHI, K., GOLD, M. & POULOS, T. 1994. The crystal structure of manganese peroxidase from *Phanerochaete chrysosporium* at 2.06-A resolution. *Journal of Biological Chemistry,* 269**,** 32759–32767.

SUNDARAMOORTHY, M., KISHI, K., GOLD, M. H. & POULOS, T. L. 1997. Crystal structures of substrate binding site mutants of manganese peroxidase. *Journal of Biological Chemistry,* 272(28)**,** 17574-17580.

TANAKA, Y., KASUGA, D., OBA, Y., HASE, S., SATO, K., OBA, Y. & SAKAKIBARA, Y. Genome sequence of the luminous mushroom *Mycena chlorophos* for searching fungal bioluminescence genes. In: 18th International Symposium on Bioluminescence and Chemiluminescence, 2014 Uppsala, Sweden. 47-48.

THORN, R. G., REDDY, C. A., HARRIS, D. & PAUL, E. A. 1996. Isolation of saprophytic basidiomycetes from soil. *Applied Environmental Microbiology,* 62**,** 4288-4292.

TORRES, E. & AYALA, M. 2010. Biocatalysis based on heme peroxidases. *In: Peroxidases as Potential Industrial Biocatalysts.* Springer Science & Business Media.

TSINGALIA, M. H. 1990. Habitat disturbance, severity and patterns of abundance in Kakamega Forest, Western Kenya. *African Journal of Ecology,* 28**,** 213-226.

UEDA, H., MATSUMOTO, H., TAKAHASHI, N. & OGAWA, H. 2002. *Psathyrella velutina* mushroom lectin exhibits High Affinity toward Sialoglycoproteins Possessing TerminalN-Acetylneuraminic Acid α2, 3-Linked to Penultimate Galactose Residues of Trisialyl N-Glycans COMPARISON WITH OTHER SIALIC ACID-SPECIFIC LECTINS. *Journal of Biological Chemistry,* 277**,** 24916-24925.

UJANG, S., ANDREW, H. H. & WONG E.B.G, J. 2007. Wood degrading fungi. *In:* E.B.G. JONES, K. D. H., S. VIKNESWARY (ed.) *Malaysian Fungal Diversity* 1ed.: Mushroom Research Centre, University of Malaya & Ministry of Natural Resources and Environment.

ULLRICH, R., DOLGE, C., KLUGE, M. & HOFRICHTER, M. 2008. Pyridine as novel substrate for regioselective oxygenation with aromatic peroxygenase from *Agrocybe aegerita*. *FEBS Letters,* 582**,** 4100–4106.

ULLRICH, R. & HOFRICHTER, M. 2005. The haloperoxidase of the agaric fungus *Agrocybe aegerita* hydroxylates toluene and naphthalene. *FEBS Letters,* 579**,** 6247-6250.

ULLRICH, R., LIERS, C., SCHIMPKE, S. & HOFRICHTER, M. 2009. Purification of homogeneous forms of fungal peroxygenase. *Biotechnology Journal: Healthcare Nutrition Technology,* 4(11)**,** 1619-1626.

ULLRICH, R., NÜSKE, J., SCHEIBNER, K., SPANTZEL, J. & HOFRICHTER, M. 2004. Novel haloperoxidase from the agaric basidiomycete *Agrocybe aegerita* oxidizes aryl alcohols and aldehydes. *Applied and Environmental Microbiology,* 70**,** 4575-4581.

ULLRICH, R., PORAJ-KOBIELSKA, M., SCHOLZE, S., HALBOUT, C., SANDVOSS, M., PECYNA, M. J., SCHEIBNER, K. & HOFRICHTER, M. 2018. Side chain removal from corticosteroids by unspecific peroxygenase. *Journal of Inorganic Biochemistry,* 183**,** 84-93.

UPADHYAY, R. C. 1995. *Metabolism of phenolic substrates by Pleurotus flabellatus (Berk; Br.) Sack and Agrocybe aegerita (Brig.) Singer.* dissertation, Friedrich Schiller University of Jena, Germany.

VAN AKEN, B., GODEFROID, L. M., PERES, C. M., NAVEAU, H. & AGATHOS, S. N. 1999. Mineralization of ^{14}C-U-ring labeled 4-hydroxylamino-2, 6-dinitrotoluene by manganese-dependent peroxidase of the white-rot basidiomycete *Phlebia radiata*. *Journal of Biotechnology,* 68(2-3)**,** 159-169.

VAN BLOOIS, E., TORRES PAZMIÑO, D., WINTER, R. & FRAAIJE, M. 2009. A robust and extracellular heme-containing peroxidase from *Thermobifida fusca* as prototype of a bacterial peroxidase superfamily. *Applied Microbiology Biotechnology*.

VAN DEN BRINK, J. & DE VRIES, R. P. 2011. Fungal enzyme sets for plant polysaccharide degradation. *Applied Microbiology and Biotechnology,* 91(6)**,** 1477.

VÁŠUTOVÁ, M. 2006. Preliminary checklist of the genus *Psathyrella* in the Czech Republic and Slovakia. *Publication of the Czech Scientific Society for Mycology,* 58**,** 1-29.

VISSER, A. A., ROS, V. I. D., DE BEER, Z. W., DEBETS, A. J. M., HARTOG, E., KUYPER, T. W., LAESSØE, T., SLIPPERS, B. & AANEN, D. K. 2009. Levels of specificity of *Xylaria* species associated with fungus-growing termites: a phylogenetic approach. *Molecular Ecology,* 18(3)**,** 553-567.

VOŘÍŠKOVÁ, J. & BALDRIAN, P. 2013. Fungal community on decomposing leaf litter undergoes rapid successional changes. *The ISME Journal,* 7**,** 477.

VOTO, P. 2011. *Psathyrella carinthiaca* sp. nov. e nuove segnalazioni di P. bivelata. *Rivista di Micologia,* 54**,** 121-133.

WANG, X., PETER, S., ULLRICH, R., HOFRICHTER, M. & GROVES, J. 2013. Driving force for oxygen-atom transfer by heme-thiolate enzymes. *Angewandte Chemie International Edition,* 52**,** 9238–9241.

WANG, Y., VAZQUEZ-DUHALT, R. & PICKARD, M. A. 2002. Purification, characterization, and chemical modification of manganese peroxidase from *Bjerkandera adusta* UAMH 8258. *Current Microbiology,* 45(2)**,** 77-87.

WARIISHI, H., VALLI, K. & GOLD, M. H. 1992. Manganese (II) oxidation by manganese peroxidase from the basidiomycete *Phanerochaete chrysosporium*. Kinetic mechanism and role of chelators. *Journal of Biological Chemistry,* 267**,** 23688-23695.

WEGENER, S., RICHARD F. RANSOM & WALTON., J. D. 1999. A unique eukaryotic β-xylosidase gene from the phytopathogenic fungus *Cochliobolus carbonum*. *Microbiology***,** 1089-1095.

WEI, D., HOUTMAN, C. J., KAPICH, A. N., HUNT, C. G., CULLEN, D. & HAMMEL, K. E. 2010. Laccase and its role in production of extracellular reactive oxygen species during wood decay by the brown rot basidiomycete *Postia placenta*. *Applied and Environmental Microbiology,* 76**,** 2091-2097.

WELINDER, K., MAURO, J. & NORSKOVLAURITSEN, L. 1992. Structure of plant and fungal peroxidases. *Biochem Soc Trans,* 20(2)**,** 337–340.

WHALLEY, A. 1996. The xylariaceous way of life. *Mycological Research,* 100**,** 897-922.

WHITE, T. J., BRUNS, T., LEE, S. & TAYLOR, J. 1990. Amplification and direct sequencing of fungal ribosomal RNA genes for phylogenetics. *PCR protocols: a guide to methods and applications,* 18**,** 315-322.

WHITTAKER, M. M., KERSTEN, P. J., NAKAMURA, N., SANDERS-LOEHR, J., SCHWEIZER, E. S. & WHITTAKER, J. W. 1996. Glyoxal oxidase from *Phanerochaete chrysosporium* is a new radical-copper oxidase. *Journal of Biological Chemistry,* 271(2)**,** 681-687.

WOLFENDEN, B. S. & WILLSON, R. L. 1982. Radical-cations as reference chromogens in kinetic studies of ono-electron transfer reactions: pulse radiolysis studies of 2, 2′-azinobis-(3-ethylbenzthiazoline-6-sulphonate). *Journal of the Chemical Society, Perkin Transactions 2***,** 805-812.

WORRALL, J. J., ANAGNOST, S. E. & ZABEL, R. A. 1997. Comparison of wood decay among diverse lignicolous fungi. *Mycologia,* 89(2)**,** 199-219.

YAN, J.-Q. & BAU, T. 2018. The Northeast Chinese species of *Psathyrella* (Agaricales, Psathyrellaceae). *MycoKeys***,** 85.

YARMAN, A., GRÖBE, G., NEUMANN, B., KINNE, M., GAJOVIC-EICHELMANN, N., WOLLENBERGER, U., HOFRICHTER, M., ULLRICH, R., SCHEIBNER, K. & SCHELLER, F. W. 2012. The aromatic peroxygenase from *Marasmius rutola*—A new enzyme for biosensor applications. *Analytical and Bioanalytical Chemistry,* 402(1)**,** 405-412.

YIN, Y., MAO, X., YANG, J., CHEN, X., MAO, F. & XU, Y. 2012. dbCAN: a web resource for automated carbohydrate-active enzyme annotation. *Nucleic Acids Research,* 40**,** W445-W451.

YOSHIDA, T. & SUGANO, Y. 2015. A structural and functional perspective of DyP-type peroxidase family. *Archives of Biochemistry and Biophysics,* 574**,** 49-55.

YOSHIDA, T., TSUGE, H., HISABORI, T. & SUGANO, Y. 2012. Crystal structures of dye-decolorizing peroxidase with ascorbic acid and 2, 6-dimethoxyphenol. *FEBS Letters,* 586**,** 4351-4356.

YOSHIDA, T., TSUGE, H., KONNO, H., HISABORI, T. & SUGANO, Y. 2011. The catalytic mechanism of dye-decolorizing peroxidase DyP may require the swinging movement of an aspartic acid residue. *The FEBS Journal,* 278(13)**,** 2387-2394.

YU, W., LIU, W., HUANG, H., ZHENG, F., WANG, X., WU, Y. T., LI, K., XIE, X. & JIN, Y. 2014. Application of a novel alkali-tolerant thermostable DyP-type peroxidase from *Saccharomonospora viridis* DSM 43017 in biobleaching of eucalyptus kraft pulp. *PLOS One,* 9(10)**,** e110319.

YUEN, T., HYDE, K. & HODGKISS, I. 1999. Wood-degrading capabilities of tropical freshwater fungi. *Material und Organismen***,** 36-50.

ZÁMOCKÝ, M., FURTMÜLLER, P. G. & OBINGER, C. 2009. Two distinct groups of fungal catalase/peroxidases. *Biochemical Society Transactions,* 37(4)**,** 772-777.

ZÁMOCKÝ, M., HOFBAUER, S., SCHAFFNER, I., GASSELHUBER, B., NICOLUSSI, A., SOUDI, M., PIRKER, K. F., FURTMÜLLER, P. G. & OBINGER, C. 2015. Independent evolution of four heme peroxidase superfamilies. *Archives of Biochemistry and Biophysics,* 574**,** 108-119.

ZÁMOCKÝ, M. & OBINGER, C. 2010. Molecular phylogeny of heme peroxidases. *In: Biocatalysis Based on Heme Peroxidases.* Springer. Berlin, Heidelberg.

ZÁMOCKÝ, M., TAFER, H., CHOVANOVÁ, K., LOPANDIC, K., KAMLÁROVÁ, A. & OBINGER, C. 2016. Genome sequence of the filamentous soil fungus *Chaetomium cochliodes* reveals abundance of genes for heme enzymes from all peroxidase and catalase superfamilies. *BMC Genomics,* 17(1)**,** 763.

ZHANG, Y. 2008. I-TASSER server for protein 3D structure prediction. *BMC Bioinformatics,* 9**,** 40.

7 APPENDIX

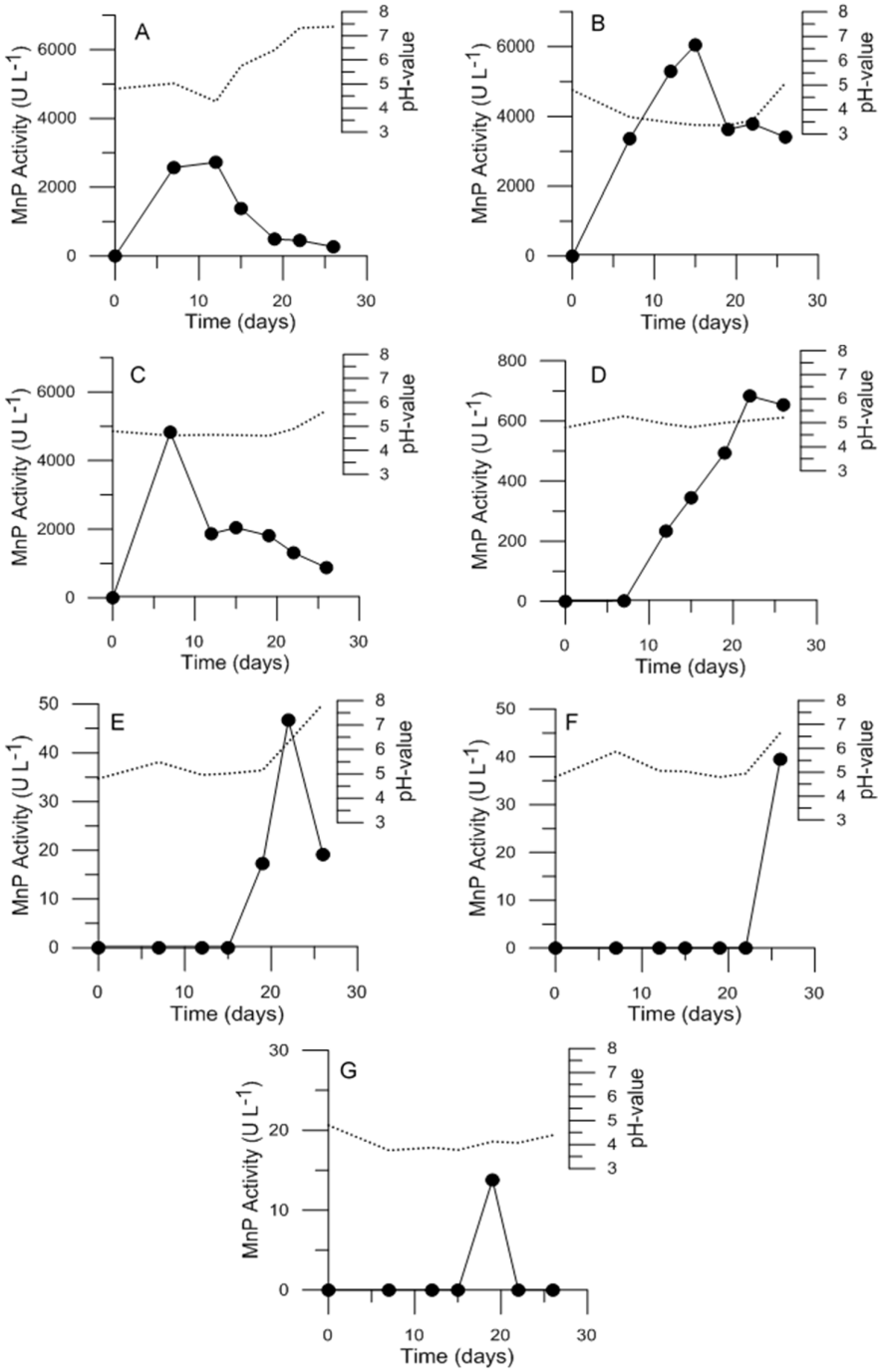

Fig. A.1: Time course of the MnP production (black circles) by *Phlebia subserialis* (A), *Stropharia rugosoannulata* (B), *Polyporales sp.* (C), *Gymnopus brunneigracilis* (D), *Cribbea sp.* (E), *Trametes gibbosa* (F), and *Microporus subaffinis* (G) from SPM media; measured with $MnCl_2$& H_20_2, dotted line-pH value.

Fig. A.2: Protein sequences that were encoded by the two genes (A: *g8238* and B: *g7491*) that encode the three UPOs isolated from *P. aberdarensis*; grey highlighted parts are internal *de-novo* peptide sequences of the purified protein identified by mass spectrometry

Fig. A.3: Protein sequence that were encoded by the gene *g488* that encode the DyP isolated from *X. grammica*; grey highlighted parts are internal *de-novo* peptide sequences of the purified protein identified by mass spectrometry.

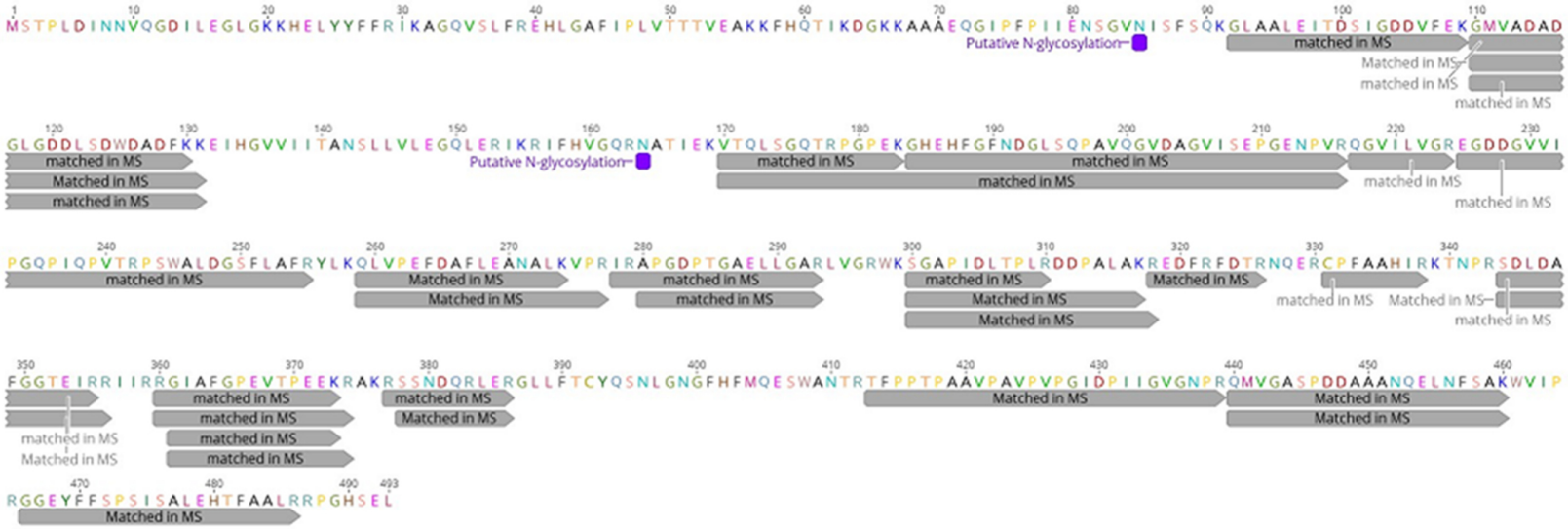

Fig. A.4: Protein sequences that were encoded by the two genes (**A:** *g9177* and **B:** *g1956*) that encode the hypothetical DyP from *X. grammica* genome

A.5 Proteomics (Peptide mapping)

Each sample was prepared for proteolytic cleavage before mass spectrometric analysis. Protein lysate was reduced (2.5 mM DTT for 1 h at 60 °C) and alkylated (10 mM iodoacetamide for 30 min at 37 °C). Proteolysis was performed overnight using trypsin (Promega, Madison, WI, USA) with an enzyme/substrate ratio of 1:25 overnight at 37 °C by trypsin (Promega). Extracted peptide lysate was desalted using a C_{18} ZipTip column (Merck Millipore).

Peptide lysates were dissolved in 0.1 % formic acid and injected into liquid chromatography mass spectrometry (LC-MS/MS) apparatus. Mass spectrometry was performed on a Q Exactive HF MS (Thermo Fisher Scientific, Waltham, MA, USA) with a TriVersa NanoMate (Advion, Ltd., Harlow, UK) source in LC chip coupling mode. First, the peptide lysates were separated on a UHPLC system (Ultimate 3000, Dionex/Thermo Fisher Scientific, Idstein, Germany). In total, 5 µL samples were first loaded for 5 min on the precolumn (µ-precolumn, Acclaim PepMap, 75 µm inner diameter, 2 cm, C18, Thermo Scientific) at 4 % mobile phase B (80 % acetonitrile in nanopure water with 0.08 % formic acid), 96 % mobile phase A (nanopure water with 0.1 % formic acid), then eluted from the analytical column (PepMap Acclaim C18 LC Column, 25 cm, 3 µm particle size, Thermo Scientific) over a 90 min non-linear gradient of mobile phase B (4-55 % B).

The mass spectrometer was set on loop count of 20 used for MS/MS scans with higher energy collision dissociation (HCD) at normalized collision energy of 30 %. MS scans were measured at a resolution of 120,000 in the scan range of 350-1,550 *m/z*. MS ion count target was set to 3×10^6 at an injection time of 80 ms. Ions for MS/MS scans were isolated in the quadrupole with an isolation window of 1.6 Da and were measured with a resolution of 15,000 in the scan range of 200-2,000 *m/z*. The dynamic exclusion duration was set to 30 s with a 10 ppm tolerance. Automatic gain control target was set to 2×10^5 with an injection time of 120 ms using the underfill ratio of 1 %.

The software Proteome Discoverer (v1.4, Thermo Scientific) was used for protein identification. Therefore, the measured MS/MS spectra (*.raw files) were searched with the Sequest HT algorithm first against the Uniprot (bacteria and archaea database). The following settings were selected for both searches: enzyme specificity was trypsin with up to two missed cleavages allowed using 10 ppm peptide ion tolerance and 0.02 Da MS/MS tolerances. Oxidation (methionine) and acetylation (any N-terminus) were

selected as a dynamic modification and carbamidomethylation (cysteine) as a static modification. Only peptides with a false discovery rate (FDR) <0.01 calculated by Percolator, (Käll et al. 2007) peptide rank =1 and XCorr >2 were considered as identified.

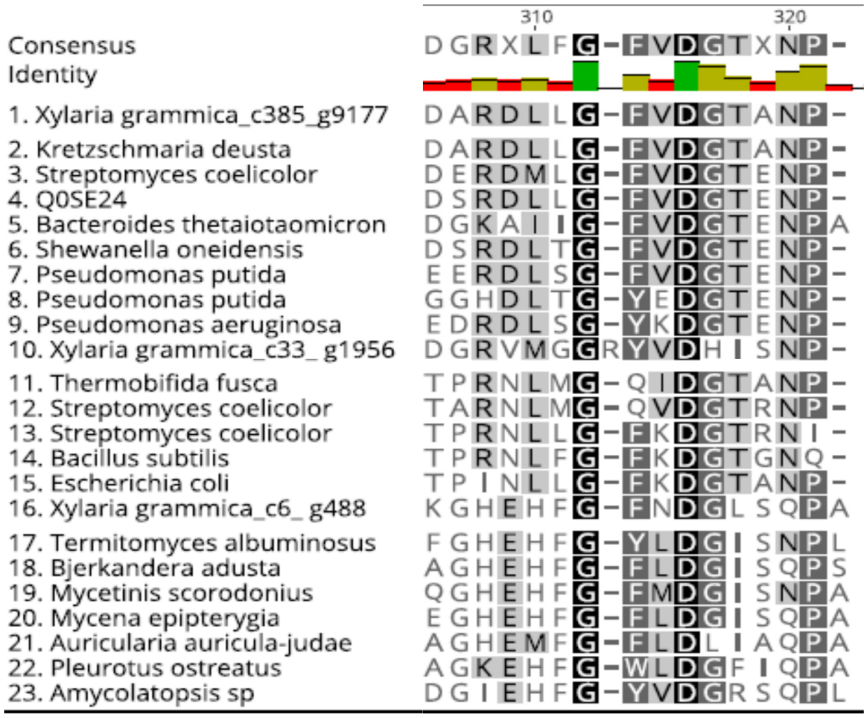

Fig. A.6: Conserved residues of the heme binding site of three *X. grammica* DyPs in comparison to other bacterial and fungal DyP-type peroxidases.

Fig. A.7: Complete alignment of characterized fungal DyPs with sequences obtained from the genome of *X. grammica* (*g9177*, *g1956* and *g488*); conserved proximal and distal residues (red) responsible for Fe-binding (blue) as well as H_2O_2-binding (F & L) or acting as acid base catalysts (D & R).

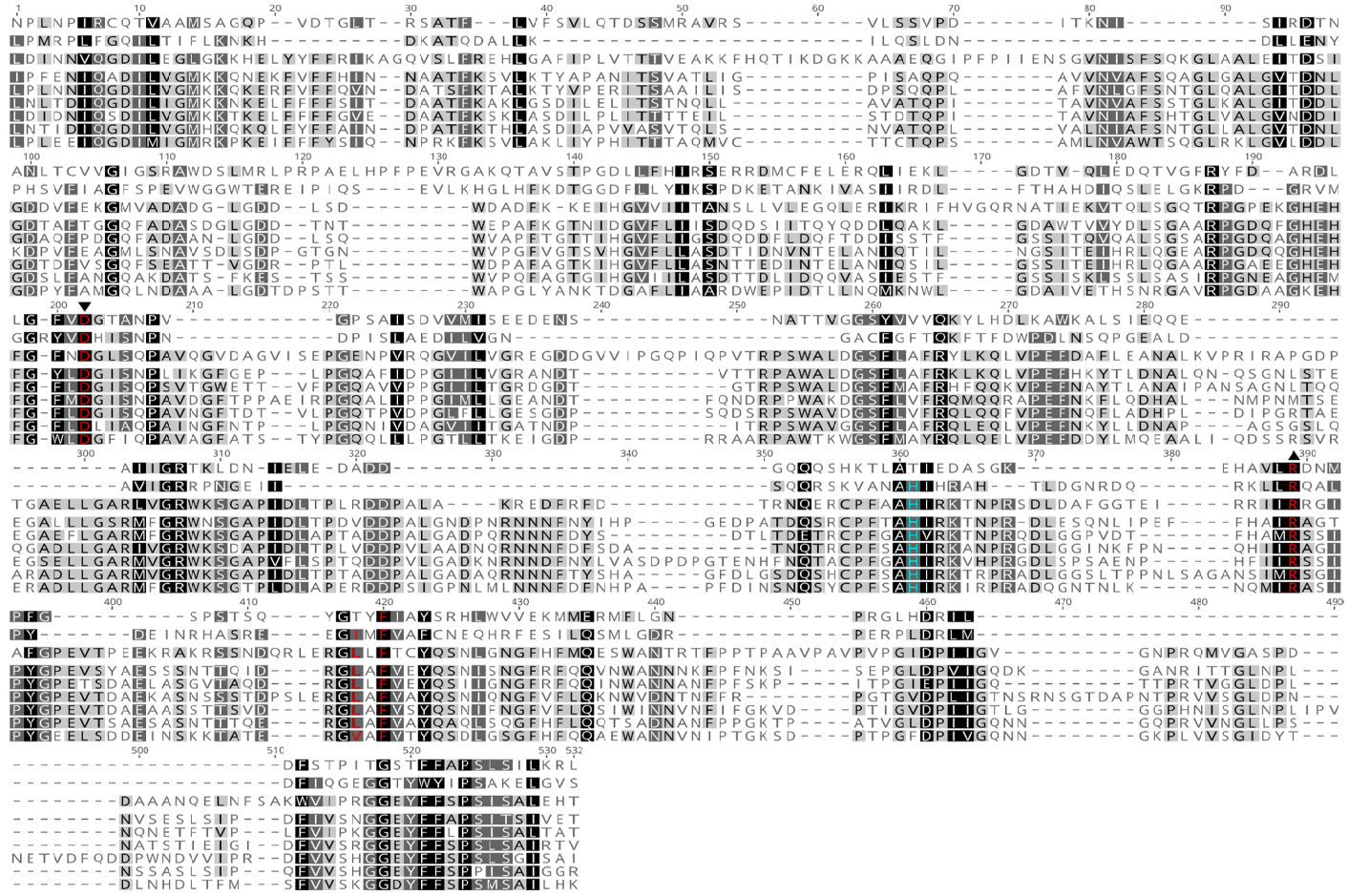

Psathyrella aberdarensis, a new species of *Psathyrella* (*Agaricales*) from a Kenyan National Park

ANDREAS MELZER
Kyhnaer Hauptstraße 5
04509 Wiedemar, Germany
E-mail: pilzmel@vielepilze.de

VIRGINIA WAMBUI KIMANI
RENÉ ULLRICH
TU Dresden - Internationales Hochschulinstitut Zittau
Markt 23
02763 Zittau, Germany
E-mails: virginia.kimani@tu-dresden.de, rene.ullrich@tu-dresden.de

Accepted 18. September 2018. © Austrian Mycological Society, published online 15. January 2019

MELZER, A., KIMANI, V. W., ULLRICH, R., 2018: A new species of *Psathyrella* (*Agaricales*) from a Kenyan National Park. – Austrian J. of Mycology 27: 23–30.

Key words: *Agaricales*, spec. nova, taxonomy, Funga of Kenya, 1 new species.

Abstract: *Psathyrella aberdarensis*, collected in the Aberdare National Park, Kenya, is described as a new species. Colour plates and drawings of the microscopic characteristics are presented. Closely related and similar species are compared with the new species and the classification within the genus *Psathyrella* is discussed. *Psathyrella aberdarensis* belongs to the *P. candolleana* alliance and is characterized by small basidiomata, a persistent veil made up of polymorphic elements and very pale spores without a recognizable germ pore.

Zusammenfassung: *Psathyrella aberdarensis*, gesammelt im Aberdare National Park, Kenia, wird als neue Art beschrieben. Farbfotos und Zeichnungen der mikroskopischen Merkmale werden vorgestellt. Eng verwandte und ähnliche Arten werden verglichen und die Klassifizierung innerhalb der Gattung *Psathyrella* wird diskutiert. *Psathyrella aberdarensis* gehört zur *P. candolleana*-Verwandtschaft und ist durch kleine Basidiomata, ein beständiges Velum aus polymorphen Elementen und sehr blasse Sporen ohne Keimporus gekennzeichnet.

The Aberdare National Park is located in Nyeri County in central Kenya and covers an area of 766 km^2. The park is part of the Aberdares Ranges, comprises the upper forest zone and includes Mount Satima, the third-highest mountain in Kenya. The climate in the ranges is characterized by alternating wet and dry seasons that are linked to the shifting intertropical convergence zone. Due to altitude differences between 1800 and 3600 m s. m., the forest harbors a high diversity of forest types within different vegetation zones. The most common tree species are *Ocotea usambarensis* ENGL., *Juniperus procera* HOCHST. ex ENDL., *Podocarpus latifolius* (THUNB.) R. BR. ex MIRB. and *Hagenia abyssinica* (BRUCE) J. F. GMEL. To our best knowledge, almost nothing is known about the local Funga.

In 2016, one of the authors (V. W. K.) collected a *Psathyrella* specimen that was growing on small twigs (of undetermined wood). Since an unambiguous identification

was impossible morphologically, we decided to carry out molecular genetic analyses alongside.

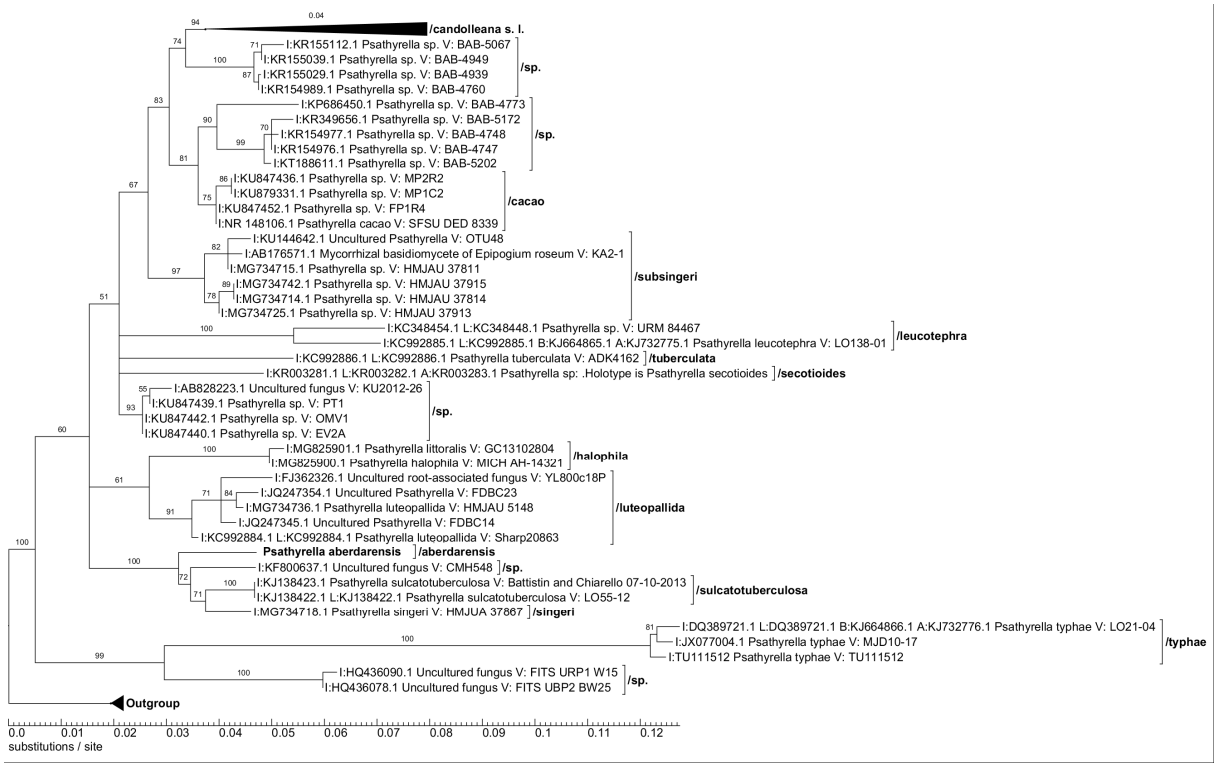

Fig. 1. Maximum Likelihood consensus tree, collapses to 50 %. Bootstrap probabilities in % noted above branches. In front of the species-name, the Genbank numbers are given, finally the name of the voucher. Abbreviations: I: ITS-region, L: LSU-region, B: β-tubulin-region, A: ef-1α-region.

Material and methods

Morphology:

Macromorphological characteristics were recorded based on fresh specimens; photographs of the basidiomata were taken *in situ*. Micromorphological analyses were performed by light microscopy using hand sections of fresh material as well as of revived exsiccata. The size of mature spores was measured in water after their collection from the stipe apex. Spore colour was assessed in plain water, ammonia solution (10 %), and in potassium hydroxide solution (5 % w/v KOH). Cystidia and other microscopic structures were studied in ammonia solution after staining with Congo red. The colour code is based on KÜPPERS (2007).

Molecular analyses:

DNA extraction was performed according to standard methods. The ITS region (ITS1, 5.8S rRNA gene, ITS2) as well as parts of the 28S rRNA gene region were amplified by PCR using standard primer pairs (WHITE & al. 1990). PCR products were Sanger sequenced by LGC Genomics (Berlin, Germany). For comparison, sequences from the NCBI Genbank were used. As outgroup, representative species of *Cystoagaricus* SINGER, *Kauffmania* ÖRSTADIUS & E. LARSSON, and *Typhrasa* ÖRSTADIUS & E. LARSSON were chosen. The alignment of the individual partitions was performed with Prank Version 140603 (VEIDENBERG & al. 2016), refined by an iterative guide tree method. The best fitting partition scheme and optimum evolution models for the Bayesian analysis were calculated with Partitionfinder (LANFEAR & al. 2016), while the Bayesian information criterion (BIC) was used for scoring. The Maximum-Likelihood analysis was performed with RAxML 8.2.10. (STAMATAKIS 2014). Out of 1000, the best tree was provided with the ML bootstrap support values. The outgroup and the subsequent *P. candolleana*-group were collapsed for better clarity.

Fig. 2. *Psathyrella aberdarensis*, young specimen. Photo: V. W. KIMANI.

Fig. 3. *Psathyrella aberdarensis,* old specimen. Photos: A. KARICH.

Cultivation:
An appropriate twig covered with mycelium was collected in the Aberdare National Park, transferred to Zittau (Germany), and placed under saturation vapour at 23 °C into an incubation chamber. After about six weeks, a few fruiting bodies and some small primordia appeared. From this material, we were able to isolate a pure culture of the fungal strain.

Results

Phylogenetical analysis

The new species belongs to the *Psathyrella* group without pleurocystidia and with a lamellar edge predominantly composed of utriform to subcylindrical marginal cells. SMITH (1972) summarized the species with such a morphology in subg. *Candolleana* (ROMAGN.) A. H. SM.; KITS VAN WAVEREN (1985) placed them in sect. *Spintrigerae* (FR.) KONR. & MAUBL. emend. KITS V. WAV. Recent molecular genetic studies (NAGY & al. 2010, 2011; ÖRSTADIUS & al. 2015) confirmed that these morphological features largely coincide with phylogenetic analysis. The number of species in this group is certainly larger than previously expected; recently, *P. secotioides* G. MORENO, HEYKOOP, ESQUEDA & OLARIAGA (MORENO & al. 2015), *P. cacao* DESJARDIN & B. A. PERRY (DESJARDIN & PERRY 2016) and *P. subsingeri* T. BAU & J. Q. YAN (YAN & BAU 2018) have been described as new species.

The closest relatives of *P. candolleana* (FR.: FR.) MAIRE comprise very similar and morphologically hardly distinguishable species. Thus, in the NCBI Genbank, many respective sequences are just deposited under "spec.". On the other hand, some more distantly related species can be easily distinguished and determined merely based on macro- and microscopic features, e.g., *P. typhae* (KALCHBR.) A. PEARSON & DENNIS and *P. leucotephra* (BERK. & BROOME) P. D. ORTON; the species described here indeed belongs to this group of *Psathyrella*.

In the phylogenetic tree (Fig. 1) the closest relatives of the new taxon *P. aberdarensis* are *P. singeri* A. H. SM., *P. sulcatotuberculosa* (J. FAVRE) EINHELL., and an unidentified sequence (KF800637) of RITTENOUR & al. (2014) which was generated from spores collected in air and dust samples indoors in Kansas City and thus cannot provide any further characters. *Psathyrella singeri* was described by SMITH (1972) from a wetland area in Florida (USA). He did not mention a veil and described the lamellae as very crowded and strikingly pale. A respective sequence in Genbank (MG734718) was analysed using a specimen from China, Jilin, Changbai Mountain National Nature Reserve (YAN & BAU 2018). It is uncertain that this sequence belongs to *P. singeri* ss. stricto; it does not match with our sequence and may rather represent a separate species. On the other hand, a good match was found between our strain and *P. sulcatotuberculosa*. This species also has small and fragile basidiomata on dead wood; its almost equally sized spores appear very pale and a distinct germ pore is absent or – at best – extremely indistinct. However, there are also significant differences to our *Psathyrella* strain. The cheilocystidia of *P. sulcatotuberculosa* are more polymorphic, the pileus surface is heavily rugulose, the veil is pale yellowish and fibrillose, does not make patches and is made up of subcylindrical to in the middle slightly enlarged, thin-walled cells, some of which are sometimes encrusted. A detailed description is given by BATTISTIN & al. (2014).

Taxonomy

***Psathyrella aberdarensis* A. MELZER, KIMANI & R. ULLRICH, spec. nov**. (Figs. 2–4)

Mycobank no.: MB 827350
Genbank accession no.: MH880928

Latin diagnosis:
Pileus usque ad 10 mm latus, primum conicus vel campanulatus, deinde planus, ad marginem tandem supra involutus, rubro-brunneus vel brunneus, non striatus, medium fuscum. Velum flocculis albis et perseverantibus plenum, usque ad medium pilei. Lamellae mediis intervallis distantes, stipiti adnatae, brunneae, in acie albae, non deliquescentes. Stipes usque ad 15 × 1 mm, cylindratus, in parte superiore albus, in parte inferiore pallide brunneus, in parte infima fibrillosus. Basidia 4-sporigera. Sporae 9,4–10,6 × 5–6,3 µm, ellipsoideae, per microscopium pallide brunneae vel flavae, porus germinativus absens. Pleurocystidia nulla. Cheilocystidia 19–33 × 8–12,3 µm, utriformia. Caulocystidia utriformia, cellulis sphaeropedunculatis et clavatis multum immixtis. Cellulae veli subcylindraceae vel subglobosae, non raro crassiparietales et brunneae. Fibulae adsunt. Basidiomata gregaria ad lignum mortuum.

Holotypus: Cultivated in Germany, Zittau, 31. May 2016, type deposited as metabolically inactive dried culture and basidiomata (GLM-F116094); origin: Kenya, Nyeri County, Aberdares National Park, -0.35220 °N; 36.80049 °E; approx. 2400 m s. m., 9. April 2016, leg. V. W. KIMANI.

Etymology: Named after the place of origin.

English description:
P i l e u s : up to 10 mm wide, at first conical to campanulate, later flattening, old with an up-rolled margin, reddish brown to brown (ca. $Y_{50}M_{50}C_{20}$ to $Y_{50}M_{70}C_{30}$), centre darker (ca. $Y_{50}M_{99}C_{60}$); parts of the universal veil well recognizable and quite persistent as patches.

L a m e l l a e : somewhat distant, adnate, brown, lamellar edge white.

S t i p e : up to 15 × 1 mm, cylindrical, in the upper part white, in the lower part brownish, base strikingly white tomentose.

B a s i d i o s p o r e s : 7.5–8(–8.8) × 4.4–5 µm, average 7.8 × 4.6 µm, Q=1.6–1.75, $Q_{av.}$=1.7; in front view ellipsoid, in side view adaxially slightly flattened, often somewhat phaseoliform, apiculus tiny, germ pore not visible; in water and ammonia solution pale yellowish brown, in KOH nearly hyaline.

B a s i d i a : 15–16.5 × 6.8–8 µm, 4-spored, clavate to sphaeropedunculate.

C h e i l o c y s t i d i a : 19–33 × 8–12.3 µm, predominantly utriform, rarely lageniform, numerous but moderately crowded, sometimes with small golden-brown deposits; intermixed with variously frequent clavate and sphaeropedunculate cells (paracystidia), 16.5–27 × 9.5–19 µm; all marginal cells thin-walled and colourless.

P l e u r o c y s t i d i a : aubsent.

C a u l o c y s t i d i a : 24.5–43.7 × 12.3–16.5 µm, utriform, scattered; sphaeropedunculate and clavate cells also present, these 19–33 × 11–24.5 µm.

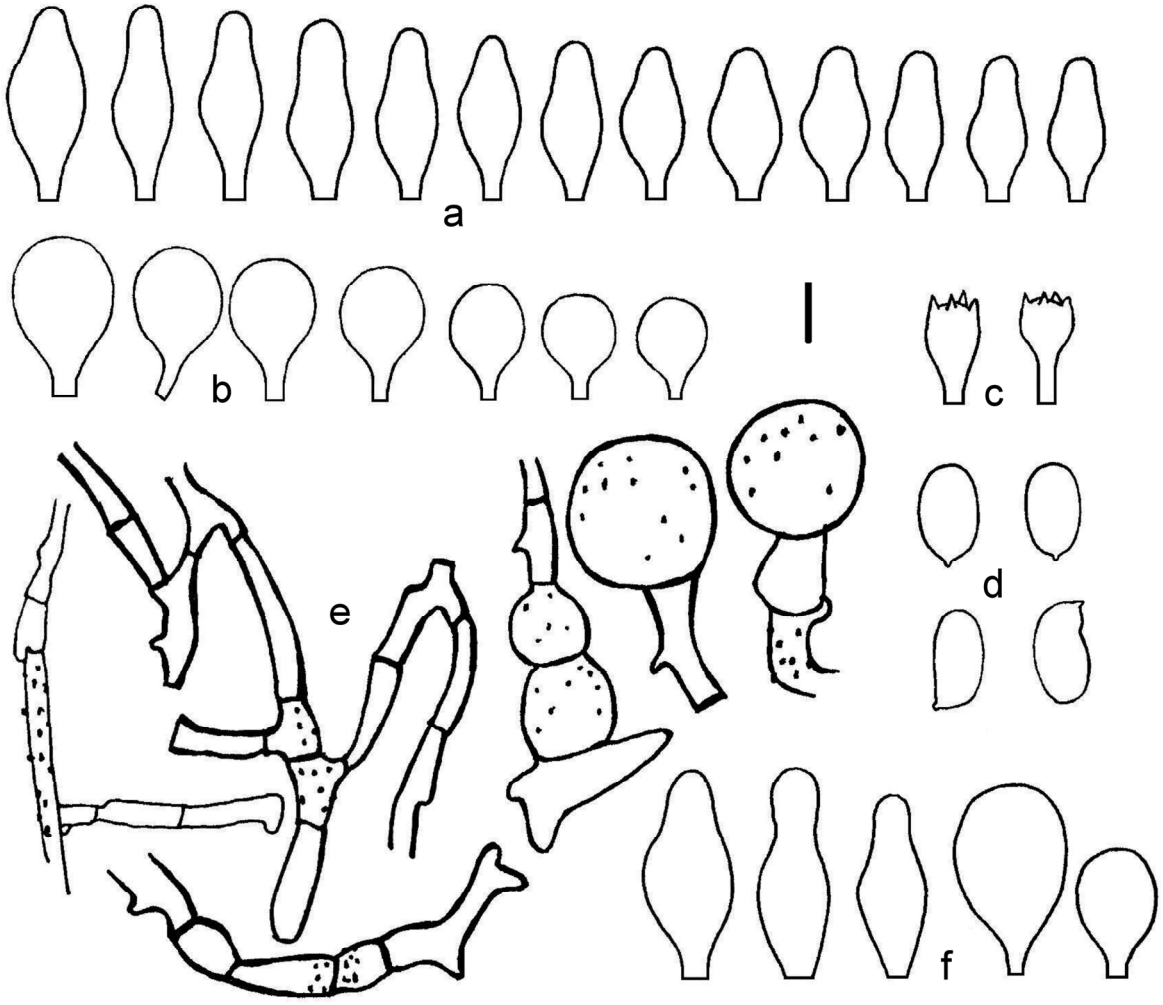

Fig. 4. Microcharacters of *Psathyrella aberdarensis; a* cheilocystidia, *b* paracystidia, *c* basidia, *d* spores, *e* veil elements, f caulocystidia. Bar: 5 µm (spores), 10 µm (others). – Drawing by A. MELZER.

V e i l : made up mainly of heavily branched, slightly diverticulate, often thick-walled and brownish pigmented cells, 13.7–50 × 4–11 µm, beside globose elements, these 16.5–30 µm in diam.; all cells often slightly to strongly encrusted.

C l a m p c o n n e c t i o n s : present, e.g., in mycelium and veil.

Habitat: gregarious on dead wood (fallen twigs).

Discussion

Psathyrella aberdarensis is characterized by small basidiomata, a persistent veil made up of polymorphic elements and very pale spores without a recognizable germ pore. Some other species without pleurocystidia, with pale spores and without germ pore, are mentioned below along with species suggesting a closer relationship to our *Psathyrella* species for other reasons. Since sequences of these species are currently not available in GenBank or Unite, distinctions are made based on other characteristics that - as a whole - appear to be plausible.

Psathyrella aequatoriae SINGER was described from Ecuador. According to SINGER (1978) it is a very small species with a pileus diameter of 6–14 mm and without (or with invisible) veil. The lamellae are crowded and only pale brownish.

Psathyrella atroumbonata PEGLER is habitually quite similar but has larger basidiomata with the veil hanging on the margin of the pileus and consisting of hyaline hyphae. The spores are pale brownish, and the germ pore is small and sometimes indistinct. However, the drawings in PEGLER (1966, 1973) show strongly truncate spores.

Psathyrella bivelata CONTU is probably a closely related species due to a similar veil structure (globose elements mixed with branched-cylindrical, slightly thick-walled ones). The spores, however, are larger, darker and have a germ pore. Moreover, the species is currently known only from the Mediterranean region (CONTU 1991, VOTO 2011, SAMMUT & MELZER 2012).

Psathyrella pallidispora DENNIS has 8–11 × 4–5 µm large and slenderer spores, the cheilocystidia are often capitate (DENNIS 1970: fig. 9G). No records are known outside South America.

Psathyrella varicosa A. PEARSON has relatively large basidiomata with up to 60 mm wide pilei and up to 120 mm long stipes. PEARSON (1950) does not mention a veil. The spores measure (6–)9 × (4–)4.5–5 µm, are frontally ellipsoid to amygdaloid, laterally phaseoliform, yellowish, and the germ pore is absent. This terrestrial species was described from South Africa.

The authors would like to thank ALEXANDER KARICH for supplying photographs, DIETER WÄCHTER, HARALD KELLNER and ENRICO BÜTTNER for gaining and interpreting the molecular genetical data, as well as BEATE NOACK and MARTIN HOFRICHTER for assistance in Latin and English language, respectively. We also thank the National Research Foundation (Kenya) in cooperation with the German Academic Exchange Service (NRF-DAAD) for the doctoral fellowship to V.W.K at the TU Dresden (ST 32 DAAD – Stipendienprogramm Afrika*)*.

References

BATTISTIN, E., CHIARELLO, O., VIZZINI, A., ÖRSTADIUS, L., LARSSON, E., 2014: Morphological characterisation and phylogenetic placement of the very rare species *Psathyrella sulcatotuberculosa*. – Sydowia **66**(2): 171–181.

CONTU, M., 1991: *Psathyrella bivelata* spec. nov., une nouvelle espèce de la section *Cystopsathyra*. – Bull. Trimest. Soc. Mycol. France **107**(3): 85–89.

DENNIS, R. W. G., 1970: Fungus flora of Venezuela and adjacent countries. – Kew Bull. Addit. Ser. **3**: 1–531.

DESJARDIN, D. E., PERRY, B. A., 2016: Dark-spored species of *Agaricineae* from Republic of São Tomé and Principe, West Africa. – Mycosphere **7**(3): 359–391.

KITS VAN WAVEREN, E., 1985: The Dutch, French and British species of *Psathyrella*. – Persoonia, Suppl. **2**: 1–300.

KÜPPERS, H., 2007: DuMont Farbenatlas (10th edn). – Köln: DuMont.

LANFEAR, R., FRANDSEN, P. B., WRIGHT, A. M., SENFELD, T., CALCOTT, B., 2016: Partition Finder 2: new methods for selecting partitioned models of evolution for molecular and morphological phylogenetic analyses. – Mol. Biol. Evol. **34**(3): 772–773.

MORENO, G., HEYKOOP, M., ESQUEDA, M., OLARIAGA, I., 2015: Another lineage of secotioid fungi is discovered: *Psathyrella secotioides* sp. nov. from Mexico. – Mycol. Prog. **14**(6/34): 1–8.

NAGY, L. G., URBAN, A., ÖRSTADIUS, L., PAPP, T., LARSSON, E., VÁGVÖLGYI, C., 2010: The evolution of autodigestion in the mushroom family *Psathyrellaceae* (*Agaricales*) interferred from Maximum Likelihood and Bayesian methods. – Mol. Phylogenet. Evol. **57**(3): 1037–1048.

NAGY, L. G., WALTHER, G., HAZI, J., VÁGVÖLGYI, C., PAPP, T., 2011: Understanding the evolutionary processes of fungal fruiting bodies: correlated evolution and divergences times in the *Psathyrellaceae*. – Syst. Biol. **60**(3): 303–317.

ÖRSTADIUS, L., RYBERG, M., LARSSON, E., 2015: Molecular phylogenetics and taxonomy in *Psathyrellaceae* (*Agaricales*) with focus on psathyrelloid species: introduction of three new genera and 18 new species. – Mycol. Progress **14**(5/25): 1–42.

PEARSON, A. A., 1950: Cape agarics and boleti. – Trans. British Mycol. Soc. **33**(3–4): 276–314.

PEGLER, D. N., 1966: Tropical African *Agaricales*. – Persoonia **4**(2): 73–124.

PEGLER, D. N., 1973: A preliminary Agaric flora of East Africa. – Kew Bull. Addit. Ser. **6**: 1–615.

RITTENOUR, W. R., CIACCIO, C. E., BARNES, C. S., KASHON, M. L., LEMONS, A. R., BEEZHOLD, D. H., BRETT J. GREEN, B. J., 2014: Internal transcribed spacer rRNA gene sequencing analysis of fungal diversity in Kansas City indoor environments. – Environ. Sci. Process Impacts **16**(1): 33–43.

SAMMUT, C., MELZER, A., 2012: *Psathyrellaceae* from Malta, a preliminary survey. – Micol. Veget. Medit. **27**(1): 33–44.

SINGER, R., 1978: Interesting and new species of *Basidiomycetes* from Ecuador II. – Nova Hedwigia **29**(1–2): 1–98.

SMITH, A. H., 1972: The North American species of *Psathyrella*. – Mem. New York Bot. Gard. **24**: 1–633.

STAMATAKIS, A., 2014: RaxML, version 8: a tool for phylogenetic analysis and post-analysis of large phylogenies. – Bioinformatics **30**(9): 1312–1313.

VEIDENBERG, A., MEDLAR, A., LÖYTYNOJA, A., 2016: Wasabi: an integrated platform for evolutionary sequence analysis and data visualization. – Molec. Biol. Evol. **33**(4): 1126–1130.

VOTO, P., 2011: *Psathyrella carinthiaca* sp. nov. e nuove segnalazioni di *P. bivelata*. – Riv. Micol. **54**(2): 121–133.

WHITE, T. J., BRUNS, T., LEE, S., TAYLOR, J., 1990: Amplification and direct sequencing of fungal ribosomal RNA genes for phylogenetics. – In: INNIS, M., GELFAND, D., SNINSKY, J., WHITE, T. (Eds.): PCR protocols: a guide to methods and applications, pp. 315–322. – Orlando: Academic Press.

YAN, J.-Q., BAU, T., 2018: The Northeast Chinese species of *Psathyrella* (*Agaricales*, *Psathyrellaceae*). – MycoKeys **33**: 85–102.

ACKNOWLEDGEMENT

The conception of this PhD research project would not have been possible without the cooperation between the German Academic Exchange Service (DAAD) and the Government of Kenya through National Research Foundation (NRF) under the ST32 DAAD-Stipendium program Afrika. I will forever be grateful for the funding support I received from these two organizations.

My gratitude goes to Prof. Dr. Martin Hofrichter, for admitting me into his doctoral work group. Working with Prof. Dr. Martin Hofrichter saw me not only grow academically but also tremendously contributed to my personal development. He went out of way to ensure an enabling environment for me to undertake my research as well as take care of my daughter. This played a big role in the successful completion of my research as I had peace of mind and tranquility.

I cherish the support and encouragement that I received from my co-supervisor Prof. Dr. Christiane Liers. Her constant and direct supervision; keen eye for details coupled with her patience and understanding is highly appreciated. I am also grateful to Dr. Rene Ullrich, from whom I learnt a great deal about unspecific peroxygenase (UPOs), his work ethics and commitment is highly admirable and a virtue to be emulated.

The molecular part and genomics analysis would not have been complete without the great guidance of Dr. Harald Kellner to whom am grateful. Special thanks also go to my colleagues; Enrico, Alexander, Sabrina, Britta, Conni, Robert, Ania and Ulrike whose invaluable input in my research is much appreciated. I am especially thankful to Enrico for the initial assembly of the genomes and Alexander for the amazing photos included in this thesis as well as guidance on how to carry out experiments at various stages. To Ulrike, I am truly thankful for the support, love, and training. She was like a mother to me, and I will always cherish our friendship.

My stay at Zittau would not have been an exciting experience had it not been for the enthusiastic colleagues: Tobias, Marek, Judith, Martin and Suzanne. They taught me amazing cuisines. I am thankful to Marek for Pymol lessons. I will never forget the fun we shared with Tobias and Martin during the numerous winters that experienced in Germany. They made me change my perception of winter from a period of gloom to a

fun filled and joyful period. The numberless invitations they extended to me made my stay great and enabled me to smoothly gel into the German culture.

My appreciation also extends to Kenya Wildlife Service (KWS), National Commission for Science, Technology and Innovation (NACOSTI), National Environment Management Authority (NEMA), Kenya Plant Health Inspectorate Service (KEPHIS) for providing permission that was necessary for undertaking this study. In particular, I want to acknowledge Kenya Industrial Research and Development Institute (KIRDI) for the study leave and financial support during the field study. Lastly, I am indebted to my family for the support and encouragement; I am sincerely grateful for the care of my daughter during the study period, it meant a lot to me and made my work easy. To Sharlene, thanks for understanding our special circumstance that was beyond your age, you truly made it possible for us.

Versicherung an Eides statt

Hiermit versichere ich, dass ich die vorliegende Arbeit ohne unzulässige Hilfe Dritter und ohne Benutzung anderer als der angegebenen Hilfsmittel angefertigt habe; die aus fremden Quellen direkt oder indirekt übernommenen Gedanken sind als solche kenntlich gemacht.

Bei der Auswahl und Auswertung des Materials sowie bei der Herstellung des Manuskripts habe ich keine Unterstützungsleistungen erhalten.

Weitere Personen waren an der Abfassung der vorliegenden Arbeit nicht beteiligt. Die Hilfe eines Promotionsberaters habe ich nicht in Anspruch genommen. Weitere Personen haben von mir keine geldwerten Leistungen für Arbeit erhalten, die nicht als solche kenntlich gemacht worden sind.

Die Arbeit wurde bisher weder im Inland noch im Ausland in gleicher oder ähnlicher Form einer anderen Prüfungsbehörde vorgelegt.

Zittau, den 27. May 2019

Virginia Wambui Kimani